The regulation of E-cadherin turnover at the cell surface by p120-catenin

By
Joshua Greig

The Department of Biomedical Science
Faculty of Science
University of Sheffield

A Thesis submitted in consideration for the award of the degree of *Doctor of Philosophy*

March 2019

“To explain all nature is too difficult a task for any one man or even for any one age. Tis much better to do a little with certainty & leave the rest for others that come after than to explain all things by conjecture without making sure of anything.”

— Sir Isaac Newton

This Thesis is dedicated to the memory of one who saw this work begun but did not live to see its end.

For the time we had, for the time we did not, you shall be ever with me.

Abstract

E-cadherin (E-cad) is the primary cell adhesion molecule in epithelial tissue. It has multiple levels of regulation to mediate correct expression and localization in space and time within the cell and tissue. Intracellularly the C-terminus of E-cad interacts with the catenin protein family which mediate all intracellular functions. This family comprises three members: β-catenin which is a component of the Wnt signalling pathway, α-catenin which binds actin, and p120-catenin (p120ctn). Prior work established that p120ctn is the master regulator of E-cad levels at the cell surface, but the precise manner of this regulation and the downstream effectors were unknown.

In this work I show that p120ctn acts via a clathrin-mediated mechanism to both promote and inhibit E-cad endocytosis by recruiting and activating two GTPases: Rho and Arf1. Rho has been known to regulate cortical actin and adhesion dynamics, and I demonstrate that p120ctn acts on this pathway to prevent E-cad internalization and stabilize its surface levels. At the same time, p120ctn interacts with Arf1, which has been traditionally viewed as being resident at the Golgi, which I found has a functional role at the plasma membrane. Through the Arf1 pathway p120ctn promotes E-cad internalization and targets it for endosomal recycling. I further dissect how these two signalling pathways operate in a hierarchical fashion with Rho predominating over Arf1, an effect which is dependent on the levels of p120ctn. In parallel, I describe a novel function of p120ctn in regulating the tension present at the cell surface and thus, show that p120ctn is a mechanotransducer. Finally, I characterize the wider implications of altered E-cad internalization and p120ctn expression on the endocytic and intracellular trafficking machinery. Altogether, this work elucidates the signalling pathways which are downstream of p120ctn and how they interact to modulate the levels of E-cad at the cell surface.

List of Contents

Declaration and statement of originality

I, Joshua Greig, do declare and confirm that the work contained within this Thesis is my own, save where explicitly stated, and that the data contained within it has not been submitted for consideration for the award of any other degree, either in part or in full, at this or any other university.

Signature……

Date……

Chapter 1 Introduction

1.1) Cell-cell adhesion: Purpose, Principles, and Evolutionary Development

Cell-cell adhesion is the capacity and organized attachment of one cell to another by means of specialized proteins present upon its surface. This has taken slightly different forms in different species and has become more complex with the evolutionary emergence of larger and more complex organisms, however many elementary principles are applicable to all cell-cell adhesion in all biological organisms. To enable the formation of higher order biological structures, by which is meant those with complex 3-dimensional geometry, cells must act collectively to arrange themselves in space (Gloerich et al., 2017; Wickström and Niessen, 2018). This requirement for higher order structure is further iterated by the necessity of the organisation to be specific in time and in many instances to operate in a choreographed sequence to allow ordered but intricate patterns of form and function observed throughout biological systems (Halbleib and Nelson, 2006; Thiery, 2003). All of these structures are dependent upon cells attaching to one another in a manner which can be regulated and highly dynamic, but which can also be present in a steady-state homeostasis for prolonged periods, sometimes up to many years.

The question of how cells first began to act collectively is one of the great questions of evolutionary history, indeed the transition from a single cell condition to that of multicellularity is one of the three great evolutionary hurdles (Szathmáry and Smith, 1995). Most biological organisms exist as unicellular entities but can form multicellular aggregates under specific conditions (Lyons and Kolter, 2015). A prime example of this is the existence of biofilms, produced by several bacterial species, and other examples of partial or conditional multicellular action by unicellular organisms (de la Fuente-Núñez et al., 2013; Kragh et al., 2016; Lyons and Kolter, 2015). Though these do not constitute true multicellularity as we would define it, it is however an example of the evolutionary advantageous arrangement that can emerge amongst unicellular organisms from collective action. It would therefore not be unreasonable to hypothesize that early multicellularity arose from the collective action which conferred a survival advantage. The early emergence of cell attachments would probably have been indirect, the consequence of adhesion from secreted proteins, still observed in some bacterial biofilms, prior to the development of specialized proteins and molecules which were presented at the surface specifically for their adhesive properties (Abedin and King, 2010; Gul et al., 2017; Hynes and Zhao, 2000). While the secretion of inherently adhesive or “sticky” proteins which have an affinity for the adhesive

secretions of other cells may have served the purpose of forming a multicellular conglomerate, it does not allow the co-ordinated regulation of action, nor the orderliness of structure required for the formation of complex geometric structures. For this, cells required more precise control over the levels and spatiotemporal distribution of adhesion. This in all probability occurred in tandem with the evolution of cues within cell which confer orientation and polarity, in so doing spatially segregate function and protein specialization at distinct surfaces in 3-dimentional space (Bryant and Mostov, 2008; Dickinson et al., 2011; Goldstein and Macara, 2007; Miller et al., 2013; Nelson et al., 2013).

One of the remaining aspects of selective multicellularity which has persisted is observed in many fungal species, which can exist as both unicellular and multicellular states dependent upon environmental conditions (Bleichrodt et al., 2015; Chu et al., 2018). Many fungal species exhibit complex 3-dimentional geometric structures, comprable to bacterial biofilms, and express many components of the specialized proteins used in obligate multicellular eukaryotic cells for the purpose of cell-cell adhesion (Abedin and King, 2008; Lipke, 2018; Murray and Zaidel-Bar, 2014; Nichols et al., 2012; Tronchin et al., 1991). Yet their adhesion is not direct cell-cell but rather cell to extracellular substrate, more comparable to the integrin mediated attachment to the extracellular matrix (cell-ECM) observed in mammalian organisms (Delon and Brown, 2008, 2009). Given what has been remarked upon about the early attachments being to secreted biofilm matrix proteins or related inherently sticky proteins, it is logical to suppose that the first specialized extracellular attachment proteins evolved to mediate this attachment, with direct cell-cell attachment emerging later. A reasonable deduction would be that as some cells spent longer periods of their lifetime in such conglomerates a degree of direct communication and organisation beyond secretions and modification of the extracellular substrate matrix became advantageous. This impetus gave rise to the first true cell-cell adhesion molecules, which in many respects utilized many of the pre-existing components of the intracellular cytoskeletal machinery (Dickinson et al., 2011).

In obligate multicellular eukaryotic organisms, a series of specialized proteins have evolved to mediate the process of attachment to neighbouring cells. Collectively these proteins are known as cell adhesion molecules (CAM). The notion of the existence of these CAM extends to the early investigation of the natural philosophers of the 19th century. The first evidence for a function of attachment in arrangement of structures and organs arose from seminal work in the 1950s, Townes paper in 1955 (Steinberg and Gilbert, 2004) in which spontaneous sorting of a disrupted cell mixture was observed. This phenomenon was

attributed to some property on the cell surface determining the configuration or arrangement of cells in the mass, thus enabling a discrimination of cell types and the correct sorting and compartmentalization of the emerging organism. This aspect of cell adhesion, as a sorting process, was one of the first demonstrations that cell-cell adhesion was not merely a passive process of providing attachment, analogous to bricks and mortar, but rather actively participated in the process of development. In part this led to the development of the differential adhesion hypothesis (DAH) by which cellular sorting was a property of distinct adhesion molecules present upon their surface with specific affinity for either cells expressing the same molecule or a complementary molecule, thereby allowing cells to discriminate between those destined for a different fate (Pieters et al., 2016; Schäfer et al., 2014). At the time this was formulated, the precise nature of these CAM or how many and varied the molecules were was unknown. Later seminal work (Takeichi, 1977) provided the first distinction between CAM which were dependent upon calcium ions (Ca^{2+}) or were insensitive to the presence of calcium. The authors concluded that two independent pathways were present in the same cell type, with the calcium-dependent pathway appearing to be more influential for the formation of specific cellular aggregates (termed flocculation), thereafter these molecules were termed the Calcium-Dependent Cell Adhesion Molecules or Cadherins for short (Takeichi et al., 1986; Yoshida and Takeichi, 1982).

1.2) Cadherins: Family members and General characteristics

The cadherin family contains multiple members which fall into three broad categories: the classical, the non-classical and the protocadherins. Further division and classification can be made dependent upon domain and structure. In humans these total 114 distinct members (Gul et al., 2017). Despite the distinction and different classifications varying by number of domains and regulation, the one unifying characteristic of the group is that they require interaction with calcium ions in their extracellular ectodomains (EC) to form the junctional bridges with cadherins present on neighbouring cells.

Members of the family have differing numbers of EC in the extracellular space, with Dachsous, a non-classical cadherin, having 35 which greatly exceed the junctional diameter (Sharma and McNeill, 2013; Tsukasaki et al., 2014). Therefore, it is hypothesised that a degree of folding and thus conformational regulation has emerged in this particular non-classical cadherin to allow an additional layer of regulation. By contrast most of the classical cadherin family members contain only 5 EC, with requirement for 2 calcium ions to allow integration between the EC of 2 and 5 (Harrison et al., 2011; Perez and Nelson, 2004; Wu et

al., 2010). The diversity and difference in the number and composition of the EC domains is reflective of the specificity required for adhesion, in accordance with the differential adhesion hypothesis this allows cells to discriminate type (Foty and Steinberg, 2005; Pawlizak et al., 2015; Steinberg, 1996). Many cadherins exhibit homophilic binding preferences or specific heterophilic interactions which allow planar polarity within a tissue (Chappuis-Flament et al., 2001; Labernadie et al., 2017; Renaud-Young and Gallin, 2002).

The largest family within the cadherin superfamily is the protocadherins with 65 members, they consist of approximately 2/3 of the family members expressed in humans, with most being expressed in neuronal tissue (Hayashi and Takeichi, 2015; Kohmura et al., 1998; Tan et al., 2010). The function and regulation of these protocadherins has been subject to less work than the classical family member but they have been implicated, given their neuronal expression patterns, with numerous neuropsychiatric conditions, postulated to arise from abnormal or defective neuronal pathfinding and synaptogenesis. Two of the best studied examples of this are protocadherin 17 and 19 (*PCDH17* and *PCDH19*). Both of these proteins have been implicated in the abnormal synaptogenesis observed in autism (Breuillard et al., 2016; Redies et al., 2012; Tsai and Huber, 2017) which is viewed primarily as an abnormality arising from perturbed neural development (PDD). In such cases abnormal dendritic arborization with reduced long-range connections and increased local connections is observed, the so-called disconnection hypothesis (Friston et al., 2016). Further evidence suggests that it is the initial formation and pathfinding of these neurones which is abnormal, with a loss of adhesion or perturbed adhesion affinity affecting the discrimination of cell type, which is particularly imperative for the formation of the synaptic junctions. *PCDH17* has been further implicated in Schizophrenia (Friston et al., 2016) and in cases of oesophageal cancer (Haruki et al., 2010; Lin et al., 2017). All of these cases attest to the fundamental nature of the requirement for cell-cell adhesion for normal physiological function. Most interestingly these protocadherins lack the intracellular domains which distinguish the classical cadherins (Gul et al., 2017; Oda and Takeichi, 2011). This removes their capacity to directly regulate the cytoskeleton but does not exclude their capacity to have some signalling function. The most superficial explanation would be that the simple process of having a molecule which can discriminate cell types by a mechanism of pure affinity preference would be sufficient. However, without additional mechanism to sense and respond accordingly the function could not be fulfilled. One possible explanation which has been posited is that they have a membrane bound co-receptor which could either directly interact or sense the affinity preference of the binding or perhaps the consequent change in the

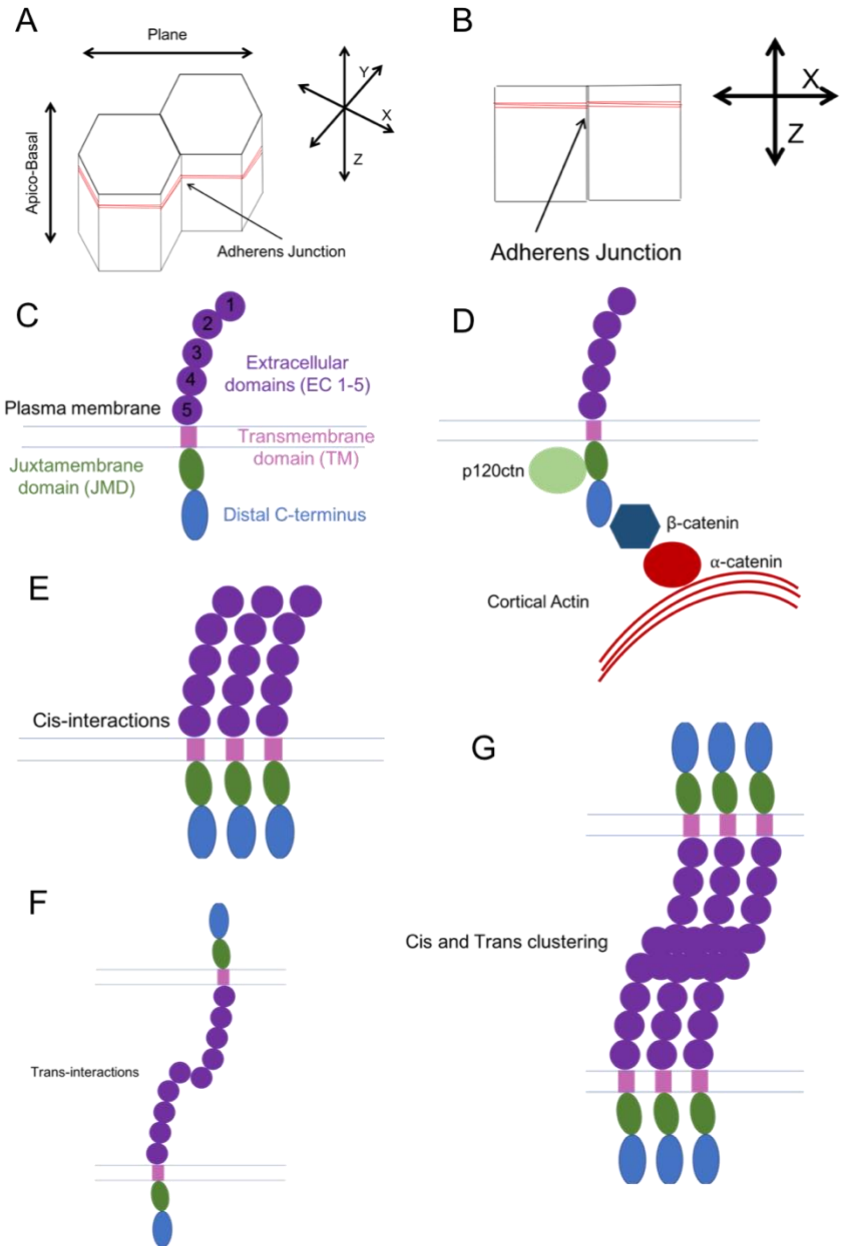

Figure 1.1 The Adherens junction in epithelia cells and the composition and dynamics of the E-cad molecule. (A) The three-dimensional orientation of epithelia cells with the adherens junction located on the apicolateral surface. (B) Two-dimensional rendering of the epithelial cells with the AJs represented by the surface contact between adjacent cells and the band of the cortical actin cytoskeleton which lies below the junctions. (C) Representation of the domain structure of a single E-cad molecule. The major domains are indicted and termed by their position along the polypeptide sequence and final cellular position. (D) The E-cad complex with associated Catenin family proteins and the respective binding sites of the catenin molecules on the cadherin complex. (E) The dimerization and clustering of molecules on the same surface (i.e. within the same cell) is termed Cis-interactions and is determined by both the JMD and the EC domains. (F) Dimerization across the intercellular space between E-cad molecules in adjacent cells is termed Trans-interactions. This is mediated by the EC1 and EC3 domains. (G) The formation of more stable adhesion complex and a mature AJ requires both cis and trans interactions to form larger clusters of the molecules. These clusters account for the immobile fraction in FRAP and are presumed to have high association with the underlying cortical actin cytoskeleton.

surrounding lipid viscosity and fluidity (Chen and Maniatis, 2013, 2013; Mah and Weiner, 2017; Weiner and Jontes, 2013). Alternatively, they may have a signalling function which is as yet unknown and could account for the observed capacity to discriminate cell types and form intricate neuronal pathways observed in mammalian brains. The protocadherin family are illustrative of the discriminating potential of having specific cell surface proteins which can distinguish themselves by binding affinities. However, the classical cadherins, which are the most studied members of the cadherin family, all share an intracellular domain with the capacity to regulate some signalling pathways or the actin cytoskeleton (Aberle et al., 1996; Nelson, 2008).

The classical cadherins are the most extensively studied members of the cadherin family because of their implications with a plethora of disease processes and their expression in a highly tissue-specific manner. All the family members have conserved EC domains and a similar intracellular domain facilitating the stereotypic interactions with the signalling pathways and actin cytoskeleton (Oda and Takeichi, 2011). The main members are classified according to the tissue in which they are expressed: epithelial (E-cadherin, E-cad), neuronal (N-cadherin), vascular endothelial (VE-cadherin), placental (P-cadherin).

1.3) Epithelial cadherin: Identification and Characteristics

The first member of the classical cadherin family, so-called because it was the first identified and has been the most extensively studied, is E-cad encoded by the *CDH1* gene. As with the identification and study of the first member of any protein family the characteristics of E-cad have been used as a comparative standard for other members of the classical cadherins as well as the other members of the cadherin superfamily. In humans E-cad has the textbook structure (Fig.1) with 5 EC domains bridging the inter-cellular space, a transmembrane domain, and a well characterised C-terminus with juxtamembrane and distal tail domains.

As previously alluded, the primary reason E-cad has been so extensively studied, and informed further research on other cadherins, and CAM in a more general sense, is that epithelial tissues constitute one of the four fundamental tissue types found in all animal organisms. Epithelial tissue covers all organs and cavities of animal bodies (the other tissues types being neuronal, skeletal and muscular) but more importantly because it is from epithelia tissues that the majority of cancerous conditions arise (CRUK). E-cad binds in an exclusively homophilic manner with E-cad present on other cells, or artificially deposited on a surface (Collins et al., 2017; Drees et al., 2005a; Nagaoka et al., 2006). This binding has, due to E-cad being the first discovered, viewed as the stereotypical binding between CAMs,

with characteristic interactions between the EC2 and EC4 with the EC1 and EC5 respectively of adjacent cells, forming trans dimers between neighbouring cells. Early studies identified this using calcium depletion assays with cultured cells, observing a rapid destabilization in EGTA/EDTA containing media and a swift re-establishment of binding when the chelating agent was washed out of the culture media. This trans interaction requires the presence of two calcium ions between the respective domain pairs. These experiments were the first indication that environmental cues and the binding potential of a CAM could influence its dynamics at the cell membrane, that is to say the time duration (lifespan) of the CAM at the plasma membrane. These trans interaction are in conjunction with the formation of cis interaction between the E-cad molecules present in the same plasma membrane to strengthen and re-enforce adhesion (Cailliez and Lavery, 2006; Ozawa, 2002; Troyanovsky et al., 2007). The precise mechanism of the assembly and disassembly of these dimers and clusters, particular the question of which first forms are still the question of ongoing research (Yap et al., 2015). These clusters and dimers directly influence the degree of attachment the cell exhibits at any one time and provided a conceptual basis for the inference that elements within the cell must be present to sense the degree of attachment to the neighbouring cells and respond to either reinforce adhesion or to remove the E-cad from the surface, to reduce adhesion, when not required or when stimulated to do so.

It was these observations *in vitro* in tandem with studies of the role of E-cad in development and disease which directed attention towards the study of the regulation of E-cad in cell adhesion. What has emerged is a multi-layer and complex, yet intricately balanced system of regulation which has been and continues to be the subject of much study due the fundamental nature of cell-cell adhesion for all multicellular processes. These are subjects which are discussed respectively in the following sections.

1.4) Roles of E-cadherin in development.

During the embryonic development of all multicellular organisms substantial cellular rearrangement and patterns emerge which give rise to the varied forms observed throughout nature. The critical importance of E-cad from the onset of development is evident from the fact that mammalian embryos which lack, or are mutant for, E-cad fail to progress beyond the morula stage and the embryo dies. In *Xenopus* the maternal contribution of E-cad can enable some embryos which are deficient to establish a degree of blastulation but without the zygotic expression this mRNA is swiftly depleted and further development fails (Nandadasa et al., 2009). Due to the early critical nature of E-cad expression, any mutation which results

in loss of expression or sufficient perturbation of expression is lethal. Therefore, any developmental conditions or defects associated with cell adhesion dysfunction which present beyond this stage, would be by definition the result of milder perturbations to cell adhesion, which either only mildly perturb function or affect some element of its regulation (Li et al., 2014).

The emergence of three distinct cell lineages during gastrulation also involve E-cad. How all of these processes are co-ordinated by the genetic machinery and the co-ordination and consistency of the patterning was first described in the late 19th century (Haeckel, 1872) and remains the subject of much research to this day. The three germ layers are distinguished by their adhesive properties by the expressional transition from E-cad to other cadherins which define the endoderm, mesoderm or ectoderm respectively (Choi and Gumbiner, 1989; Schäfer et al., 2014; Wang et al., 2004). This is an early manifestation of the differential adhesion which is used to facilitate cellular sorting and rearrangement simultaneously: as the different lineages emerge they become separated and sorted from the neighbouring tissues while simultaneously undergoing invagination and ingression that defines the gastrulation stage of embryonic development (Shimizu et al., 2005; Winklbauer, 2012).

From the gastrulation stage organisms undergo a process of organogenesis in which the organs which constitute the adult body emerge and more specific functions and adaptations manifest. All of these processes require the regulated modification of cell adhesion to enable the development of mature structures. One of the most commonly known defects of this process is the failure of the closure of the neural tube resulting in spina bifida. This has been studied in both human patients and *Xenopus* in which the involvement of both E-cad and N-cad have been implicated (Greene and Copp, 2014; Nandadasa et al., 2009).

In *Drosophila*, another organism like *Xenopus* which has been extensively studied during the embryonic stages of development, E-cad is also required early in development (Karim et al., 2016; Oda et al., 1998). Analogous to vertebrate development, the *Drosophila* embryo undergoes rapid divisions after fertilization (Gilbert, 2000). However, this occurs in a multinuclear syncytium in which only the nuclei divide with no cell membranes or adhesion. Only after the 13th division and migration to the edges of the syncytial embryo do the individual nuclei acquire the membranes which separate them from the neighbour. Once formed this structure could be viewed as being equivalent to the vertebrate blastula with a hollow fluid-filled cavity surrounded by an array of cells (blastocysts), which are in essence a single layered epithelium (Choi and Gumbiner, 1989; Nandadasa et al., 2012). There is a significant maternal mRNA contribution which can sustain a deficient zygote for some time,

and *Drosophila* E-cad zygotic mutants complete most of embryogenesis with defects in dynamic cell rearrangements during organogenesis (Uemura et al., 1996)

Another morphological process which requires the dynamic functional alternation of E-cad is in the process of an epithelial to mesenchymal transition (EMT), whereby static and stable epithelia cells in a tissue transition to a migratory pattern of behaviour by downregulating cellular attachment and modify the regulation of their cytoskeleton to facilitate this process. Upon completion these cells might undergo the reverse process known as the mesenchymal to epithelia transition (MET), for example during the formation of the midgut in *Drosophila* (Campbell and Casanova, 2015) or differentiation of hepatocytes (Li et al., 2017).

Both EMT and MET were originally identified as processes required for morphogenesis but latterly it has become apparent that this can be co-opted in various pathological conditions (see next section). The involvement of E-cad in these processes was initially thought be analogous to a handbrake, that is to say to establish a stable epithelium, and the mesenchymal state requiring the suppression of this and all cell-cell adhesion (Lamouille et al., 2014; Wendt et al., 2011). However, it has emerged that this view is incomplete, in mesenchymal cells the mRNA levels of E-cad in some cases remain the same as those prior to EMT and after MET (Campbell and Casanova, 2015). It is the surface levels of E-cad which are affected in these cases. For many EMT events the cells do not migrate individually but in fact exhibit a degree of ordered and orchestrated collective action (Cousin, 2017; Elisha et al., 2018; Hwang et al., 2012). It has been observed that these collective migrating cells do in fact present E-cad in discrete spots/ puncta on their surface specifically in regions in which they are in contact with neighbouring mesenchymal cells, but not on the external surface of the migrating mass (Campbell and Casanova, 2015). Further examination revealed that these puncta spots are highly dynamic and never persist for long on the surface, presumably they are internalized by mechanisms induced by the Twist/Snail transcription factors and the continued manifestation of E-cad at the surface results from some independent recycling mechanism (Le Bras et al., 2012). This would ensure that while the fleeting presence of E-cad at the surface would confer a degree of integrity to the migrating mass of cell, it would not allow the establishment of a stable adhesion between the cells, which is a hallmark of a mature fully differentiated epithelial cell.

The processes described in this section constitute the normal range of functions that cell-adhesion and particular E-cad have in normal animal development. Many of these persist in the adult, being used to maintain homeostatic stability of tissues. However, many are also

present in pathological processes, and it is the study of the role of E-cad in disease which has shed the greatest light upon its function.

1.5) Roles of E-cadherin in disease and infection

In a similar fashion to importance of cell adhesion for developmental processes, due to its fundamental importance, dysfunction of cell adhesion is observed in multiple disease states (El-Amraoui and Petit, 2010, 2013; Vestweber, 2015). These can either be directly causative (aetiology) or arise during the course (symptomatic) of these conditions. As many diseases arise within epithelial tissue the study of cell adhesion within these tissues has been the most explored, indeed most of the information known about E-cad is derived from work describing and characterising its role in various disease states (Ellis et al., 2008; Grabowska and Day, 2012; Petrova et al., 2016; Schneider and Kolligs, 2015). Broadly, diseases may be divided into two: those arising from internal dysfunction, and those arising from external agents, e.g. infection and toxins.

For internally arising conditions, cancer and tumorous growths are the most characterised in relation to cell adhesion, these are discussed in detail in the following section. For those which primarily arise from external agents, study has been made of infections which infiltrate the epithelial tissue and the inflammatory response to this infection. The bacterium *Listeria Monocytogenes* which causes the severe infection condition listeriosis, characterised by: inflammation of epithelial tissue, meningitis and septicaemia, uses specialized proteins to integrate into epithelia tissue. These specialized proteins called *Internalins* enable the bacterium to attach to E-cad and to initiate a process of internalization, which carries the bacterium into the cell, by a currently poorly characterized mechanism (Bonazzi et al., 2008, 2009; Lecuit, 2005; Lecuit et al., 2004). Presumably this initiates a mechanism of induced endocytosis rather than merely being passively carried with E-cad during constitutive endocytosis, however direct evidence for this is scant and only the rate of transmission and some preliminary work on the virulence factors provide such clues (Coelho et al., 2018). Superficially this is similar to other transmission routes for intracellular pathogens co-opting the normal cellular process for their own replication and transmission. However, this bacterium is of interest as it is one of the few instances that cell adhesion molecules themselves have been used by bacterium to infiltrate cells. This phenomenon is further evident in viral infections, naturally as viruses are obligate intracellular pathogens, with emerging evidence that Hepatitis C and other epithelia specified viruses use E-cad as an entry factor (Li et al., 2016). It could be argued that the examples outlined above are not the

direct result of E-cad but the result of an external agent merely using an existing cell adhesion molecule for their own end. This is evidenced in the case of some human papilloma viruses in which the infected cells undergo a transition to a more mesenchymal state, by virally inducted epigenetic suppression of the expression E-cad (D'Costa et al., 2012; Laurson et al., 2010; Lefevre et al., 2017; Leong et al., 2010).

Of greater potential importance in these conditions is the inflammatory response which arises to counteract the infection. Cell adhesion is required to attach an immune cell to any infected cell and enable screening by cell of the innate or adaptive immune system (Van den Bossche et al., 2012). But of more direct importance and interest from the perspective of the epithelia cell is the anti-inflammatory role played by E-cad. Rather than merely attaching immune cells to epithelial to enable screening, a large volume of evidence indicates that E-cad has direct roles in the inflammatory cascade (Saito et al., 2014; Smyth et al., 2012; Van den Bossche et al., 2015). Loss of E-cad increases the expression of several inflammatory markers, particularly the master regulator Nf-kB (Chua et al., 2007; Solanas et al., 2008). Further the loss of specific components of the adherens junction, e.g. p120ctn and β-catenin can also result in inflammation (Hu, 2012; Perez-Moreno et al., 2008; Stefanatos et al., 2013; Zhu et al., 2014). Why this should be, is an interesting question, the inflammatory response in the initial phase requires the identification and destruction of the invasive agent, and the unbuckling of epithelial adhesion permits the passing of immune cells across epithelia barriers (Chi and Melendez, 2007; Dejana et al., 2008; Sandig et al., 1997; Sidibé and Imhof, 2014). However, more direct evidence indicates that epithelial cells themselves can phagocytose under certain conditions (Monks et al., 2005), though this does appear to be a back-up system to the primary professional phagocytic cells. Moreover, the increase in inflammatory markers in cells resulting from the downregulation of E-cad would enable the extrusion and identification of infected cells. This cell extrusion phenomena can be utilized by cancerous cells to aid metastasis (see next section).

All of the disease cases outlined above involve cell adhesion and E-cad for initiation or progression, however they are for the most part the result of some external pathogen or action which is ultimately responsible for the resulting disease state. To fully understand the role of E-cad in disease we must turn to the role it has in cancerous conditions. It is this field which has provided the largest contribution to the understanding of cell adhesion and E-cad.

1.6) Roles of E-cadherin in cancer cell progression and metastasis

Cancer is a term which applies to a range of diseases which are grossly characterised by the acquisition of aberrant growth and the potential to spread from the original site (primary tumour) to form secondary tumorous growths (Steeg, 2016). This definition encompasses the pathological progression of the disease but does not define each form, type or characteristic of cancerous cells. A comprehensive analysis of the properties of cancerous cells was done in a seminal work by Weinberg (Hanahan and Weinberg, 2000, 2011) in which all of the cellular hallmarks of cancer and the available evidence for how they arise are described extensively. At each stage of cancer progression: from formation, primary tumour growth, detachment of cells from the primary mass, and the reintegration of these cell to colonise proximal and distal tissue, there is extensive evidence to implicate the involvement of cell adhesion and E-cad in particular for tumours of epithelial origin (Canel et al., 2013; Jeanes et al., 2008; Liu and Chu, 2014; Onder et al., 2008; Pećina-Šlaus, 2003; Petrova et al., 2016; Rosso et al., 2017). It is a natural inference if one considers the fundamental nature of cell adhesion, but to fully understand the role that E-cad plays one must examine each stage in turn and the types of carcinoma in which E-cad has been studied and known to have a contributory role to the aetiology and progression of the disease, these are discussed below.

The majority of cancerous conditions arise from epithelial tissue (CRUK). Many reasons have been postulated from this phenomenon, however one of the consistent themes is that the epithelium is under a higher rate of turnover or proliferation compared to muscular, skeletal and neuronal tissues, some of which have a turnover in the range of many years or practically none in smaller shorter-lived organisms (Rawlins and Hogan, 2008; Tunn et al., 1989). This requirement of constant turnover and proliferation in tandem with the presence of epithelial tissue in all organs and cavities of animal bodies is the very reason that most cancers arise from this tissue type and why most research has focused on the various forms of cancer from the epithelium. Traditionally cancers of the epithelium have been characterised by the area of the body in which they form and the histological characteristics of the tumours mass upon observation (Chen et al., 2019). For this the Grade and Stage of the condition are the two clinical and histological metrics used (CRUK). The grade of the tumour is commonly referred to as the aggressiveness, in actuality grade is a classification of how well differentiated or epithelial-like the tumour appears. A higher grade (range 1-3) indicates that the tumorous mass is highly undifferentiated, that is to say less epithelial in appearance, which usually results in a higher degree of invasion of adjacent tissue and metastasis (Kristensen et al., 1999; Maeyama et al., 2018). The stage is a measure of the progression of

the cancerous condition. Independent staging systems have emerged to describe cancers which arise in different organs, for instance the Dukes system for colorectal cancer (Akkoca et al., 2014). However, they share many of the same principles, and have been unified by the TNM system which describes in turn: the primary tumour characteristics (T), the invasion of lymph nodes and how extensive this is (N), and finally the presence or absence of metastasis (M). It is the presence of metastasis which is the single diagnostic criterion which distinguishes a benign tumour from a malignant tumour. Therefore, much work has been, and continues to be, done to understand not only how cancers develop but on understanding the steps of progression to metastasis (Hunter et al., 2008; Pachmayr et al., 2017). With advances in the rapid genetic profiling of patient cancers it is becoming possible to obtain the full range of genetic and chromosomal abnormities which give rise to cancer and to correlate these with the grade stage and histological type (Ghadimi and Grade, 2010; Lu et al., 2018). In the future it is highly likely that this genetic profiling system will replace the definition of cancer based solely on anatomical position in the patient and provide the opportunity for tailored therapeutic intervention with a higher likelihood of successful remission or cure.

Many studies have implicated the *CHD1* (E-cad) gene as being involved at some stage with cancer, every level of the regulation of E-cad has been implicated in some fashion with a type of cancer, details about the E-cad regulatory systems are discussed in the following section. In the first instance the formation of primary tumours requires the alteration of divisional dynamics within the mass to accommodate the elevated growth of the tumours. Cell adhesion has been long indicated as providing dimensional cues for the orientated division of cells (Gloerich et al., 2017). Indeed, substantial evidence has correlated the presence of E-cad at the surface with the grade of the tumour (aggressiveness), which increases the proliferation rate and the probability of metastasis by altering several growth signalling pathways (Andl et al., 2006; Arend et al., 2013; Heuberger and Birchmeier, 2010; Sharif and Wellstein, 2015; Thievessen et al., 2003). In several cancers the expression of E-cad is absent or supressed, in most of the cancer types studied at the primary stage the expression of E-cad is not affected but rather the levels at the plasma membrane are significantly reduced (Gross et al., 2009; Klymenko et al., 2017; Maiden et al., 2016; Onder et al., 2008; Petrova et al., 2016). In breast cancer cases the loss of E-cad is particularly pronounced in the case of triple negative tumours (Kashiwagi et al., 2010; Shen et al., 2016; Yadav et al., 2015). In a similar fashion in colorectal cancer (CRC), lung, and melanoma the loss of E-cad is correlated with the progression and high grade (Christou et al., 2017; Danen et al., 1996; Dorudi et al., 1993; Grigoraş et al., 2017; Hsu et al., 2000; Lim et al., 2000;

Palaghia et al., 2016; Pećina-Slaus et al., 2007). This is logically consistent with the requirement that the cancerous cells lose adhesion in the primary tumour to enable them to detach and disseminate to form secondary tumours in the epithelia of other organs. The first observations of the characteristics of these secondary tumours indicated that E-cad was present and usually in a physiologically normal amount and the cells were more histologically normal that those of the primary tumour (Chao et al., 2010; Kanazawa et al., 2002; Putzke et al., 2011; Wells et al., 2008). If one takes only these two data sets it is possible to make the inference that while loss of E-cad is advantageous for the primary tumour the reverse is the true for the secondary, as it requires a measure of cell attachment to enable reintegration into epithelia tissue. Therefore, the view that E-cad reduction alone is the only associated characteristic in cancerous conditions is not complete. In fact, the dynamic modulation of E-cad rather than complete loss would be the most advantageous position from the perspective of the metastatic cancer cell (Aiello et al., 2016). To determine the veracity of this view one is required to examine the intermediary step between the primary and secondary tumours, specifically to investigate the metastatic cells themselves. This has proven to be technically challenging but not impossible. Studies in mice have been able to isolate circulating tumour cells (CTC) which are cells which have detached from the primary tumours and are circulating within the bloodstream of the host organism before finding a niche in which to establish a secondary tumour (Lin et al., 2018; Millner et al., 2013). The view which is emerging from these studies is that metastasis is a highly inefficient process and that CTCs require some expression of E-cad or related CAM to enable attachment between CTC and host epithelia, or in many cases the CTC migrate as an adhesive mass of several cells with internal cohesion (Elisha et al., 2018). In a recent studies it was found that these collective CTC masses constitute different cell forms with some assuming a more stem-like form, which is presumed to enable the CTC mass to survive and replenish lost cells (Bulfoni et al., 2016; Luo et al., 2018; Mansoori et al., 2017; May et al., 2018; Yang et al., 2015). Further evidence is emerging that these collective CTC masses, which express E-cad to maintain integrity, have a higher metastatic potential (Elisha et al., 2018). This would be logically consistent with the requirement of such CTC to attach and reintegrate into tissue to form secondary tumours. However, direct observation and study of this process is exceedingly challenging *in vivo* and is the subject of ongoing research in *Drosophila* (Martorell et al., 2014). Attempts are being made to make use of organoid cultures to replicate the conditions and artificially induce the transition from CTC to secondary tumours

(Luo et al., 2018; Praharaj et al., 2018). This aspect is of great interest from a clinical perspective in developing effective means to prevent this process.

This progression of cancerous cells from primary to secondary tumours is similar to the process of EMT/MET during normal development discussed in the previous section. However, the precise molecular mechanism and pathway is distinct from normal EMT, such that this abnormal EMT has been called EMT class II/ III (Li et al., 2017; Roche, 2018). The nature of the molecular mechanisms which are similar and those which are distinct is the subject of ongoing work. Therefore, E-cad expression as a function of the total amount of transcript in the cancerous cells in not the most reliable indicator of prognosis, and progression of cancerous cells from primary tumours to CTC, and eventually secondary tumours, is dependent upon modulation of cell adhesion rather than the absolute binary of presence or absence. The emerging view is that it is rather the dynamics and regulatory elements of cell adhesion which are primarily responsible (Campbell and Casanova, 2015; Elisha et al., 2018). As metastasis requires the dynamic shift during the stages, both the regulation of cell surface amounts leading to metastasis and the ability to return to the surface which is required for the formation of secondary tumours. Therefore, it is the regulation of the cell surface levels of E-cad which is the primary contributory mechanism. Hence, to more fully understand the role of E-cadherin in both development and disease, which exhibit remarkable similarity, one must understand the mechanisms which have evolved to regulate its amount at the cell surface.

1.7) Regulation of E-cadherin

All proteins are subjected to many levels and degrees of expressional regulation. This notion was first apparent from the emergence of the central dogma of molecular biology, whereby information flows from DNA to RNA and then to protein, proposed by Crick in 1958 (Cobb, 2017). In the instance of the production of a protein the earlier stages of transcriptional regulation have the largest proportional effect on the outcome and as such have attracted much attention for long-term modification of the cellular program (Lee and Young, 2013; Stavreva et al., 2012). Later stages in this production process allow modulation of activity and localization, thus permitting more fine-tuned regulation of a particular protein. The expression of E-cad or related adhesion molecules is a prerequisite for the establishment and maintenance of tissues. Because of this many redundant systems have evolved to maintain the levels and expression to protect the integrity of tissues (Delva and Kowalczyk, 2009; Gumbiner, 2000; Liu et al., 2005; Petrova et al., 2016; van Roy and Berx, 2008). However,

these can be co-opted by other pathways which override this system and lead to pathologies (Peinado et al., 2004). Therefore, to understand how this occurs we must look further into the precise nature and components of these regulatory pathways.

E-cad has been extensively studied in this context, transcriptionally E-cad is regulated by a multitude of transcription factors (Liu et al., 2005). The dysregulation of E-cad in cancer is more complex than merely an antagonistic relationship with growth factor pathways (e.g. Wnt) by which suppression of one leads to the upregulation of the other. Indeed E-cad has been documented to be involved with Notch, Hippo, Hedgehog and multiple other growth signalling pathways (Ferreira et al., 2012; Grammont, 2007; Gumbiner and Kim, 2014; Sharif and Wellstein, 2015; Wang et al., 2017; Xiao et al., 2010). With a highly complex interplay between these pathways to either promote or inhibit proliferative pathways and orientate cell division. Much of this data has been obtained from pathological studies of various diseases. As many, if not most, diseases have some implication of cell adhesion (see section 1.5). EGFR signalling and WNT pathways are the classical examples in which the conventional view is that an antagonistic relationship between attachment and growth. This contrast between contact inhibition deriving from cell adhesion, and the antithetical effect of replication and proliferation being dependent on growth factors which supress attachment does not give a complete appreciation of the true nature of the transcriptional regulation of E-cad. JAK-STAT pathways and various proto-oncogenic pathways as well as nearly all growth pathway have some degree of transcriptional regulator function (Bausek, 2013; Xiong et al., 2012). Why this should be so, remains a question of debate, conceivably one could suggest that cell types in which strong attachment is required would be antithetical to rapid growth as epithelia represent a steady state tissue which is performing a normal function. However, such transcriptional regulation is reflective of a prolonged state or transition of the cell into another gross morphological or phenotypic response or behaviour, which requires prolonged exposure to the growth factor and/or prolonged duration of the modification for some enduring outcome.

Post-transcriptional and post-translational modifications can often be used in tandem with transcription repression or activation to enhance the effect or in isolation to provide a more nuanced regulatory mechanism (Spoel, 2018). A large body of evidence exists for the mRNA and post-transcriptional modification by viral infections which are co-opting various natural cellular pathways. Indeed, knowledge about the regulation of E-cad has arisen from the study of viral oncogenes (Arzumanyan et al., 2012; Colpitts et al., 2016; D'Costa et al., 2012), but for the purposes of understanding the role of E-cad in the processes described in

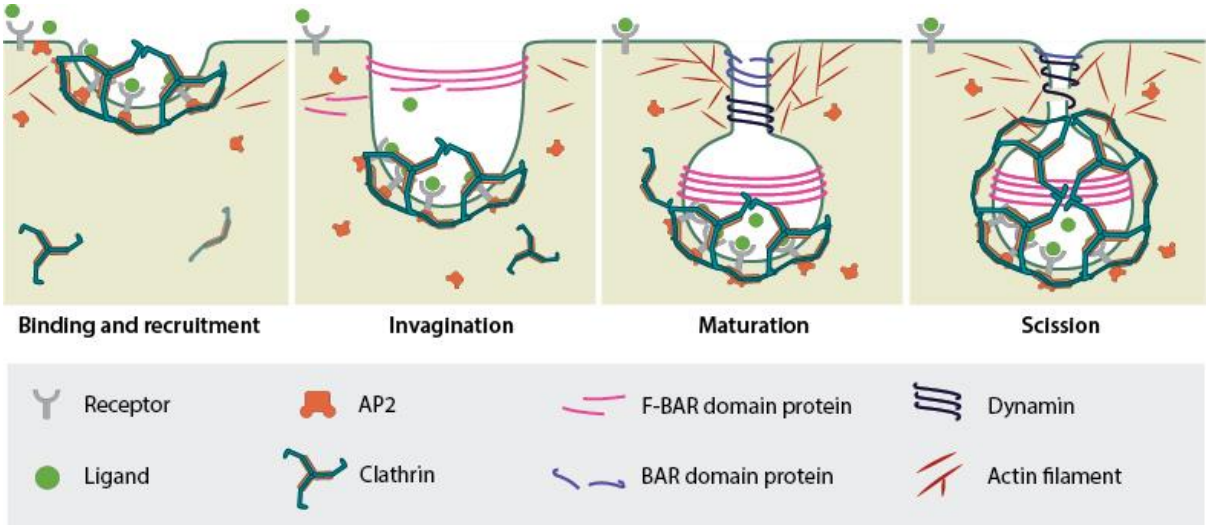

Figure 1.2. The process of Clathrin-Mediated Endocytosis. The internalization of a cargo on the surface begins with the recruitment of adaptor proteins (AP) which in turn recruit clathrin to the site. This results in the invagination of the plasma membrane and the further recruitment of clathrin to form a clathrin coated pit. As the process proceeds the plasma membrane at the neck of the invagination begins to undergo negative curvature and be brought into closer proximity by actin which encircles the neck of the maturing vesicle. Finally, the clathrin lattice fully encases the vesicle and the scission from the plasma membrane is brought about by dynamin constricting the actin encircling the neck of the vesicle, this separate the plasma membrane and vesicle, the latter now undergoes trafficking within the endosomal system. Adapted from MBinfo

the previous sections one must focus specifically on the regulatory mechanisms which influence the levels at the plasma membrane (see description in previous section).

What one might view as the regulation at the end of the production process, that of the turnover of mature fully formed proteins and the complexes they form, is for membrane bound proteins the function of endocytosis and recycling (Doherty and McMahon, 2009), which enables the membrane bound proteins at the cell surface to be in a state of dynamic equilibrium (for full description of endocytosis see next section). The theoretical advantages of such a system are the rapidity with which cell surface adhesion may be modulated. On a rapid timescale the cell may reduce or increase its surface adhesion, while in tandem regulating the amount of synthesis and degradation to couple short- and long-term modulation. The precise interaction between these pathways; how they are connected, and the nature of the cross talk between them, is the subject of ongoing work. To delve further into the regulation of E-cad at the cell surface we shall now focus on the process of endocytosis and recycling at the plasma membrane.

1.8) Endocytosis: overview of initiation and trafficking

Endocytosis is a highly conserved and fundamental cellular process for internalizing proteins and various components present upon the surface of cells. While it is not the purpose of this work to provide too detailed an insight into the various pathways which exist, an overview of the general mechanism of the pathway which was studied as part of this work will be presented and discussed in this section.

At the most fundamental level the process of endocytosis commences with the selection or targeting of a membrane bound cargo (defined as a substrate protein or agent attached at the surface of the cell which is internalized during the process of endocytosis and trafficked within the cell) by various means to assemble a complex which mediates the process of internalization (Fig 1.2, Ref). Various mechanisms have evolved to mediate the internalization method used, with various carriers and scaffolding proteins being employed (Doherty and McMahon, 2009; Ferreira and Boucrot, 2018; Grant and Donaldson, 2009). The best characterized, and therefore viewed as the classical pathway, is that of clathrin-mediated endocytosis (CME), whereby specific adaptor proteins are recruited to the cargo and mediate the recruitment of clathrin to the site to enable the formation of the membrane invagination which later forms the vesicle (McMahon and Boucrot, 2011). These invaginations are coated with the clathrin lattice and progress to form mature clathrin-coated pits and eventually vesicles which are abscised (detached) from the membrane (Fig 1.2). Following this, vesicles undergo a process of sorting and trafficking within the endosomal system. First the cargo is delivered to the early endosome (marked by Rab5) which acts as the first sorting station (Jovic et al., 2010). After this the cargo can be: targeted for direct recycling to the membrane, progress to form late endosomes, which determine a degradative pathway, or can be trafficked to the Golgi for reprocessing (Bonifacino and Rojas, 2006; Grant and Donaldson, 2009). This endosomal pathway is known to be important for the regulation of all membrane bound proteins (Kelly and Owen, 2011).

The work presented here focuses on the initiation of endocytosis and how a cargo is either targeted for endocytosis or is prevented from doing so by specific signalling pathways and cortical actin regulation. Therefore, this following sub-section will focus on the known elements of these events and the specific details pertaining to the known regulation implications for E-cad. The initiation of endocytosis is stimulated by a cargo being marked on the surface for internalization. There are numerous known methods by which this may be achieved, including ubiquitination, phosphorylation and recruitment of adaptor proteins (Chiasson et al., 2009; Delva and Kowalczyk, 2009; Levayer et al., 2011; Miyashita and

Ozawa, 2007; Park and Guo, 2014). The precise nature of the recruitment of the systems which targets the E-cad cargo for internalization is still the subject of ongoing research, but clear common elements are apparent. A distinguishing mark is conferred upon the protein to be internalized, whether this occurs in a targeted manner or is simply due to a proportion of the cargo being tagged remains an open question. Some evidence indicates that ubiquitination kinetics are proportional to the amount of internalized cargo in a given system (González Flecha, 2017; Xu and Qu, 2012). This enables a regulation of membrane protein levels in a dynamic equilibrium or steady-state, the advantages of which are to enable or allow a rapid readjustment of the steady state as required by the conditions of the cellular environment or in response to specific cellular or signalling stimulation.

Once targeted for internalization, specific adaptor proteins are recruited to the cytoplasmic tail of the membrane protein. Classically at the plasma membrane this is the AP2 protein though many other variants exist, which is presumed to accommodate a variety of cargos or determine fates, or may even specify cargo destination (Paczkowski et al., 2015). Once recruited, individual clathrin triskelion molecules are recruited to the site and begin to form a lattice. The source of the initial deformation of the membrane accounting for the invagination is still in question. What is certainly evident is that clathrin recruitment as a carrier or coat protein is required to enable progression of the invagination into a more mature clathrin coated pit (McMahon and Boucrot, 2011; Scott et al., 2018). Conflicting models exist to account for this maturation process: the constant curvature mode (Dannhauser and Ungewickell, 2012) or the constant area model (Bucher et al., 2018), with recent evidence that both are proportional contribution dependent upon the force required to deform the membrane (Maib et al., 2018), which is itself a consequence of the nature and properties of the cargo which is being internalized. Once the invagination has reached the point at which a neck is forming by negative membrane force actin acini begin to form around the neck (Fig 1.2, (Ferguson and De Camilli, 2012). These are regulated and manipulated by a group of GTPase enzymes which mediate the abscission of the vesicle from the membrane (Guha et al., 2003; Kroll et al., 2015). This process involves the processive constriction of the neck of the invagination until such a point that the membranes are in contact and energetic resolution is brought about by the formation of a spherical vesicle and the closing of the plasma membrane (Fig 1.2).

Once complete the vesicle is trafficked to the early endosomal compartment and the clathrin coating lattice is disassembled either by specific enzyme mediation or spontaneous (in the chemical sense of the term) dissociation (Sousa et al., 2016). Once within the endosomal

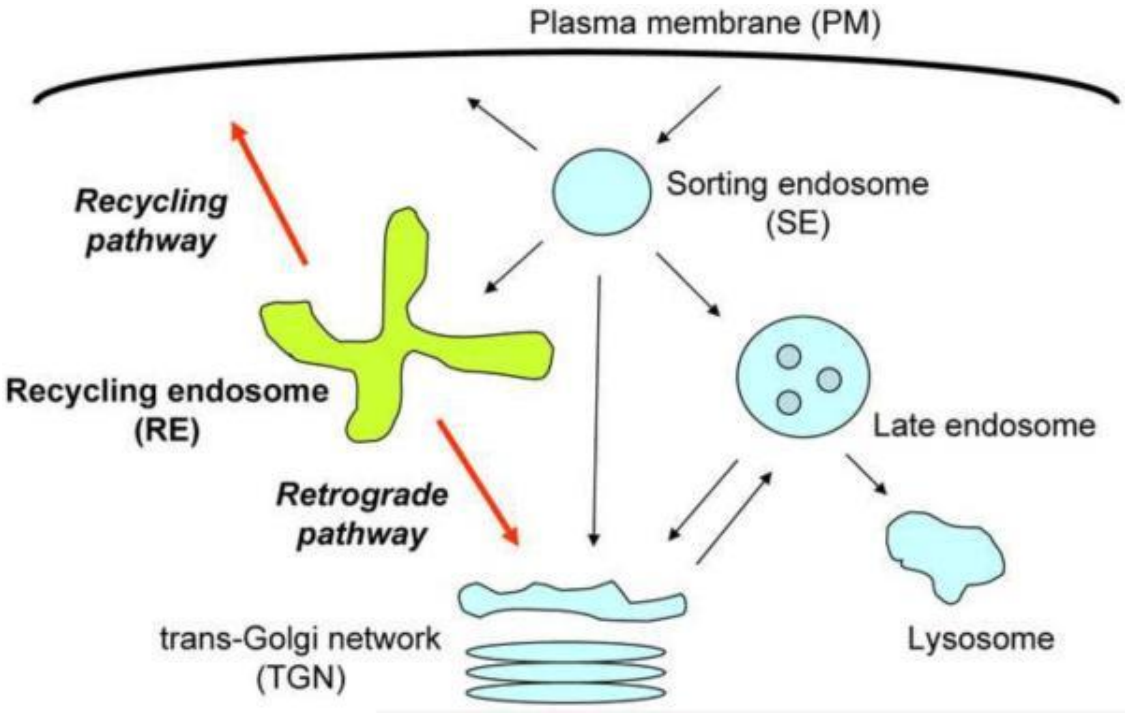

Figure 1.3. Endosomal trafficking. Schematic of the pathways and compartments within the endosomal system. After cargo had been internalized from the plasma membrane it is directed towards the early/sorting endosome (EE/SE) (marked by Rab5) from here a sorting decision is made and the cargo can be trafficked to the Golgi via the TGN, or it can be immediately targeted for degradation via the late endosomes (marked by Rab7), which fuse with the lysosomes to complete the process. From the Golgi the cargo can be directed to return to the plasma membrane via the recycling endosome (marked by Rab11). Adapted from (Prekeris, *et al* 2010)

pathway the proteins can be degraded or recycled back to the plasma membrane. This process and fate decision are the result of an equally elaborate array of proteins and regulators (Bishop, 2003; Frankel and Audhya, 2018; Kelly and Owen, 2011). A proportion of the internalized protein is recycled in what may be a constitutive manner, however if triggered by signalling events this proportion can be increased by redirecting the proportion which would be degraded back through this recycling pathway (Goldenring, 2015; Hsu and Prekeris, 2010; Poythress et al., 2013).

The Arf (ADP-ribosylation factor) are a family of GTPase proteins that are intimately involved in all stages of endocytosis and sorting of intracellular vesicles. The three classes of Arfs are distinguished by spatial separation of localization the specific sorting pathway with which they are involved (Donaldson and Honda, 2005; Donaldson and Jackson, 2011). However, all share a commonality of mechanism in that they recruit coat proteins to facilitate the trafficking of vesicles between intracellular compartments (D'Souza-Schorey and Chavrier, 2006). E-cad has been documented to undergo Arf1 mediated recycling in the Golgi and to require Arf6 for internalization from the plasma membrane in mammalian cells

(Xu et al., 2015). However, the role and function of these *in vivo* and how evolutionarily conserved between species of these mechanisms is unknown.

To understand the role of E-cad in intracellular signalling and the mediation of its cell surface regulation by endocytosis one must examine the function that the known E-cad binding partners and interactors have, and how this is implicated in the processes previously described.

1.9) Catenin family and signalling

To enable the communication between the extracellular environment and intracellular signalling pathways requires an interaction between E-cad and components which mediate such processes. Unlike tyrosine kinases such as JAK or EGFR, E-cad is not itself auto-active and requires intermediaries to mediate the signalling pathways. This enables E-cad to have a multitude of interactions which enable the repertoire of signalling outputs and potential actions. The family of proteins which has evolved to mediate this process, the Catenins (Latin for link or chain), are a broad group of proteins which bind to the intracellular C-terminus of E-cad and mediate all its intracellular functions (Gul et al., 2017; Hulpiau et al., 2013; Nelson et al., 2013; Shapiro and Weis, 2009). These are divided into three groups: β-catenin which is a component of the WNT signalling pathway, α-catenin which binds to β-catenin and in turn binds to actin filament of the cytoskeleton (Fig 1.1), thus tethering the extracellular adhesion with the internal cytoskeleton, and p120-catenin (p120ctn), which binds to the Juxtamembrane domain of E-cad and regulates its turnover (Davis et al., 2003; Miyashita and Ozawa, 2007; Reynolds, 2007).

The most well characterised member of the catenin family is β-catenin, which in *Drosophila* is named *armadillo* and was known as a component of WNT signalling before the discovery of mammalian β-catenin and its role in E-cad adhesion (Clevers and Nusse, 2012; Kraus et al., 1994; Krishnamurthy and Kurzrock, 2018; MacDonald et al., 2009; Morel and Arias, 2004; Peifer et al., 1994; Peyriéras et al., 1985). The expression of β-catenin is required to enable the initial trafficking of E-cad to the plasma membrane, and the association of β-catenin with E-cad sequesters it at the plasma membrane (Chen et al., 1999; Dupre-Crochet et al., 2007; Nelson and Nusse, 2004; Ramis-Conde et al., 2008; Tian et al., 2011). When uncoupled from E-cad β-catenin acts in the Wnt pathway as a transcription factor which activates various signalling and growth pathways (Clevers and Nusse, 2012). The pathways which regulate the activation and deactivation of β-catenin are perhaps the most

studied of any of the catenin family, principally because this interaction with E-cad and the direct role it has in cancer progression, which has led to it being one of the classical proto-oncogenes (Koesters et al., 1999; Thievessen et al., 2003). The dissociation of β-catenin would naturally remove the ability of E-cad to bind to cortical actin as this is mediated by the α-catenin and β-catenin dimer (Fig 1.1). This uncoupling has been shown to be modulated by various kinase, including Pak, GTPases, including Cdc42, and other proteins involved in the establishment and maintenance of apicobasal polarity (Daugherty and Gottardi, 2007; Fang et al., 2007; He et al., 2008; Wu et al., 2006). What if any interaction β-catenin has with the third catenin family member, p120ctn, is unknown. Presumably there is a degree of interaction as they are in close proximity on the C-terminus of E-cad, and indeed of the other classical cadherins: VE-cad and N-cad, but if some manner of cross-regulation or interaction occurs has not been determined.

The other member of the catenin family, α-catenin, is it could be argued not a *bona fide* member of the catenin family at all but a derivative of the vinculin family, which is primarily involved in the function of focal adhesion and integrin regulation at the basal membrane (Gul et al., 2017; Shapiro and Weis, 2009). The function of α-catenin is to bind filaments of cortical actin which reside immediately below the band of the mature adherens junctions in cells (Niessen and Gottardi, 2008; Troyanovsky, 2012; Yap et al., 2015) (Fig 1.1). In turn, it binds to β-catenin, although the precise nature of this relationship between α-catenin and β-catenin in the context of actin binding has proved somewhat contentious. The debate about the mechanism of α-catenin function was triggered by the fact that *in vitro* recombinant purified α-catenin has exclusive binding to β-catenin or actin (Drees et al., 2005b). More recently, work by several groups has shown the nature of α-catenin interactions *in vivo* is dependent upon tension inducted conformation changes (Desai et al., 2013; Escobar et al., 2015). The view which emerged is that the unfolding of α-catenin occurs for cross-binding or bridging between actin and β-catenin at higher tension (Kim et al., 2015; Yao et al., 2014). Later work further postulated a bimodal function by which α-catenin enables AJ to resist the application of deformation forces up until a threshold after which it yields to the forces (Personal communication R.Sarpal, U.Tepass lab). Theoretically this has the advantage of not allowing the cell to indefinitely resist force, to do so would result in the rupturing of the cell and compromising the integrity of the tissue. This enable the deformation and remodelling of issues in both regimes, with weaker applications of force resulting in resistance and stronger resulting in compliance.

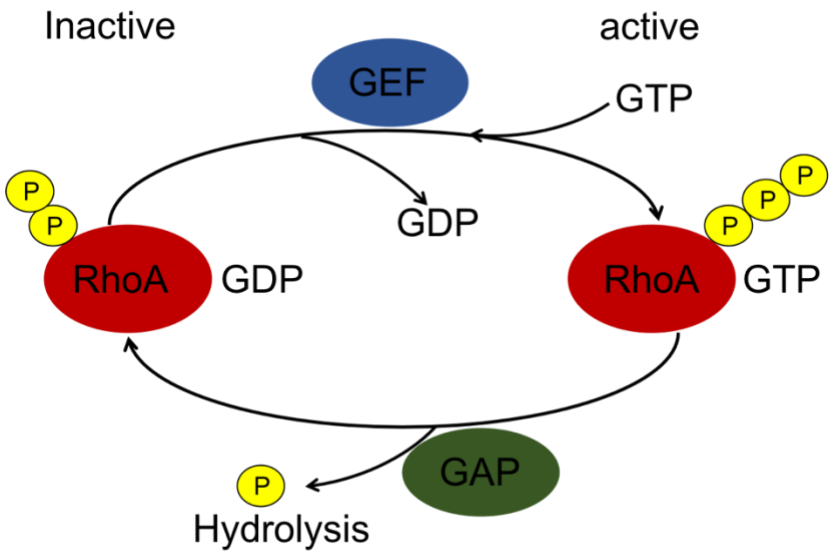

Figure 1.4 The regulation of small GTPases by GEF and GAP proteins. The activity of most GTPases is subject to a molecular switch dependent on the nucleotide Guanosine triphosphate (GTP). In the inactive form the GTPase (RhoA) is bound by a GDP molecule. This can spontaneously dissociate but in most cases requires the action of another enzyme to remove and facilitate the nucleotide switch. This activation switch is performed by Guanine exchange factors (GEF) which enable the dissociation of the GDP and allow GTP to bind to the GTPase. As GTPases have a low functional capacity to hydrolyze the GTP bound to them they require another family of molecules to stimulate the hydrolysis of GTP. These proteins are called GTPase accelerating proteins (GAPs) for their ability to bind GTPases and enhance their innate hydrolytic activity. Thus, the action of GAP proteins on GTPases is to affect the off molecular switch by removing a phosphate group from the GTP resulting in the reaction product GDP and the inactivation of the GTPase.

The third member of the catenin family, p120ctn, is considered primarily as the regulator of cadherin dynamics at the plasma membrane. Though it has been the subject of substantially less research than its more famous cousins the important and central role this protein plays in adherens junctional dynamics is becoming more apparent. This is discussed in detail in the following sections along with the works which lead to the findings presented in this work.

1.10) p120-catenin identification, evolutionary history, and initial characterization

p120ctn was first identified after the other two classical family members, α- and β-, in separate work by another group. It was identified by a screen for Src interacting proteins in chicken (Reynolds et al., 1989). This was rationalized as a screen for interactors of a kinase known to be implicated in multiple cancer cases. The full significance of this protein was not apparent at that time but became so by follow-up work performed by the same group which found that this 120kDa protein was in complex with cell adhesion molecules (Reynolds et al., 1994), in the first instance the authors examined the localization of this protein with E-cad in

the chicken equivalent in histological sections (Daniel and Reynolds, 1995; Reynolds et al., 1994; Shibamoto et al., 1995; Staddon et al., 1995). This observation of co-localization with cell adhesion molecules and the determination that this 120kDa protein contained armadillo domains, similar to those present in β-catenin and other catenin family members, resulted in it being designated: protein of 120kDa of catenin family (p120ctn). Subsequent examination has revealed that it is not the sole protein in mammalian cells but is the archetype of a protein family in its own right (Carnahan et al., 2010). The protein described as p120ctn in mammalian cells (*CTNND1*) is also elaborated by the presence of other members from the related delta catenin group (*CTNND2*) which encompasses, ARVCF, p00071, and the plakophilin group (Carnahan et al., 2010).

Despite this identification and classification as a member of a catenin family, the functional role of this protein remained in question, naturally if it was so consistently found in complex with adhesion molecules it must serve some vital function in relation to cell adhesion (Ohkubo and Ozawa, 1999; Reynolds et al., 1996; Thoreson et al., 2000; Yap et al., 1998). This initial characterization determined that p120ctn expression was required to maintain cadherin molecules at the surface of mammalian cells (Davis et al., 2003; Ireton et al., 2002; Thoreson et al., 2000). Though efforts to explore the mechanism of this would not come until much later, it was supposed to either stabilize or actively prevent the removal of the cadherin molecules from the cell surface. In multiple cancerous conditions p120ctn was observed to be mislocalised or absent (Dillon et al., 1998; Gold et al., 1998; van Hengel and van Roy, 2007; Mo and Reynolds, 1996; Peglion and Etienne-Manneville, 2013; Roy and McCrea, 2005; Skoudy et al., 1996; Syrigos et al., 1998). It was further noted that the expression of E-cad, or the equivalent cell adhesion molecules, was either absent or the protein was retained within the cytoplasm away from the plasma membrane (Gold et al., 1998; Jawhari et al., 1999) with immunostaining indicating that the retained cadherin molecules localized within cellular vesicles resembling the known endosomal compartments (Thoreson et al., 2000). These papers gave rise to the notion that p120ctn was acting either to enable presentation of E-cad at the plasma membrane or was responsible for providing some stability to the protein by preventing internalization.

Interest in p120ctn assumed more prominence with the publication of a range of pathological studies which identified that the mis-expression or mislocalization of p120ctn was involved in many cancer types. Indeed, it was evident that the severity of the abnormal localization of p120ctn was correlated with the severity of the cancer itself, that is to say the

grade and stage of the cancer (for detailed description of both see section 1.6).This was the state of knowledge at the turn of the last century, and further mechanistic evidence has emerged which elucidated these initial observations and lead to the work presented in this thesis. The precise condition of the field and details of the works leading to the state of knowledge prior to, and during the course of, the work undertaken during this project are detailed in the following section.

1.11) Evidence for p120ctn function and knowledge prior to this project

From the initial identification and histological observations of p120ctn localization within cells, in tandem with the observations from histopathological sections of cancerous conditions, it was evident that expression and the correct localization were required to maintain normal cell adhesion and localization of E-cad. A systematic and fundamental biological investigation began to understand how p120ctn functions within cells. Early work in cell culture substantiated the initial observations and findings (Anastasiadis and Reynolds, 2000; Davis et al., 2003; Ireton et al., 2002; Thoreson et al., 2000) that p120ctn is a core component of the adherens junctions and binds to the juxtamembrane domain (JMD) of classical cadherins in a consistent manner, that is to say binding is observed in multiple tissue types and between different classical cadherins and p120ctn (Montonen et al., 2001). Moreover, the uncoupling of p120ctn from this JMD leads to complete internalization of the E-cad from the cell surface (Miyashita and Ozawa, 2007; Thoreson et al., 2000). These works used the observation of multiple intracellular vesicles to infer that the presence of p120ctn either inhibited E-cad endocytosis or was required for some measure or stability at the cell surface. Other works have attempted to identify the mechanism of p120ctn interaction in the context of internalization by ectopically expressing the JMD on an organelle or other membrane protein to mitigate the effect of losing cell adhesion (Gu et al., 2015; Hartsock and Nelson, 2012; Yap et al., 1998). These works showed that the JMD resulted in a high proportion of the protein being internalized. These findings were further supported by more detailed mechanistic insight in to the precise binding of p120ctn to the JMD, which identified specific domains which couple p120ctn to the JMD of E-cad, mutation of which exposed the site and lead to internalization of E-cad (Ishiyama et al., 2010)

Further examination in mammalian cell cultures and murine models indicated that this notion of p120ctn presence being required to keep E-cad at the cell surface was further supported (Hartsock and Nelson, 2012; Shrestha et al., 2017) with evidence that the JMD was also bound by a ubiquitin ligase which target E-cad for internalization. This ubiquitin ligase,

Hakai, is in competition with p120ctn for access to the JMD and thus the balance between the two determines how much E-cad is internalised from the plasma membrane and degraded (Hartsock and Nelson, 2012).

This evidence lead to the formulation of the "Cap model" of p120ctn function, which describes the primary function of p120ctn as an obligate binding partner of E-cad, which competes with Hakai for access to the JMD. The binding of p120ctn thus caps and protect the JMD from ubiquitination preventing the endocytosis of E-cad. The plethora of papers emerging from the Reynolds lab and a few others (van Hengel and van Roy, 2007; Kowalczyk and Reynolds, 2004; Peifer and Yap, 2003) all substantiate the critical role that p120ctn played in preventing endocytosis in mammalian cells; in both cell culture and murine *in vivo*. This lead the discoverer of p120ctn to propose that p120ctn was a master regulator of E-cad stability at the cell membrane (Reynolds, 2007). Later work further elaborated that p120ctn binds to the JMD in a regulated manner, consistent with p120ctn having first being identified as a Src interacting protein (Castaño et al., 2007; Fukumoto et al., 2008; Mariner et al., 2001).

The Cap model provided a logically consistent explanation for the results of the previous work insofar that all evidenced in favour of p120ctn binding and preventing endocytosis, measured using internalization assays. However, this model was first challenged in mammalian cells when it was demonstrated that contrary to this Cap model p120ctn could promote the internalization of VE-cadherin by interacting with Numb (Sato et al., 2011). In this work the authors used a variety of approaches to demonstrate the phosphorylation-specific interaction of Numb with p120ctn could initiate the internalization of VE-cadherin. Again, this was measured by using internalization assays, and no direct measurement of the dynamics of VE-cadherin or other cadherins at the surface was undertaken.

In lower organisms the essential stabilizing nature of p120ctn for the adherens junction was demonstrated to be less important and indeed mutants in several model organisms showed no overt phenotype, certainly non-comparable to the complete loss of adhesion observed in mammalian cells. The *Drosophila*, *C.elegans*, and *Xenopus* models in a series of papers published in the same year evidenced that the p120ctn in non-mammalian organisms was dispensable for viability (Ciesiolka et al., 2004; Myster et al., 2003; Pacquelet et al., 2003; Pettitt et al., 2003). This brings one to an interesting consideration and argument about the nature of the conservation of the p120ctn protein between organism and its evolutionary lineage and divergence. p120ctn in all organisms this is derived from a common ancestor encoded by the *CTNND1* gene (Carnahan et al., 2010; Hatzfeld, 2005). During the

course of mammalian evolution this was duplicated and gave rise to the *CTNND2* and related family members (delta catenin family and the plakophilins). At the same time, the *CTNND1* gene (p120ctn) assumed greater importance for the regulation of cadherins by a concurrent modification in the binding domain of the mammalian E-cad JMD. These LL and DEE domains in the JMD of mammalian E-cad render it more sensitive to ubiquitination. The removal or mutation of these domains is sufficient to obviate the effect of internalization in the absence of p120ctn (Nanes et al., 2012). Therefore, a valid argument would be that the p120ctn which is present in *Drosophila Xenopus* and *C.elegans* more closely resembles the more ancestral form and exhibits the more conserved function of p120ctn, which have been overlooked by the study of mammalian cells, where the protein has acquired additional functions. Moreover, these lower organisms permits the study of p120ctn functions which are impossible to examine in the mammalian system due to the loss of adhesion resulting from the increased sensitivity of mammalian E-cad to the presence of p120ctn.

The advance of the challenge to the Cap model first made in mammalian cells (Sato et al., 2011) was made by the work which immediately preceded, and formed the foundation for, the work undertaken during this doctorate. In this work the authors demonstrate that p120ctn is required to promote the internalization of an E-cad fraction which is in association with Bazooka (Baz or Par-3) at the plasma membrane. This was shown by measuring the dynamic properties of E-cad using Fluorescence Recovery After Photobleaching (FRAP) and pulse chase assays to measure the internalization (Bulgakova and Brown, 2016). In consideration of the authors preceding work identifying two pools (sub-populations) of E-cad at the plasma membrane distinguished by their dynamic properties and association with Baz (Bulgakova et al., 2013), it was a possibility that p120ctn may have a differential effect on the two pools accounting for the experimental findings. However, the work, nor any other work, has shown definitively if p120ctn can inhibit endocytosis in *Drosophila* in a manner comparable to that observed in mammalian cells (Larson et al., 2008). Further the great outstanding question about the mechanism of p120ctn dependent regulation of E-cad remained unknown.

What had been determined was an interaction of p120ctn with some small GTPases. In mammalian cells it has been ascertained that the localization of p120ctn itself determines the nature of the interaction with RhoA, with uncoupled or cytoplasmic p120ctn inhibiting the activity of the pathway (Anastasiadis and Reynolds, 2001; Anastasiadis et al., 2000; Castaño et al., 2007; Chiasson et al., 2009). This characteristic is purported to be involved in the anoikis resistance of tumours cells (Schackmann et al., 2011). At the membrane p120ctn

is reported to interact with Rac1 and enable the migratory phenotype required for the formation of branches dendrites in neuronal cells (Hou et al., 2006). The consistent theme which emerges from these studies is the interaction of p120ctn with small GTPase enzymes which regulate actin (Boguslavsky et al., 2007; Noren et al., 2000; Rajput et al., 2013). The precise identification of the interactor has remained elusive though the notion of an upstream regulatory GEF or GAP , specifically p190RhoGAP, has been posited (Kim et al., 2008; Wildenberg et al., 2006; Zebda et al., 2013). Conceptually this would be consistent with the evolutionary interaction between other armadillo domain proteins and actin GTPase regulators, and is posited to be an evolutionarily ancient mechanism (Hulpiau et al., 2013; Nandadasa et al., 2012; Nelson et al., 2013). In the *Drosophila* system the very interaction with RhoA itself is contested not merely in the nature of the interaction with the signalling pathway. One group identified an interaction with RhoA directly in S2 cells (Magie et al., 2002). A later publication challenged these findings and found no interaction between p120ctn and RhoA (Fox et al., 2005). Different tissues and techniques were used in these two studies, so no reconciliation of the conflicting data had yet been undertaken. However, in light of other data a more satisfactory explanation which would account for both findings would be that p120ctn has a weak transient interaction with some component of the RhoA signalling pathway (See Figure 1.4 for details of activity regulation). This has been substantiated by studies measuring the binding efficiency of p120ctn with E-cad itself (Ishiyama et al., 2010) and using immunoprecipitation with other components using chemical crosslinking or other detergents (Lee et al., 2017). How this directly relates to the primary function of p120ctn in regulating the turnover of E-cad is another matter which no group had attempted to address.

Therefore, at the commencement of this project the state of knowledge could be summarized thus: p120ctn is a regulator of E-cad at the plasma membrane, it modulates this by endocytosis using an unknown mechanism and potentially interacts with some GTPases enzymes, but the nature and mechanism of this is unknown.

1.12) Hypothesis and aims of the work

Hypothesis

p120ctn regulates the endocytosis of E-cad by recruiting and activating Rho signalling and other mediators of the endocytic machinery

Aims

I) Identify the protein interactors of p120ctn which mediate E-cadherin endocytosis by using a genetic screen of proposed candidates, identified from review of the existing literature

II) Identify the molecular mechanism of the interaction of these proteins with p120ctn, and how this mediates the endocytosis of E-cadherin

III) Determine the reason for the differential action of p120ctn on the two identified subpopulations of E-cadherin

Chapter 2: Materials and Methods

2.1) Materials

All chemicals were obtained in analytical grade quality from the following companies: Sigma -Aldrich, Bio-Rad, Invitrogen, Thermo. All solutions were made up with MilliQ water and autoclaved prior to use. All enzymes required for molecular work were purchased from New England Biosciences (NEB).

A table of all chemical reagents, solutions, and antibodies used in this research is included below:

Name	Chemical composition	Source
Acetone		Fisher Chemical
Ampicillin		Sigma
AP buffer		NEB
Apple juice agar		Tesco/Fisher Chemical
Bead wash buffer	50mM Tris-Hcl pH 8.0, 150mM NaCl, 1mM MgCl	
Bleach		Arco
BSA		NEB
Canada Balsam		Sigma
Cross-linking buffer	50mM Tris-Hcl pH 8.0, 150mM NaCl, 1mM MgCl 20mM DSP/DMP	
Crosslinking solution	50mM Tris-Hcl pH 8.0, 150mM NaCl, 1mM MgCl 40mM DSP/DMP	
Development solution		GC heathcare
DMP		Sigma
DNA extraction Buffer	10mM Tris-Hcl pH 8.2, 25mM NaCl, 1mM EDTA, 0.2% Triton 100X, 200mM Proteinase K	
DNA Loading buffer		NEB
DSP		Sigma
EDTA		Sigma
Embryo Wash buffer	120mM NaCl, 0.2% Triton 100X	
Ethanol		Fisher Chemical
Fly media		Fly facility, BMS, UOS
Formaldehyde		Sigma
Glycerol		Fisher Chemical
Glycine		Sigma

Halocarbon oil 27		Fisher Chemical
Heptane		Fisher Chemical
Immersion oil (Airyscan)		Zeiss
Immersion oil (olympus)		Olympus
Isopropanol		Fisher Chemical
LB		Sigma
LB agar		Invitrogen
Ligation Buffer		NEB
Loading Buffer		NEB
Lysis buffer	50mM Tris-Hcl pH 8.0, 150mM NaCl, 0.5% Triton, 1mM MgCl	
Methanol		Fisher
MgCl2		Sigma
Milk powder		Marvel Milk
MilliQ water		UOS
NaCL		Sigma
PBS		Sigma
PBST (Triton)	1x PBS with 0.05% triton 100x	
PBST (Tween)	1 x PBS with 0.2% Tween20	Applichem
Restriction buffer		NEB
Running Buffer DNA	1x TAE	
Running Buffer PAGE	25mM Tris, 190nM Glycine, 0.1% SDS	
SDS		Sigma
Sepharose beads		GC Heathcare
SOC media		NEB
Staining Solution		
Sybre Safe		Invitrogen
Transfer Buffer	25mM Tris, 190nM Glycine, 20% Methanol	
Tris base		Sigma
Tris-HCl pH 8.0		Sigma
Tris-HCl pH 8.2		Sigma
Vectashield		Vectorlabs
Nail Varnish		Maybelline

Antibodies

Primary

Name	Epitope	host species	mono/poly	Conc IF	Con WB
DECAD2	E-cadherin	Rat	Mono	1:100	1:1000
a-p120ctn	p120ctn	Mouse	Poly		1:1000
b-p120ctn	p120ctn	Mouse	Poly	1:100	
Atub	Alph-Tubulin	Rat	Mono	1:100	1:1000
a-GFP	GFP	Rabbit	Mono	1:100	1:200 (IP)
a-Rab5	Rab5	Rabbit	Poly	1:200	

Secondary

Name	Epitope	host species	Pre-absorbed	Conc IF	Con WB
Anti-rat Cy3	Any rat primery	Goat	Yes	1:300	
Anti-Rat-647	Any rat primery		Yes	1:300	
Anti-Rabbit 647	Any rabbit primery		Yes	1:300	
Anti-Mouse Cy3	Any mouse primery		Yes	1:300	
Anti-Mouse 647	Any mouse primery		Yes	1:300	
Anti-Rat HRP	Any rat primery		No		1:5000
Anti-Mouse HRP	Any mouse primery		No		1:5000
Anti-Rabbit HRP	Any rabbit primery		No		1:5000

2.2) Methods

Drosophila husbandry and histological preparations

All flies were raised on standard medium (Fly facility, BMS, University of Sheffield) and maintained at 25°C or 18°C inside environmentally controlled rooms unless otherwise indicated. Stocks were stored in standard vials containing approximately 10 ml of media provided by Fly facility, BMS, University of Sheffield. Stocks amplified for experiments were maintained in larger bottles. Crosses for embryo collection were performed in adapted 100ml kitchenware measuring pots which were capped by interchangeable pre-prepared and pre-warmed apple juice agar set in standard petri dishes (Fly facility, BMS, University of Sheffield). To sustain crosses and encourage egg deposition on the apple juice surface a small

measure of yeast paste (Allison Flour) was applied to the surface after pre-warming and removal of condensation from post-preparation storage at 4°C. For larval collection a larger cylindrical bottles containing a sufficed quaintly of the standard fly medium was used. When necessary a quantity of dry yeast or water was added to encourage larvae to thrive. For selection and sorting of adults, flies were anesthetized using a CO_2 gas exposure. These were then placed upon a CO_2 emitting pad under a standard dissection microscope and selected manually by means of a small paint brush or pooter instrument. Those adults which were not required or surplus to requirement were culled in a fly morgue (bottle containing 70% IMS solution) followed by disposal and incineration in accordance with regulations pertaining to GM organisms.

Stocks and Genetics

The following fly stocks were used in this study (Bloomington number included where applicable):

Genotype	Source
ubi::E-cad-GFP	
en::Gal4 ubi::E-cad-GFP	
en::Gal4 ubi::E-cad-GFP/CyO, twi::GFP; UAS::CD8-Cherry/TM6, dfd::YFP	
shg::E-cad-Cherry	Bloomington 59014
shg::E-cad-GFP	Bloomington 60584
en::Gal4 shg::E-cad-GFP	
arm::β-catenin-YFP	CPTI-001198
arm::β-catenin-YFP; en::Gal4	
p120ctn[308]	Bloomington 6664
p120ctn[308]/CyO, twi::GFP; UAS::CD8-Cherry/TM6, dfd::YFP	
p120ctn[308] en::Gal4/ CyO, twi::GFP	
p120ctn[308] ubi::E-cad-GFP/ CyO, twi::GFP	
p120ctn[308] shg::E-cad-GFP/ CyO, twi::GFP	
Df(2)M41A8/ CyO, twi::GFP (Δp120ctn)	Bloomington 740
arm::β-catenin-YFP; p120ctn[308]/CyO, twi::GFP	
w[1118]	
w; Dr/ TM3 Sb Ser, twi::Gal4 UAS::GFP	Bloomington 6663
w; Dr/ TM6 Sb Tb, dfd::YFP	
w; Gla, Bc/ CyO	
w; TM3/ TM6B	
en::Gal4	Bloomington 30564
en::Gal4; UAS::CD8-Cherry/TM6, dfd::YFP	
en::Gal4 Zipper-YFP/ CyO, twi::GFP	

en::Gal4/ CyO, twi::GFP; sqh::Rok[K116A]-Venus/ TM3, twi::GFP	
arm::Gal4 x2/ TM3, Sb	Bloomington 1561
act::Gal4/ CyO, twi::GFP	Bloomington 4414
prd::Gal4/ TM3, Sb	Bloomington 1947
prd::Gal4 UAS::CD8-Cherry/ TM3, Sb	
pnr::Gal4	Bloomington 25758
Baz-YFP	CC01941
w; GFP-Rho1	Bloomington 9528
w; UAS::Rho1-V14 (CA)	Bloomington 7330
w; UAS::Rho1-N19 (DN)/ TM6, dfd::YFP	Bloomington 7328
UAS::RhoGEF2-RNAi/ CyO, twi::GFP	VDRC, 110577
Zipper-YFP	CPTI-100036
w; UAS::CD8-Cherry	Bloomington 27391
w; UAS::CD8-Cherry	Bloomington 27392
UAS::ClC-GFP	Bloomington 7107
UAS::ClC-GFP/ TM6	Bloomington 7109
shg::E-cad-Cherry,en::Gal4; UAS::CLC-GFP/TM6, dfd::YFP	
UAS::Arf1-GFP (Arf79F)	T.Harris
UAS::Arf1 RNAi	T.Harris
UAS::p120ctn-GFP	Myster 2003
UAS::p120ctn	
Arf1-GFP	
Arf1-mCherry	
UAS::Arf1 (CA)	Wang 2017
UAS::Arf1 (DN)	Wang 2017
shg::Ecad-GFP, en::Gal4; tubulin::Gal80 (ts)	
en::Gal4 Zipper-YFP/ CyO, twi::GFP; UAS::CD8-mCherry	
en::Gal4; UAS::Arf1-GFP	
en::Gal4; UAS::p120ctn	
Rab11-YFP	
Rab7-YFP	

For all crosses, virgin females were collected twice daily, virginity determined by time interval, pale abdomen and presence of meconium in the intestinal tract. Collected females were kept at 18°C until used, all virgins were used within a week of elcosion. Crosses consisted of >50 virgin females and 15-30 males, depending upon availability. Once established the crosses were transferred to 25°C and collections were commenced after a period of two days to allow acclimatization and mating events to occur. Therefore, collections were undertaken during the optimum laying rate at the peak of mated female egg

deposition. For all the p120ctn null experiments a transdeficiency was used consisting of p120ctn^{308} crossed to a chromosomal deficiency line Δp120ctn (Df(2R)M41A8/ CyO, *twi::*Gal4, *UAS::*GFP), both of which are completely devoid of the p120ctn locus. Thus, the resulting progeny of the desired genotype (p120ctn^{308}/ Δp120) lacked both maternal and zygotic contributions of p120ctn transcripts.

2.2.1) Principles of the GAL4-UAS system

The GAL4/UAS system is a powerful and widely applied genetic tool for the specific expression of a transgenes or RNAi construct in a cell or tissue of interest (Brand, 1993). It is based on binary expression system present in yeast, relying upon the selectivity and specificity of the Upstream Activator Sequence (UAS) to respond only to the presence of the GAL4 transcription factor protein which is not naturally found in *Drosophila* or non-yeast cells. The presence of the GAL4 protein alone has no deleterious effect on the physiological function of the fly and expression of GAL4 alone does not have marked effect on procreation, development or lifespan. The system requires the incorporation of the GAL4 protein downstream of a promotor or enhancer element, therefore the expression of the GAL4 is under the control of a cis-acting genomic element termed a driver.

Thus, the expression of the GAL4 protein is restricted to the cell type or lineage in which the driver is active. The second component of the binary system relies upon a transgene or RNAi sequence being under the control of the exogenous yeast promotor (UAS). These lines can be generated using conventional P-element modifications incorporating any desired sequence. As the GAL4 and UAS stocks are stored separately there is minimal concern about the effects of establishing a stable transgenic expressing stock. For experimental purposes all one requires is to cross the adult of the desired driver GAL4 with the adult of a stock containing the desired transgene or RNAi.

In this study a range of transgenes and RNAi lines were used (see Stocks Table) with several GAL4 drivers. For the most part the data presented utilized the *engrailed*-GAL4 (*en::*GAL4) driver. *engrailed* is a segment polarity protein which is expressed in discreet segment bands (posterior halves of segments) along the long axis of the embryonic epidermis and is required for the specificity of the posterior compartment of the wing disc and adult wing.

2.2.2) Acute induction using GAL80^{ts} system

For the specific temporal induction of a transgene, in this case dominant negative variants of Arf1 or RhoA, under the GAL4/UAS system the thermally sensitive variant of GAL4

inhibitor GAL80 was used. GAL80 is a related yeast protein which, like, GAL4, does not itself have any detrimental or deleterious effect when expressed. For the research undertaken in this project a GAL80 under the expression of the ubiquitous tubulin promotor was used (*tub::*GAL80^{ts}). The GAL80 protein works by inhibiting the binding of the GAL4 transcription factor at the lower and more common experimental temperature of 18°C or 25°C. To inactive the function of GAL80 and thereby allow the GAL4 to induce the expression of the DN transgenes, the embryos were switched to 29°C for four hours before proceeding with fixation. The accelerated development of the embryos by the elevated temperature was accounted for by inducing the four-hour GAL80 suppression 12 hours after egg collection and maintaining apple juice agar plates at 25°C. Thereafter the embryos were fixed in accordance with the standard protocol detailed below.

2.2.3) Collection and fixation of Embryo tissue

Embryos were collected at 25°C for a 3-hour time interval and allowed to develop at 18°C for 21 hours to reach the desired developmental stage, at the end of dorsal closure corresponding to late stage 15. Embryos were dislodged from the apple juice agar surface by applying a small measure of water and brushing surface with paint brush. Embryos were dechorionated by immersing in a 1:1 sodium hypochlorite (bleach, Invitrogen) and water solution for 5 minutes followed by filtration through an in-house made cell filtration net and extensively washing with deionized water prior to fixation. Chemical fixation was performed in scintillation vials with total volume of 6ml of a 1:1 solution of 4% formaldehyde (Sigma) in PBS (Phosphate Buffed Saline) and heptane (Sigma) for 20 minutes on an orbital shaker at room temperature. Embryos were then devitellinized by first removing the lower liquid phase containing the PBS and formaldehyde and adding an equal volume of methanol. In this 1:1 solution of methanol and heptane the embryos were vigorously agitated using a vortex mixer for 20 seconds. The precipitated embryos were transferred to a 1.6 ml centrifugation tube and following three subsequent washes with 1 ml of methanol the fixed embryos were stored at -20°C in methanol until required.

2.2.4) Dissection and fixation of larval wing discs

Larvae progress through three moulting stages before pupation in the *Drosophila* life cycle. These stages are dependent on nutrient signalling and entail a substantial increase in the mass of the larvae. The period between the moulting's are termed instars and are a common feature of insect species. For the first two instar stages the larvae remain buried in the media at the

bottom of the vials or vessels in which they are contained. In the third instar they have obtained a sufficed mass and nutrient store that they are prepared to undergo the next stage of the *Drosophila* life cycle and pupate to undergo the metamorphosis into adults. As such 3rd instar larvae emerge from the media and ascend the walls of the vial, these "wandering" larvae contain all of the material required for morphogenesis and the primordial tissue, termed imaginal discs, which form all of the anatomical feature of the adult *Drosophila*. For the dissection of the wing imaginal discs, which constitutes a single layer epithelium, larvae were staged by only selecting those which had reached the 3rd instar or wandering phase. These larvae were selected from the bottle and vials by either the shaft of a needle or by picking with forceps. These larvae were placed into a watch glass containing 1 ml of PBS, once a sufficient number of larvae were selected the genotype was determined by negatively selecting against fluorescently labelled balancer chromosomes from the parental stocks, under an epifluorescence dissection microscope (Leica). The larvae of correct genotype were placed on a slide with cavity (SLS, slides single cavity 16x0.5mm) into a drop of PBS for dissection. Dissection was performed by placing a pair of forceps in the centre of the larvae and bifurcating along the long axis of the larvae. The posterior of the larvae was discarded, and the cuticle of the anterior half inverted to expose the visceral organs. This inversion was achieved by grasping the head tip with one forceps and angling a single prong of the other forceps along the shaft of the cuticle and grasping when 2-3mm inside of the cuticle. This has the effect of forcing the cuticle between the prongs of the forceps and inversion is by drawing one pair of forceps over the over. Once achieved the viscera were exposed and surplus organs were removed before fixation. The inverted cuticle with wing disc attached we transferred to a fresh watch glass containing 1 ml PBS. Subsequent dissection proceeded in like fashion for a period of 20 minutes, after which all the dissected cuticles in the watch glass were fixed. The cuticles were fixed for 20 minutes by adding the fixation solution (200ul of a 4% formaldehyde solution in PBS) to the watch glass and allowing to stand at room temperature for a period of 20 minutes. After fixation the cuticle were washed three times in 200ul of PBST (PBS with 0.05% triton) for 15 minutes each at room temperature without agitation. Once compete the cuticles were immediately processed either for immunostaining or direct mounting of the wing discs dependent upon the genotype or application required.

2.2.5) Mounting of adult wings

Adult flies to be used for wing dissection were grown from vials which were changed daily to prevent overcrowding of the emerging larvae which can affect the metabolic state and growth

of the adults. For comparative analysis between the wild type and p120ctn null mutant adult wings females were anesthetised and placed in centrifugation tubes. The adults were freeze-killed by placing the centrifugation tubes at -20°C for a minimum of 30 minutes. To prepare histological wings a dehydration series was performed on the intact adults. Following freeze-killing the adults were immersed in 1 ml of 50% ethanol solution for 10 minutes at room temperature without agitation, then further dehydrated by 2 separate 10 minute immersions in a 75% ethanol solution. Final dehydration was performed by 2 addition immersions in 1ml of a 98% ethanol solution for 10 minutes. To remove the ethanol solution the adults were washed one in 100% acetone for 10 minutes followed by overnight incubation in a fresh 100% acetone solution overnight at room temperature. To mount wings the adults were removed individually from the centrifugation tube by forceps and excess acetone removed by delicate dabbing against absorbent tissue paper. To mount wings microscope slide (Thermo) were prepared with a single streak of Canada Balsam (Sigma) along the centre of the slide. Adults were placed atop this to hold in position while wings were removed by using a pair of forceps to detach the wings at the hinge to ensure the majority of the epithelium of the blade was intact. These detached wings were placed in the Canada balsam and the remaining adult body was removed and discarded. Once 7-10 wings had been placed in the Canada balsam a 22X40mm coverslip (Thermo) was placed atop and delicate pressure applied to disperse the Canada Balsam mount media below. The slides were allowed to set for 2 days afterward by leaving slides at room temperature in microscope slide boxes.

2.2.6) Immunostaining of embryos

The methanol storage solution was removed, and the embryos were washed three times in 1 ml of PBST (PBS with 0.05% Triton) with gentle rocking on bench top orbital shaker (Thermo). Blocking of the embryos prior to staining was in 300 µl of a 1% NGS (Normalized Goat Serum) in PBST for 1 hour at room temperature with gentle rocking. For staining the blocking solution was removed and 300 µl of a 1:100 dilution of the primary antibody (rat anti-E-cad, DCAD2, DSHB) was added and the embryos were incubated overnight at 4°C with orbital rotation. Next day, primary antibody solution was removed, and embryos were washed three times with 1 ml of PBST for 15 minutes each at room temperature with gentle rocking. A 300 µl of a 1:300 dilution of the secondary antibody (goat Cy3-conjugated anti-rat-IgG, Invitrogen) in PBST was added and the embryos incubated either overnight at 4°C with orbital rotation, or for 2 hours at room temperature with gentle rocking. Following this the staining solution was removed, and embryos were washed three time with PBST as

above. To mount the embryos, they were incubated with 50-70 µl of Vectashield and allowed to equilibrate for a period of 2 hours at room temperature. Once sedimented at the bottom of the centrifugation tubes, 50-70 µl of the embryo Vectashield mixture was transferred to microscope slides and a 22x40 mm coverslip applied (Superfrost, Thermo). These slides were sealed with nail varnish and stored at 4°C until being imaged. All embryos slides were imaged within a week of being prepared.

2.2.7) Immunostaining of larvae

As wings discs (WD) could not be stored after dissection the immunostaining of the tissue proceeded directly after the fixation and washing detailed in the previous section. Prior to staining the tissue was blocked with 200 µl of blocking solution (PBST+1%BSA) for 30 minutes on the lab bench at room temperature without agitation. Incubation of the WD with 200 µl of the primary antibody solution diluted in PBST (rat anti-E-cad, DCAD2, DSHB, 1:100) was overnight at 4°C in a pre-prepared wet chamber without agitation. The following day the primary antibody solution was removed and the WD washed 3 times with 1 ml of PBST for 15 minutes each at room temperature without agitation. Staining with the secondary antibody was by addition of 200 µl of the secondary antibody (goat Cy3-conjugated anti-rat-IgG, Invitrogen, 1:300) in PBST overnight at 4°C without agitation in a wet chamber. To mount the WD on microscope slides the cuticles were washed 3 times with 1 ml of PBST for 15 minutes each at room temperate without agitation. Following this the cuticle were transferred to a PBS solution in fresh watch glass for further dissection. To detach the WD from the cuticle forceps were used to delicately remove the tissue at the notum tip leaving in many instances ruminants of the trachea and peripodial membrane intact. These detached WD were transferred into a fresh watch glass containing 1 ml of PBS and the cuticle discarded. Once 7-10 WD were prepared they were transferred to a microscope slide (Superfrost, Thermo) using a Gilson pipette with 200 µl tip, which had been pre-soaked in BSA (NEB) to prevent attachment of the WD in the plastic interior of the disposable pipette tips. A total volume of 50 µl of the PBS containing the WD was transferred. To correctly position and orientate the WD with dorsal pouch facing upwards on slide, forceps were used to manipulate the WD in the PBS solution and pipette to incrementally remove the liquid to prevent displacement of positioned WD by the force of surface tension disruption while positioning other WDs. Once all WD had been positioned on the microscope slide the remain PBS was removed with a pipette, but some residual liquid was allowed to remain to prevent desiccation of tissue. To prepare slides 7 µl of Vectashield

mounting medium was added to the centre of the WD clusters on the microscope slide and a 22x22 mm coverslip applied to the area. Once sealed with nail varnish the slides were stored at 4°C and were imaged within a week of preparation.

2.2.8) Embryo mounting for live imaging and FRAP

Embryos were collected for a shorter 1.5-hour period at 25°C and allowed to develop to late stage 14 by placing the apple juice collection plates at 18°C for 22.5 hours after collection. The embryos were dechorionated as previously described and washed extensively with deionized water. Once in the collection nets used for washing the embryos were transferred to apple juice agar segments which had been prepared on a microscope slide, by using a paint brush. Those embryos of the correct genotype and stage were determined by examination under a florescent dissection microscope (Leica) and were manually picked using the shaft of a needle to a fresh segment of apple juice agar adjacent to the first. The embryos were positioned on their lateral side and orientated relative to the anterior-posterior axis of one another into a column consisting of 6-10 embryos. The microscope slide onto which the embryos were to be transferred was prepared by affixing two 22x22 mm coverslips at either end on the same side and placing a strip of scotch tape orthogonal to the long axis of the slide between the two cover slips. The prepared embryos on the apple juice agar were transferred to this slide by inverting the imaging slide and delicately touching the surface to the agar segment containing the embryos allowing contact with the scotch tape without exerting too great a force. Once transfer was confirmed by visual inspection, the embryos were embedded with 50 µl of Halocarbon oil 27 (Sigma) and left to aerate for 10 minutes at room temperature. Before imaging the embryos were covered using a 22x40 mm coverslip, and the short ends sealed and fixed in position by using nail varnish- Once it dried, the embryos were taken immediately for imaging.

Molecular Techniques

2.2.9) Extraction of genomic DNA

To perform screening or identify recombinant lines the genomic DNA of adult flies was extracted. Representative adults of the stock to be tested were selected while anesthetised under a dissection microscope. Males were selected in the instances of crosses, as any unlaid but fertilized eggs in the female would have confounded subsequent analysis because the genotype of the progeny differed from the parental. These adults were placed individually in

1.6 ml centrifugation tube and freeze killed by placing at -20°C for a minimum of 30 minutes. To each centrifugation tube 50 µl of the extraction buffer was added and the adults were ground by compaction against side of tube with pipette tip. To allow complete lysis of cells and release of DNA the centrifugation tubes were incubated for 30 minutes at 37°C in a water bath. To heat inactivate the Proteinase K the centrifugation tubes were incubated for 10 minutes at 95°C in a heating block. To separate the extracted DNA from the rest of the material the centrifugation tubes were cooled on ice for 5 minutes then centrifuged at 5000 rpm for 5 minutes and the supernatant transferred to fresh centrifugation tubes to be stored at -20°C until required.

2.2.10) Polymerase Chain Reaction (PCR) of genomic and plasmid DNA

PCR was used in this research to: amplify regions of interest from the genome, generate the homology arms for the CRISPR/Cas9 mediated genetic modifications, screen recombinants and progeny from injections, and to amplify regions from plasmid DNA. The precise composition and conditions of the reaction depended upon the application and the polymerise enzyme used.

For routine PCR used in the screening of CRISPR stocks and recombinants a standard Taq polymerase reaction was used (total volume 25ul):

Component	Vol (ul)	Conc
10xStandard Taq buffer (NEB)	2	1X
dNTPS (Roche/NEB)	0.5	10um
Forward Primer	0.5	10um
Reverse Primer	0.5	10um
Template DNA	1	variable
Taq polymerase (NEB)	0.5	
MilliQ H2O	15	

The programme run on the thermocycler in the case of Taq was as follows:

Step	Temp C	Time	Purpose
1	95	30sec	Initial denaturation
2	95	30 sec	denaturation

3	50-65	30sec	annealing
4	68	1min/Kbp	extension
5	68	5 min	final extension

Reaction cycled between steps 2 and 4 for 30-35 cycles to adjust yield of DNA amplicon product.

For homology arm and related amplifications in which sequence fidelity was paramount the Phusion (NEB) proof-reading polymerase was used (total volume of 50ul):

Component	Vol (ul)	Conc
5xHF buffer (NEB)	10	1X
dNTPS (Roche/NEB)	1	10um
Forward Primer	2.5	10um
Reverse Primer	2.5	10um
Template DNA	2	variable
Phusion Polymerase (NEB)	0.5	
MilliQ H2O	31.5	

The programme run on the thermocycler for Phusion was as follows:

Step	Temp C	Time
1	98	30sec
2	98	10 sec
3	50-65	30 sec
4	72	30sec/Kbp
5	72	5 min

2.2.11) TOPO cloning of PCR product

The homology arms (HA) for the CRISPR/Cas9 mediated modifications of Arf1 were cloned into TOPO vector (Invitrogen) after PCR amplification. After the completion of the Phusion amplification reaction the PCR product underwent a further reaction of A-tailing to add an adenosine residues to the terminus of the PCR product, enabling the TA cloning reaction, which is the basis of TOPO vector cloning. The A-tailing reaction proceeded immediately after the end of the Phusion amplification of the HA regions from the genomic DNA. Once the initial PCR was complete the reaction was supplemented with 1 µl of Taq polymerase and

incubated at 72°C for 20 minutes. This product was used immediately for a TOPO reaction (Invitrogen). Following a 5-minute incubation at room temperature on the bench the reaction product was transformed into competent cell in accordance with the procedure detailed elsewhere in this chapter.

2.2.12) Restriction digestion of plasmid DNA

To excise fragments of DNA from plasmid for the sub-cloning of the homology arms for CRISPR and the sub-cloning of the p120ctn cDNA standard restriction digestion was used. The sequences were fist input to specialist software (EnzymeX, https://nucleobytes.com/enzymex/index.html) and the restriction sites were mapped. This enabled a design of the entire procedure, including consideration for subsequent applications. Digestion of the DNA was performed in a total volume of 20 µl with approximately 20 units of enzyme per 1 µg of DNA. For both single and double digestions the total volume of enzyme did not exceed 10% of the reaction volume to prevent star activity. All restriction digestion enzymes were provided by NEB, digestion was performed at 37°C for one hour before heat inactivation at 65-90°C (depending upon the enzyme) for 5 minutes. The product was then immediately used for subsequent applications.

2.2.13) Dephosphorylation of digested plasmids

Restriction-digested vectors were dephosphorylated to prevent reannealing of un augmented vector. After digestion 20% of the reaction volume was removed and the remaining volume supplemented with Alkaline Phosphatase buffer and Antarctic phosphatase (NEB). Reaction proceeded at 37°C for 30 minutes followed by heat inactivation at 80°C for 10 minutes

2.2.14) Sub-cloning and ligation of restriction digested DNA inserts and plasmid vectors

Digested DNA from plasmid or PCR was sub-cloned into recipient plasmid vectors using standard sticky-end ligation. A total reaction volume of 20 µl was used and the reaction calculated to contain 50 ng of the vector with a 3:1 molar excess of insert. Standard T4 DNA ligase was used (NEB) in a reaction which was left overnight at room temperature.

2.2.15) Transformation of competent cells

Bacterial cells (DH5a, Invitrogen) were removed from -80°C storage and thawed on ice for a minimum of 5 minutes before use. 2-3 µl of ligation reaction product was added and the tubes mixed by several flicks with the index finger. Mixture was incubated on ice for 30

minutes. Heat shock of cells was performed in a water bath set to 42°C for 45 seconds before returning to ice. After 1 minute of incubation on ice 200 µl of SOC media (Invitrogen) was added to each tube, and the tubes incubated at 37°C with orbital shacking at 250 RPM for 1 hour. After this the transformed cell cultures were plated onto LB agar plates which had been pre-prepared to contain standard concentration of ampicillin or kanamycin (Addgene). To plate cells, 100 µl was dispensed in the centre of the plate and a sterile spreader was used to ensure even coverage over the surface of the agar. Plates were then incubated overnight at 37°C without shaking.

2.2.16) Culturing bacterial cell monocultures

After overnight incubation of plated transformed cells individual colonies were picked using a sterile 10 µl pipette tip and placed in test tubes containing 5 ml of liquid LB with ampicillin or kanamycin. These tubes were incubated either overnight or for a minimum of 14 hours at 37°C with orbital shaking at 250 RPM. After this time the cultures were either processed or stored at 4°C for a maximum of a week. If longer storage was required the cultures were stored at -80°C in a 50% glycerol solution, prepared by flash freezing with dry ice.

2.2.17) Extraction and purification of plasmid DNA by miniprep

The amplified monocultures in the liquid LB were centrifuged at 9000 RPM for 3 minutes to precipitate bacterial cells from media. Plasmid DNA was extracted and purified by using the standard protocol in a miniprep kit (Qiagen). The only variation to this protocol was in the final elution, MilliQ water rather than the included elution buffer was used at a volume of 30 µl. The concentration of the DNA was measured using Nanodrop (Thermo) and the eluted plasmids stored indefinitely at -20°C.

2.2.18) Agarose gel electrophoresis of DNA

DNA samples were separated for visualisation using standard protocol for agarose gel electrophoresis. For most applications a 1% agarose (Invitrogen) in TAE buffer was prepared, to which a 1:10,000 dilution of the Sybr Safe View DNA dye was added (Invitrogen) before casing the gel in the cassette. DNA samples and standard 10 Kb ladder (NEB) were prepared containing a 1:6 dilution of loading dye (NEB) with variable volumes added to gels dependent upon the size of the gel used and the dimensions of the wells. Electrophoresis was performed by running a 100V current with constant amplitude for 40-60 minutes.

2.2.19) Imaging of DNA agarose gels

To visualize the DNA embedded within the agarose gels and determine size, the gels were imaged under expose to UV radiation using standard imaging apparatus (Bio-Rad) variable exposure time and parameters were used, determined automatically by the instrument, to adjust ad hoc for the most intense bands visible. The images were stored and printed. Determination of the size and number of bands present in each sample lane informed subsequent experiments.

2.2.20) DNA extraction and purification from agarose gels

DNA embedded within agarose gels after electrophoresis were excised for the gel by using a sterile scalpel or razor blade under exposure to safe view illumination of the gel (Invitrogen). Once the agarose fragment was excised and transferred to an 1.6 ml centrifugation tube, extraction of the DNA was performed using a standard column extraction protocol (Qiagen). Only variation to this protocol was to elute with MilliQ water in lieu of the included elution buffer. Once extracted the DNA concentration was determined using Nanodrop spectrophotometry (Thremo) and the DNA was either used immediately for ligation or stored for an indefinite period at -20°C.

2.2.21) Sequencing of DNA samples

All samples for applications in which sequence fidelity was paramount were submitted for sequencing to the in-house facility (Core Genomic Facility, University of Sheffield) either using primers available from the facility or submitting bespoke primers.

Genetic engineering by CRISPR/Cas9 and P-element insertion

2.2.22) Principles of CRISPR

To perform genetic modification and tag the endogenous Arf1 with GFP, the newly emerging method of CRISPR/Cas9 mediated homologous recombination was used. This relied upon the selection of gRNA targeting sites and design of the exogenous repair template incorporating genomic regions flanking the insertion site, termed Homology Arms (HA).

2.2.23) Selection of GFP insertion site in genome

Selection was based upon know function of Arf1 and examining the functional domains using available software (https://www.uniprot.org/). This enabled the insertion site to be selected to result in minimal theoretical disruption to the functioning of Arf1. The C-terminus of Arf1 was selected as the N-terminus contained a myristoylation domain. No amino acids were lost as the stop codon was replaced with the start of the GFP linker sequence consisting of a chain of serine residues.

2.2.24) Design of Homology arms

The flanking HA of the Arf1 GFP were selected to be in the range 500-1500bp, this allowed a satisfactory number of gRNA targets to be included and the primers to be selected to provide the greatest specificity for the intended region. Primer were designed using Primer3 software (http://primer3.ut.ee/) and selected for: limited off-targets, minimal dimerization, similar melting temperature, and comparable GC content.

2.2.25) Selection of gRNA targeting sites

gRNA guides for the Cas9 enzyme were identified within the HA by examination using available software (http://www.e-crisp.org/E-CRISP/) selection was based upon proximity to the insertion site and lack of off-targets predicted to include the PAM region. Two gRNA targets were selected, one in each HA.

2.2.26) Amplification of Homology arms from genomic DNA and TOPO cloning

Wild-type (WT) control adult flies were selected to obtain the HA regions which flank the insertion site. Phusion polymerase PCR was used to amplify the regions. The product was run on an agarose gel to determine the size of the product and specificity of the reaction. These bands were extracted and purified (Qiagen). These products were cloned into TOPO vector using TA cloning method (Invitrogen) and first screened and sequenced (Core Genomic Facility, University of Sheffield) before being used for subsequent sub-cloning.

2.2.27) Subcloning of HA into GFP vector

HA regions were transferred from TOPO vector into pBSSK-mGFP6 vector using double restriction digestion with either *Not*1 and *Hind*III or *Xho*I and *Kpn*I (NEB). Followed by ligation using T4 DNA ligase.

2.2.28) PCR of gRNA with pCFD5 plasmid

Primers were designed to incorporate the sequences for the designated gRNA targeting site in accordance with the pCFD5 protocol for tandem gRNA targeting (Addgene). These primers were used in a Phusion PCR with the pCFD5 vector plasmid as a template to amplify the overlapping region and generate the insert containing the genome specific gRNA sequences. The reaction product was run on an agarose gel to determine size and be extracted.

2.2.29) Gibson Assembly of gRNA and pCFD5 plasmid

To incorporate the insert, the pCFD5 vector was digested with *Bam*HI and the gel-extracted vector added at a 3:1 excess molar ration. A 2X Gibson Assembly master mix solution was added in equal volume (NEB) and the reaction incubated for 1 hour at 50°C before proceeding directly to transformation of the product into bacterial cells.

2.2.30) Site directed mutagenesis of Homology arms

The Q5 site-directed mutagenesis kit (NEB) was used to mutate a single base in the PAM region for the gRNA target site in each homology arm. Reaction proceeded according to standard protocol and reaction product was transformed into bacterial competent cells.

2.2.31) Preparation of samples and injection

Prior to submitting the samples for injection both the donor plasmid and the gRNA plasmid were sequences (Core Genomic Facility, University of Sheffield). Separate Miniprep purified samples of the plasmids were submitted for injection into the *nos::*Cas9 transgenic line (Bloomington 54591) to GenetiVision (http://www.genetivision.com/), with the stipulation that a midiprep was undertaken to provide a supply at the company should the injection procedure or modification fail.

2.2.32) Screening of injected F0 founders and F1 progeny

Returned injected larvae were allowed to develop and separated to prevent mating between the founders. The F0 were crossed individually with 3-4 balancer flies of the complementary sex. After fertility had been determined the founders were sacrificed for PCR screening. This PCR was a two-stage selection process, first determination of GFP incorporation was undertaken by using internal GFP primers, second a determination of correct genomic locus incorporation was undertaken by using either the forward or reverse GFP primer with a locus specific primer which was outside of the range of the homology arms. Once confirmed by

PCR the localization of the Arf1-GFP was examined using confocal microscopy of fixed Embryos.

2.2.33) Transgenesis with P-element insertion for UAS::p120ctn, overexpression construct.

The p120ctn full length cDNA was obtained from Berkeley Drosophila Genome Project (BDGS), supplied in a pBSSK vector. This was sub-cloned into a (pUAS-k10.attB) plasmid (Addgene) using standard restriction digestion with *Not*I and *Bam*HI (NEB) followed by ligation with T4 DNA ligase (NEB) and transformation into DH5a competent *E.coli* cells (Thermo). Prior to injection plasmids were test digested and sequenced (Core Genomic Facility, University of Sheffield). Plasmids were prepared for injection using standard miniprep extraction (Qiagen) and submitted for injection (Microinjection service, Department of Genetics, University of Cambridge) into the attP-86Fb stock (Bloomington stock 24749). Successful incorporation of the transgene was determined by screening for (w^+) in the F1 progeny.

Proteomics and Biochemistry

2.2.34) Protein extraction from embryos

Protein extraction from embryos was constrained to crosses or genotypes in which all of the resulting progeny would be isogenic, therefore circumventing the necessity of manual section or reducing the prospective yield of the extract. Further most applications used a collection which encompassed the full range of embryonic stages. This was done to enhance the yield of protein from each extraction. Embryos were collected overnight at 25°C (5pm to 9am) and allowed to develop at 18°C for a period of 6 hours, this was to allow younger embryos to develop into later stages. At this point the embryos were dechorionated as previously described (see section 2.2.3) after this the embryos were washed with embryo washing buffer and transferred to a 1.6 ml centrifugation tube containing 1ml of washing buffer. To dislodge embryos from the cell sieve membrane used during dechorionation, they were delicately agitated with the membrane being held at the side and immersed and removed from the wash buffer in the centrifugation tube. After all the embryos had been placed in the centrifugation tubes and allowed to sediment at the bottom the liquid was removed. 200 µl of the embryo lysis buffer containing the protease inhibitors was added. Lysis of the embryos was by application of a plastic homogenizer and the alteration of plunger and grinding actions to

disrupt the cell membranes. Once lysed the samples where kept on ice whenever possible. Following lysis, the samples were centrifuged at 5000 rpm for 5 minutes. The supernatant was removed and placed in fresh centrifugation tubes on ice. During this supernatant removal the volume extracted was measured by using standardized pipetting volumes, usually amounting to 200 µl. To the supernatant in the fresh centrifugation tube, an equal volume of 2x SDS loading buffer with 200mM DTT was added. The samples were mixed and boiled at 98°C for 10 minutes. Following this the samples were returned to ice for 5 minutes, centrifuged to precipitate any condensation and then stored at -20°C until required for Western blot, samples where used within a period of a week following lysis and protein extraction.

2.2.35) Lysis of proteins form embryos for crosslinking (detergent free)

To perform the chemical crossing-linking of proteins in the embryos the tissue was first disrupted in a detergent-free buffer and then a solution containing the crosslinking chemical was added during cellular lysis. Embryos were dechorionated and washed as previously described (see previous section). Following this they were transferred to centrifugation tubes using wash buffer, as the outer vitelline membrane of the embryos is hydrophobic this buffer contained a low concentration of detergent, this enabled the embryos to be transferred into solution. To remove this before lysis the embryos were washed three times with 1 ml of crosslinking buffer. After removing final wash solution 200 µl of the crosslinking buffer was added and the tissue disrupted by homogenization of the samples.

2.2.36) Crosslinking with DMP or DSP before Immunoprecipitation

To the samples described in the section above an equal volume of the 2x crosslinking solution (200 µl, crosslinking buffer containing either DSP or DMP) was added, and the solution incubated on a roller at room temperature for 30 minutes to allow the crosslinking reaction to occur. To quench the reaction and prevent aberrant cross-linking 20 µl of Tris-HCl (pH 8.0) was added and the samples further incubated for a period of 15 minutes on the roller at room temperature. Following this the samples were centrifuged for 5 minutes at 5000rpm and the supernatant transferred to a fresh centrifugation tube on ice, either for storage at -20°C or further use in Western blot or Immunoprecipitation.

2.2.37) Immunoprecipitation (IP) of proteins from embryo lysate

Following lysis of proteins from the embryos, both with and without crosslinking, the supernatant of the protein extract in the fresh centrifugation tubes on ice (see previous sections). A 10 µl aliquot of this supernatant was removed and stored in a separate centrifugation tube at -20°C for comparative analysis after the IP to ascertain the efficiency of the pull-down. To the extracted supernatant a volume of Glycerol was added to adjust the volume to (10%v/v) and Triton X-100 detergent to a concentration of. After thoroughly mixing the solution, 2 µl of anti-GFP (or other antibody against protein of interest) was added and the sample incubated for a period of 2 hours at 4°C with gentle agitation. During this time the sepharose beads were prepared (GE Healthcare) by washing the beads with 1 ml of lysis buffer, centrifuging at 10,000 rpm for 20 sec and removing the supernatant, taking care not to disturb the beads. The final solution (50% slurry) consisted of the volume of the beads with equal volume of lysis buffer, altogether 50 µl for each protein sample to be precipitated. After the two-hour incubation of the protein extracts with the antibody, 50 µl of the bead solution was added an incubated overnight at 4°C with gentle agitation. The following day, while maintaining all solutions and reagents at 4°C, the samples were centrifuged for 20 sec at 10,000 rpm and the supernatant transferred to separate centrifugation tubes. These provided an additional control to determine the degree of pull-down in subsequent analysis. Following this the beads were washed further three times by the addition of 1 ml of lysis buffer (pre-cooled to 4°C), inverting the tubes and then centrifuging for 20 sec at 10,000 rpm and discarding the supernatant without disturbing the beads. After this the samples were either prepared for Western blot or mass spectral analysis. In the former case the samples, including the aliquot of the lysate and post-IP supernatant were prepared by adding equal volume of 2x SDS loading dye with (200mM DTT). These were boiled for 10 minutes at 98°C and then transferred to ice before being centrifuged at 5000 rpm for 5 minutes. The supernatant, which now contained the denatured proteins dissociated from the beads, was removed and transferred to a fresh centrifugation tube. All the samples were then stored at -20°C until required for Western blot. All samples were used within the period of a week after preparation.

2.2.38) Western Blotting I: Electrophoresis

To separate protein samples by mass, standard electrophoresis using SDS-PAGE was performed using pre-cast mini-protean gels with a 4%-15% gradient filtering (Biorad). These gels were placed in an upright electrophoresis tank using standard insert cassettes to hold 1-2

gels with the tanks holding a maximum of 4 gels if required (Biorad) and the volume of running buffer indicated on the instrument was added. Combs were removed manually with care and the integrity of the well walls examined by optical diffraction of ambient light prior to loading protein samples. The protein samples previous prepared (See protocol above) were removed from -20C and placed on ice. For each gel a standard protein ladder was added to the first well of each respective replicate on the gel (Thermo Fisher). For the protein samples a standard volume was added to the wells dependent upon the application and concentration. For lysates and post-IP supernatants, 2ul of the protein sample was added to the wells, for Pull-down precipitates the entire volume available in the wells (15ul) was added. Once loaded the running buffer was topped-up to the maximum level of the insert cassette. The accompanying power supply attachment and power pock was attached (Bio-Rad) and the samples first run for 10 minutes at 75Voltes. After this time the voltage was increased to 150V and the samples run from a period of 30-40 minutes, until the leading dye front in the samples was within an inch of the bottom of the gel.

2.2.39) Western Blotting II: Transfer to membrane

During the electrophoresis of the protein samples the transfer equipment was prepared. preparation required the cooling of the transfer buffer to 4C and the incubation of the PVDF membrane with methanol (using base of old pipette box as vessel). A tray containing ice was prepared with the transfer tank (alternative was using 4C room when space permitted). Once electrophoresis was complete the gels were removed from the cassette and the plastic container prised open using standard equipment (Bio-Rad). Residual running buffer was removed by rinsing with DI water. A standard wet transfer protocol was applied: a transfer cassette (sandwich) was prepared containing sponges and watchman paper. These were bathed in transfer buffer before the gel was placed within the cassette atop a sponge and Whatman paper on one side. To this the PVDF membrane, removed from methanol and rinsed once in transfer buffer, was applied. The transfer cassette was completed by adding a layer of Whatman paper and a sponge to this completing the stack and closing the plastic transfer inset cassette before placing in transfer tank. Care was taken to ensure any air bubbles were displaced during the final assembly of the transfer cassette. Transfer buffer was added to the top of the tank, to ensure transfer at low temperature an ice pack was added to the transfer tank when performed in the lab with the ice tray. Transfer was performed at 100V for a period of 90 minutes, with a brief pause half-way for the exchange of the ice pack. Once

complete the success of transfer was ascertained by the visible bands of the protein ladder on the PVDF membrane.

2.2.40) Western Blotting III: Immunoblotting

After transfer the membranes were divided into each replicate or experimental group, as required, using a sterile razor and placing the membrane in a 50ml falcon tube. To remove transfer buffer, the membranes were washed in PBST (PBS+ 0.2% Tween20) three times, first a quick wash, the latter two for 15 minutes at room temperature on the tube roller. For each sample a blocking solution of was prepared; PBST with 5% milk powder (Marvel milk). To block the membranes before immunoblotting the membranes were incubated with 5ml of the blocking solution for 30 minutes at room temperature on the roller. Staining solution was PBST with 5% milk powered to which the appropriate primary antibody was added at a concentration of 1:500-1:2000, according to the antibody used (E-cad and GFP used at 1:1000). After blocking the membrane, the solution was removed an 5ml of the primary antibody staining solution was added. The membranes were incubated with the primary antibody solution overnight at 4C on a roller. The following day the primary antibody solution was removed and the membranes washed three times with PBST (PBS+ 0.2% Tween20) at room temperature on the tube roller in the lab. Secondary antibody soluton for each sample was 5ml of PBST with 5% milk powder to which was added a HRP conjugated secondary against the host species of the primary at a 1:5000 concentration (Darko). Membranes were incubated with secondaries for a period of 2 hours at room temperature on a roller. After which time the membranes were washed three times with PBST.

2.2.41) Imaging of WB membranes

Following washing of the PVDF membranes with PBST the immunoblotting was detected using standard colorimetric development. The final wash buffer was removed from the membranes and the excess liquid removed by grasping the edge with forceps and placing next to absorbent tissue paper. The membranes were placed protein side up on sections of clingfilm, 1ml of the developer solution, Amersham ECL Prime (GE healthcare), was added to cover the surface of the membrane. This reaction was allowed to proceed for 1 minute before the solution was removed by upturning the membrane using forceps and placing edge on absorbent tissue paper. The membrane was then placed with the protein-side down on fresh clingfilm which had been starched flat upon the bench. This was wrapped to prevent dehydration of the membrane and taken for immediate imaging. Gels were imaged using the

Gel Doc XR machine (Bio Rad) with standard settings, exposure time varied and was optimized for each protein detected by taking range of exposures which ranged from 10 sec to 15 minutes. Once imaging was complete the membranes were either disposed or washed and stored for future re-probing if required.

Microscopy

2.2.42) Fixed embryo data acquisition

All experiments except for laser ablation were performed using an up-right Olympus FV1000 confocal microscope with a 60x/1.40 NA oil immersion objective. All measurements were made on dorsolateral epidermal cells of embryos, which were near or just after completion of dorsal closure, corresponding to the end of Stage 15 of embryogenesis. For fixed samples 16-bit images were taken at a magnification of 0.051µm/pixel (1024x1024 pixel XY-image) with a pixel dwell of 4µm/pixel. For each embryo, a Z-axis sectional stack through the plane of the AJs was taken, which consisted of six sections with a 0.38 µm intersectional spacing. The images were saved in the Olympus binary image format for further processing.

2.2.43) Live embryo data acquisition and FRAP

For E-cad FRAP (adapted from Bulgakova et al., 2013) 16-bit images were taken at a magnification of 0.093 µm/pixel (320x320 pixel XY-image). In each embryo, several circular regions of 1 µm radius were photobleached at either DV or AP junctions resulting in one bleach event per cell. Photobleaching was performed with 8 scans at 2 µs/pixel at 50-70% 488 nm laser power, resulting in the reduction of E-cad-GFP signal by 60–80%. A stack of 6 z-sections spaced by 0.38 µm was imaged just before photobleaching, and immediately after photobleaching, and then at 20 s intervals, for a total of 15 minutes.

For CLC-GFP FRAP, 16-bit images were taken at a magnification of 0.051µm/pixel (256x256 pixel XY-image). In each embryo a single plane was selected in centre of the AJ band using Shg-Cherry for positioning. An area encompassing a transverse region orthogonal to the axis of the engrailed expressing cells was selected (140x60 pixels) was photobleached with 1 scan at 2 µm/pixel using 100% 488nm laser power resulting in reduction of CLC-GFP signal by 70-80%. Images were taken using continuous acquisition at a frame rate of 2 sec^{-1}. Prior to bleaching a sequence of 10 images was taken, and a total of 400 frames corresponding to 3.5 minutes were taken.

2.2.44) Data processing and statistical analysis

Membrane intensity: Images were processed in Fiji (https://fiji.sc) by generating average intensity projections of the channel required for quantification. Masks were created by processing background-subtracted maximum intensity projections using the Tissue Analyzer plugin in Fiji (Aigouy and Bivic, 2016). Quantification of the membrane intensity at the AP and DV borders was done as described previously using a custom-built Matlab script (Bulgakova and Brown, 2016) found at (https://github.com/nbul/Intensity). Statistical analysis was performed in Graphpad Prism (https://www.graphpad.com/scientific-software/prism/). First, the data was cleaned using ROUT detection of outliers in Prism followed by testing for normal distribution (D'Agostino & Pearson normality test). Then, the significance for parametric data was tested by either a two-way ANOVA or two-tailed t-test with Welch's correction.

E-cad FRAP: images were processed by using the grouped Z-projector plugin in Fiji to generate average intensity projections for each time-point. Following this the bleached ROI, control ROI and background intensity were manual measured for each time point. This data was processed in Microsoft Excel. First the intensity of the bleached ROI at each time point was background subtracted and normalized as following: $I_n = (F_n - BG_n)/(FC_n - BG_n)$, where F_n – intensity of the bleached ROI at the time point *n*, FC_n – intensity of the control unbleached ROI of the same size at the plasma membrane at the time point *n*, and BG_n – background intensity, measured with the same size ROI in cytoplasm at the time point *n*. Than the relative recovery at each time point was calculated using the following formula: $R_n = (I_n - I_1)/(I_0 - I_1)$, where I_n, I_1 and I_0 are normalized intensities of bleached ROI and time point *n*, immediately after photobleaching, and before photobleaching respectively. These values were input to Prism and nonlinear regression analysis was performed to test for best fit model and if recoveries were significantly different between cell borders or genotypes. The recovery was fit to either single exponential model in a form of $f(t) = 1 - F_{im} - A_1 e^{-t/T_{fast}}$, or to bi-exponential model in a form of $f(t) = 1 - F_{im} - A_1 e^{-t/T_{fast}} - A_2 e^{-t/T_{slow}}$, where F_{im} is a size of the immobile fraction, T_{fast} and T_{slow} are the half times, and A_1 and A_2 are amplitudes of the fast and slow components of the recovery. An F-test was used to choose the model and compare datasets.

CLC-GFP FRAP: measurements of all intensities, i.e. the bleached ROI, control ROI and the background, and normalization were done using a custom-build Matlab script (http://github.com/nbul/FRAP) using the same algorithm as described for E-cad FRAP.

Curve fitting and statistical analysis was performed in Graphpad Prism using a nonlinear regression analysis as described for E-cad FRAP.

CLC-GFP puncta: Images were analysed using a custom script in MATLAB described in (Strutt et al., 2016). This was modified for unpaired data by calculating a threshold value for puncta detection using a mean calculated from all of the control images and applying this threshold to the experimental images. Statistical analysis of the recovery was performed in Graphpad Prism using nonlinear regression analysis.

Total membrane intensity: the masks generated using the Tissue analyzer plugin were processed using a custom-built Matlab script (https://github.com/nbul/Intensity/tree/master/TissueAnalyzer). In short, the outlines of the cells were determined from the binary masks, and the length of outline was used as a measure of cell perimeter. Then, the outlines of individual cells were dilated using a YxY structuring element, so that the resulting mask covered all visible E-cad signal on the borders of the cell, and the mean pixel intensity of the mask was measured. The total protein amount was calculated as a product of cell perimeter by mean pixel intensity of the mask. Statistical analysis was performed in Graphpad Prism: using a two-tailed t-test with Welch's correction.

2.2.45) Laser Ablation

Nanoablation of single junctions was performed to provide a measure of junctional tension. Embryos were imaged on a Zeiss LSM 880 microscope with an Airyscan detector, an 8-bit image at 0.053 µm/pixel (512x512 pixel XY-Image) resolution with a 63x objective (NA 1.4) at 5x zoom and 2x averaging was used. An illumination wavelength of 488 nm and 0.5% laser power were used. Images were captured with a 0.5 µm z-spacing. Narrow rectangular ROIs were drawn across the centre of single junctions and this region was ablated using a pulsed TiSa laser (Chameleon), tuned to 760 nm at 45% power. Embryos were imaged continuously in a z-stack consisting of 3 z-slices. The initial recoil rate between vertices at the ends of ablated junctions was quantified by measuring the change in distance between the vertices and dividing by the initial time step. Statistical analysis was performed in Graphpad Prism: using a two-tailed t-test with Welch's correction.

Chapter 3: E-cadherin endocytosis is modulated by p120-catenin through the opposing actions of RhoA and Arf1

Manuscript prepared for Submission in academic journal

Declaration of content and author contribution

The following chapter contains the work undertaken in this project which has been prepared as a manuscript for publication in a peer-review academic journal. As such the format will differ from the other chapters contained in this thesis. In accordance with the regulations of the alternative format thesis submission, the author states and declares that the work presented in the manuscript was done by the author with the exception of the experiments presented in Figure 7. The experiments and analysis in that Figure were the work of the co-author on the manuscript N.A.B.

The author of this Thesis is the first author listed on the manuscript and was the primary contributor to the enclosed manuscript. All of the other experiments, save for those of Figure 7, were designed and performed by the author.

The manuscript is presented in full so that the examiners have the opportunity to view the manuscript as presented to the editors and reviewers of the academic journal.

E-cadherin endocytosis is modulated by p120-catenin through the opposing actions of RhoA and Arf1

Joshua Greig[1], Natalia A. Bulgakova[1, *]

[1] Department of Biomedical Science and Bateson Centre, The University of Sheffield, Sheffield S10 2TN, United Kingdom.

[*] Corresponding author: n.bulgakova@sheffield.ac.uk

Running title: E-cad turnover by p120ctn

Keywords: Arf1, Cell adhesion, Clathrin, E-cadherin, Endocytosis, p120-catenin, RhoA

Word count: 6995

Summary Statement

Greig and Bulgakova reveal that p120-catenin, the regulator of E-cadherin endocytosis, carries out its action through activation of two actin-remodelling pathways which bi-directionally adjust E-cadherin junctional levels, fine-tuning cell adhesion.

Abstract

The regulation of E-cadherin at the plasma membrane by endocytosis is of vital importance for development and disease. p120-catenin, which binds to the E-cadherin C-terminus, can both promote and inhibit E-cadherin endocytosis. However, little is known about what determines the directionality of p120-catenin activity, and the molecules downstream. Here, we have discovered that p120-catenin fine-tunes the clathrin-mediated endocytosis of E-cadherin in *Drosophila* embryonic epidermal cells. It simultaneously activated two actin-remodelling pathways with opposing effects: RhoA, which stabilized E-cadherin at the membrane, and Arf1, which promoted internalization. Epistasis experiments revealed that RhoA additionally inhibited Arf1. E-cadherin was efficiently endocytosed only in the presence of intermediate p120-catenin amounts with too little and too much p120-catenin inhibiting E-cadherin endocytosis. Finally, we found that p120-catenin levels altered the tension of the plasma membrane. Altogether, this shows that p120-catenin is a central hub which co-ordinates cell adhesion, endocytosis, and actin dynamics with tissue tension.

Introduction

Cell-cell adhesion is a fundamental requirement for the formation of tissues and organs. Such adhesions link cells to their neighbours and provide orientational information to a cell in a tissue (Wickström and Niessen, 2018). In the epithelium, it is mediated by Adherens Junctions (AJs), with the principal component E-cadherin (E-cad), a transmembrane protein which binds in a homophilic fashion to E-cad molecules on adjacent cells (van Roy and Berx, 2008; Takeichi, 1977). Intracellularly E-cad interacts with the catenin protein family (Ozawa et al., 1990; Shapiro and Weis, 2009). At its distal C-terminus E-cad binds β-catenin, with α-catenin binding β-catenin and actin, thus tethering extracellular adhesion with the cytoskeleton (Buckley et al., 2014; Ozawa et al., 1990). The p120-catenin (p120ctn) binds to the JuxtaMembrane Domain in the proximal C-terminus of E-cad (Daniel and Reynolds, 1995; Shibamoto et al., 1995; Yap et al., 1998). These catenins are represented by a single gene for each in invertebrates including *Drosophila*, whereas both α-catenin and p120ctn families have several members in vertebrates. p120ctn family has 7 members in humans with different expression patterns and functional requirements, reflecting an increase in tissue types and functional complexity (Carnahan et al., 2010; Gul et al., 2017; Hatzfeld, 2005).

The spatio-temporal expression and localization of E-cad is a prerequisite for the development of multi-cellular organisms: mutations of E-cad result in early embryonic lethality (Riethmacher et al., 1995; Shimizu et al., 2005). The loss of E-cad from the cell surface has been implicated in the progression of cancer cells towards metastatic spread (Elisha et al., 2018). Concurrently, the return of E-cad to the plasma membrane is required for cells to re-integrate into tissues to form secondary tumours (Petrova et al., 2016; Wells et al., 2008). Therefore, knowledge of the mechanisms that modulate E-cad levels at the cell surface is crucial for understanding regulation of E-cad in development and disease.

E-cad has multiple levels of regulation, with endocytic recycling providing a rapid response to changing environment (Levayer et al., 2011; Troyanovsky et al., 2006). The p120ctn family is as the key regulator of E-cad endocytosis in mammalian cells (Cadwell et al., 2016; Garrett et al., 2017; Ireton et al., 2002; Oas et al., 2013; Reynolds, 2007; Sato et al., 2011; Yu et al., 2016). Most studies have focused on the founding family member, p120ctn, however other members, δ-catenin and ARVCF, function in the same way and can substitute for p120ctn (Davis et al., 2003). In mammalian cells, p120ctn maintains E-cad at the plasma membrane: uncoupling p120ctn from E-cad or suppressing its expression results in internalization of E-cad (Davis et al., 2003; Ireton et al., 2002; Ishiyama et al., 2010), which

has been reported in several cancers (Gold et al., 1998; Shibata et al., 2004; van de Ven et al., 2015). Thus, a "cap model" was proposed whereby p120ctn concealed endocytosis triggering motifs on E-cad (Nanes et al., 2012; Reynolds, 2007). This model of unidirectional p120ctn activity has recently been augmented in mammalian cells, when it was found that p120ctn promotes endocytosis of E-cad through interaction with Numb (Sato et al., 2011).

By contrast, in *Drosophila* and *C. elegans* p120ctn was thought less important playing supporting role in adhesion as genetic ablation failed to replicate the effects observed in mammalian systems (Myster et al., 2003; Pacquelet et al., 2003; Pettitt et al., 2003). This is thought to be due to a greater similarity of invertebrate p120ctn to mammalian δ-catenin, ablation of which is similarly viable in mice (Carnahan et al., 2010; Israely et al., 2004). However, δ-catenin expression is restricted to neural and neuroendocrine tissues (Ho et al., 2000), which is likely to explain the mildness of knockout phenotypes. Invertebrate p120ctn is broadly expressed in both epithelia and neurons (Myster et al., 2003), suggesting the potential functional similarity with mammalian p120ctn which shares the broad expression pattern (Davis et al., 2003). Additionally, it has recently been reported that *Drosophila* p120ctn is required to stabilize E-cad in the pupal wing (Iyer et al., 2019) and promotes the endocytosis of E-cad in the embryo and larval wing discs (Bulgakova and Brown, 2016), indicating an evolutionary conservation of p120ctn function.

One key aspect of endocytic regulation of cell adhesion is the remodelling of the cortical actin cytoskeleton by small GTPases (Baum and Georgiou, 2011; Cavey and Lecuit, 2009; Smythe and Ayscough, 2006). One these GTPase regulators is RhoA, whose activity results in focal points of actin contraction. The interaction between Rho and E-cad has been well documented in mammalian systems (Derksen and van de Ven, 2017). In *Drosophila*, Rho promotes the regulated endocytosis of E-cad by Dia and AP2 (Levayer et al., 2011). Conversely, Rho activity antagonises endocytic events in the early embryo (Lee and Harris, 2013), indicating the pivotal role RhoA plays in E-cad endocytic dynamics. In mammalian cells, p120ctn can directly inhibit RhoA, indirectly inhibit it via p190RhoGAP, localize its spaciotemporal activity, or activate it (Anastasiadis et al., 2000; Derksen and van de Ven, 2017; Lang et al., 2014; Taulet et al., 2009; Yu et al., 2016; Zebda et al., 2013), suggesting a context-dependent role of p120ctn in RhoA signalling. p120ctn role in the RhoA pathway in *Drosophila* is unclear (Fox and Peifer, 2007; Fox et al., 2005; Magie et al., 2002).

Another group of GTPases important in the endocytosis are Arf (ADP-Ribosylating Family) proteins (Paterson et al., 2003). Arf GTPases recruit coat proteins to facilitate the

intracellular trafficking of vesicles. The member of the family Arf1 is classically viewed as a Golgi resident and responsible for anterograde transport from the Golgi to the plasma membrane (Donaldson and Jackson, 2011; McMahon and Boucrot, 2011). Recently, however, Arf1 was detected at the plasma membrane and found to participate in trafficking by co-operating with Arf6-dependent endocytosis (Humphreys et al., 2013; Padovani et al., 2014). Arf1 activity has been suggested to balance the initiation and impediment of endocytosis (Lee and Harris, 2013). In *Drosophila*, Arf1 is required for the remodelling of the actin cytoskeleton and facilitating endocytosis in the early syncytial embryo (Humphreys et al., 2012; Lee and Harris, 2013; Rodrigues et al., 2016). Furthermore, Arf1 interacts with E-cad and another known component of AJs, Par-3 (Shao et al., 2010; Toret et al., 2014).

Here, we demonstrate that p120ctn acts to both inhibit and promote endocytosis of E-cad within the same tissue. These activities are dependent on the amount of p120ctn and determine the levels and dynamic properties of E-cad. We show that the interaction of p120ctn with Rho and Arf1 signalling regulates clathrin-mediated endocytosis, with these two pathways acting in an opposing but coupled fashion to set the E-cad turnover rate. Additionally, we found that p120ctn determines tension at the tissue-level. Finally, we present a new model by which p120ctn fine-tunes adhesion through the regulation of actin dynamics and E-cad endocytosis, and thus modulates tissue tension.

Results

Both loss and overexpression of p120ctn stabilize E-cadherin at the plasma membrane via clathrin-mediated endocytosis

In previous work, describing the requirement of p120ctn to promote E-cad endocytosis in *Drosophila* (Bulgakova and Brown, 2016), an E-cad expressed from a ubiquitous (*Ubi-p63E*) promoter was used (*Ubi::E-cad*-GFP). This expression was in the presence of untagged endogenous E-cad, potentially leading to E-cad overexpression and skewing the effects of p120ctn loss. We sought to substantiate these findings using an E-cad tagged at its endogenous locus: *shotgun::*E-cad-GFP (E-cad-GFP) (Huang et al., 2009). The cells of the epidermis of stage 15 *Drosophila* embryos exhibit a distinct rectangular morphology (Fig. 1A) with long cell borders which are orthogonal to the Anterior-Posterior axis of the embryo (AP borders) and short borders which are orthogonal to the Dorsal-Ventral axis (DV borders). E-cad-GFP localizes in a narrow continuous band of fully formed mature AJs at these borders (Adams et al., 1996; Tepass and Hartenstein, 1994). To measure protein amounts, we quantified fluorescent intensities directly emitted by EGFP: an approached well-established

in various models due to linear scaling of EGFP signal with the amount of protein (Coffman and Wu, 2012; Strutt et al., 2016). E-cad-GFP localized asymmetrically with a 1:2 (AP:DV) ratio between the two cell borders (Fig. 1A-C, Table S1) (Bulgakova et al., 2013). In the absence of both maternal and zygotic p120ctn, the amount of E-cad was reduced at both the AP and DV borders by approximately 15% ($p=0.008$ and $p=0.035$, respectively, Fig. 1A-C).

Additionally, we measured the dynamics of E-cad-GFP using Fluorescence Recovery After Photobleaching (FRAP). In previous work, using the *Ubi::*E-cad-GFP, recovery was 70% for DV and 50% for the AP borders in control. Recovery curves were best-fit by a bi-exponential model (Bulgakova *et al*., 2013), with the fast and slow components attributed to diffusion and endocytic recycling, respectively (Bulgakova et al., 2013; Iyer et al., 2019; Lippincott-Schwartz et al., 2003). The recovery was reduced to approximately 35% at both cell borders in *p120ctn* mutant embryos, resulting in an increase of immobile *Ubi::*E-cad-GFP amounts and therefore *Ubi::*E-cad-GFP stabilization within AJs (Bulgakova and Brown, 2016). In the *p120ctn* mutant, a single exponential curve best described the data with the slow recovery component being absent (Bulgakova and Brown, 2016). We replicated the above experiments using endogenously tagged E-cad-GFP, confirming that the effect of p120ctn loss was the same when E-cad was expressed at endogenous levels: the increase of the immobile fraction, and loss of the slow recovery component (Fig. S1, best-fit data in Table S1). Combining our results with published data, we conclude that p120ctn loss leads to the stabilization of E-cad at the membrane by affecting the slow endocytic component of recovery (de Beco et al., 2009; Bulgakova and Brown, 2016; Bulgakova et al., 2013).

To further explore the function of p120ctn we examined the effect of its overexpression on E-cad. In mammalian cell culture, overexpression of p120ctn resulted in the elevation of VE-cad at plasma membranes by inhibiting endocytosis (Xiao et al., 2003). We created a p120ctn overexpression construct under the control of a *UAS* promoter (*UAS*::p120ctn). We expressed it in the posterior half of each embryonic segment using the *engrailed*::GAL4 (*en*::GAL4) driver and marking the cells with a *UAS::*CD8-Cherry (Fig. 1D). This resulted in an increase of E-cad-GFP at AP but not DV borders relative to the adjacent internal control cells ($p=0.002$ and $p=0.27$, respectively, Fig. 1E, Table S1). The result at the AP border was the reverse of that observed for the *p120ctn* mutant (Fig. 1C, Table S1). No increase at the DV might be due to E-cad being saturated at these borders in normal conditions. Measuring the dynamics of E-cad-GFP, using FRAP, we discovered that E-cad-GFP was less dynamic at both border types of the p120ctn overexpressing cells. Recovery was approximately 40% and 30% for AP and DV borders respectively (Fig. 1F),

resulting in increased fraction of immobile E-cad-GFP at both borders (Table S1). Additionally, the slow recovery phase was lost, comparable to that observed in *p120ctn* mutants, indicating impairment of endocytic recycling (Table S1). The rate of fast recovery phase was the same in all cases. Therefore, both loss and overexpression of p120ctn impaired E-cad mobility and internalization.

Previously, the function of p120ctn in E-cad endocytosis was mostly studied by measuring the localization and internalization rate of E-cad (e.g. Davis et al., 2003; Pieters et al., 2016). We decided to directly examine the effect p120ctn has on the endocytic machinery and determine if p120ctn acts through clathrin-mediated endocytosis. We used Clathrin Light Chain (CLC) tagged with GFP (*UAS*::CLC-GFP), to monitor clathrin localization and behaviour using light intensity released from the EGFP tag. CLC tagged with GFP incorporates functionally into clathrin-coated pits without interfering with basic clathrin functions, and is widely used to study dynamics of clathrin-mediated endocytosis (Chang et al., 2002; Gaidarov et al., 1999; Kochubey et al., 2006). Although there is some evidence that biochemically it is not identical to the untagged protein, it does reflect the physiological normal activity of clathrin (Hoffmann et al., 2010). CLC-GFP expressed using the *en*::GAL4 driver was found in spots (puncta) both on the plasma membrane in the plane of AJs and in the cytoplasm (Fig. 2A), a localization consistent with the known function (Kaksonen and Roux, 2018). In the absence of p120ctn we observed a change in localization with more signal localizing with the E-cad at the membranes (Fig. 2B). Quantification of the puncta (see Materials and Methods) revealed that in the absence of p120ctn, CLC-GFP puncta were larger in area, fewer in number and more intense ($p=0.002$, $p=0.0001$, and $p=0.0003$, respectively, Fig. 2C-2E). As these are average measures, we cannot distinguish if loss of p120ctn specifically increased CLC-GFP amounts and puncta size at the plasma membrane, or had an additional, likely indirect effect in cytoplasm. To explore the effect of p120ctn on clathrin dynamics we measured CLC-GFP recovery in the plane of the AJs using FRAP and found that CLC-GFP in the *p120ctn* mutants was less mobile, indicated by a smaller mobile fraction ($p=0.0001$, Fig. 2F).

As E-cad had a smaller mobile fraction in p120ctn overexpression (Fig. 1F) we sought to determine whether this was due to an effect on the clathrin-mediated endocytic pathway. To explore this, we overexpressed p120ctn in conjunction with CLC-GFP. To balance the GAL4-UAS copy number, we co-expressed CD8-Cherry with CLC-GFP in the control (Fig 2G). CLC-GFP puncta in the p120ctn overexpressing cells were smaller in area and less intense ($p=0.01$ and $p=0.03$, respectively, Fig. 2H-2J), and overall puncta number was

unchanged (Fig. 2M), indicating a defect in the formation of mature vesicles which abscise from the membrane. FRAP of CLC-GFP in these cells revealed that p120ctn overexpression reduced the mobile fraction of CLC-GFP (p=0.0001, Fig. 2N). Therefore, as both the removal and overexpression of p120ctn resulted in reduction of clathrin mobility, we reasoned that p120ctn levels act in a bell-curve fashion to regulate clathrin-mediated endocytosis of E-cad.

p120ctn acts via the Rho signalling pathway to stabilize E-cad at the adherens junctions

A primary candidate to link p120ctn to clathrin-mediated endocytosis is the GTPase RhoA. To test this we turned to the downstream effectors of RhoA: the enzyme Rho-Kinase (Rok), which specifically binds RhoA in its activated form, resulting in Rok recruitment to membranes (Leung et al., 1995); and the actin cross-linker non-muscle Myosin II, a Rho-kinase target which requires Rho-kinase for recruitment to AJs (Amano et al., 2010; Schwayer et al., 2016; Shewan et al., 2005).

We used a tagged kinase-dead variant of Rok (Venus-Rok^{K116A}, referred to as Rok-Venus) driven by the *spaghetti squash* promoter as an established readout for the normal localization of Rok without overactivation of the pathway (de Matos Simões et al., 2010). In the epidermis we observed a distinct asymmetry of Rok-Venus localisation between the AP and DV borders in the order 2:1 (AP:DV, Fig.3A-D) consistent with previous reports (Bulgakova et al., 2013; de Matos Simões et al., 2010). In the *p120ctn* mutant embryos this asymmetry was lost, specifically due to a reduction of the Rok-Venus levels at the AP borders (p=0.013, Fig. 3A-C). To confirm the interaction, we examined the effect of p120ctn overexpression. We found an increase in the amount of Rok-Venus at the AP borders (p=0.0043, Fig. 3A-B,D). Therefore, the levels of Rok-Venus at the plasma membrane positively change with those of p120ctn.

To directly demonstrate an effect of p120ctn on the cytoskeleton we used an endogenously tagged variant of the non-muscle Myosin II (MyoII-YFP), which reproduces the localization of untagged Myosin II (Shewan et al., 2005). The localization of the MyoII-YFP protein corresponded to that of Rok-Venus (Fig. 3E-F). The loss of p120ctn resulted in the same effect on MyoII-YFP as on Rok-Venus: loss of asymmetry due to a reduction at the AP borders (p=0.0011, Fig. 3E-G). Similarly, p120ctn overexpression resulted in an increase of MyoII-YFP at the AP borders by comparison to the internal control (p=0.025, Fig. 3E-F,H). Together, these results support a mechanism whereby p120ctn activates Rho signalling in a dose-dependent manner.

Having established an interaction between RhoA and p120ctn, we examined the impact on E-cad endocytosis using constitutively active (Rho^{CA}) and dominant negative (Rho^{DN}) constructs to modulate Rho signalling. Dampening of Rho activity using suppression of the activator RhoGEF2 reduced E-cad levels at plasma membranes (Bulgakova et al., 2013). As this was a mild suppression by RNAi we decided to measure the effect of expressing Rho^{DN}. Expressed using the strong driver *en::GAL4*, it resulted in a complete loss of E-cad at the membrane by stage 15 of embryogenesis (data not shown). Therefore, we acutely induced the expression of the Rho^{DN} using temperature sensitive $GAL80^{ts}$ expressed from the *tubulin84B* promoter (Pilauri et al., 2005). We measured the amount of E-cad-GFP at the plasma membranes four hours post-induction of the Rho^{DN} expression, with time adjusted to obtain stage 15 of embryogenesis. In this case, cells presented the residual E-cad-GFP at the plasma membranes but, strikingly, it was reduced to discrete puncta along the membrane (arrowhead, Fig. 4A). The levels of E-cad-GFP at the plasma membranes were reduced at the AP borders ($p=0.0039$, Fig. 4B).

To complement these data, we examined the effect of overactivation of Rho signalling using the Rho^{CA} construct. This construct resulted in stark changes in cell morphology (Fig. S2) and an increase of E-cad-GFP membrane levels at DV borders ($p<0.0001$, Fig. 4C-D). Cells rounding complicated the division into AP and DV borders, therefore we also measured the mean intensity of E-cad-GFP at the membrane as a total of the entire membrane (Fig. S2). As expected E-cad-GFP intensity was significantly increased in the Rho^{CA} cells ($p<0.0001$, Fig. S2). Overall, these results showed that RhoA activity positively correlated with E-cad localization at the plasma membrane.

To investigate if the observed effects of manipulating Rho activity were the result of an endocytic mechanism, we measured the effects of these Rho constructs on clathrin using CLC-GFP. Co-expression of CLC-GFP with Rho^{CA} resulted in a localization change of the clathrin puncta in comparison to co-expression with CD8-Cherry in the control (Fig. 4E). A larger proportion of protein was localizing with E-cad at the membrane, and the puncta were of greater area and fewer in number ($p=0.0009$ and $p<0.0001$, respectively, Fig. 4F, 4H). Finally, we measured the dynamics of clathrin in these cells. The recovery of CLC-GFP was lower ($p<0.0001$, Fig. 4I), suggesting that Rho activity impairs the budding of clathrin coated vesicles, leading to retention at the plasma membrane. In conclusion, our data is consistent with p120ctn-dependent activation of Rho signalling resulting in the inhibition of clathrin mediated endocytosis, enabling p120ctn to stabilize E-cad at the cell surface.

p120ctn promotes the internalization of E-cadherin through Arf1 signalling

Due to the reported interactions of Arf1 with E-cad and Par-3 (Shao et al., 2010; Toret et al., 2014) we examined if Arf1 acts downstream of p120ctn. We used a transgenic GFP tagged variant of Arf1 (*UAS*::Arf1-GFP) driven by *en::*GAL4. Arf1 tagged with GFP has reduced affinity for ArfGAPs and ArfGEFs, as well as nucleotide exchange rate (Jian et al., 2010), which was beneficial for the experiments described below allowing the study of Arf1 without hyperactivating the pathway. We observed large and distinct Arf1-GFP puncta in the cytoplasm including in proximity to the plasma membrane, which corresponded to the Golgi-resident Arf1 population (Fig. 5A, Fig. S3). To lesser extent, Arf1 localized at the plasma membranes in the plane of AJs, similarly to what was reported before (Shao et al., 2010) (Fig. 5A, highlighted by arrows). As we were interested in the localization of Arf1 at the plasma membrane not the Golgi we excluded the puncta signal from our quantification (see Materials and Methods). Removing p120ctn resulted in a decrease in the amount of Arf1-GFP at both the AP and DV borders ($p<0.0001$ and $p<0.0001$, respectively, Fig. 5A-C). In a complementary experiment, we overexpressed p120ctn: in these cells the amount of Arf1-GFP at the membrane was reduced at the AP borders ($p=0.02$, Fig. 5D-F). Therefore, both the loss and overexpression of p120ctn reduced the amount of Arf1 at the membrane. This was highly reminiscent of the result we observed for clathrin. As Arf1 is a known recruiter of clathrin at the Golgi (Ren et al., 2013), we inferred that plasma membrane-resident Arf1 downstream of p120ctn may link it to the clathrin-mediated endocytic machinery.

Having determined an interaction between p120ctn and Arf1, we asked whether Arf1 activity had a more directive role in p120ctn-mediated endocytosis of E-cad. Expression of a dominant negative variant of Arf1 ($Arf1^{DN}$, Wang et al., 2017) using *en*::GAL4 increased the amount of E-cad-GFP at the AP borders with no change detected at the DV ($p=0.02$ and $p=0.5$, respectively Fig. 6A-B). This was accompanied by an abnormal cell morphology (Fig. 6A and Fig. S4). No surviving larvae were observed, consistent with previous reports (Carvajal-Gonzalez et al., 2015). We attributed this lethality to perturbation of post-Golgi protein transport by prolonged exposure to $Arf1^{DN}$, leading to cell death (Jian et al., 2010; Luchsinger et al., 2018).

To ascertain if Arf1 was acting on E-cad membrane localization via clathrin we measured the effect of expressing $Arf1^{DN}$ on the localization and amount of CLC-GFP. Co-expression of CLC-GFP with $Arf1^{DN}$ resulted in a substantial reduction in CLC-GFP puncta area, intensity, and number ($p<0.0001$, $p=0.0005$, and $p<0.0001$, respectively, Fig. 6C-F). Therefore, we conclude that Arf1 is required for the normal recruitment of clathrin to the AJs.

Finally, to confirm that Arf1 is functionally downstream of p120ctn we designed a rescue experiment using a constitutively active Arf1 ($Arf1^{CA}$). We expressed this in a *p120ctn* mutant background and measured the effect on CLC-GFP (see Fig. 2). We compared this to control co-expressing CLC-GFP with CD8-Cherry in an otherwise wild-type genetic background. Control clathrin puncta localization was as previously observed (Fig. 6G). In the *p120ctn* mutant expressing $Arf1^{CA}$ the clathrin puncta were no different in area, intensity or number from control (p=0.21, p=0.19, and p=0.33, respectively, Fig, 6H-J). Measuring the dynamics of clathrin revealed that recovery was no longer different from the wild-type control (Fig. 6K). From both fixed and dynamic measures of clathrin we concluded that the expression of $Arf1^{CA}$ rescues the clathrin defect observed in the *p120ctn* mutant (see Fig. 2). This is consistent with Arf1 being a downstream interactor of p120ctn, which links the p120ctn–E-cad complex to the clathrin-mediated endocytic machinery. Overall, this allows p120ctn to promote the internalization of E-cad in addition to the previously described anti-endocytic function with RhoA signalling.

The Rho signalling pathway is upstream of Arf1

Having established that Arf1 and RhoA signalling are regulated by p120ctn, resulting in the internalization or retention of E-cad respectively, we sought to determine if these two pathways act upon one another or exist independently. As Arf1 was reported to regulate RhoA (Schlienger et al., 2014), we explored the possibility of an interaction between Arf1 and Rho signalling. To address this, we perturbed signalling in one pathway and measured the effect on the other.

First, we measured the membrane localization of MyoII-YFP, as a readout of RhoA signalling activity, upon upregulation of Arf1 signalling using $Arf1^{CA}$. MyoII-YFP localization was indistinguishable between cells expressing $Arf1^{CA}$ and control cells (Fig. 7A-B), demonstrating that Rho signalling in embryonic epidermis is independent of Arf1 function. In a complementary experiment, we impaired RhoA signalling using an RNAi against RhoGEF2, which results in a milder E-cad reduction at AJs than the severe loss observed with Rho^{DN} (Fig. 4 and Bulgakova et al., 2013). We measured the membrane levels of Arf1-GFP in cells expressing RhoGEF2-RNAi or CD8-Cherry (Fig. 7C, D). Downregulation of RhoGEF2 resulted in an increase in the amount of Arf1-GFP at both AP and DV borders (p=0.045 and p=0.022, respectively, Fig. 7E), demonstrating that RhoA signalling activity limits Arf1 localization to the plasma membrane. This was reminiscent of the phenotype observed upon p120ctn overexpression, in which Arf1-GFP was reduced at the

plasma membrane (see Fig. 5). Therefore, as the overexpression of p120ctn is accompanied by upregulation of Rho signalling (see Fig. 3), we suggest that the reduction of Arf1 previously observed (Fig. 5) is caused by the regulation of Arf1 recruitment by Rho signalling. However, the reduction of Arf1 at the plasma membrane in the absence of p120ctn (see Fig. 5) is independent of RhoA and is caused by regulation of Arf1 recruitment and/or activation more directly by p120ctn.

p120ctn levels modulate plasma membrane tension

Having identified two actin-remodelling pathways downstream of p120ctn we sought to understand their functional outcome at the tissue-level. Actin assembly on clathrin-coated pits, which requires Arf activity (Myers and Casanova, 2008), is suggested to counteract cortical tension to enable membrane deformation (Boulant et al., 2011). In light of the MyoII results (see Fig. 3E-F), we decided to test if p120ctn modulated membrane tension. We analysed this using microablation of membranes and measured the initial recoil as a readout of tension (Mao et al., 2013), as it is proportional to the tension in the system rather than other variables (Liang et al., 2016). We examined AP membranes as these presented an enrichment of MyoII (see Fig. 3E-F). The initial recoil was measured as the distance between the two cell vertices of the ablated membrane immediately post-ablation, as a change in the length proportional to pre-ablation length (Fig. 8A). In control embryos expressing E-cad-GFP alone, the recoil distance post-ablation increased by 5% over pre-ablation distance (Fig. 8A-B). The overexpression of p120ctn resulted in a higher mean initial recoil of 10% ($p<0.0001$, Fig 8A-B). Conversely, in *p120ctn* mutant cells the recoil was decreased ($p=0.022$) to a mean value of 2% (Fig. 8A-B). Therefore, membrane tension positively correlated with p120ctn levels at the plasma membrane.

Discussion

In this study we have focused on the mediators and mechanism of E-cad turnover downstream of p120ctn. We present several advances to the understanding of p120ctn activity and its role in cell-cell adhesion. First, we showed that p120ctn acts bi-directionally as a set point for E-cad at the plasma membrane via a clathrin-mediated mechanism. Second, we demonstrated that p120ctn regulates RhoA signalling, which regulates the internalization of E-cad. This places *Drosophila* p120ctn in the same context as its mammalian orthologue, which interacts with Rho (Reynolds and Roczniak-Ferguson, 2004). Third, we discovered an Arf1-dependent mechanism by which p120ctn promotes the internalization of E-cad. The

described changes in protein amounts following manipulation of p120ctn were in the range of 10%-40%, which may be considered subtle and is consistent with the notion that p120ctn has supportive rather than essential role in non-chordate adhesion (Myster et al., 2003; Pettitt et al., 2003). We speculate that the mildness of changes is due to redundancies and feedback interactions which ensure robustness of cadherin adhesion, essential in a multicellular organism (Priya et al., 2015). Altogether, we propose a new model of p120ctn action, in which the activity of p120ctn is a function of the differential interaction with RhoA and Arf1 (Fig. 8C). In this model, p120ctn regulates membrane tension through RhoA, reinforcing cortical actin, which inhibits E-cad endocytosis. Simultaneously, p120ctn regulates the formation of clathrin-coated vesicles through Arf1, promoting E-cad endocytosis, until a threshold is passed and further increase of p120ctn results in Arf1 inhibition, due to the concordant increase in RhoA activity. The balance between these pathways depends on p120ctn levels and determines the amount of E-cad endocytosis. Therefore, we suggest that p120ctn co-ordinates cell adhesion with endocytosis and the actin cytoskeleton to dictate cellular behaviour and tissue tension.

Previous work established a cap model whereby p120ctn prevents the internalization of E-cad in mammalian cells (Kowalczyk and Reynolds, 2004; Nanes et al., 2012; Su and Kowalczyk, 2016; Thoreson et al., 2000). This function is ascribed to two motifs in mammalian E-cad (LL and DEE), which are absent in *Drosophila* E-cad (Nanes et al., 2012). This explains why *Drosophila* E-cad is not completely internalised in *p120ctn* mutants (Myster et al., 2003). Here, we showed that p120ctn overexpression inhibits E-cad endocytosis. Superficially, this is similar to mammalian cells, in which stabilization results from p120ctn outcompeting access to the E-cad LL and DEE motifs (Hartsock and Nelson, 2012). However, our findings represent a distinct phenomenon resulting from the perturbed balance of downstream signalling. It is more similar to the mechanism of E-cad internalisation in mammalian cells, which does not require p120ctn dissociation from E-cad, but instead relies on recruitment of clathrin adaptor AP2 through direct interaction between p120ctn and Numb (Sato et al., 2011). An outstanding question is whether this mechanism in mammalian cells also involves regulation of actin remodelling by p120ctn.

Both RhoA and Arf1 regulate actin remodelling and endocytosis, but their functions are fundamentally different. RhoA leads to increased cortical tension via the phosphorylation of non-muscle Myosin II, which in turn, counteracts membrane bending required for vesicle formation and endocytosis (Curtis and Meldolesi, 2012; Hodge and Ridley, 2016; Jarsch et al., 2016). In mammalian cells, p120ctn is a well-established regulator of RhoA, and in most

cases directly or indirectly inhibits it, which plays an important role in regulation of epithelial cell shape (Menke and Giehl, 2012; Yu et al., 2016). However, it was unclear if this p120ctn function is present in *Drosophila*: p120ctn physically binds RhoA, but is not required for RhoA localization and does not genetically interact with it (Fox et al., 2005; Magie et al., 2002). Here, we demonstrated that Rho activity positively correlates with p120ctn levels at the membrane. An interesting question is whether *Drosophila* p120ctn can also inhibit RhoA or localize its activity in other tissues or developmental contexts, and whether activation of RhoA is an ancestral function. If so, this would imply that RhoA inhibition is a more novel acquisition in chordates which arose during the diversification of the p120ctn family (Carnahan et al., 2010). We have found that this p120ctn-RhoA interaction stabilizes E-cad: elevated p120ctn and RhoA activity impair the formation of vesicles to internalize E-cad, and therefore increases the duration E-cad spends at the membrane.

In contrast, Arf1 promotes E-cad endocytosis by recruiting clathrin adaptor proteins and facilitating the remodelling of actin required for vesicle formation and abscission. We showed a role for Arf1 in the clathrin-mediated trafficking of E-cad from the membrane. Prior to our work the Arf1 recruitment of clathrin had only been shown at the Golgi by recruiting the Adaptor 1 protein (AP1) (Carvajal-Gonzalez et al., 2015). The function of Arf1 at the plasma membrane had been described in dynamin-independent endocytosis, which was presumed to be clathrin-independent (Kumari and Mayor, 2008). However, the involvement of Arf1 in multiple endocytic pathways has not been fully explored. We have shown that Arf1's capacity to recruit clathrin is exploited by p120ctn to facilitate the endocytosis of E-cad. Whether this requires AP2, a well-documented membrane resident clathrin adaptor, has yet to be determined. Our findings provide a mechanistic insight into the pro-endocytic activity of p120ctn which has only recently come to light (Bulgakova and Brown, 2016; Sato et al., 2011) and elaborates the number of known p120ctn interactors. The activities of Arf1 and RhoA are antagonistic, which was also seen in previous studies on the early embryo (Lee and Harris, 2013).

We propose that by balancing the RhoA and Arf1 pathways p120ctn determines the precise amount of E-cad endocytosis. Further, using laser ablation we demonstrated that p120ctn directly modulates tension, providing a broader view for the function of p120ctn on the tissue-level. Considering that all of the components of this regulatory network are expressed in all epithelia across evolution, we speculate that this system is likely to be more broadly applicable in development and a general feature of cell biology.

Materials and Methods

Fly stocks and genetics

Flies were raised on standard medium. The GAL4/UAS system (Brand and Perrimon, 1993) was used for all the specific spatial and temporal expression of transgenic and RNAi experiments. The GAL4 expressional driver used for all experiments was *engrailed::GAL4* (*en*::GAL4, Bloomington number 30564). The following fly stocks were used in this study (Bloomington number included where applicable): E-cad-GFP (*shg::E-cadherin-GFP*) (60584), Shg-Cherry (*shg::mCherry*, 59014), *UAS*::CLC-GFP (7109), *UAS*::Arf1-GFP (gift from T.Harris), Zipper-YFP (*Myosin II*-YFP, Kyoto Stock Center 115082), *sqh*::Rok^{K116A}-Venus (gift from J.Zallen), *UAS*::Arf1-T31N (DN) and *UAS::*Arf1-Q71L (CA) (Wang et al., 2017), *UAS*::Rho1-N19 (DN) (7328), and *tubulin*::GAL80^{TS} (7017). The p120ctn mutant genotype (p120ctn^{308}/ Δp120) used was derived from crossing two deficiency stocks: homozygously viable p120ctn^{308} females (Myster et al., 2003) with homozygously lethal Df(2R)M41A8/ CyO, *twi::*Gal4, *UAS::*GFP males (740). Thus, the p120ctn mutants examined lacked both maternal and zygotic contributions.

Embryo collection and fixation

Embryos were collected at 25°C at 3-hour time intervals and allowed to develop at 18°C for 21 hours to reach the desired developmental stage, except for the acute induction experiments, where embryos were allowed to develop for 13 hours at 18°C and shifted to 29°C for 4 hours. Then embryos were dechorionated using 50% sodium hypochlorite (bleach, Invitrogen) in water for 4 minutes, and extensively washed with deionized water prior to fixation. Fixation was performed with a 1:1 solution of 4% formaldehyde (Sigma) in PBS (Phosphate Buffered Saline) and heptane (Sigma) for 20 minutes on an orbital shaker at room temperature. Embryos were then devitellinized in 1:1 solution of methanol and heptane for 20 sec with vigorous agitation. Following subsequent methanol washes the fixed embryo specimens were stored at -20°C in methanol until required.

Embryo live imaging

Embryos were collected and dechorionated as described above. Once washed with deionized water embryos were transferred to apple juice agar segments upon microscope slide. Correct genotypes were selected under a fluorescent microscope (Leica) using a needle. Embryos were positioned and orientated in a row consisting of 6-10 embryos per genotype. Following

this, embryos were transferred to pre-prepared microscope slides with Scotch tape and embedded in Halocarbon oil 27 (Sigma). Embryos were left to aerate for 10 minutes prior to covering with a cover slip and imaging.

For laser ablation, following orientation and positioning the embryos were transferred to a 60mm x 22mm coverslip which had been pre-prepared by applying 10 µl of Heptane glue along a strip in the middle of the coverslip orientated with the long axis. The coverslip was attached to a metal slide cassette (Zeiss), and the embryos were embedded in Halocarbon oil 27 before imaging.

Molecular cloning

The p120ctn full length cDNA was obtained from Berkeley Drosophila Genome Project (BDGP), supplied in a pBSSK vector. This was sub-cloned into a (pUAS-k10.attB) plasmid using standard restriction digestion with NotI and BamHI (New England Biolabs) followed by ligation with T4 DNA ligase (New England Biolabs) and transformation into DH5a competent E.coli cells (Thermo Fisher Scientific). Prior to injection plasmids were test digested and sequenced (Core Genomic Facility, University of Sheffield). Plasmids were prepared for injection using standard miniprep extraction (Qiagen) and submitted for injection (Microinjection service, Department of Genetics, University of Cambridge) into the attP-86Fb stock (Bloomington stock 24749). Successful incorporation of the transgene was determined by screening for (w^+) in the F1 progeny.

Immunostaining

The embryos were washed three times in 1 ml of PBST (PBS with 0.05% Triton) with gentle rocking. Blocking of the embryos prior to staining was done in 300 µl of a 1% NGS (Normal Goat Serum) in PBST for 1 hour at room temperature with gentle rocking. For staining the blocking solution was removed, 300 µl of the primary antibody: either 1:100 dilution of a rat anti-E-cad (DCAD2, DSHB) or 1:10 of a mouse anti-engrailed (4D9, DSHB) in fresh blocking solution was added and the embryos were incubated overnight at 4°C with orbital rotation. Then, embryos were washed three times with 1 ml of PBST. A 300 µl 1:300 dilution of the secondary antibody (goat Cy3- or Cy5-conjugated anti-rat-IgG, Invitrogen) was added, and the embryos incubated either overnight at 4°C with orbital rotation or for 2 hours at room temperature with gentle rocking. Then embryos were washed three time with PBST, following which they were incubated with 50-70 µl of Vectashield (Vector Laboratories) and allowed to equilibrate for a period of 2 hours before being mounted on microscope slides (Thermo).

Microscopy, data acquisition and FRAP

All experiments except for laser ablation were performed using an up-right Olympus FV1000 confocal microscope with a 60x/1.40 NA oil immersion objective. All measurements were made on dorsolateral epidermal cells of embryos, which were near or just after completion of dorsal closure, corresponding to the end of Stage 15 of embryogenesis. For fixed samples 16-bit images were taken at a magnification of 0.051µm/pixel (1024x1024 pixel XY-image) with a pixel dwell of 4µm/pixel. For each embryo, a Z-axis sectional stack through the plane of the AJs was taken, which consisted of six sections with a 0.38 µm intersectional spacing. The images were saved in the Olympus binary image format for further processing.

For E-cad FRAP (adapted from Bulgakova et al., 2013) 16-bit images were taken at a magnification of 0.093 µm/pixel (320x320 pixel XY-image). In each embryo, several circular regions of 1 µm radius were photobleached at either DV or AP junctions resulting in one bleach event per cell. Photobleaching was performed with 8 scans at 2 µs/pixel at 50-70% 488 nm laser power, resulting in the reduction of E-cad-GFP signal by 60–80%. A stack of 6 z-sections spaced by 0.38 µm was imaged just before photobleaching, and immediately after photobleaching, and then at 20 s intervals, for a total of 15 minutes.

As rate of endocytosis depends on external factors, such as temperature (Weigel and Oka, 1981), controls were examined in parallel with experimental conditions in all experiments with CLC-GFP. This dependence might also account for slight variation between datasets, e.g. compare Fig. 2A and 2G. For CLC-GFP FRAP, 16-bit images were taken at a magnification of 0.051µm/pixel (256x256 pixel XY-image). In each embryo a single plane was selected in centre of the AJ band using Shg-Cherry for positioning. An area encompassing a transverse region orthogonal to the axis of the engrailed expressing cells was selected (140x60 pixels) was photobleached with 1 scan at 2 µm/pixel using 100% 488nm laser power resulting in reduction of CLC-GFP signal by 70-80%. Images were taken using continuous acquisition at a frame rate of 2 sec^{-1}. Prior to bleaching a sequence of 10 images was taken, and a total of 400 frames corresponding to 3.5 minutes were taken.

Data processing and statistical analysis

Membrane intensity: Images were processed in Fiji (https://fiji.sc) by generating average intensity projections of the channel required for quantification. Masks were created by processing background-subtracted maximum intensity projections using the Tissue Analyzer plugin in Fiji (Aigouy and Bivic, 2016). Quantification of the membrane intensity at the AP and DV borders was done as described previously using a custom-built Matlab script

(Bulgakova and Brown, 2016) found at (https://github.com/nbul/Intensity). In the case of quantification of Arf1-GFP membrane intensity, due to high Arf1-GFP presence inside cells both in Golgi and cytoplasm, the mean intensity of embryonic areas not expressing the GFP-tagged transgene were used for background subtraction. Statistical analysis was performed in Graphpad Prism (https://www.graphpad.com/scientific-software/prism/). First, the data was cleaned using ROUT detection of outliers in Prism followed by testing for normal distribution (D'Agostino & Pearson normality test). Then, the significance for parametric data was tested by either a two-way ANOVA or two-tailed t-test with Welch's correction.

E-cad FRAP: images were processed by using the grouped Z-projector plugin in Fiji to generate average intensity projections for each time-point. Following this the bleached ROI, control ROI and background intensity were manual measured for each time point. This data was processed in Microsoft Excel. First the intensity of the bleached ROI at each time point was background subtracted and normalized as following: $I_n = (F_n - BG_n)/(FC_n - BG_n)$, where F_n – intensity of the bleached ROI at the time point *n*, FC_n – intensity of the control unbleached ROI of the same size at the plasma membrane at the time point *n*, and BG_n – background intensity, measured with the same size ROI in cytoplasm at the time point *n*. Than the relative recovery at each time point was calculated using the following formula: $R_n = (I_n - I_1)/(I_0 - I_1)$, where I_n, I_1 and I_0 are normalized intensities of bleached ROI and time point *n*, immediately after photobleaching, and before photobleaching respectively. These values were input to Prism and nonlinear regression analysis was performed to test for best fit model and if recoveries were significantly different between cell borders or genotypes. The recovery was fit to either single exponential model in a form of $f(t) = 1 - F_{im} - A_1 e^{-t/T_{fast}}$, or to bi-exponential model in a form of $f(t) = 1 - F_{im} - A_1 e^{-t/T_{fast}} - A_2 e^{-t/T_{slow}}$, where F_{im} is a size of the immobile fraction, T_{fast} and T_{slow} are the half times, and A_1 and A_2 are amplitudes of the fast and slow components of the recovery. An F-test was used to choose the model and compare datasets.

CLC-GFP FRAP: measurements of all intensities, i.e. the bleached ROI, control ROI and the background, and normalization were done using a custom-build Matlab script (http://github.com/nbul/FRAP) using the same algorithm as described for E-cad FRAP. Curve fitting and statistical analysis was performed in Graphpad Prism using a nonlinear regression analysis as described for E-cad FRAP.

CLC-GFP puncta: Images were analysed using a custom script in MATLAB described in (Strutt et al., 2016). This was modified for unpaired data by calculating a threshold value for

puncta detection using a mean calculated from all of the control images and applying this threshold to the experimental images. Statistical analysis of the recovery was performed in Graphpad Prism using nonlinear regression analysis.

Total membrane intensity: the masks generated using the Tissue analyser plugin were processed using a custom-built Matlab script (https://github.com/nbul/Intensity/tree/master/TissueAnalyzer). In short, the outlines of the cells were determined from the binary masks, and the length of outline was used as a measure of cell perimeter. Then, the outlines of individual cells were dilated using a YxY structuring element, so that the resulting mask covered all visible E-cad signal on the borders of the cell, and the mean pixel intensity of the mask was measured. The total protein amount was calculated as a product of cell perimeter by mean pixel intensity of the mask. Statistical analysis was performed in Graphpad Prism: using a two-tailed t-test with Welch's correction.

Laser Ablation

Nanoablation of single junctions was performed to provide a measure of junctional tension. Embryos were imaged on a Zeiss LSM 880 microscope with an Airyscan detector, an 8-bit image at 0.053 µm/pixel (512x512 pixel XY-Image) resolution with a 63x objective (NA 1.4) at 5x zoom and 2x averaging was used. An illumination wavelength of 488 nm and 0.5% laser power were used. Images were captured with a 0.5 µm z-spacing. Narrow rectangular ROIs were drawn across the centre of single junctions and this region was ablated using a pulsed TiSa laser (Chameleon), tuned to 760 nm at 45% power. Embryos were imaged continuously in a z-stack consisting of 3 z-slices. The initial recoil rate between the vertices at the ends of ablated junctions was quantified by measuring the change in distance between the vertices and dividing by the initial time step. Statistical analysis was performed in Graphpad Prism: using a two-tailed t-test with Welch's correction.

Acknowledgments

The authors wish to thank Rob Tetley and Yanlan Mao for assistance with laser ablation experiments. The authors also with to thank Professor David Strutt, University of Sheffield, and his lab; and the technical staff of the Wolfson Light Microscopy Facility (LMF) and the Fly Facility, the University of Sheffield. This work was supported by grant BB/P007503/1 from the UK Biotechnology and Biological Sciences Research Council.

Author Contribution

J.G and N.A.B. designed and performed experiments and wrote the manuscript.

Conflicts of Interest

The authors declare and confirm that there is no conflict of interest for the work presented in this paper.

References

Adams, C.L., Nelson, W.J., and Smith, S.J. (1996). Quantitative analysis of cadherin-catenin-actin reorganization during development of cell-cell adhesion. J. Cell Biol. *135*, 1899–1911.

Aigouy, B., and Bivic, A.L. (2016). The PCP pathway regulates Baz planar distribution in epithelial cells. Sci. Rep. *6*, srep33420.

Amano, M., Nakayama, M., and Kaibuchi, K. (2010). Rho-Kinase/ROCK: A Key Regulator of the Cytoskeleton and Cell Polarity. Cytoskelet. Hoboken Nj *67*, 545–554.

Anastasiadis, P.Z., Moon, S.Y., Thoreson, M.A., Mariner, D.J., Crawford, H.C., Zheng, Y., and Reynolds, A.B. (2000). Inhibition of RhoA by p120 catenin. Nat. Cell Biol. *2*, 637–644.

Baum, B., and Georgiou, M. (2011). Dynamics of adherens junctions in epithelial establishment, maintenance, and remodeling. J. Cell Biol. *192*, 907–917.

de Beco, S., Gueudry, C., Amblard, F., and Coscoy, S. (2009). Endocytosis is required for E-cadherin redistribution at mature adherens junctions. Proc. Natl. Acad. Sci. U. S. A. *106*, 7010–7015.

Boulant, S., Kural, C., Zeeh, J.-C., Ubelmann, F., and Kirchhausen, T. (2011). Actin dynamics counteract membrane tension during clathrin-mediated endocytosis. Nat. Cell Biol. *13*, 1124–1131.

Brand, A.H., and Perrimon, N. (1993). Targeted gene expression as a means of altering cell fates and generating dominant phenotypes. Dev. Camb. Engl. *118*, 401–415.

Buckley, C.D., Tan, J., Anderson, K.L., Hanein, D., Volkmann, N., Weis, W.I., Nelson, W.J., and Dunn, A.R. (2014). Cell adhesion. The minimal cadherin-catenin complex binds to actin filaments under force. Science *346*, 1254211.

Bulgakova, N.A., and Brown, N.H. (2016). Drosophila p120-catenin is crucial for endocytosis of the dynamic E-cadherin-Bazooka complex. J. Cell Sci. *129*, 477–482.

Bulgakova, N.A., Grigoriev, I., Yap, A.S., Akhmanova, A., and Brown, N.H. (2013). Dynamic microtubules produce an asymmetric E-cadherin–Bazooka complex to maintain segment boundaries. J. Cell Biol. *201*, 887–901.

Cadwell, C.M., Su, W., and Kowalczyk, A.P. (2016). Cadherin Tales: Regulation of Cadherin Function by Endocytic Membrane Trafficking. Traffic Cph. Den.

Carnahan, R.H., Rokas, A., Gaucher, E.A., and Reynolds, A.B. (2010). The Molecular Evolution of the p120-Catenin Subfamily and Its Functional Associations. PLOS ONE *5*, e15747.

Carvajal-Gonzalez, J.M., Balmer, S., Mendoza, M., Dussert, A., Collu, G., Roman, A.-C., Weber, U., Ciruna, B., and Mlodzik, M. (2015). The clathrin adaptor AP-1 complex and Arf1 regulate planar cell polarity in vivo. Nat. Commun. *6*, 6751.

Cavey, M., and Lecuit, T. (2009). Molecular Bases of Cell–Cell Junctions Stability and Dynamics. Cold Spring Harb. Perspect. Biol. *1*.

Chang, H.C., Newmyer, S.L., Hull, M.J., Ebersold, M., Schmid, S.L., and Mellman, I. (2002). Hsc70 is required for endocytosis and clathrin function in Drosophila. J. Cell Biol. *159*, 477–487.

Coffman, V.C., and Wu, J.-Q. (2012). Counting protein molecules using quantitative fluorescence microscopy. Trends Biochem. Sci. *37*, 499–506.

Curtis, I. de, and Meldolesi, J. (2012). Cell surface dynamics – how Rho GTPases orchestrate the interplay between the plasma membrane and the cortical cytoskeleton. J Cell Sci *125*, 4435–4444.

Daniel, J.M., and Reynolds, A.B. (1995). The tyrosine kinase substrate p120cas binds directly to E-cadherin but not to the adenomatous polyposis coli protein or alpha-catenin. Mol. Cell. Biol. *15*, 4819–4824.

Davis, M.A., Ireton, R.C., and Reynolds, A.B. (2003). A core function for p120-catenin in cadherin turnover. J Cell Biol *163*, 525–534.

Derksen, P.W.B., and van de Ven, R.A.H. (2017). Shared mechanisms regulate spatiotemporal RhoA-dependent actomyosin contractility during adhesion and cell division. Small GTPases 1–9.

Donaldson, J.G., and Jackson, C.L. (2011). ARF family G proteins and their regulators: roles in membrane transport, development and disease. Nat. Rev. Mol. Cell Biol. *12*, 362–375.

Elisha, Y., Kalchenko, V., Kuznetsov, Y., and Geiger, B. (2018). Dual role of E-cadherin in the regulation of invasive collective migration of mammary carcinoma cells. Sci. Rep. *8*, 4986.

Fox, D.T., and Peifer, M. (2007). Cell Adhesion: Separation of p120's Powers? Curr. Biol. *17*, R24–R27.

Fox, D.T., Homem, C.C.F., Myster, S.H., Wang, F., Bain, E.E., and Peifer, M. (2005). Rho1 regulates Drosophila adherens junctions independently of p120ctn. Development *132*, 4819–4831.

Gaidarov, I., Santini, F., Warren, R.A., and Keen, J.H. (1999). Spatial control of coated-pit dynamics in living cells. Nat. Cell Biol. *1*, 1–7.

Garrett, J.P., Lowery, A.M., Adam, A.P., Kowalczyk, A.P., and Vincent, P.A. (2017). Regulation of endothelial barrier function by p120-catenin·VE-cadherin interaction. Mol. Biol. Cell *28*, 85–97.

Gold, J.S., Reynolds, A.B., and Rimm, D.L. (1998). Loss of p120ctn in human colorectal cancer predicts metastasis and poor survival. Cancer Lett. *132*, 193–201.

Gul, I.S., Hulpiau, P., Saeys, Y., and van Roy, F. (2017). Evolution and diversity of cadherins and catenins. Exp. Cell Res. *358*, 3–9.

Hartsock, A., and Nelson, W.J. (2012). Competitive Regulation of E-Cadherin JuxtaMembrane Domain Degradation by p120-Catenin Binding and Hakai-Mediated Ubiquitination. PLOS ONE *7*, e37476.

Hatzfeld, M. (2005). The p120 family of cell adhesion molecules. Eur. J. Cell Biol. *84*, 205–214.

Ho, C., Zhou, J., Medina, M., Goto, T., Jacobson, M., Bhide, P.G., and Kosik, K.S. (2000). δ-catenin is a nervous system-specific adherens junction protein which undergoes dynamic relocalization during development. J. Comp. Neurol. *420*, 261–276.

Hodge, R.G., and Ridley, A.J. (2016). Regulating Rho GTPases and their regulators. Nat. Rev. Mol. Cell Biol. *17*, 496–510.

Hoffmann, A., Dannhauser, P.N., Groos, S., Hinrichsen, L., Curth, U., and Ungewickell, E.J. (2010). A comparison of GFP-tagged clathrin light chains with fluorochromated light chains in vivo and in vitro. Traffic Cph. Den. *11*, 1129–1140.

Huang, J., Zhou, W., Dong, W., Watson, A.M., and Hong, Y. (2009). Directed, efficient, and versatile modifications of the Drosophila genome by genomic engineering. Proc. Natl. Acad. Sci. *106*, 8284–8289.

Humphreys, D., Liu, T., Davidson, A.C., Hume, P.J., and Koronakis, V. (2012). The Drosophila Arf1 homologue Arf79F is essential for lamellipodium formation. J. Cell Sci. *125*, 5630–5635.

Humphreys, D., Davidson, A.C., Hume, P.J., Makin, L.E., and Koronakis, V. (2013). Arf6 coordinates actin assembly through the WAVE complex, a mechanism usurped by Salmonella to invade host cells. Proc. Natl. Acad. Sci. *110*, 16880–16885.

Ireton, R.C., Davis, M.A., van Hengel, J., Mariner, D.J., Barnes, K., Thoreson, M.A., Anastasiadis, P.Z., Matrisian, L., Bundy, L.M., Sealy, L., et al. (2002). A novel role for p120 catenin in E-cadherin function. J. Cell Biol. *159*, 465–476.

Ishiyama, N., Lee, S.-H., Liu, S., Li, G.-Y., Smith, M.J., Reichardt, L.F., and Ikura, M. (2010). Dynamic and Static Interactions between p120 Catenin and E-Cadherin Regulate the Stability of Cell-Cell Adhesion. Cell *141*, 117–128.

Israely, I., Costa, R.M., Xie, C.W., Silva, A.J., Kosik, K.S., and Liu, X. (2004). Deletion of the Neuron-Specific Protein Delta-Catenin Leads to Severe Cognitive and Synaptic Dysfunction. Curr. Biol. *14*, 1657–1663.

Iyer, K.V., Piscitello-Gómez, R., Paijmans, J., Jülicher, F., and Eaton, S. (2019). Epithelial Viscoelasticity Is Regulated by Mechanosensitive E-cadherin Turnover. Curr. Biol. *29*, 578-591.e5.

Jarsch, I.K., Daste, F., and Gallop, J.L. (2016). Membrane curvature in cell biology: An integration of molecular mechanisms. J Cell Biol *214*, 375–387.

Jian, X., Cavenagh, M., Gruschus, J.M., Randazzo, P.A., and Kahn, R.A. (2010). Modifications to the C-terminus of Arf1 alter cell functions and protein interactions. Traffic Cph. Den. *11*, 732–742.

Kaksonen, M., and Roux, A. (2018). Mechanisms of clathrin-mediated endocytosis. Nat. Rev. Mol. Cell Biol. *19*, 313–326.

Kochubey, O., Majumdar, A., and Klingauf, J. (2006). Imaging Clathrin Dynamics in Drosophila melanogaster Hemocytes Reveals a Role for Actin in Vesicle Fission. Traffic *7*, 1614–1627.

Kowalczyk, A.P., and Reynolds, A.B. (2004). Protecting your tail: regulation of cadherin degradation by p120-catenin. Curr. Opin. Cell Biol. *16*, 522–527.

Kumari, S., and Mayor, S. (2008). ARF1 is directly involved in dynamin-independent endocytosis. Nat. Cell Biol. *10*, 30–41.

Lang, R.A., Herman, K., Reynolds, A.B., Hildebrand, J.D., and Plageman, T.F. (2014). p120-catenin-dependent junctional recruitment of Shroom3 is required for apical constriction during lens pit morphogenesis. Dev. Camb. Engl. *141*, 3177–3187.

Lee, D.M., and Harris, T.J.C. (2013). An Arf-GEF Regulates Antagonism between Endocytosis and the Cytoskeleton for Drosophila Blastoderm Development. Curr. Biol. *23*, 2110–2120.

Leung, T., Manser, E., Tan, L., and Lim, L. (1995). A novel serine/threonine kinase binding the Ras-related RhoA GTPase which translocates the kinase to peripheral membranes. J. Biol. Chem. *270*, 29051–29054.

Levayer, R., Pelissier-Monier, A., and Lecuit, T. (2011). Spatial regulation of Dia and Myosin-II by RhoGEF2 controls initiation of E-cadherin endocytosis during epithelial morphogenesis. Nat. Cell Biol. *13*, 529–540.

Liang, X., Michael, M., and Gomez, G.A. (2016). Measurement of Mechanical Tension at Cell-cell Junctions Using Two-photon Laser Ablation. Bio-Protoc. *6*.

Lippincott-Schwartz, J., Altan-Bonnet, N., and Patterson, G.H. (2003). Photobleaching and photoactivation: following protein dynamics in living cells. Nat. Cell Biol. *Suppl*, S7-14.

Luchsinger, C., Aguilar, M., Burgos, P.V., Ehrenfeld, P., and Mardones, G.A. (2018). Functional disruption of the Golgi apparatus protein ARF1 sensitizes MDA-MB-231 breast cancer cells to the antitumor drugs Actinomycin D and Vinblastine through ERK and AKT signaling. PloS One *13*, e0195401.

Magie, C.R., Pinto-Santini, D., and Parkhurst, S.M. (2002). Rho1 interacts with p120ctn and α-catenin, and regulates cadherin-based adherens junction components in Drosophila. Development *129*, 3771–3782.

Mao, Y., Tournier, A.L., Hoppe, A., Kester, L., Thompson, B.J., and Tapon, N. (2013). Differential proliferation rates generate patterns of mechanical tension that orient tissue growth. EMBO J. *32*, 2790–2803.

de Matos Simões, S., Blankenship, J.T., Weitz, O., Farrell, D.L., Tamada, M., Fernandez-Gonzalez, R., and Zallen, J.A. (2010). Rho-kinase directs Bazooka/Par-3 planar polarity during Drosophila axis elongation. Dev. Cell *19*, 377–388.

McMahon, H.T., and Boucrot, E. (2011). Molecular mechanism and physiological functions of clathrin-mediated endocytosis. Nat. Rev. Mol. Cell Biol. *12*, 517–533.

Menke, A., and Giehl, K. (2012). Regulation of adherens junctions by Rho GTPases and p120-catenin. Arch. Biochem. Biophys. *524*, 48–55.

Myers, K.R., and Casanova, J.E. (2008). Regulation of actin cytoskeleton dynamics by Arf-family GTPases. Trends Cell Biol. *18*, 184–192.

Myster, S.H., Cavallo, R., Anderson, C.T., Fox, D.T., and Peifer, M. (2003). Drosophila p120catenin plays a supporting role in cell adhesion but is not an essential adherens junction component. J Cell Biol *160*, 433–449.

Nanes, B.A., Chiasson-MacKenzie, C., Lowery, A.M., Ishiyama, N., Faundez, V., Ikura, M., Vincent, P.A., and Kowalczyk, A.P. (2012). p120-catenin binding masks an endocytic signal conserved in classical cadherins. J Cell Biol *199*, 365–380.

Oas, R.G., Nanes, B.A., Esimai, C.C., Vincent, P.A., García, A.J., and Kowalczyk, A.P. (2013). p120-catenin and β-catenin differentially regulate cadherin adhesive function. Mol. Biol. Cell *24*, 704–714.

Ozawa, M., Ringwald, M., and Kemler, R. (1990). Uvomorulin-catenin complex formation is regulated by a specific domain in the cytoplasmic region of the cell adhesion molecule. Proc. Natl. Acad. Sci. U. S. A. *87*, 4246–4250.

Pacquelet, A., Lin, L., and Rorth, P. (2003). Binding site for p120/delta-catenin is not required for Drosophila E-cadherin function in vivo. J. Cell Biol. *160*, 313–319.

Padovani, D., Folly-Klan, M., Labarde, A., Boulakirba, S., Campanacci, V., Franco, M., Zeghouf, M., and Cherfils, J. (2014). EFA6 controls Arf1 and Arf6 activation through a negative feedback loop. Proc. Natl. Acad. Sci. U. S. A. *111*, 12378–12383.

Paterson, A.D., Parton, R.G., Ferguson, C., Stow, J.L., and Yap, A.S. (2003). Characterization of E-cadherin Endocytosis in Isolated MCF-7 and Chinese Hamster Ovary Cells THE INITIAL FATE OF UNBOUND E-CADHERIN. J. Biol. Chem. *278*, 21050–21057.

Petrova, Y.I., Schecterson, L., and Gumbiner, B.M. (2016). Roles for E-cadherin cell surface regulation in cancer. Mol. Biol. Cell *27*, 3233–3244.

Pettitt, J., Cox, E.A., Broadbent, I.D., Flett, A., and Hardin, J. (2003). The Caenorhabditis elegans p120 catenin homologue, JAC-1, modulates cadherin-catenin function during epidermal morphogenesis. J. Cell Biol. *162*, 15–22.

Pieters, T., Goossens, S., Haenebalcke, L., Andries, V., Stryjewska, A., De Rycke, R., Lemeire, K., Hochepied, T., Huylebroeck, D., Berx, G., et al. (2016). p120 Catenin-Mediated Stabilization of E-Cadherin Is Essential for Primitive Endoderm Specification. PLoS Genet. *12*, e1006243.

Pilauri, V., Bewley, M., Diep, C., and Hopper, J. (2005). Gal80 Dimerization and the Yeast GAL Gene Switch. Genetics *169*, 1903–1914.

Priya, R., Gomez, G.A., Budnar, S., Verma, S., Cox, H.L., Hamilton, N.A., and Yap, A.S. (2015). Feedback regulation through myosin II confers robustness on RhoA signalling at E-cadherin junctions. Nat. Cell Biol. *17*, 1282–1293.

Ren, X., Farias, G.G., Canagarajah, B.J., Bonifacino, J.S., and Hurley, J.H. (2013). Structural Basis for Recruitment and Activation of the AP-1 Clathrin Adaptor Complex by Arf1. Cell *152*, 755–767.

Reynolds, A.B. (2007). p120-catenin: Past and present. Biochim. Biophys. Acta BBA - Mol. Cell Res. *1773*, 2–7.

Reynolds, A.B., and Roczniak-Ferguson, A. (2004). Emerging roles for p120-catenin in cell adhesion and cancer. Oncogene *23*, 7947–7956.

Riethmacher, D., Brinkmann, V., and Birchmeier, C. (1995). A targeted mutation in the mouse E-cadherin gene results in defective preimplantation development. Proc. Natl. Acad. Sci. *92*, 855–859.

Rodrigues, F.F., Shao, W., and Harris, T.J.C. (2016). The Arf GAP Asap promotes Arf1 function at the Golgi for cleavage furrow biosynthesis in Drosophila. Mol. Biol. Cell *27*, 3143–3155.

van Roy, F., and Berx, G. (2008). The cell-cell adhesion molecule E-cadherin. Cell. Mol. Life Sci. CMLS *65*, 3756–3788.

Sato, K., Watanabe, T., Wang, S., Kakeno, M., Matsuzawa, K., Matsui, T., Yokoi, K., Murase, K., Sugiyama, I., Ozawa, M., et al. (2011). Numb controls E-cadherin endocytosis through p120 catenin with aPKC. Mol. Biol. Cell *22*, 3103–3119.

Schlienger, S., Campbell, S., and Claing, A. (2014). ARF1 regulates the Rho/MLC pathway to control EGF-dependent breast cancer cell invasion. Mol. Biol. Cell *25*, 17–29.

Schwayer, C., Sikora, M., Slováková, J., Kardos, R., and Heisenberg, C.-P. (2016). Actin Rings of Power. Dev. Cell *37*, 493–506.

Shao, W., Wu, J., Chen, J., Lee, D.M., Tishkina, A., and Harris, T.J.C. (2010). A modifier screen for Bazooka/PAR-3 interacting genes in the Drosophila embryo epithelium. PloS One *5*, e9938.

Shapiro, L., and Weis, W.I. (2009). Structure and biochemistry of cadherins and catenins. Cold Spring Harb. Perspect. Biol. *1*, a003053.

Shewan, A.M., Maddugoda, M., Kraemer, A., Stehbens, S.J., Verma, S., Kovacs, E.M., and Yap, A.S. (2005). Myosin 2 Is a Key Rho Kinase Target Necessary for the Local Concentration of E-Cadherin at Cell–Cell Contacts. Mol. Biol. Cell *16*, 4531–4542.

Shibamoto, S., Hayakawa, M., Takeuchi, K., Hori, T., Miyazawa, K., Kitamura, N., Johnson, K.R., Wheelock, M.J., Matsuyoshi, N., and Takeichi, M. (1995). Association of p120, a tyrosine kinase substrate, with E-cadherin/catenin complexes. J. Cell Biol. *128*, 949–957.

Shibata, T., Kokubu, A., Sekine, S., Kanai, Y., and Hirohashi, S. (2004). Cytoplasmic p120ctn regulates the invasive phenotypes of E-cadherin-deficient breast cancer. Am. J. Pathol. *164*, 2269–2278.

Shimizu, T., Yabe, T., Muraoka, O., Yonemura, S., Aramaki, S., Hatta, K., Bae, Y.-K., Nojima, H., and Hibi, M. (2005). E-cadherin is required for gastrulation cell movements in zebrafish. Mech. Dev. *122*, 747–763.

Smythe, E., and Ayscough, K.R. (2006). Actin regulation in endocytosis. J Cell Sci *119*, 4589–4598.

Strutt, H., Gamage, J., and Strutt, D. (2016). Robust Asymmetric Localization of Planar Polarity Proteins Is Associated with Organization into Signalosome-like Domains of Variable Stoichiometry. Cell Rep. *17*, 2660–2671.

Su, W., and Kowalczyk, A.P. (2016). The VE-cadherin cytoplasmic domain undergoes proteolytic processing during endocytosis. Mol. Biol. Cell.

Takeichi, M. (1977). Functional correlation between cell adhesive properties and some cell surface proteins. J. Cell Biol. *75*, 464–474.

Taulet, N., Comunale, F., Favard, C., Charrasse, S., Bodin, S., and Gauthier-Rouvière, C. (2009). N-cadherin/p120 catenin association at cell-cell contacts occurs in cholesterol-rich membrane domains and is required for RhoA activation and myogenesis. J. Biol. Chem. *284*, 23137–23145.

Tepass, U., and Hartenstein, V. (1994). The development of cellular junctions in the Drosophila embryo. Dev. Biol. *161*, 563–596.

Thoreson, M.A., Anastasiadis, P.Z., Daniel, J.M., Ireton, R.C., Wheelock, M.J., Johnson, K.R., Hummingbird, D.K., and Reynolds, A.B. (2000). Selective Uncoupling of P120ctn from E-Cadherin Disrupts Strong Adhesion. J. Cell Biol. *148*, 189–202.

Toret, C.P., D'Ambrosio, M.V., Vale, R.D., Simon, M.A., and Nelson, W.J. (2014). A genome-wide screen identifies conserved protein hubs required for cadherin-mediated cell–cell adhesion. J Cell Biol *204*, 265–279.

Troyanovsky, R.B., Sokolov, E.P., Troyanovsky, S.M., and Nusrat, A. (2006). Endocytosis of Cadherin from Intracellular Junctions Is the Driving Force for Cadherin Adhesive Dimer Disassembly. Mol. Biol. Cell *17*, 3484–3493.

van de Ven, R.A.H., Tenhagen, M., Meuleman, W., van Riel, J.J.G., Schackmann, R.C.J., and Derksen, P.W.B. (2015). Nuclear p120-catenin regulates the anoikis resistance of mouse lobular breast cancer cells through Kaiso-dependent Wnt11 expression. Dis. Model. Mech. *8*, 373–384.

Wang, Y., Zhang, H., Shi, M., Liou, Y.-C., Lu, L., and Yu, F. (2017). Sec71 functions as a GEF for the small GTPase Arf1 to govern dendrite pruning of Drosophila sensory neurons. Development *144*, 1851–1862.

Weigel, P.H., and Oka, J.A. (1981). Temperature dependence of endocytosis mediated by the asialoglycoprotein receptor in isolated rat hepatocytes. Evidence for two potentially rate-limiting steps. J. Biol. Chem. *256*, 2615–2617.

Wells, A., Yates, C., and Shepard, C.R. (2008). E-cadherin as an indicator of mesenchymal to epithelial reverting transitions during the metastatic seeding of disseminated carcinomas. Clin. Exp. Metastasis *25*, 621–628.

Wickström, S.A., and Niessen, C.M. (2018). Cell adhesion and mechanics as drivers of tissue organization and differentiation: local cues for large scale organization. Curr. Opin. Cell Biol. *54*, 89–97.

Xiao, K., Allison, D.F., Buckley, K.M., Kottke, M.D., Vincent, P.A., Faundez, V., and Kowalczyk, A.P. (2003). Cellular levels of p120 catenin function as a set point for cadherin expression levels in microvascular endothelial cells. J. Cell Biol. *163*, 535–545.

Yap, A.S., Niessen, C.M., and Gumbiner, B.M. (1998). The juxtamembrane region of the cadherin cytoplasmic tail supports lateral clustering, adhesive strengthening, and interaction with p120ctn. J. Cell Biol. *141*, 779–789.

Yu, H.H., Dohn, M.R., Markham, N.O., Coffey, R.J., and Reynolds, A.B. (2016). p120-catenin controls contractility along the vertical axis of epithelial lateral membranes. J. Cell Sci. *129*, 80–94.

Zebda, N., Tian, Y., Tian, X., Gawlak, G., Higginbotham, K., Reynolds, A.B., Birukova, A.A., and Birukov, K.G. (2013). Interaction of p190RhoGAP with C-terminal domain of p120-catenin modulates endothelial cytoskeleton and permeability. J. Biol. Chem. *288*, 18290–18299.

Figures

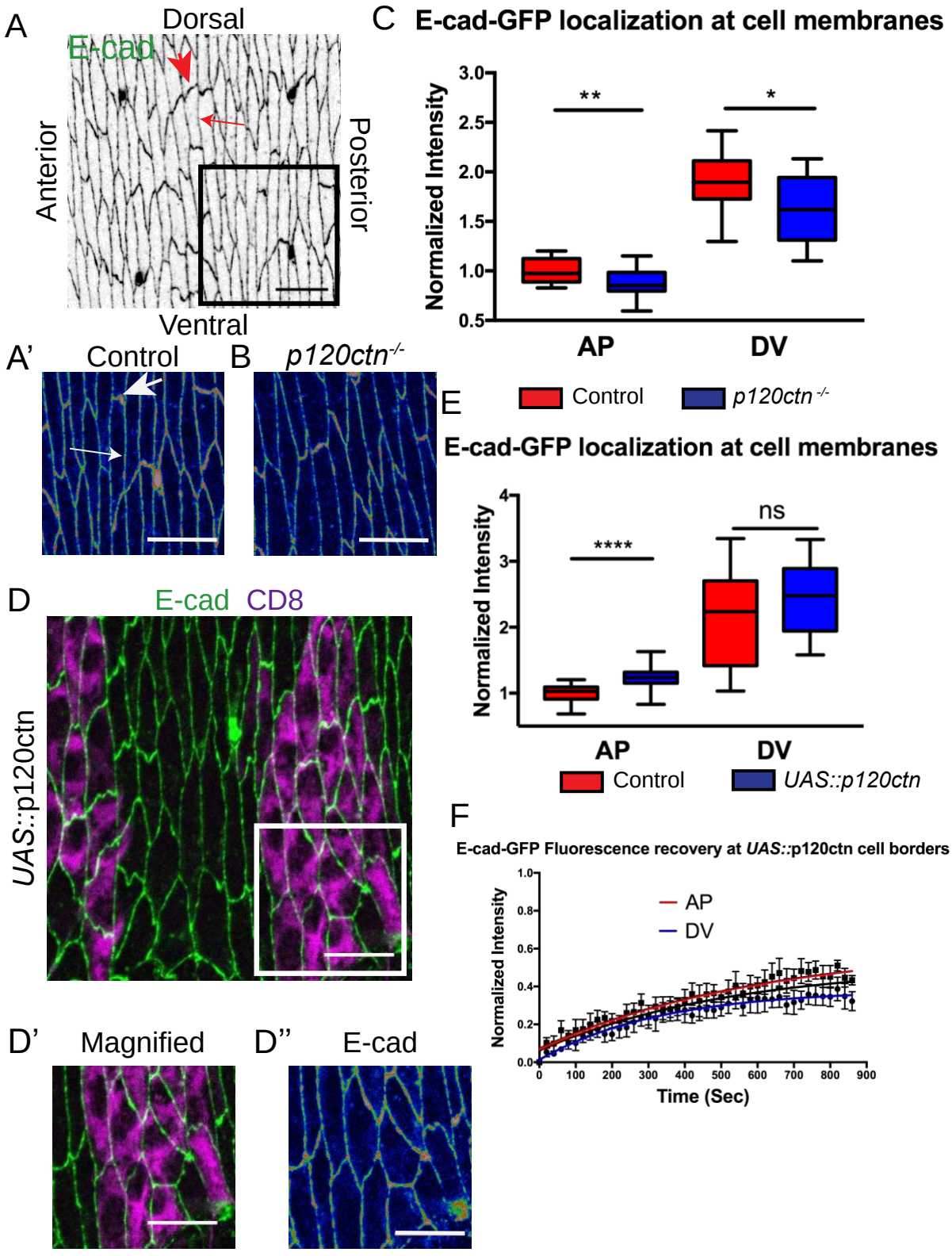
A
Dorsal
E-cad
Anterior
Posterior
Ventral
A'
Control
B
p120ctn-/-
C
E-cad-GFP localization at cell membranes
Normalized Intensity
3.0
2.5
2.0
1.5
1.0
0.5
**
*
AP
DV
Control
p120ctn -/-
D
E-cad CD8
UAS::p120ctn
D'
Magnified
D''
E-cad
E
E-cad-GFP localization at cell membranes
Normalized Intensity
4
3
2
1
****
ns
AP
DV
Control
UAS::p120ctn
F
E-cad-GFP Fluorescence recovery at UAS::p120ctn cell borders
Normalized Intensity
1.0
0.8
0.6
0.4
0.2
0.0
AP
DV
0
100
200
300
400
500
600
700
800
900
Time (Sec)

Figure 1. p120ctn levels determine the amount and dynamics of E-cad at the membrane. **A-B.** Apical view of the dorsolateral epidermis of stage 15 *Drosophila* wild type (**A-A'**) and *p120ctn*$^{-/-}$ mutant embryos (**B**) with cell outlines visualized by endogenously tagged E-cad-GFP using the rainbow spectrum for pixel intensity. Two distinct cell borders exist: the longer Anterior-Posterior (AP, large arrow) and the short Dorsal-Ventral (DV, small arrow). (**A'**) Magnified image indicated in the box of (A), scale bar is 10 µm. **C.** Quantification of the E-cad-GFP amount at the plasma membranes. **D.** Apical view of epidermis co-expressing *UAS::*p120ctn with *UAS::*CD8-Cherry using *en::*GAL4 with E-cad-GFP (green in D-D' and rainbow in D'') and *UAS::*CD8-Cherry (magenta in D-D'). *UAS::*CD8-Cherry was used to mark cells expressing transgenes. (**D'-D''**) magnified region indicated in (D), scale bar is 10 µm. **E.** Quantification of the E-cad-GFP at the plasma membrane in *UAS::*p120ctn and internal control. **F.** Dynamics of E-cad-GFP measured by FRAP in the *UAS::*p120ctn. Average recovery curves (mean ± s.e.m.) and the best-fit curves (solid lines) are shown. All best-fit and membrane intensity data are in Table S1. Bars in C and E represent difference between cell borders in genotypes measured by two-way ANOVA. *, $P < 0.05$; **, $P < 0.01$ ***, $P < 0.001$. 10-20 embryos per genotype were used for intensity quantifications; 8-10 embryos for FRAP.

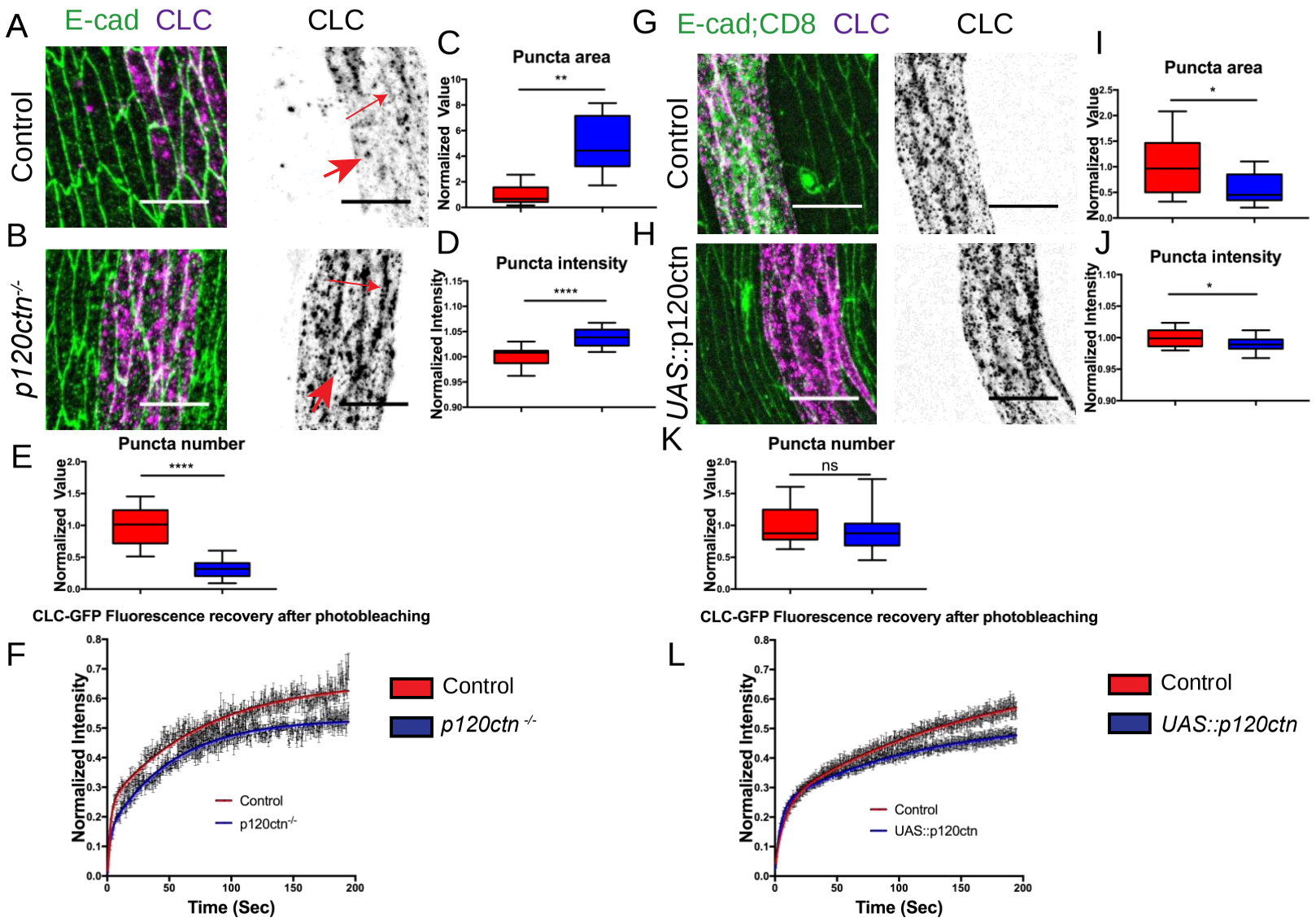
A
E-cad CLC
CLC
Control
B
p120ctn-/-
C
Puncta area
**
Normalized Value
D
Puncta intensity
****
Normalized Intensity
E
Puncta number
****
Normalized Value
CLC-GFP Fluorescence recovery after photobleaching
F
Normalized Intensity
Time (Sec)
Control
p120ctn -/-
G
E-cad;CD8 CLC
CLC
Control
H
UAS::p120ctn
I
Puncta area
*
Normalized Value
J
Puncta intensity
*
Normalized Intensity
K
Puncta number
ns
Normalized Value
CLC-GFP Fluorescence recovery after photobleaching
L
Normalized Intensity
Time (Sec)
Control
UAS::p120ctn

Figure 2. p120ctn regulation of E-cad is via the clathrin-mediated endocytic pathway. The localization of the clathrin light chain (*UAS*::CLC-GFP) in *p120ctn*$^{-/-}$ mutant embryos (**A**), and embryos overexpressing p120ctn (*UAS*::p120ctn, **G**). **B** and **H** show the corresponding controls. Distinct puncta (spots, magenta in left and black in right images, arrows) are observed at the membrane and in the cytoplasm. Cell outlines are visualized by anti-E-cad antibody staining (green in left images). Note that in control for p120ctn overexpression, there is additionally signal from UAS::CD8-mCherry in green. (**C-E** and **I-K**) Quantification of the clathrin puncta in *p120ctn*$^{-/-}$ mutant embryos (**C**-**E**), and embryos overexpressing p120ctn (*UAS*::p120ctn) (**I-K**) by measuring the area (size, **C** and **I**), intensity (**D** and **J**), and the number (**E** and **K**). (**F** and **L**) FRAP of *UAS*::CLC-GFP in *p120ctn*$^{-/-}$ mutant (**F**), and embryos overexpressing p120ctn (*UAS*::p120ctn) (**L**). Average recovery curves (mean ± s.e.m.) and the best-fit curves (solid lines) are shown in F and L. Statistical analysis is a two-tailed students t-test with Welch's correction. All best-fit and membrane intensity data are in Table S1. *, $P < 0.05$; **, $P < 0.01$ ****, $P < 0.0001$. 10-20 embryos per genotype were used for puncta quantifications; 8-10 embryos – for FRAP.

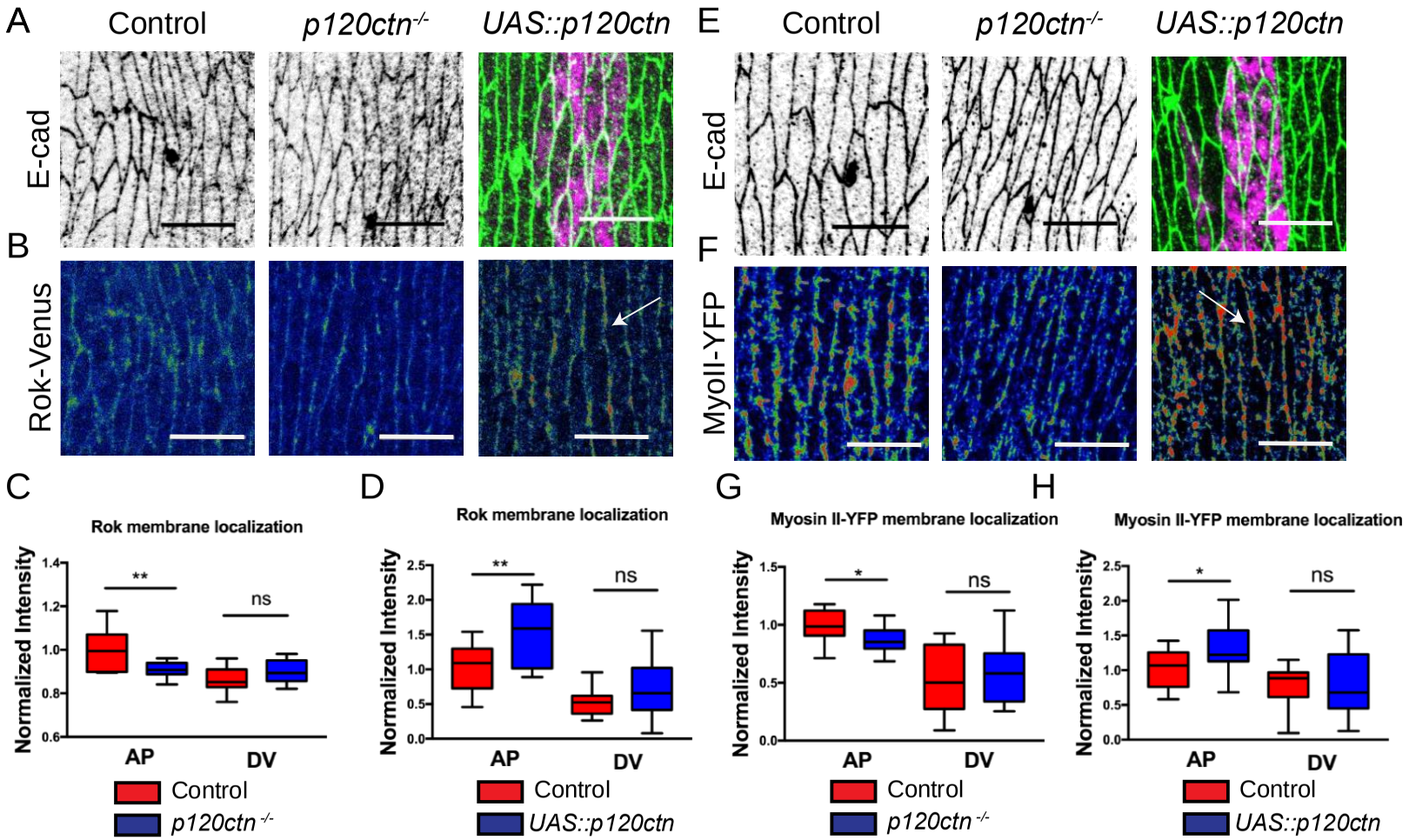
A
Control
p120ctn-/-
UAS::p120ctn
E-cad
B
Rok-Venus
E
Control
p120ctn-/-
UAS::p120ctn
E-cad
F
MyoII-YFP
C
Rok membrane localization
Normalized Intensity
**
ns
AP
DV
Control
p120ctn -/-
D
Rok membrane localization
Normalized Intensity
**
ns
AP
DV
Control
UAS::p120ctn
G
Myosin II-YFP membrane localization
Normalized Intensity
*
ns
AP
DV
Control
p120ctn -/-
H
Myosin II-YFP membrane localization
Normalized Intensity
*
ns
AP
DV
Control
UAS::p120ctn

Figure 3. p120ctn activates RhoA signalling at the plasma membrane.

A-B. Apical view of the epidermis of control, *p120ctn*$^{-/-}$ mutant, and p120ctn overexpression (*UAS::*p120ctn) embryos visualized with anti-E-cad antibody (**A**, grey in the left and middle images, green in the right image), *UAS*::CD8-mCherry (**A**, magenta in the right image, marks cells expressing *UAS::*p120ctn) and Rho-Kinase (Rok) tagged with Venus (**B,** rainbow pixel intensity spectrum, membrane indicated by arrow). **C-D.** Quantification of Rok-Venus in the *p120ctn*$^{-/-}$ mutant (**C**) and p120ctn overexpressing embryos (**D**). **E-F.** The epidermis of control, *p120ctn*$^{-/-}$ mutant and p120ctn overexpression (*UAS::*p120ctn) embryos visualized with anti-E-cad antibody (**E**, grey in the left and middle images, green in the right image), *UAS*::CD8-mCherry (**E**, magenta in the right image, marks cells expressing *UAS::*p120ctn), and Myosin II (MyoII) tagged with YFP (**F,** rainbow pixel intensity spectrum, membrane indicated by arrow). **G-H.** Quantification of MyoII-YFP in the *p120ctn*$^{-/-}$ mutant (**G**) and p120ctn overexpressing embryos (**H**). All membrane intensity data are in Table S1. Scale bars – 10 µm. Upper bars in **C, D, G** and **H** represent difference between genotypes and the lower - between cell borders measured by two-way ANOVA. *, $P < 0.05$; **, $P < 0.01$. 12-20 embryos per genotype were quantified.

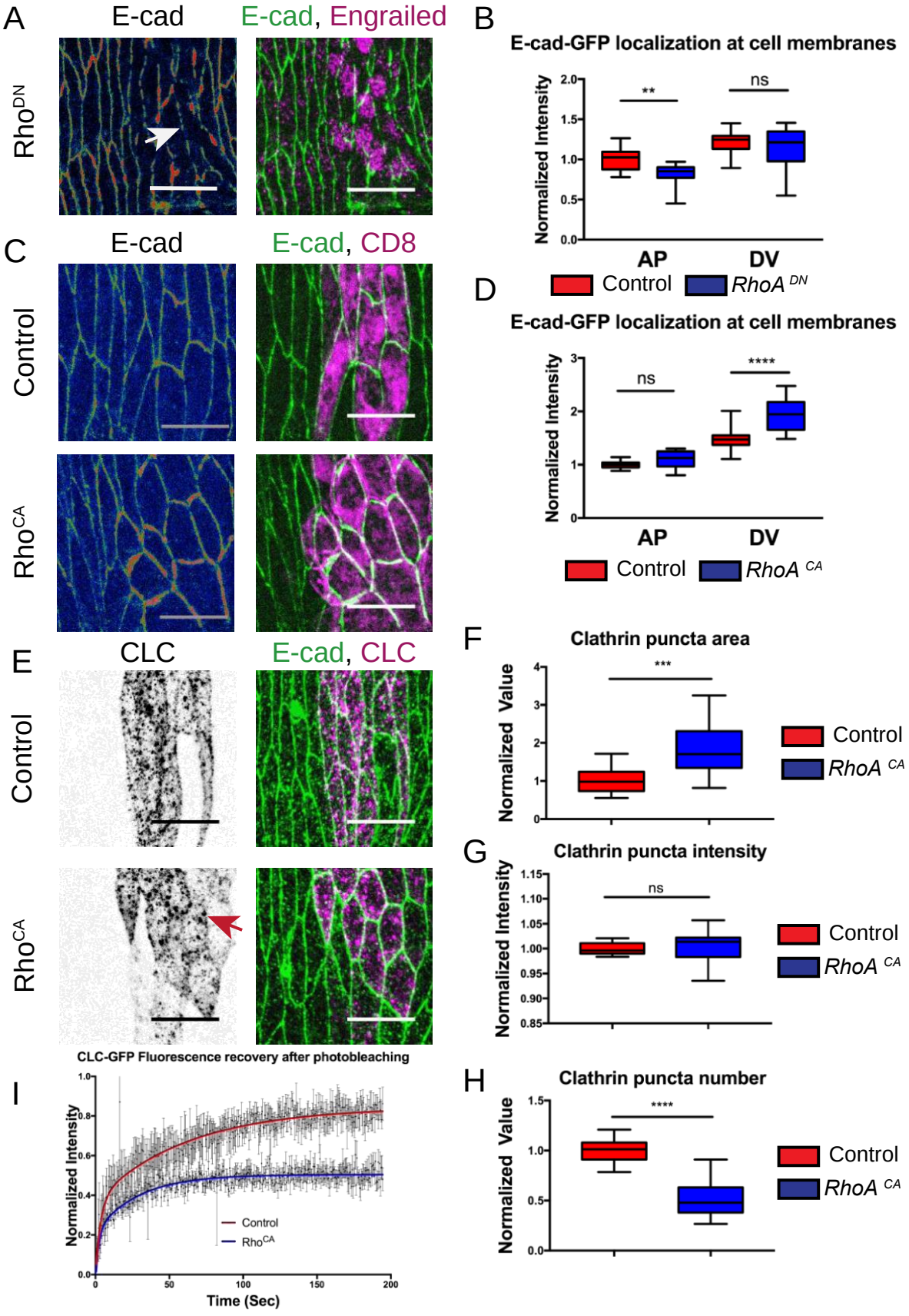
A
E-cad
E-cad, Engrailed
Rho^DN
B
E-cad-GFP localization at cell membranes
Normalized Intensity
**
ns
AP
DV
Control
RhoA DN
C
E-cad
E-cad, CD8
Control
Rho^CA
D
E-cad-GFP localization at cell membranes
Normalized Intensity
ns
****
AP
DV
Control
RhoA CA
E
CLC
E-cad, CLC
Control
Rho^CA
F
Clathrin puncta area
Normalized Value
***
Control
RhoA CA
G
Clathrin puncta intensity
Normalized Intensity
ns
Control
RhoA CA
H
Clathrin puncta number
Normalized Value
****
Control
RhoA CA
I
CLC-GFP Fluorescence recovery after photobleaching
Normalized Intensity
Control
Rho^CA
Time (Sec)

Figure 4. RhoA activity promotes the stabilization, and opposes the internalization, of E-cad at the membrane.

A-D. Localization of E-cad in the epidermis following downregulation (the induction of Rho^{DN} expression for 4 hours, **A-B,** membrane indicated by arrow) or upregulation (expression of Rho^{CA}, **C-D)** of Rho signalling. Top images in **C** are the corresponding control expressing *UAS*::CD8-Cherry alone. Cell borders are marked by E-cad-GFP (rainbow spectrum in left, green in right images). Cells expressing transgenes are marked with an antibody for Engrailed (**A**) or by *UAS::*CD8-Cherry (**C**). Quantification of the E-cad-GFP at the membrane of the Rho^{DN} (**B**) or Rho^{CA} (**D**) expressing cells in comparison to internal control (**B**) or external controls (**D**). The total amount of E-cad-GFP per cell upon Rho^{CA} expression is in Fig. S3. **E.** Localization of clathrin (*UAS*::CLC-GFP, grey in left, magenta in right images) in cells co-expressing Rho^{CA} (bottom) and corresponding control co-expressing *UAS*::CD8-Cherry (top). Cell borders are visualized by anti-E-cad antibody staining (green in right images, arrow indicates membrane localized puncta). **F-H.** Quantification of the clathrin puncta area (F), intensity (G), and number (H) in the Rho^{CA} expressing cells. **I.** FRAP of *UAS*::CLC-GFP in Rho^{CA} expressing cells. Average recovery curves (mean ± s.e.m.) and the best-fit curves (solid lines) are shown. All best-fit and membrane intensity data are in Table S1. Scale bars – 10 μm. **, $P < 0.01$ ***, $P < 0.001$; ****, $P < 0.0001$. 10-20 embryos per genotype were used for puncta quantifications; 8-10 embryos – for FRAP.

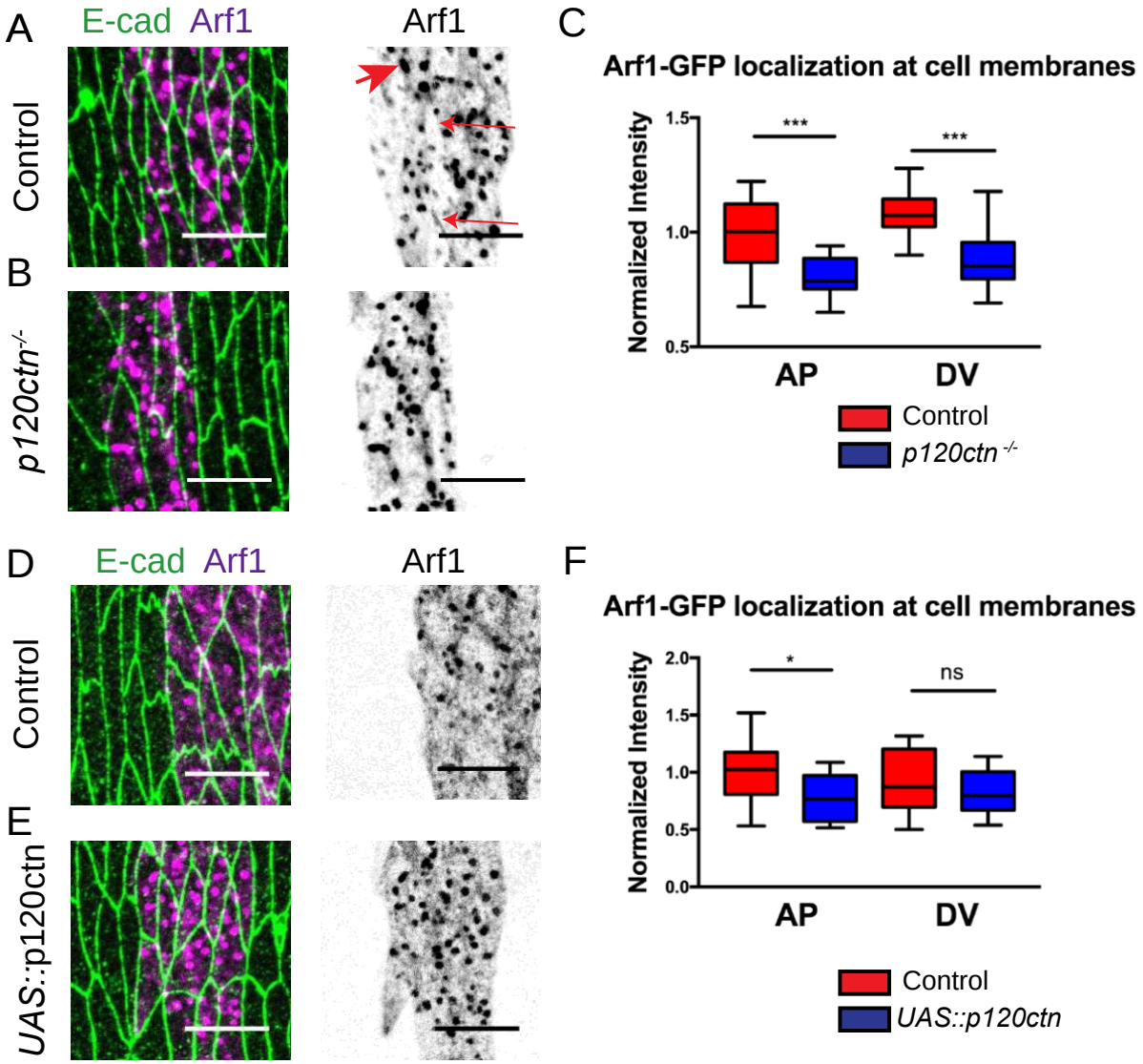
A
E-cad Arf1
Arf1
Control
B
p120ctn-/-
C
Arf1-GFP localization at cell membranes
Normalized Intensity
1.5
1.0
0.5
***
***
AP
DV
Control
p120ctn -/-
D
E-cad Arf1
Arf1
Control
E
UAS::p120ctn
F
Arf1-GFP localization at cell membranes
Normalized Intensity
2.0
1.5
1.0
0.5
0.0
*
ns
AP
DV
Control
UAS::p120ctn

Figure 5. Arf1 is a downstream interactor of p120ctn.

Apical views of the epidermis expressing *UAS*::Arf1-GFP (Arf1, magenta in left , grey in right images) with *en*::Gal4 in *p120ctn*$^{-/-}$ mutant (**B**), overexpressing p120ctn (*UAS*::p120ctn, **E**), and corresponding control embryos (**A** and **D**). Cell outlines are visualized with anti-E-cad antibody staining (green in left images). The large UAS::Arf1-GFP puncta in the cytoplasm (large arrow in A) marks the Golgi (see Fig. S3). The small arrow in A indicates the membrane resident population of Arf. (**C** and **F**) Quantification of the amount of *UAS*::Arf1-GFP at the plasma membrane between a control and *p120ctn*$^{-/-}$ mutant (**C**), and control and p120ctn overexpressing (**F**) embryos. All membrane intensity data are in Table S1. Scale bars – 10 µm. Upper bars in C and F represent difference between genotypes and the lower - between cell borders measured by two-way ANOVA. *, $P < 0.05$; ***, $P < 0.001$. 10-20 embryos per genotype were quantified.

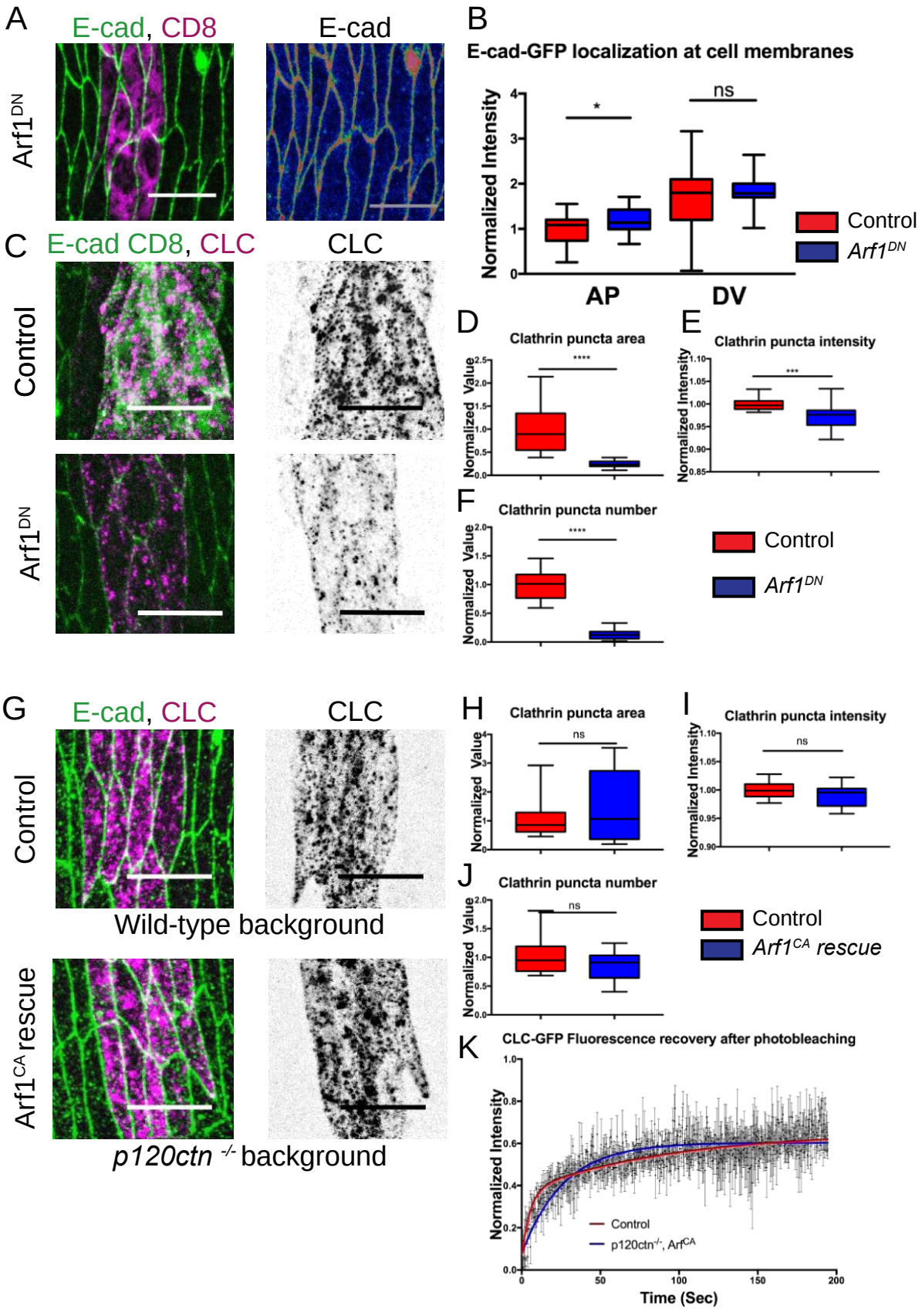
A
E-cad, CD8
E-cad
Arf1DN
B
E-cad-GFP localization at cell membranes
Normalized Intensity
*
ns
AP
DV
Control
Arf1DN
C
E-cad CD8, CLC
CLC
Control
Arf1DN
D
Clathrin puncta area
Normalized Value
****
E
Clathrin puncta intensity
Normalized Intensity
***
F
Clathrin puncta number
Normalized Value
****
Control
Arf1DN
G
E-cad, CLC
CLC
Control
Wild-type background
Arf1CA rescue
p120ctn -/- background
H
Clathrin puncta area
Normalized Value
ns
I
Clathrin puncta intensity
Normalized Intensity
ns
J
Clathrin puncta number
Normalized Value
ns
Control
Arf1CA rescue
K
CLC-GFP Fluorescence recovery after photobleaching
Normalized Intensity
Control
p120ctn-/-, ArfCA
Time (Sec)

Figure 6. Arf1 activity promotes the clathrin-mediated internalization of E-cad, and rescues the defects in clathrin localization and dynamics in p120ctn mutant background. Localization of E-cad (E-cad-GFP, **A**, grey in left, green in right image) and *UAS*::CLC-GFP (**C**, grey in left, green in right images) in cells expressing a dominant negative variant of Arf1 ($Arf1^{DN}$) with *en*::GAL4. Cell borders are visualized with E-cad-GFP (A) and anti-E-cad antibody staining (C, right image). *UAS*::CD8-Cherry was used to mark cells expressing $Arf1^{DN}$ in A (magenta, right image) and to balance the dose of GAL4-UAS (C, green, top images). (**B**) Quantification of the amount of E-cad-GFP at the plasma membranes of the $Arf1^{DN}$ cells compared to adjacent internal control cells. (**D**-**F**) Quantification of the *UAS*::CLC-GFP puncta area (**D**), intensity (**E**), and number (**F**) in the plane of AJs in the $Arf1^{DN}$ cells. (**G**) Localization of *UAS*::CLC-GFP (grey in left, magenta in right images) in *wt* control, expressing *UAS*::CLC-GFP alone (top), and in embryos expressing a constitutively active Arf1 ($Arf1^{CA}$) in a $p120ctn^{-/-}$ mutant genetic background (bottom). Cell borders were visualized with anti-E-cad antibody staining (green in right images). (**H**-**J**) Quantification of the *UAS*::CLC-GFP puncta area (**H**), intensity (**I**), and number (**J**) in the plane of AJs in the $Arf1^{CA}$; $p120ctn^{-/-}$ embryos. (**K**) FRAP of *UAS*::CLC-GFP in the plane of AJs in the $Arf1^{CA}$; $p120ctn^{-/-}$ embryos. Average recovery curves (mean ± s.e.m.) and the best-fit curves (solid lines) are shown in K. All best-fit and membrane intensity data are in Table S1. Scale bars – 10 µm. *, $P < 0.05$; ***, $P < 0.001$; ****, $P < 0.0001$. 10-20 embryos per genotype were used for puncta quantifications; 8-10 embryos – for FRAP.

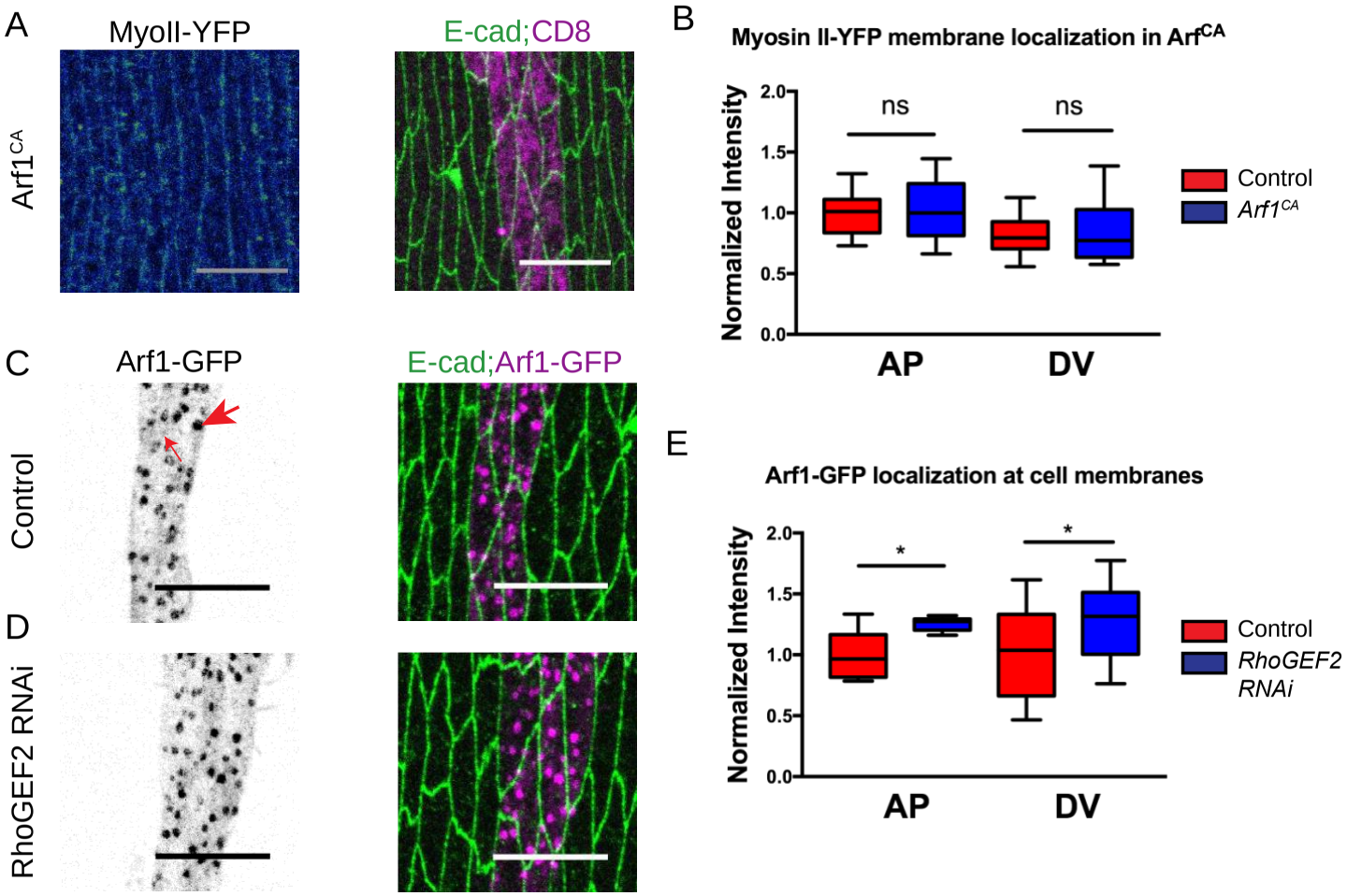
A
MyoII-YFP
E-cad;CD8
Arf1CA
B
Myosin II-YFP membrane localization in ArfCA
Normalized Intensity
2.0
1.5
1.0
0.5
0.0
ns
ns
AP
DV
Control
Arf1CA
C
Arf1-GFP
E-cad;Arf1-GFP
Control
D
RhoGEF2 RNAi
E
Arf1-GFP localization at cell membranes
Normalized Intensity
2.0
1.5
1.0
0.5
0.0
*
*
AP
DV
Control
RhoGEF2
RNAi

Figure 7. RhoA signalling inhibits Arf1 and is independent of it.

A. Localization of MyoII-YFP (rainbow in left image) in the cells expressing a constitutively active Arf1 ($Arf1^{CA}$) with *en*::GAL4 marked by *UAS::*CD8-Cherry (magenta in right image). Cell borders are visualized with anti-E-cad antibody staining (green in right image). **B.** Quantification of the MyoII-YFP at the plasma membranes of the $Arf1^{CA}$ cells and the adjacent internal control cells. **C**-**D.** The localization of *UAS::*Arf1-GFP (grey in left images, magenta in right images) in control (**C)** and cells expressing RhoGEF2 RNAi (**D**). Large arrow indicates the Golgi resident Arf1 and the small arrow indicate the membrane resident population **(C)**. Cell borders were visualized with anti-E-cad antibody staining (green in right images). **E.** Quantification of the amount of *UAS::*Arf1-GFP at the plasma membranes of the RhoGEF2RNAi expressing cells. All membrane intensity data are in Table S1. Scale bars – 10 μm. *, $P < 0.05$. 10-20 embryos per genotype were quantified.

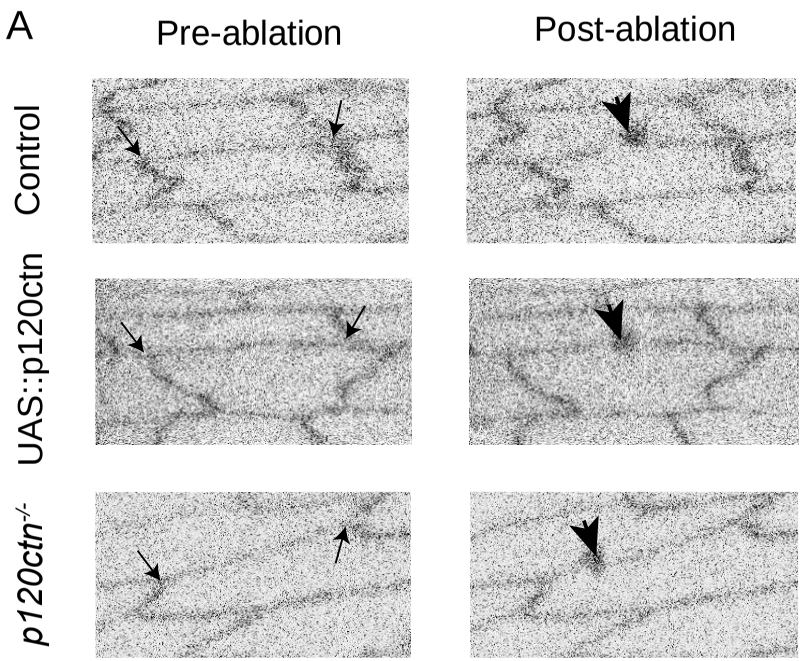
A
Pre-ablation
Post-ablation
Control
UAS::p120ctn
p120ctn-/-

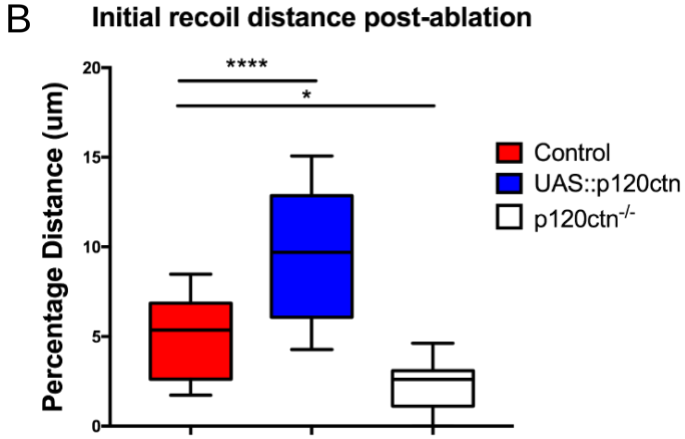
B
Initial recoil distance post-ablation
Percentage Distance (um)
20
15
10
5
0
****
*
Control
UAS::p120ctn
p120ctn-/-

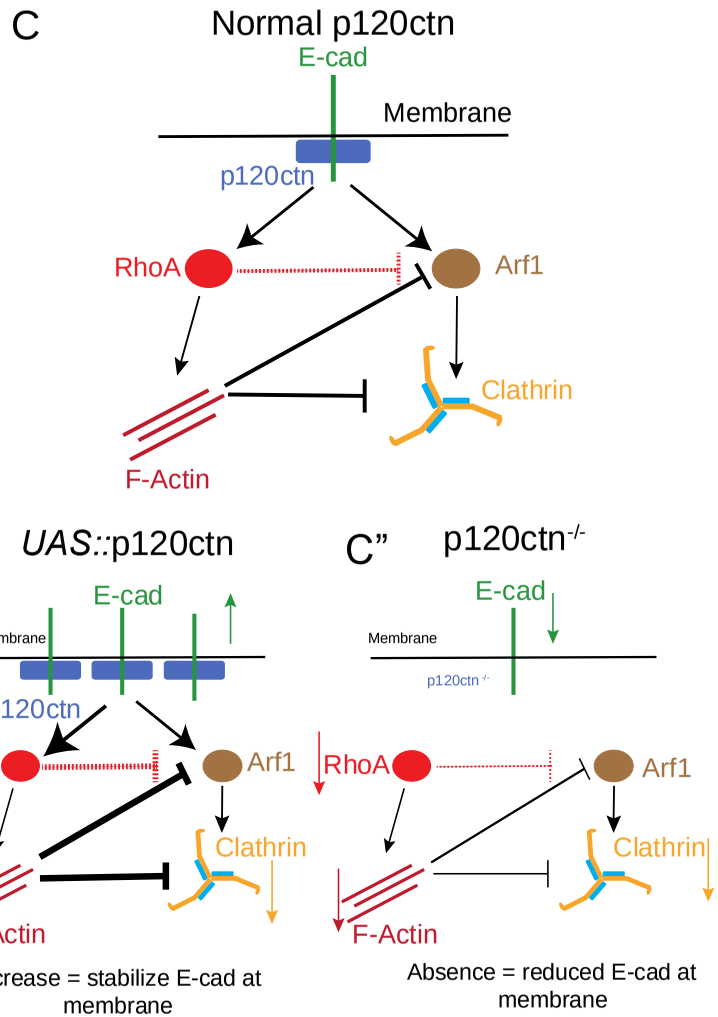
C
Normal p120ctn
E-cad
Membrane
p120ctn
RhoA
Arf1
Clathrin
F-Actin
C'
UAS::p120ctn
C"
p120ctn-/-
Increase = stabilize E-cad at membrane
Absence = reduced E-cad at membrane

Figure 8. p120ctn increases the tension at the plasma membrane, and the model of p120ctn action.

A. Examples of laser ablation in epidermal cells in control (top), p120ctn mutant (*p120ctn*$^{-/-}$, middle), and p120ctn overexpressing (*UAS*::p120ctn, bottom). Cells shown immediately before (left) and after ablation (right). Cell borders are visualized with E-cad-GFP (grey). The small arrows indicate the connected vertices of the ablated membrane used to measure distance. The large arrows represent the position of microablation, for which a small spot of discolouration can be observed. **B.** Quantification of the initial recoil, expressed as a percentage increase in distance relative to the length of the membrane prior to ablation. **C.** Model of the interaction between p120ctn, RhoA, Arf1, clathrin, and actin. p120ctn acts on both Arf1 and RhoA signalling pathways: RhoA promotes the stabilization of E-cad and Arf1 promotes E-cad internalization by recruiting clathrin. RhoA additionally inhibits Arf1, possibly directly (dashed red lines) or indirectly by increasing the density of the cortical actin. (**C'**) Overexpression of p120ctn leads to overactivation of the RhoA, resulting in an increase in cortical actin and suppression of Arf1. This results in an increase in E-cad amount and stability at the membrane. (**C"**) In the absence of p120ctn the RhoA and Arf1 are not stimulated. Therefore, cortical actin tension, clathrin mediated endocytosis, and E-cad levels are reduced. Scale bar – 10μm. *, $P < 0.05$; ***, $P < 0.001$. 14-20 embryos per genotype.

Supplementary Information

Table S1. Numerical values for each experiment presented in paper.

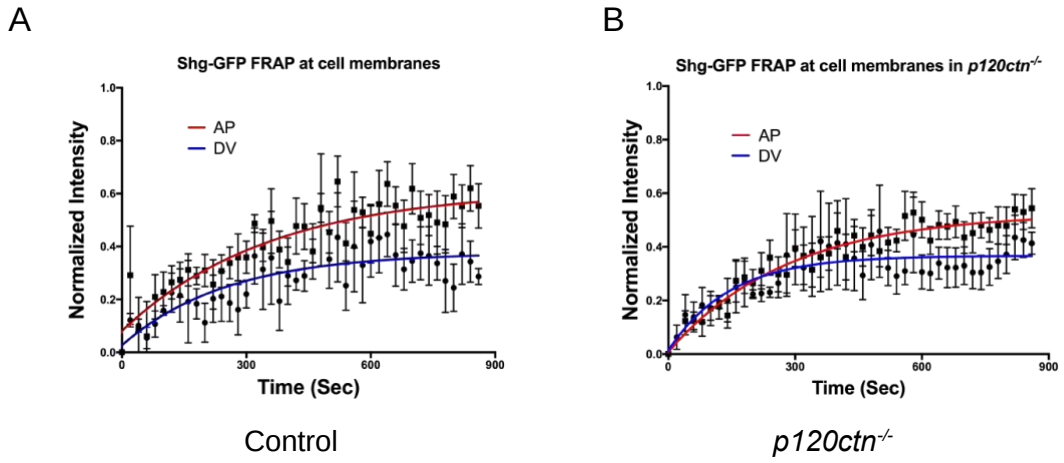

Figure S1. Shg-GFP is less dynamic at both cell borders in the p120ctn mutant.

A-B. Recovery of fluorescent intensity during the course of a FRAP experiment for the control (**A**) and p120ctn mutant embryos (**B**), measured at both the AP and DV cell borders. Average recovery curves (mean ± s.e.m.) and the best-fit curves (solid lines) are shown. All best-fit and membrane intensity data are in Table S1.

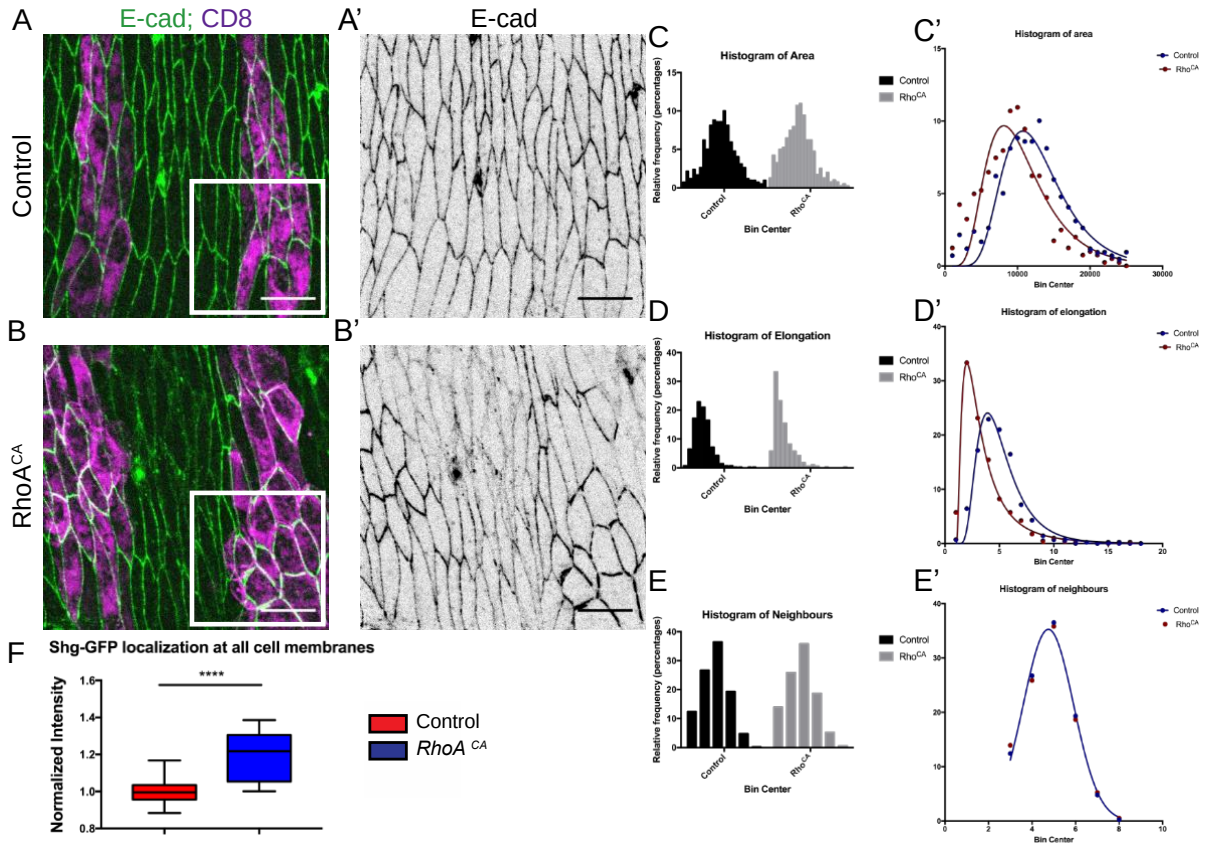

Figure S2. Rho^{CA} induces substantial changes in cellular morphology and an increase in Shg-GFP at the membrane.

A-B .Apical view of the dorsolateral epidermis of control embryos (expressing CD8-m-Cherry transgene, **A-A'**, magenta in **A**), and embryos expressing RhoA^{CA} transgene with *en*::Gal4 (B-B', visualized with CD8-m-Cherry, magenta in **A**). Lower magnification images presented with white square representing region are shown in main figure (see Fig. 4). The cell membranes marked by E-cad-GFP are shown in green (**A, B**) and black (**A',B'**). **C.** Histograms of the cell area, comparing engrailed regions of control and RhoA^{CA} expressing cells: individual distributions (**C**) and overlaid frequency distributions (**C'**). **D.** Histograms of the elongation of the cells, shown as individual (**D**) and overlaid (**D'**). **E.** Histograms of the distribution of cell neighbours, both as individual distributions (**E**) and overlaid curves (**E**'). **F.** Quantification of the amount of Shg-GFP at the cell membrane, calculating total membrane without angle dependence (division into AP and DV borders). Statistical analysis is a two-tailed students t-test with Welches correction *, $P < 0.05$; **, $P < 0.001$; ***, $P < 0.0001$. Scale bar is 10 µm.

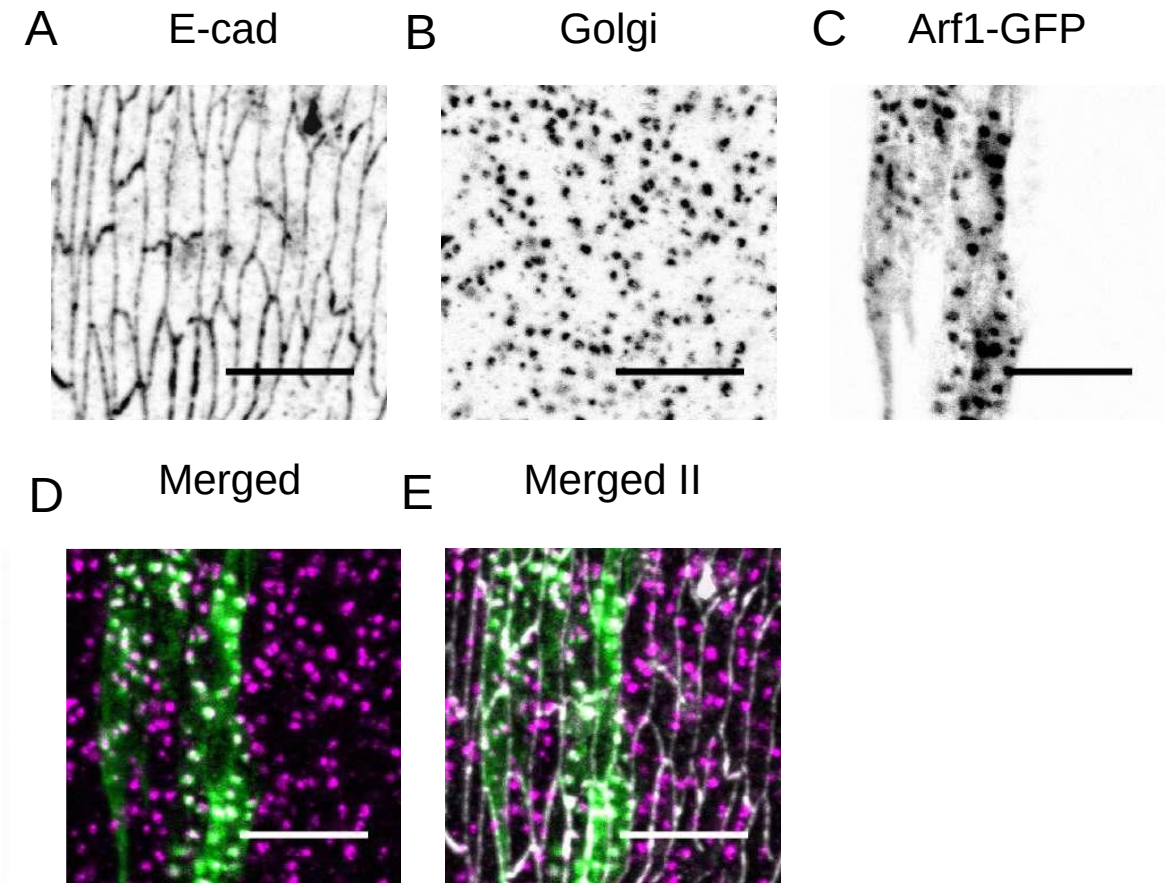

Figure S3. Arf1-GFP cytoplasmic puncta are representative of the Golgi apparatus.
A-E. Apical view of the dorsolateral epidermis of *UAS::*Arf1-GFP expressing control embryo with cells borders are marked by antibody staining of E-cad (black in **A**, white in **E**), Golgi marked by immunostaining of Trans-Golgi (black in **B**, magenta in D and E), and Arf1-GFP localization in the engrailed expressing cells (black in **C,** green in **D** and **E)**. The same region is shown in main text (see Fig. 5). Scale bar is 10 µm.

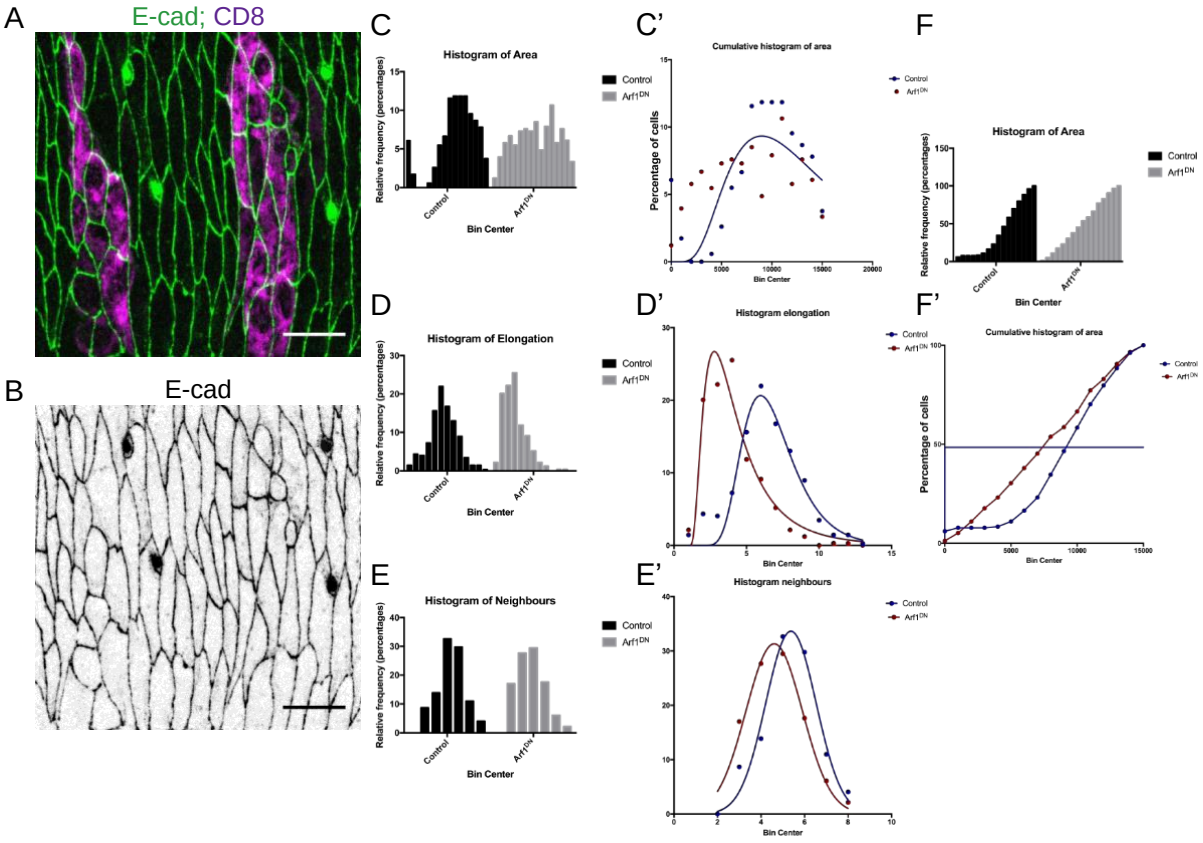

Figure S4. Arf1^{DN} induces cell morphology changes leading to cell death.

A-B. Apical view of the dorsolateral epidermis of Arf1^{DN} transgene expressing embryos, co-expressing *UAS::*CD8-cherry in the engrailed stripes to mark the cells (magenta in **A**). The cell borders are marked by Shg-GFP (green in A, black in B). Scale bar is 10 µm. **C.** Histograms of the frequency distributions of the cell area between the Arf1^{DN} expressing cells and the adjacent internal control cells, shown as both the individual distributions (**C**) and overlaid (**C'**). **D.** Histograms of the frequency distributions of the cell elongations between the Arf1^{DN} and the internal control cell. Individual and overlaid to display modal shift. **E.** Histograms of the frequency distributions of the cell neighbours shown as individual (**E**) and overlaid (**E**'). Horizontal line represents 50% threshold for each cumulative distribution (**E'**). **F.** Histograms showing the cumulative distributions of the cell area showing the individual cumulative distributions (**F**) and the overlaid curves (**F'**).

Chapter 4: Examination of the 3rd Instar Wing Imaginal Disc and p120ctn dynamics

4.1) Introduction

In the previous chapter I presented the findings obtained during the course of this research which yielded new insights into the molecular mechanism of p120ctn activity on E-cad at the plasma membrane. By necessity these results represented those which were the most complete body of evidence for elucidating the mechanism of p120ctn action on E-cad. However, during the course of this work other data were obtained which, while no less interesting than that which was previously presented, was not directly related to the mechanistic understanding of p120ctn presented in the previous chapter. Therefore, for narrative simplicity and the ease of comprehension of the reader these were omitted. In the following three results chapters the unpublished data which was obtained during this research project shall be presented. They represent in turn: the examination of the interactors in the wing disc (see explanation below) with exploration of the dynamics of the p120ctn protein itself, the investigation of p120ctn action beyond the plasma membrane by using Arf1 to examine the Golgi and the associated transportation and trafficking which occurs therein, and finally an investigation of the endosomal trafficking pathway directly using the p120ctn mutant genotype to characterise the specific processes and pathways within the endosomal sorting system which are affected by the absence of p120ctn.

The current chapter presents the work undertaken in the larval wing disc. During the initial screen of candidate p120ctn interactors a combination of the embryonic epidermis and 3rd instar larval wing disc were used to provide two complementary epithelial tissue. This was done to ensure that any results obtained were not merely the result of the developmental stage examined, nor the result of some special or particular feature of a specific epithelial tissue. The results presented are the initial screen of tagged interactors using the genetic ablation of p120ctn (*p120ctn* $^{-/-}$ mutants, see Chapter 2) with fluorescently tagged candidate interactors. A limited volume of data is available because the use of the wing disc was largely abandoned in favour of the embryonic epidermis in experiments beyond the initial genetic screen. This was done to ensure consistency of the experimental tissue used for all the findings which formed the results presented in the manuscript derived from this work (see Chapter 3). The reasoning behind the choice of the embryonic epidermis over the wing disc was both scientific and scholastic. First, the embryonic epidermis has the advantage of ease of observation by being a superficial structure as well as ease of live imaging, and has a consistent pattern of morphogens and, as I came to appreciate later, a stereotypic and

opposing pattern of mechanical force distribution which correlates to the asymmetry of E-cad localization between the two district cell borders (see Chapter 3 Figure 8). The second scholastic argument arises from the previous literature in the field. Most prior studies, including those from within the lab, have used the embryonic epidermis to investigate E-cad and the function of p120ctn, while using the wing disc for specific experimental purposes when the embryonic tissue would be technically difficult to access (Bulgakova and Brown, 2016).

The 3rd instar larval wing disc (WD) is a well characterised and commonly used epithelial tissue to study the expression of transgenic constructs to examine the role of proteins and genes in the development of the tissue and the regulation of the multiple morphogenic events such as cell proliferation and tissue folding which occur during the maturation of the tissue (Bryant, 1975; Liu et al., 2016; Sui et al., 2018). The use of this tissue predates that of the embryonic epidermis but not that of the embryo in entirety (Bryant, 1975), the WD has distinctive patterns of growth factor expression and well characterised compartmentalization between the anterior and posterior sections, and the proximal and distal sections which can all be marked by the patterns of the wingless and hedgehog signalling pathways (Gou et al., 2018; Irvine and Harvey, 2015; Zecca and Struhl, 2002). In much the same fashion as the study of segmentation in the embryo the pattern of growth and signalling has formed the basis for much of the understanding about the function, role, and molecular mechanism of these growth pathways in the development of multiple organisms and the dysfunction which occurs during the aberrant signalling observed in disease states (Ingham, 2018; Swarup and Verheyen, 2012; Widmann and Dahmann, 2009). In addition to the examination of the gross morphology of the tissue it is possible to isolate stages of development during the maturation of the tissue and explore the effect of any perturbation on the cellular and tissue processes which are most prevalent at the stage in question. Taking these considerations into account provides the basis for the use of the tissue and the results presented in this chapter support the three-key findings presented in the previous Chapter: 1) That p120ctn acts via a clathrin-mediated pathway, 2) p120ctn activates Rho signalling at the plasma membrane, 3) p120ctn recruit and acts via Arf1 at the plasma membrane. The last section of this chapter presents the results of the examination of p120ctn directly using both analysis of its localization in fixed tissue and dynamics using FRAP. This analysis of p120ctn was undertaken to address a key question of its mechanism of action, specifically in reference to the two subpopulations of E-cad (Bulgakova and Brown, 2016; Bulgakova et al., 2013). It was found that p120ctn promotes the internalization of one of the subcomplexes of E-cad,

mobile in association with Par-3 (Bulgakova and Brown, 2016), but the question as to whether this was due to differential binding of p120ctn or differential action remained unknown. The findings presented here have relevance beyond this and point to interesting elements of the dynamics of the protein. As this aspect of the work undertaken in this project are not easily accommodated into the other chapters they are included in the latter section of the current chapter to highlight the interest of the findings.

4.2) Clathrin is mislocalised in p120ctn mutant larvae

To examine the interaction between p120ctn and clathrin in the larval wing disc (WD) I used the same crosses as those used to obtain the embryonic data (see Chapter 3 Fig. 3) and allowed the F1 progeny to develop to the larval stage (further development to the adult stage was undertaken in most experiments to assess adult viability and evidence of overt phenotype in the posterior compartment of the adult wings, data not shown). When using the *engrailed* driver, used for all experiments shown, in the WD there is a clear distinction between the posterior compartment which expressed the driver and the anterior compartment which does not (Guillen et al., 1995). This permits the use of the anterior compartment of each WD to serve as an internal comparative control. To exclude the possibility that some difference was innate between the anterior and posterior compartments I analysed the cell morphology and plasma membrane levels of E-cad-GFP in control genotypes which expressed the *UAS::*CD8-mCherry construct alone (used to balance the ratio between the driver and UAS constructs in all of the controls throughout this work). This analysis indicated that no significant difference was evident between the anterior and posterior compartments, neither cell morphology nor the plasma membrane levels of E-cad-GFP (data not shown). This result enabled me to proceed with the use of the anterior compartment of the experimental genotypes as the internal control for the plasma membrane levels of the protein. This was not possible with the use of transgenes, in these cases the use of an external control was routinely included. The first screen using the transheterozygous loss of p120ctn (*p120ctn* $^{-/-}$ mutants) explored the genetic interaction between p120ctn and the candidate interactors, the first of which was to identify the endocytic pathway used by p120ctn by using a tagged Clathrin light chain construct (*UAS::CLC*-GFP).

Clathrin localized in large distinct puncta through the cytoplasm in the pouch epithelium cells of the WD (Fig. 4.1 A). I further observed some localization at the plasma membrane localizing with E-cad in the plane of the AJ in the images (Fig. 4.1 A, indicated by arrow). In the *p120ctn*$^{-/-}$ mutant larvae the clathrin puncta were more numerous and appeared to be

increased in area to the unaided eye (Fig. 4.1 B). Indeed, in the overlaid image it appeared that some cells were saturated with clathrin in the plane of the AJ (Fig. 4.2 B" lower right quarter of the image). Quantification of these puncta indicated that they were significantly larger in area (p=0.0042, Fig. 4.1 C), were not different in intensity on average (p=0.42, Fig. 4.1 D), and were fewer in number (p=0.0013, Fig. 4,1 D) in the *p120ctn*$^{-/-}$ mutant larvae. This data replicated the results obtained in the analysis of clathrin in the embryonic epidermis (Chapter 3 Fig. 3), although it was more difficult to detect the specific accumulation of clathrin at the plasma membrane due to small apical cell surface area in comparison to embryonic epidermis and simultaneous increase in intracellular puncta size. However, this data supports the data in the embryonic epidermis (Chapter 3), and allowed me conclude that the previous observation; that p120ctn loss resulted in clathrin becoming increased at the plasma membrane leading to a loss of dynamic exchange in the plane of the AJs, is not merely a feature of the embryonic epidermis but is apparent in multiple tissues and would therefore lend greater credence to the conclusion that the findings presented are representative of a general cellular mechanism.

4.3) Rok-Venus is reduced at the plasma membrane in the p120ctn mutant WD

In a similar fashion to the validation of the interaction of clathrin with p120ctn I examined the consistency of my finding with the Rho signalling pathway. For this I used the downstream enzyme Rho-Kinase as previously presented in the embryonic epidermis (Chapter 3), to study the normal localization of the protein without overactivation the signalling pathway (Chapter 3 Fig. 3). I used the same kinase dead variant of the enzyme tagged with Venus and driven by the *spaghetti squash* promoter (Venus-Rok^{K116A})(de Matos Simões et al., 2010). In the larval WD the Rok-Venus localized to the plasma membrane in the plane of the AJ (Fig. 4.2 A) unlike the embryonic epidermis the signal is not isolated to a specific cell border relative to the organismal axis, rather the signal is uniform on average measurement in each WD with some variation in signal strength evident upon observation (Compare Fig. 4.2 and Chapter 3 Fig. 4). In the *p120ctn*$^{-/-}$ mutant larvae the Rok-Venus signal remained localized to the plasma membrane colocalizing with the E-cad signal in the plane of the AJs, however the signal was notably reduced, an effect evident to the unaided eye (Fig. 4.2 B). To quantify the membrane levels of Rok-Venus between the genotypes I used a variation of the membrane script previously used to measure the membrane levels of proteins in the embryo (Chapter 3, 2016 paper). As no AP and DV borders are evident in the larvae, such an angle-dependent division would be inappropriate. Therefore, the script simply

used the entirety of the membrane of the identified cells to calculate the intensity per unit area as an average (See Chapter 2). Analysis of the membrane levels indicated that Rok-Venus was significantly reduced in the *p120ctn*$^{-/-}$ mutant larvae ($p=0.0002$, Fig. 4.2 C). Further, measurement of the Rok-Venus signal present in the cytoplasm in the plane of the AJs also showed a reduction, of statistical significance but of a lower magnitude than that observed at the membrane ($p<0.0001$, Fig. 4.2 D). A similar result was observed for Myosin II-YFP (Zipper) in the WD (data not shown), both of which supported the results obtained in the embryonic epidermis (Chapter 3 Fig. 3). The reduction observed in the cytoplasmic signal was suggestive of a general reduction of the protein, which could only be substantiated by proteomic analysis directly. To this end I examined the protein levels of Rok-Venus in the embryo using a Western blot. This indicated that the total amount of Rok-Venus protein was reduced in the *p120ctn*$^{-/-}$ mutant condition (Fig. 4.2 E). The significance of this is open to interpretation. In the first instance it is evidence that a degree of protein level regulation is coupled to the degree of activation in the signalling pathway. The simplest explanation of this coupling would be that inactive but not active Rok is subjected to proteolytic degradation in a concentration-dependent fashion, therefore reduced activation of Rok in the *p120ctn*$^{-/-}$ mutant animals leads to increase in amount of inactive protein, increasing its degradation and hence the total amounts of Rok. Such a mechanism would enable a cell to detect the balance between active and inactive protein as a proportion of the total amount of protein and maintaining the active: inactive ratio by reducing total amount. Overall, I concluded that these results support the general mechanism identified in the embryonic epidermis previously described.

4.4) Arf1 puncta are reduced by the loss of p120ctn

In addition to providing evidence that p120ctn interacts with clathrin and Rok in both the embryo and the larvae I examined the interaction of p120ctn with Arf1 in the WD to substantiate the embryonic data (Chapter 3 Fig. 5). However, unlike the embryonic data presented in the previous chapter I did not undertake to create the masks to measure the levels of Arf1-GFP at the plasma membrane but analysed the puncta signal. A more detailed account of this and the reasoning behind this examination shall be presented in the next chapter (Chapter 5) but for the present moment it will be sufficient to state that this analysis was undertaken as, at the time of the screen, the script for the analysis of the membrane resident Arf1 was still undergoing validation and the use of the puncta script as a measure provided a swift means of analysing the presence of any effect of the loss of p120ctn (see

Chapter 5.2). Furthermore, as is presented in the next chapter, the analysis of the Arf1-GFP puncta presented a method of analysing the activity of the trafficking network between the plasma membrane and the Golgi apparatus.

In the larval WD the Arf1-GFP signal was present in large distinct puncta throughout the cytoplasm with some signal evident in narrow bands which corresponded with the plasma membrane (Fig. 4.3 A). Indeed, it further appeared that many of the puncta were in close association with the plasma membrane, within the limits of the spatial resolution afforded by confocal microscopy, and some cells presented with multiple puncta (Fig. 4.3 A"). This was a pattern of localization which replicated precisely that which was observed in the embryonic epidermis (Chapter 3 Fig. 5). In the *p120ctn*$^{-/-}$ mutant larvae the Arf1-GFP signal appeared strongly reduced to the unaided eye, with the same pattern of localization of puncta and partial membrane localized signal (Fig. 4.3 B). To quantify these puncta, I used the puncta script previously used for the analysis of clathrin (Chapter 3 Fig. 2) which measure the three parameters of these puncta (see next chapter for full explanation of use of this script). Quantification of these puncta indicated that they were significantly decreased in area ($p=0.018$, Fig. 4.3 C), were not significantly different in intensity as an average of the population of puncta ($p=0.99$, Fig. 4.3 D), and were substantially fewer in number ($p=0.0042$, Fig. 4.3 E) in the *p120ctn*$^{-/-}$ mutant larvae. From this data I concluded that p120ctn does have an interaction with Arf1 in the WD, supporting the embryonic data and providing the empirical basis for the examination of the Trans Golgi network which is explored further in the next chapter.

4.5) The dynamics of p120ctn-GFP replicate those of E-cadherin at the plasma membrane

The final section of this chapter presents the work that was undertaken on p120ctn directly and the study of the dynamics of the protein at the plasma membrane. This was primarily undertaken to address one of the key questions arising from one of the papers which formed the foundation of the current work (Bulgakova and Brown, 2016), where the authors described p120ctn as being required to promote the internalization of a pool of E-cad at the plasma membrane which is in association with the polarity determinant Par-3 (*Drosophila* Bazooka-BAZ). This follows from a previous publication which identified two subpopulations of E-cad present at the plasma membrane which are distinguished by their dynamic properties (hence were termed mobile and immobile pools) and the specific association of this mobile pool with BAZ (Bulgakova et al., 2013). The question which remained from these works was whether the observed differential effect of p120ctn on the

two subpopulations of E-cad was a result of differing functional outputs or merely the result of different binding capacities of the two subpopulations with p120ctn.

To test these opposing explanations and to examine p120ctn I first attempted to tag the endogenous genomic locus with GFP using the CRISPR/Cas9 approach for homology directed repair to incorporate the GFP tag (Jinek et al., 2012; Lackner et al., 2015; Roberts et al., 2017; Wiedenheft et al., 2012), comparable to the later tagging undertaken for Arf1 (see Chapter 5). Unfortunately, this endeavour proved fruitless due to the high degree of heterochromatization of the surrounding locus (N.A.B. personal communication), thus impeding the accessibility of the enzyme to the site (data not shown). Therefore, I turned to the use of a transgenic tagged construct p120ctn-GFP (*UAS::p120ctn*-GFP) (Myster et al., 2003). As a transgenic construct, this naturally has the caveat that some degree of overexpression was induced, but the localization ought to be identical to that of the endogenous p120ctn. Indeed, to exclude the possibility of abnormal localization I also examined the localization of the p120ctn-GFP construct in a *p120ctn*$^{-/-}$ mutant genetic background to ensure comparable localization with the otherwise wild-type condition (data not shown). This construct had been examined in earlier embryogenic stages but the sub-cellular localization in relation to the two cell borders of the stage 15 embryonic epidermis was unexplored.

I first measured the localization of this construct when driven by the *engrailed* driver (*en::*Gal4) in the embryonic epidermis. Within the *engrailed* expressing cells, which formed a striped pattern across the epidermis, I observed the high enrichment of the p120ctn-GFP signal at the plasma membranes (Fig. 4.4 A). This signal co-localized precisely with that of E-cad in the cells, within the limits of the resolution of the confocal microscope (Fig. 4.4 A"). To analyse the localization of this construct at the plasma membrane and to access the ratio between the AP and DV cell borders I used the embryo membrane script previously described (see Chapters 2 and 3). This analysis indicated that the membrane levels of p120ctn-GFP were present in a 1:1.5 ratio (AP:DV) (Fig. 4.4 B). This differed from the usual ratio I observed for E-cad (1:2), however I reasoned that this may be an effect of the overexpression induced by the use of the transgenic construct. To explore this, I measured the ratio of E-cad at the membranes in the same cells and identified that it too was present in a 1:1.5 ratio (Fig. 4.4 C). This was the first measurement identifying that E-cad and p120ctn were present in identical ratios at the membrane, indicative of a 1:1 stoichiometry. If the reduction in the E-cad ratio was a result of p120ctn overexpression it would be evident by measuring the E-cad in the adjacent internal control cells (Fig. 4.4 A"). Therefore, I measured

and compared the E-cad amounts at the AP and DV borders of the internal control and p120ctn-GFP expressing cells. This analysis revealed that indeed E-cad was in the normal 1:2 ratio in the control cells and the reduction in the ratio observed in the p120ctn-GFP expressing cells was specifically due to an increase in the levels of E-cad present at the AP cell borders ($p=0.0007$, Fig. 4.4 D). This finding is consistent with the increase in E-cad-GFP expressed at endogenous levels at the AP cell borders upon overexpression of untagged p120ctn (see Chapter 3), further supporting the role of p120ctn in regulation of E-cad turnover.

The 1:1 stoichiometry between E-cad and p120ctn was alone suggestive of a uniform interaction with both E-cad subcomplexes, however to determine this more conclusively I had to take account of the dynamic properties of p120ctn itself. For this I used FRAP (see Chapter 2) on the p120ctn-GFP construct at both the AP and DV cell borders. This measurement indicated that the p120ctn-GFP signal recovered to approximately 65% at the AP border and approximately 50% at the AP cell borders (Fig. 4.4 E). Furthermore, I used a test to explore whether a single or biexponential best-fit model most accurately described the data. This analysis indicated that a single exponential model was the best-fit for p120ctn-GFP by contrast to E-cad itself which is best-fit by a biexponential model (2013). More interesting was the half-time of p120ctn at both borders was reminiscent of the slow recovery component of E-cad, which is attributed to endocytic recycling as previously remarked (Chapter 3). This would suggest that p120ctn recovery at the membrane is proportionally attributed to endocytic recycling.

Finally, to determine the continuous association of p120ctn with E-cad and the consistent increase in E-cad levels induced by the overexpression of p120ctn, I measured the levels of E-cad by immunofluorescence in the larval WD. For this I used the same genotype as previously presented for the embryonic data but permitted the animals to reach a later stage of development. I used the anterior compartment of the WD as the internal control (Fig, 4.4 F) and compared to the E-cad in the posterior compartment cells which expressed the p120ctn-GFP construct (Fig. 4.4 H). As expected the levels of E-cad at the cell membranes of p120ctn-GFP expressing cells were elevated ($p=0.002$, Fig. 4.4 I) but no overall increase in the cytoplasmic signal of E-cad within the plan of the AJ was detected ($p=0.72$, Fig. 4.4 J). From this data I concluded that p120ctn was in association with both E-cad subcomplexes, as both the stoichiometry in the fixed tissue and the dynamic properties of p120ctn replicated precisely those of E-cad itself. Further, the measurement of the dynamics suggests that p120ctn may be co-recycled with E-cad by an endocytic recycling pathway.

4.6) Conclusion

In this chapter I have examined the role that some of the genetic interactions previously presented in the embryo have in the larval wing disc. The use of the wing discs allows to examine the consequences of the genetic alterations in another epithelial tissue, thus countering any concern that the results obtained are the preserve of some specific epithelium or are limited to a specific developmental stage. As the majority of the results presented in this work, including the previous chapter and the following chapters, focuses on the embryonic epidermis, I tested whether my results were consistent between epithelia. Thus, while it is an important consideration that the results presented in this work were demonstrated to be consistent between different epithelial tissues, having done so with several key experiments it was no longer necessary to include both tissues for all subsequent experiments. The findings presented in this chapter support the previous reported data (Chapter 3), this allows me to state with more confidence that the results I present are accurate and that what I have studied in this work represents a general cellular mechanism for the regulation of cell-cell adhesion.

The finding that clathrin localization was perturbed in the same manner as observed in the embryonic epidermis lends support to the argument that p120ctn is a regulator of E-cad endocytosis specifically via a clathrin-mediated endocytotic mechanism (Chapter 3). This does not exclude the other clathrin-indepenent pathways (CIE) but does indicate that CME is the primary mechanism through which p120ctn acts on E-cad in multiple tissues. In a similar fashion I detect a reduction in Rok-Venus localization to the plasma membrane in the *p120ctn*$^{-/-}$ mutant larvae, replicating the result obtained in the embryonic epidermis (Chapter 3). As I used the enzyme as a proxy for the signalling output of the RhoA signalling pathway, in conjunction with MyosinII, I am more assured that p120ctn is an activator of the RhoA signalling pathway in epithelial cells. This is of particular significance as many of the data in previous studies have concluded that Rho is inhibited by p120ctn in the cytoplasm (Anastasiadis et al., 2000; van Hengel and van Roy, 2007; Noren et al., 2000). The prospect that p120ctn requires Rho activity to protect E-cadherin at the cell membrane by impeding the formation of endocytic invaginations, is a novel activity I have identified and characterised in this work. The presentation of the WD data in this chapter lends further support to this notion and serves as a useful paradigm for the future application of the study of p120ctn force transduction and mechanosensing in the WD: an aspect of this particular epithelial tissue which has been and continues to be the focus of much ongoing research.

The nature of the interaction between p120ctn and Arf1 has proved to be one of the more difficult aspects to elucidate in this work. The emerging conception is that p120ctn requires Arf1 to activate the clathrin-mediated endocytic pathway to promote the internalization of E-cad. However, as Arf1 is primarily localized at the Golgi and the functionality of the plasma membrane resident population is subsidiary to the activity of RhoA, it has proved most difficult to disentangle the direct effect of p120ctn on Arf1 by modulating the levels of p120ctn alone. Therefore, the loss of p120ctn in the *p120ctn*$^{-/-}$ mutant larvae provided the most direct means available of studying this. The results present an analysis of the Arf1 puncta, an aspect which is more closely attended in the following chapter in which I turn to the examination of the Trans-Golgi network. This Arf1 analysis is presented in this chapter in part because it is WD data which supports the embryonic data present in the next chapter (Chapter 5.2) but also because the puncta analysis provided a swift means of assaying the effect of p120ctn loss on the primary Arf1 population. This element of the discussion about the population of Arf1 and the significance of Arf1 TGN is explored extensively in the next chapter.

The final section of this chapter, it may be argued, provides the most insight and novelty, which goes beyond and not simply supports the data presented in the previous chapter. To my knowledge no direct study of the dynamics and localization of p120ctn in the embryonic epidermis of stage 15 or any other system had been undertaken. Some exploration of the localization in cell culture or in earlier morphogenesis is available (Myster et al., 2003) but in most cases these focus on gross morphology. Even the early studies of p120ctn confined themselves to the measurement in cell culture, with all of the inherent limitations in the exclusive use of 2D cell culture. I have identified that p120ctn is associated with both of the E-cad subcomplexes (Bulgakova et al., 2013) and therefore the different action of p120ctn on the mobile fraction of E-cad (Bulgakova and Brown, 2016) is due to the differential activity of p120ctn not to its binding potential. This conclusion was apparent from the stoichiometry of the fixed samples but more interestingly I show the dynamics of p120ctn at the membrane for the first time by using FRAP. This measured revealed that p120ctn has an immobile fraction at both the AP and DV cell borders. The recovery curve differs between the borders in a manner which is very close to the different dynamics and recovery of E-cad itself between the AP and DV cell borders (Bulgakova et al., 2013). What was most curious was that the recovery curve of p120ctn-GFP was reminiscent of E-cad at the AP and DV cell borders in the WT condition but not those of E-cad in the case of p120ctn overexpression (see Chapter 3). What accounts for this apparent discrepancy is difficult to answer directly

without the availability of the endogenously tagged p120ctn. If one examines the data more closely; the recovery of p120ctn was best-fit by a single exponential recovery curve by contract to E-cad itself which is fi by a bi-exponential recovery curve in normal conditions (Bulgakova et al., 2013). The point could be possibly addressed by p120ctn binding and unbinding in a reaction-limited reaction-diffusion manner (Sprague and McNally, 2005). With p120ctn dissociating from internalized E-cad complexes when internalization is initiated and re-binding when the E-cad complex is returned to the membrane. Further the saturation of the system occurring by the overexpression of p120ctn is resulting in association with newly synthesised protein as it transits to the membrane. This effect would mimic endocytic recycling within the parameters of a FRAP experiment. At the time of writing it is difficult to completely address the matter highlighted above, investigations are currently ongoing in the lab.

Overall an interesting question for future work, in light of this finding and the results presented for tissue tension in the previous chapter, is what role tension plays in the functional difference in the outcome and signalling of p120ctn, or if a reciprocal relationship exists.

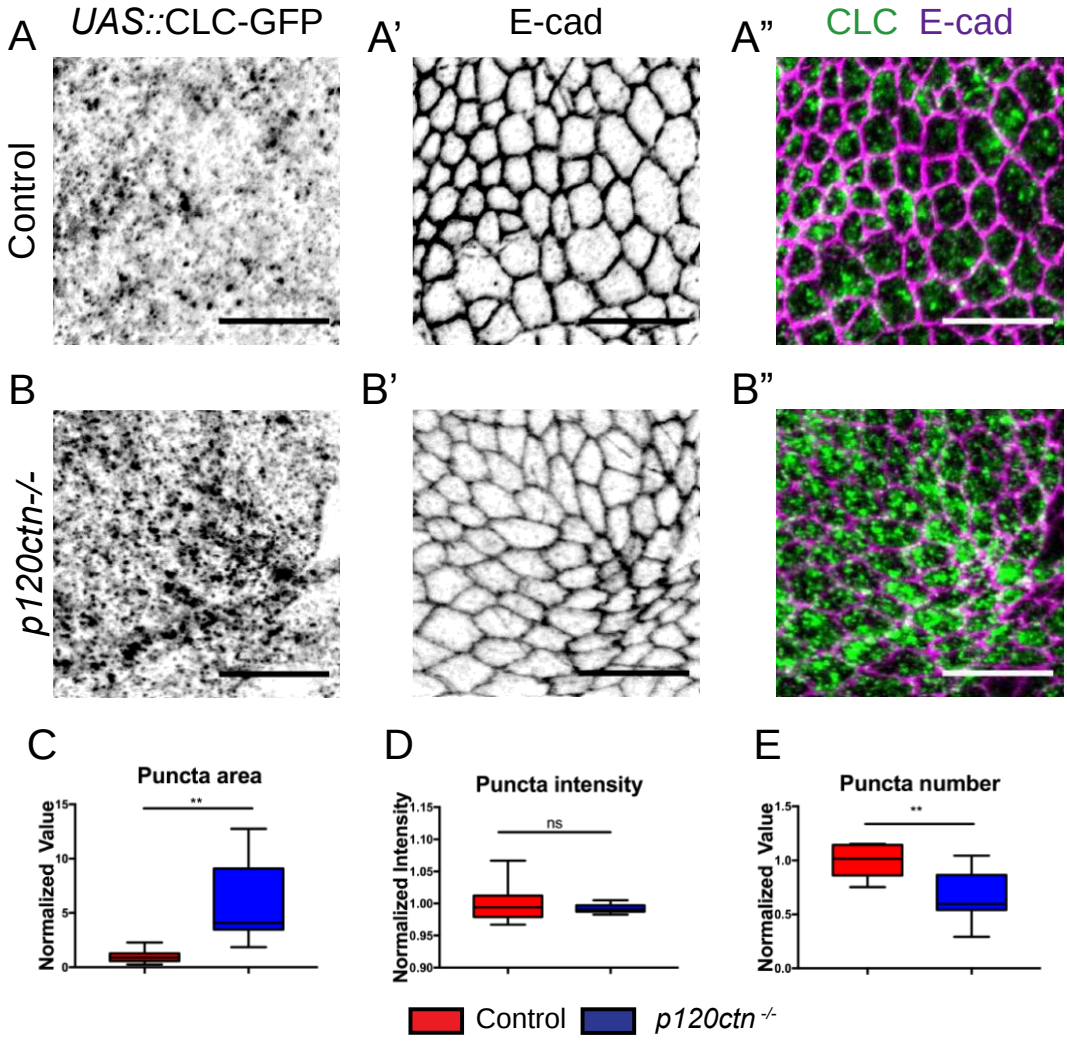

Figure 4.1. p120ctn loss increases Clathrin puncta in the WD

A-B. Localisation of the *UAS::*CLC-GFP puncta in the in the *Drosophila* 3rd instar larval wing disc (WD) in control (**A**) and *p120ctn*$^{-/-}$ mutant Larvae (**B**), with cell borders visualized by E-cad immunostaining (central panel). Grey left and central images are the individual channels (CLC-GFP and E-cad, respectively) the right panel is a merged image to show the signal of the two proteins respective to one another (CLC in green and E-cad in magenta). **C-E**. Quantification of the *UAS::*CLC-GFP signal using the puncta script, all normalized relative to the control values. (**C)** The area of the puncta as an average of all puncta. (**D**) The intensity of the puncta as an average of all measured in the images. (**E**) The number of puncta in the images as defined using a threshold set by the control. Statistical analysis was a two-tailed student t-test with Welches correction. *, $P < 0.05$; **, $P < 0.01$ ***, $P < 0.001$; ****, $P < 0.0001$. (n= 10-15 Larvae per genotype) scale bar represents 10 µm.

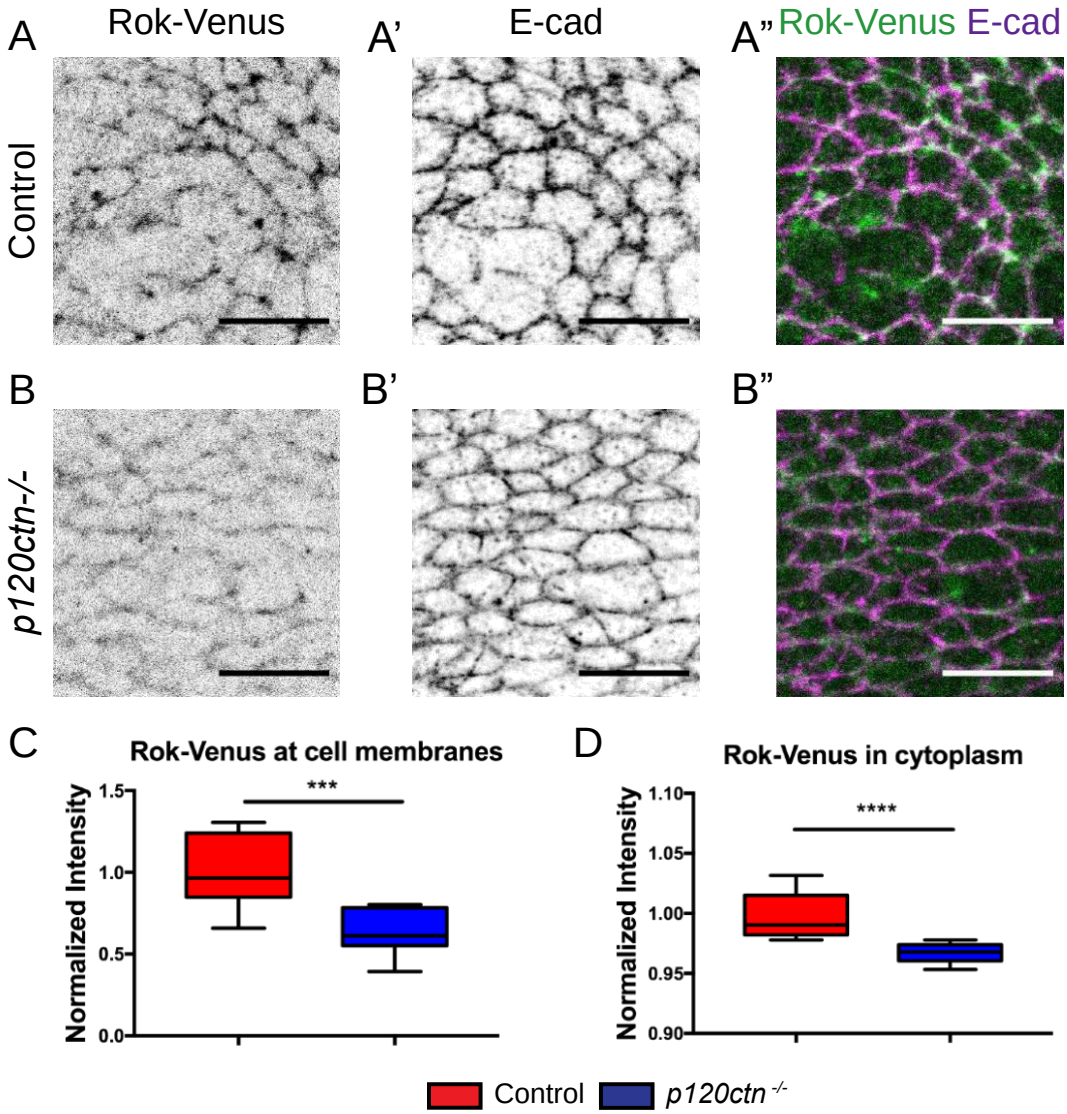

1- Control
2-*p120ctn*$^{-/-}$

Figure 4.2. Rho-Kinase is reduced by the loss of p120ctn in the WD

A-B. Localisation of Rho-kinase(Rok-Venus) in the in the *Drosophila* 3rd instar larval wing disc (WD) in control (**A**) and *p120ctn*$^{-/-}$ mutant Larvae (**B**), with cell borders visualized by E-cad immunostaining (central panel). Grey left and central images are the individual channels (Rok-Venus and E-cad, respectively) the right panel is a merged image to show the signal of the two proteins respective to one another (Rok in green and E-cad in magenta). **C-D**. Quantification of the Rok-Venus signal using the membrane intensity script, all normalized and expressed relative to the control values. (**C)** The levels of Rok at the plasma membrane of the cells as an average around the entire border of the cells. (**D**) The levels of Rok signal within the cytoplasmic space in the plasma of the AJ of the images. (**E**) Western blot membrane of control and *p120ctn*$^{-/-}$ mutant embryos. The left is the membrane probed for Venus using an Anti-GFP antibody. The right image is the membrane probed for tubulin as a loading control. The genotypes are indicated by the key below the left image. Statistical analysis was a two-tailed student t-test with Welches correction. *, $P < 0.05$; **, $P < 0.01$ ***, $P < 0.001$; ****, $P < 0.0001$. (n= 12-18 Larvae per genotype) scale bar represents 10 µm.

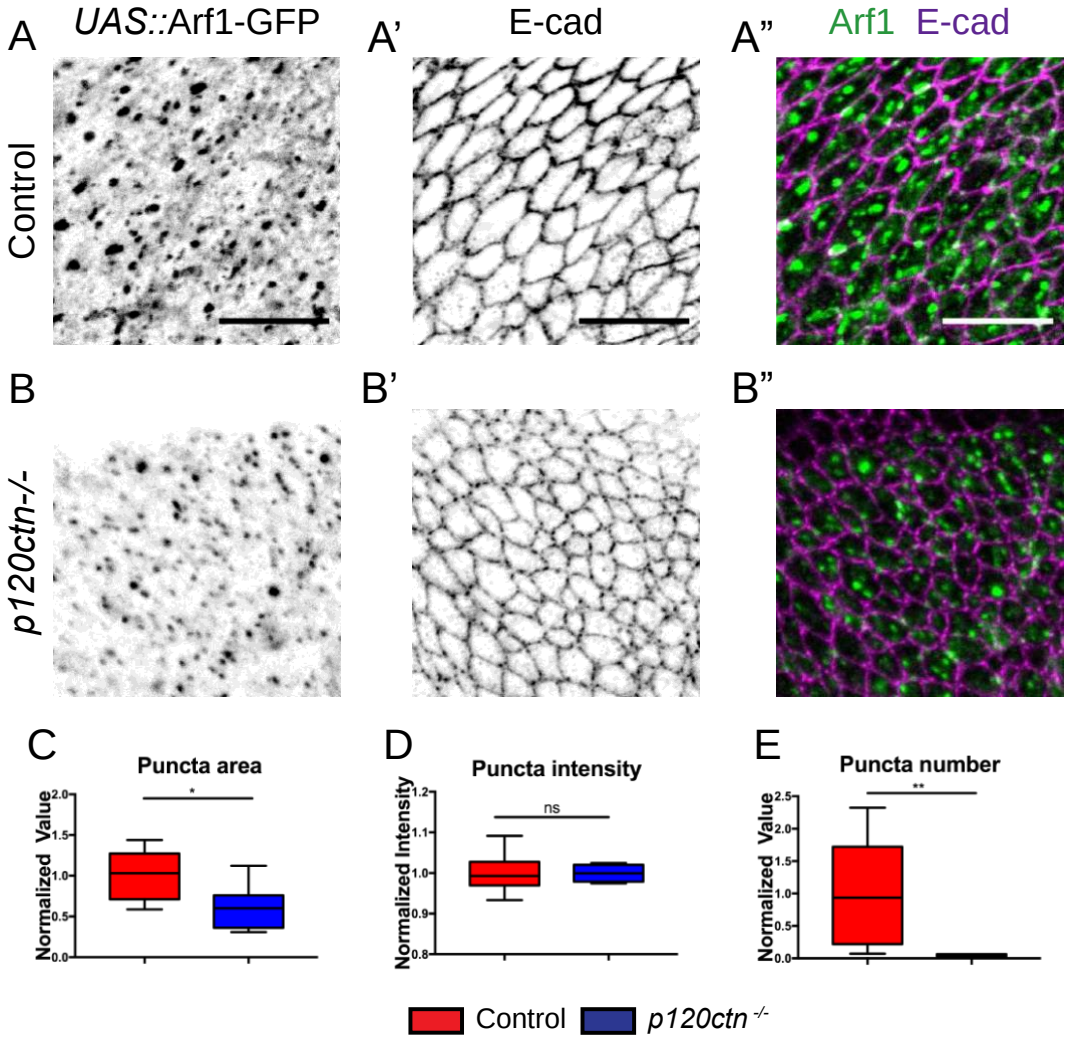

Figure 4.3. Arf1 puncta are smaller and fewer in number in the *p120ctn*$^{-/-}$ mutant WD

A-B. Localisation of the *UAS::*Arf1-GFP puncta in the in the *Drosophila* 3rd instar larval wing disc (WD) in control (**A**) and *p120ctn*$^{-/-}$ mutant Larvae (**B**), with cell borders visualized by E-cad immunostaining (central panel). Grey left and central images are the individual channels (Arf1-GFP and E-cad, respectively) the right panel is a merged image to show the signal of the two proteins respective to one another (Arf1 in green and E-cad in magenta). **C-E**. Quantification of the *UAS:*Arf1-GFP signal using the puncta script, all normalized and expressed relative to the control values. (**C)** The area of the puncta as an average of all puncta. (**D**) The intensity of the puncta as an average of all measured in the images. (**E**) The number of puncta in the images as defined using a threshold set by the control. Statistical analysis was a two-tailed student t-test with Welches correction. *, $P < 0.05$; **, $P < 0.01$ ***, $P < 0.001$; ****, $P < 0.0001$. (n= 10-15 Larvae per genotype) scale bar represents 10 µm.

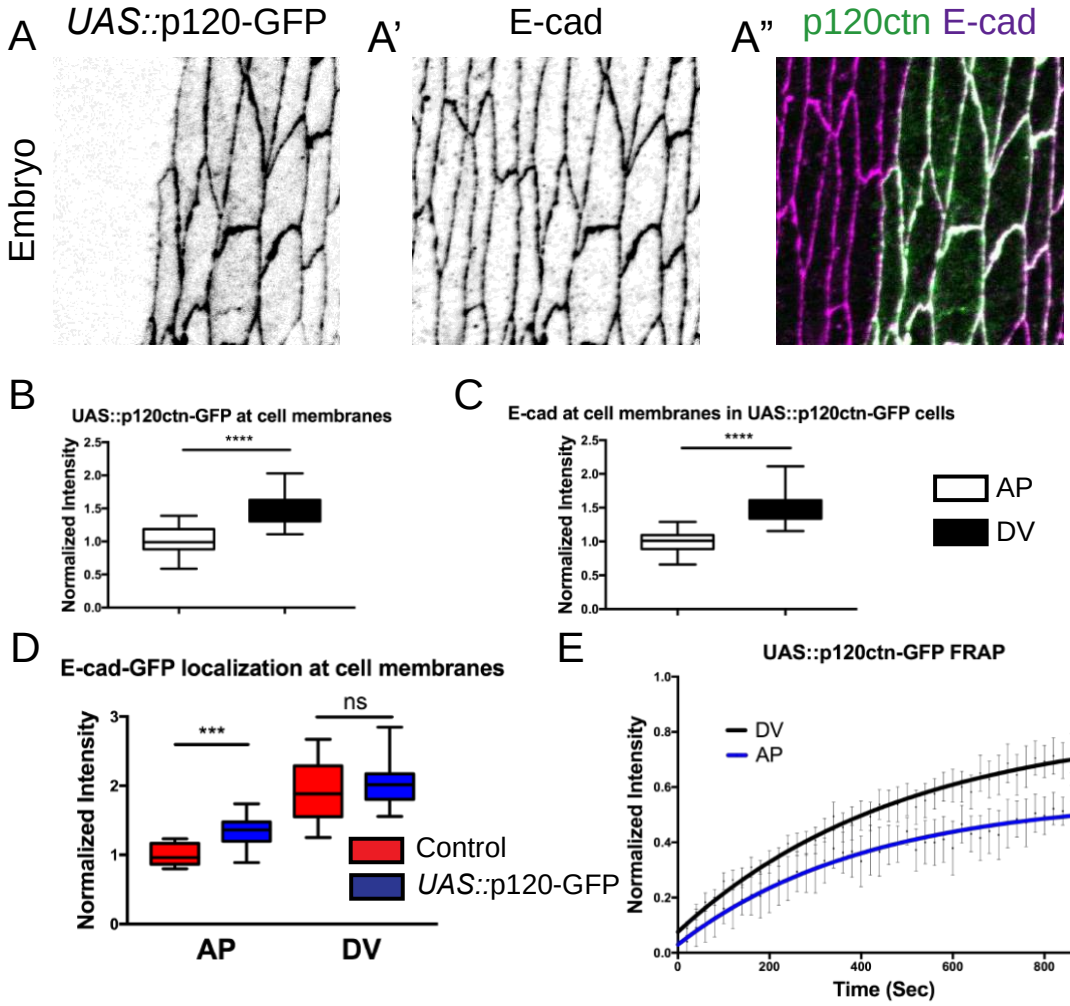
A
UAS::p120-GFP
A'
E-cad
A"
p120ctn E-cad
Embryo
B
UAS::p120ctn-GFP at cell membranes
Normalized Intensity
****
C
E-cad at cell membranes in UAS::p120ctn-GFP cells
Normalized Intensity
****
AP
DV
D
E-cad-GFP localization at cell membranes
Normalized Intensity
***
ns
Control
UAS::p120-GFP
AP
DV
E
UAS::p120ctn-GFP FRAP
Normalized Intensity
DV
AP
Time (Sec)
F
E-cad, Anterior
G
E-cad, Posterior
H
UAS::p120-GFP
Wing Disc
I
E-cad at cell membranes
Normalized Intensity
**
J
E-cad signal in the cytoplasm
Normalized Intensity
ns
Anterior
Posterior

Figure 4.4. The localization and dynamics of p120ctn-GFP are identical to those of E-cadherin

(A) The localization of the *UAS::*p120ctn-GFP construct in the dorsolateral epidermis of stage 15 *Drosophila* embryos. Left and centre panels show individual channels, cell borders are visualized using E-cad immunostaining which marks both engrailed expressing and adjacent internal control cells (right panel). (**B**) quantification of the levels of p120ctn-GFP at the two cell borders, normalized to the AP cell border value. (**C**) Quantification of the E-cad levels at the cell borders of the p120ctn-GFP expressing cells, normalized to the AP cell border value. (**D**) Comparative analysis of the E-cad levels between the internal control cells and the p120ctn-GFP expressing cells at both cell borders. Normalized to the E-cad levels at the internal control AP cell borders. (**E**) Dynamics of p120ctn-GFP measured by FRAP at both cell borders. Average recovery curves (mean ± s.e.m.) and the best-fit curves (solid lines) are shown. **F-H**. Localization of the *UAS::*p120ctn-GFP construct in the *Drosophila* 3rd instar larval wing disc (WD). Cell borders visualized by E-cad immunostaining. (**F**) Localization of E-cad in the anterior compartment. (**G**) Localization of E-cad in the posterior compartment. (**H)** visualization of the *UAS::*p120ctn-GFP in the posterior compartment. **I-J.** Quantification of the E-cad signal using the membrane intensity script, all normalized and expressed relative to the control values. (**I)** The levels of E-cad at the plasma membrane of the cells as an average around the entire border of the cells. (**J**) The levels of E-cad signal within the cytoplasmic space in the plasma of the AJ of the images. Statistical analysis was a two-tailed student t-test with Welches correction. Bars in **D** represent difference between cell borders in genotypes measured by two-way ANOVA. *, $P < 0.05$; **, $P < 0.01$ ***, $P < 0.001$; ****, $P < 0.0001$. (n= 20 embryos for intensity quantification, n= 15 for Larvae intensity quantification, n=8 embryos for FRAP) scale bar represents 10 µm.

Chapter 5: Examination of the role of p120ctn in the Trans-Golgi network.

5.1) Introduction

The Trans-Golgi Network (TGN) is one of the primary sorting and secretion networks within eukaryotic cells (Gu et al., 2001; Guo et al., 2014; Lieu et al., 2008; Lock et al., 2005). It is generally viewed from the perspective of newly synthesised protein which is transiting thought the system before arriving at a particular intracellular compartment or being targeted for secretion outside of the cell (von Blume et al., 2011; Kienzle and Blume, 2014; Rosquete et al., 2018). This view is what is described as the anterograde progression of newly synthesized protein, which transits from the Endoplasmic Reticulum through the Golgi itself before being released at the opposite end for delivery elsewhere (Huang and Wang, 2017). While this description is applicable for newly synthesized protein it is far from a complete account of the role and function of the Golgi in protein trafficking and sorting. In the introduction the existence of a retrograde pathway which is coupled to the endocytic system was partially described (See Chapter 1 section 1.8), and I shall now discuss this in more detail and how this relates to E-cad itself and to p120ctn mediated recycling.

The Golgi is a compact and folded organelle which comprises a series of folded membranes stacks (cisternae). Broadly speaking proteins are delivered to the cis-face of the Golgi from the (ER) and undergo rounds of maturation processing and post-translational modifications. Many of the transferase enzymes required for post-translation modifications are found within the structure of the Golgi (Kweon et al., 2004; Lemonidis et al., 2014; Rabouille et al., 1995; Sengupta et al., 2015; Strous, 1986). There is a degree of selective mediation and a measure of stochastic modifications dependent upon the transferase enzymes present and the substrates which are passing through the Golgi at any particular moment (Day et al., 2013; Nilsson et al., 2009; Preuss et al., 1992; Ruiz-May et al., 2012). As progression through the Golgi reaches its end the proteins reach the trans face of the Golgi, which in most instances is orientated away from the nucleus and toward the plasma membrane (Li et al., 2013; Yadav and Linstedt, 2011; Yadav et al., 2009). There are series of competing models for how cargo is sorted through the Golgi and how such vesicles are sorted for delivery (Boulant et al., 2011; Ernst et al., 2018; Füllekrug and Nilsson, 1998; Gong et al., 2010). It is not the purpose of this work to elaborate too greatly on this point, merely to say that this area is still the subject of ongoing work and given the vast number of components identified in sorting it is likely to be a substantial computational problem to solve the conundrum of Golgi sorting (Gong et al., 2010). The final secretion form the Golgi at the Trans face and delivery

of cargo to compartments of the plasma membrane usually marks the end of the discussion about the Golgi. However, the role of the Golgi is not limited to this, but it is also involved in the trafficking of cargo within the endocytic system (Chia et al., 2013). As mentioned in the introduction and discussed further in Chapter 6, once cargo is internalized by endocytosis it is sorted between endocytic compartments either for recycling or degradation (See Fig 1.3 Chapter 1and Chapter 6). One of the two known recycling routes first sorts cargo back to the Golgi (retrograde TGN, slow recycling). The precise purpose of this is questioned and no definitive answer has emerged, principally due to the difficulty of isolating only that population of protein which has undergone such recycling. However, it would not be an unreasonable deduction to infer that some reprocessing or modification of the internalized protein occurs. Indeed, it may even undergo a degree of viability testing, whereby any protein that is damaged or cannot be further modified is targeted for degradation: evidence of a transition between the TGN and the late endosomes by a Rab9 dependent mechanism has been identified in the past (Kucera et al., 2016a, 2016b).

E-cad itself has been well documented to undergo endocytic recycling (Le et al., 1999; Nanes and Kowalczyk, 2012) and has known post-translational modifiers present in the Golgi (Bonazzi et al., 2008; Geng et al., 2012; Shao et al., 2016). Some of the other work presented in this Thesis supports previous observations and reports of the endocytic sorting and recycling of E-cad (see Chapter 6). The potential role of p120ctn in the TGN is a less studied aspect of this regulation of E-cad. Primarily p120ctn has been studied as having a role at the plasma membrane. However, some works suggested a role of p120ctn when uncoupled to E-cad in the cytoplasm and more specifically in the trafficking of N-cadherin through the Golgi itself (Wehrendt et al., 2016). While the latter was studied in neuronal cells the mechanism of interaction with classical cadherins is highly likely to be conserved. Moreover, evidence has been reported for p120ctn directly participating in the endocytic recycling by retrieving cargo and trafficking vesicles along microtubules (Chen et al., 2003; Ichii and Takeichi, 2007; Xiao et al., 2007; Yanagisawa et al., 2004). Therefore, while this work was primarily directed toward the study of the regulation of the initiation of E-cad internalization by p120ctn at the plasma membrane, I used the finding of p120ctn genetic interaction with Arf1, which is primarily resident at the trans face of the Golgi, as a basis for examining the Golgi by proxy, using Arf1 as a function readout of the activity of the TGN in some of the genetic conditions examined in this work. Here, I present this analysis and the findings which may yield interesting results with further examination.

5.2) Loss of p120ctn reduces the Arf1 signal at the Golgi

To examine the TGN in the case of genetic ablation of p120ctn I used the transheterozygous genetic null previously described (See Chapter 2) and the same experimental crosses used to measure the membrane levels of Arf1 presented in a previous chapter (see Chapter 3, Fig. 4). As I had this data to hand and the large proportion of Arf1-GFP signal was localized at the Golgi, I decided to use the puncta script, previously used to measure the clathrin puncta (See Chapter 3, Fig. 3) to obtain a measure of the Arf1 signal present in these puncta, which I used as a proxy for the activity of the TGN (Donaldson et al., 2005). First I confirmed that the puncta observed in the *UAS::*Arf1-GFP cells are the Golgi by immunostaining with a Golgi antibody and observing the co-localization of the Golgi staining and the Arf1-GFP puncta (See Chapter 3 supplementary Fig 3).

In the control *UAS::*Arf1-GFP expressing cells, driven by *engrailed::*GAL4, the puncta are observed throughout the cytoplasm some of which appear to be in close association with the plasma membrane, with multiple distinct Golgi structures present in each cell, within the plane of the AJs. (Fig 5.1 A). This pattern of Golgi localization is as previously observed and reported for *Drosophila* cells (Kondylis and Rabouille, 2009; Yano et al., 2005). In the *p120ctn* mutant embryos these *UAS::*Arf1-GFP puncta presented in a similar pattern to the control cells with little distinction obvious to the eye (Fig. 5.1 B). This analysis indicated that in the *p120ctn* mutant cell the *UAS::*Arf1-GFP puncta were significantly smaller in area ($p=0.0011$, Fig 5.1 C), were of greater intensity ($p=0.0014$, Fig 5.1 D), and were not different in number ($p=0.49$, Fig 5.1 E). These measured collectively indicated that in the *p120ctn* mutant condition the levels of Arf1 resident on the Golgi, and by proxy engaged in TGN activity, are reduced in the plane of the AJs. Overall, I concluded that p120ctn is possibly required for Arf1 TGN localization in the plane of the AJs.

5.3) Overexpression of p120ctn increases the Arf1 GFP signal on the Golgi

To complement the result of the genetic ablation of p120ctn on the TGN previously measured, I turned to the use of our full-length p120ctn overexpression construct (See Chapters 2 and 3). The expression of this construct was balanced in the control by the inclusion of the *UAS::*CD8-Cherry previously described (see Chapter 3). In the control cells the pattern of *UAS::*Arf1-GFP puncta localization is as previously observed (Fig. 5.2 A). In the *UAS::*p120ctn overexpressing cells the Arf1 puncta displayed no overt distinction from the control cells, the signal presented in the same pattern and localization: distinct large puncta present throughout the cytoplasm and some in close proximity to the plasma

membrane (Fig. 5.2 B). Quantification of these puncta indicated that in the p120ctn overexpression they were larger in area (p=0.045, Fig. 5.2 C), were greater in signal intensity on average (p=0.0017, Fig. 5.2 D), and were greater in number than detected in the control cells (p=0.0157, Fig. 5.2 E). Given that the results obtained with the overexpression of p120ctn were the reverse of those obtained for the loss of p120ctn I concluded that a genetic association existed between p120ctn and Arf1-dependent TGN activity. Further this data is compatible with, and indeed complements, the data I obtained by measuring the Arf1-GFP population at the plasma membrane in the same genetic conditions (See Chapter 3). Possibly indicating that p120ctn has a broader function in the balance between endocytic internalization and recycling.

5.4) Tagging endogenous Arf1 with GFP using CRISPR and observation of TGN

Following the identification of Arf1 as a genetic interactor of p120ctn and the determination of functional consequences for E-cad at the membrane with the Arf1 regulatory constructs (see Chapter 3) I sought to create an endogenously tagged variant of Arf1 with various fluorophores using CRISPR-mediated homologous recombination (see Chapter 2 for specific details). I intended to use this to provide a direct measure of the endogenous Arf1 and to address any concern that previous measurements and results using the transgene were an overexpression artefact.

After microscopy and PCR screening to confirm the successful tagging of the Arf1 genetic locus with EGFP or mCherry independently, I first observed the localization of the construct in the embryonic epidermis and the larval wing disc (for the latter the data is not shown). The pattern of the signal detected corresponded to the previous observation of the *UAS::*Arf1-GFP transgene, large distinct puncta are present throughout the cytoplasm with some signal observable and measurable on the plasma membrane (Fig. 5.3 A). This provided bidirectional reassurance, first that the tagging was replicating the transgene, indicating no aberrant localization, and second that the transgene itself was localizing normally, validating the previous analyses using the transgene. Once I confirmed that the endogenous Arf1 had been tagged and that this construct localized normally I sought to repeat the initial experiments with the *p120ctn* mutant and overexpression construct, to substantiate our previous results using the Arf1 transgene. The endogenous Arf1-GFP (Cherry was the same but is not shown here) localized in a similar fashion in both the control and *p120ctn* mutant embryos (Fig. 5.3 A and B) with no overt discrepancy in localization, consistent with observations of the transgenic Arf1-GFP. I quantified both the membrane localized Arf1-GFP

and the puncta in these conditions. This analysis indicted no reduction in the area (p=0.21, Fig. 5.3 C), a significant increase in the intensity (p<0.0001, Fig. 5.3 D) and an increase in the number (p=0.022, Fig. 5.2 C) between the control and *p120ctn* null embryos. Further to this I replicated the experiment using the p120ctn overexpression construct previously described (see Chapter 3). The localization of the endogenous Arf1-GFP between the *engrailed* expressing cells and the internal control cells exhibited no overt difference (Fig. 5.3 F). Quantification of the puncta indicated an increase in area (p=0.0265, Fig. 5.3 G), no difference in intensity (p=0.99, Fig. 5.3 H) and no significant difference in the number (p=0.543, Fig. 5.3 I) between the internal control cells and the *UAS::*p120ctn expressing cells. The question of why the endogenously tagged construct failed to replicate the findings of the transgenic *UAS::*Arf1-GFP raised some interesting possibilities discussed at the end of this Chapter.

5.5) Effect on the TGN of the expression of Arf1 regulatory constructs

Finally, to ascertain the consequences on the TGN of perturbing the function of Arf1 I measured the Golgi directly using the antibody for the Golgi in the presence of the constitutively active (CA) and dominant negative (DN) construct of Arf1 previously described and used (see Chapter 3). I used this construct primarily to examine the role of Arf1 activity on E-cad levels at the plasma membrane (Chapter 3 Fig. 6). However, as the majority of the Arf1 population is located at the Golgi I decided to complement this analysis with an examination of the Golgi directly. To measure the Golgi in these experiments I turned to the use of the antibody previously used to confirm that the Arf1-GFP puncta observed were representative of the Golgi (Chapter 3 Supplementary Fig. 3) this antibody specifically targets the Trans face of the Golgi to isolate the activity of the TGN.

In the internal control cells the Golgi staining pattern presented in the manner previously observed and consistent with expectations: large discrete puncta present throughout the cytoplasm with reasonably low background or non-specific staining (Fig. 5.4 A). The expression of the CA construct manifested no overt difference in the gross morphology of the Golgi (compare cells expressing CD8 marker, with the internal control cells on the right side of the central panel, Fig. 5.4 A). Quantification of these puncta using the script previously described (using the same settings that were used for Arf1) identified that their area was increased (p=0.0008, Fig. 5.4 B) with no difference in intensity (p=0.48, Fig. 5.4 C) nor any difference in the number of Golgi puncta (p=0.38, Fig. 5.4 D) within the

plane of the AJ. As the antibody used specifically marked the Trans face of the Golgi the increase in the area would be indicative of the expanded area for the function of the TGN. It is possible that the absence of any change in the intensity or number is a result of the antibody marking the entirety of the Trans-face of the Golgi. Unlike the previous analysis which used Arf1-GFP, the resident population of which varies more than that of the Golgins used as an epitope for the antibody. This may be a consequence of the more dynamic exchange of Arf1 as only active Arf proteins can interact with membranes (Gommel et al., 2001)

To complement the examination of the Golgi using the Arf1 CA construct I also examined the Golgi structure when in the presence of the Arf1 DN construct. This construct induced a highly abnormal cellular morphology and is lethal beyond the embryonic stage (See Chapter 3, Fig. 6). Staining for the Golgi revealed a peculiar pattern of localization, with multiple smaller puncta present in the cytoplasm (Fig. 5.4 E) which suggested that the Golgi may be fragmenting or forming into smaller units: at least the Trans face which is marked by this antibody was undergoing some gross morphological change in the presence of the DN construct (Top right of central panel Fig. 5.4 E). This pattern was highly variable and fluctuated in a similar manner to the magnitude of the cell morphology abnormalities previously observed (Chapter 3, Fig. 6 and Supplementary Fig. 4). Comparative analysis of these Golgi between the internal control cells and the DN expressing cells indicated a significant decrease in area ($p=0.0495$, Fig. 5.4 F) with no change observed in the intensity ($p=0.97$, Fig. 5.4 G) nor in the number of puncta detected on average ($p=0.99$, Fig. 5.4 H). The reason for this absence of change in number or intensity may be attributed to an averaging effect which mitigates the most striking morphological defects apparent in the cells which are presumably expressing more, or have expressed for longer, the DN construct (Wang et al., 2017).

As the DN showed a decrease in the area of the Trans face of the Golgi, which is the reverse of the effect observed with the CA, I reasoned that the constructs are affecting the TGN in the manner predicted. This deduction operates on the premise that the area of the Trans face of the Golgi is proportional to the function or activity of the TGN. Moreover, it validates the premise of the previous experiments in which I used the punctate pattern of Arf1-GFP as a proxy measure for the TGN, insofar as the area metric is concerned. Overall, I conclude that the Arf1 regulatory constructs are affecting the TGN in the manner predicted and this adds an interesting paradigm to the network from the perspective of p120ctn mediated regulatory activity.

5.6) Conclusion

In this chapter I have explored the role and function that p120ctn may play beyond the direct effect on E-cad at the plasma membrane by examining the TGN. Although the primary objective of the research undertaken in this work was to examine the regulation at the plasma membrane, the role p120ctn may have elsewhere has been postulated and partially studied by others (Carnahan et al., 2010; Casagolda et al., 2010; Duñach et al., 2017). In the case of the current work it arose from the identification of Arf1 as an interactor of p120ctn, while I did focus on the plasma membrane localized population of Arf1, I also decided to explore the effect present upon the primary population of Arf1, which is resident on the Trans face of the Golgi. I reasoned that the use of Arf1-GFP may have the additional advantage of being a useful proxy measure for the TGN (Donaldson et al., 2005).

Using the same genotypes and micrographs used for the analysis of the effect of altering p120ctn levels on the plasma membrane population of Arf1 I used the puncta script initially developed by Prof D. Strutt and optimized by Dr N. Bulgakova for the analysis of clathrin to examine the Golgi resident population of Arf1 and infer the TGN effect. At this points it is worth discussing what the parameters measured represent. Puncta or spots in space have two spatial dimensions (size and number) and one intensity dimension which can be quantified, these are represented in the puncta script as the area (size), intensity, and number present in a given image or subsection of an image. In themselves each can be informative but to provide an indication of the amount of a protein in a given area within the cell it is useful to apply all three metrics.

The area of the puncta is representative of the average of the spatial occupancy of the protein present on the Trans face of the Golgi, the intensity provides an indication of the density, while the number is representative of the average number in an image which exceed the threshold intensity value, determined in each case by the average of the control. These are by no means a precise quantification of the activity of the TGN, but they do provide a useful comparative approximation of TGN activity for which I reasoned that Arf1 localization is a valid proxy. For, despite being an overexpression condition, it marks Arf1 localization without functional overexpression. Evidence from cell culture indicates that tagging a small GTPases like Arf1 perturbs function by decreasing the possibility of a substrate accessing the active site of the enzyme (Snapp, 2005). This has been shown directly for Arf1 (Jian et al., 2010) in this case the authors described the shift in functional kinetics of the tagged Arf1-GFP. Further, in consideration of the fact that the CRISPR tagged Arf1-GFP stocks are not homozygotically viable, event those arising from different founder adults, indicates that the

CRISPR tagged endogenous construct cannot fully substitute for the activity of the untagged protein on the balancer chromosome.

I found that in the cases of p120ctn mutation or overexpression there is a corresponding change in the Arf1 present in puncta, which complements and corresponds with the previous measurement of the effect of p120ctn levels on the plasma membrane population of Arf1 (Chapter 3 Fig. 5). Taking both data sets into account it would be a reasonable conclusion that in the absence of p120ctn there is a reduction in the activity of the Arf1 generally with both the plasma membrane bound and Golgi bound population of Arf1 being decreased. This may result from the reduction in amount due to re-localization elsewhere in the cell or from the increased degradation of the protein when the requirement for its function is lowered (Schrader et al., 2009). However, the question does arise as to whether the changes in Arf1 localization are due to direct effects of p120ctn on the TGN or due simply to a reduction of internalized cargo which can undergo recycling (see Chapter 6 for further exploration of this problem). The prospect of p120ctn having a more direct role in TGN trafficking is supported by the overexpression experiments in which the Arf1 is correspondingly decreased at the plasma membrane (Chapter 3 Fig 5) and increased at the Golgi. This would suggest that although the Arf1 activity and cargo (E-cad) internalization are impaired at the plasma membrane by Rho signalling activity (Chapter 3 Fig. 3 and 6), the elevation of p120ctn levels have stimulated the activity of the TGN.

I endeavoured to measure the endogenous Arf1 by tagging it with fluorophores using the CRIPSR-mediated homologous recombination technique. However, analysis using this tagged variant when repeating the experiments with the alterations of p120ctn levels failed to replicate the result and in some instances contradicted the previous findings. I postulate that this is due to complementation with transcriptional feedback compensation which is skewing the results, in case of endogenously but not UAS expressed Arf1. Indeed, there is a gene encoding an antisense RNA transcribed from a complementary DNA strand overlapping Arf1 promoter (http://flybase.org/reports/FBgn0267631): a hallmark of a potential transcriptional inhibition mechanism (Janowski et al., 2005; Osato et al., 2007) This question is the subject of ongoing work in the lab but is outside of the scope of the work presented here.

Finally, I measured the effect on the TGN of exposure to the Arf1 regulatory constructs previously used to measure the effect on Arf1 on E-cad at the plasma membrane (Chapter 3 Fig. 6). This confirmed the expected alteration in the Trans face of the Golgi when subjected to the activity of either CA of DN Arf1 and validated the use of Arf1 as a proxy for the activity of the TGN. Collectively the work of this chapter has revealed, or at least

indicates, that p120ctn seems to have a broader cellular function than purely the regulation of E-cad at the plasma membrane. This prospect has been suggested by previous work, indeed some direct examination of the extra-plasma membrane function of p120ctn has been undertaken by other groups (Anastasiadis et al., 2000; Daniel, 2007), some of which have identified p120ctn in the trafficking of N-cadherin through the Golgi, while others have identified the interaction of p120ctn with motor proteins and the involvement of the delivery of recycling vesicles along microtubules (Ichii and Takeichi, 2007; Wehrendt et al., 2016). However, it has proved technically challenging in mammalian cell culture systems used for these studies to disentangle the effects p120ctn has within the cells from its more well characterised function on E-cad at the plasma membrane. Some work has attempted to use an p120ctn uncoupled from E-cad to explore cytoplasmic or nuclear activity (Ishiyama et al., 2010), but this has always been complicated by the complete loss of adhesion observed in mammalian cells following such uncoupling (Davis et al., 2003; Reynolds and Roczniak-Ferguson, 2004). An interesting prospect for future work would be to make use of the *Drosophila* or other non-mammalian system, in which E-cad does not have this enhanced dependence on p120ctn, to explore this broader role of p120ctn in the TGN and cellular trafficking of cargo and vesicles.

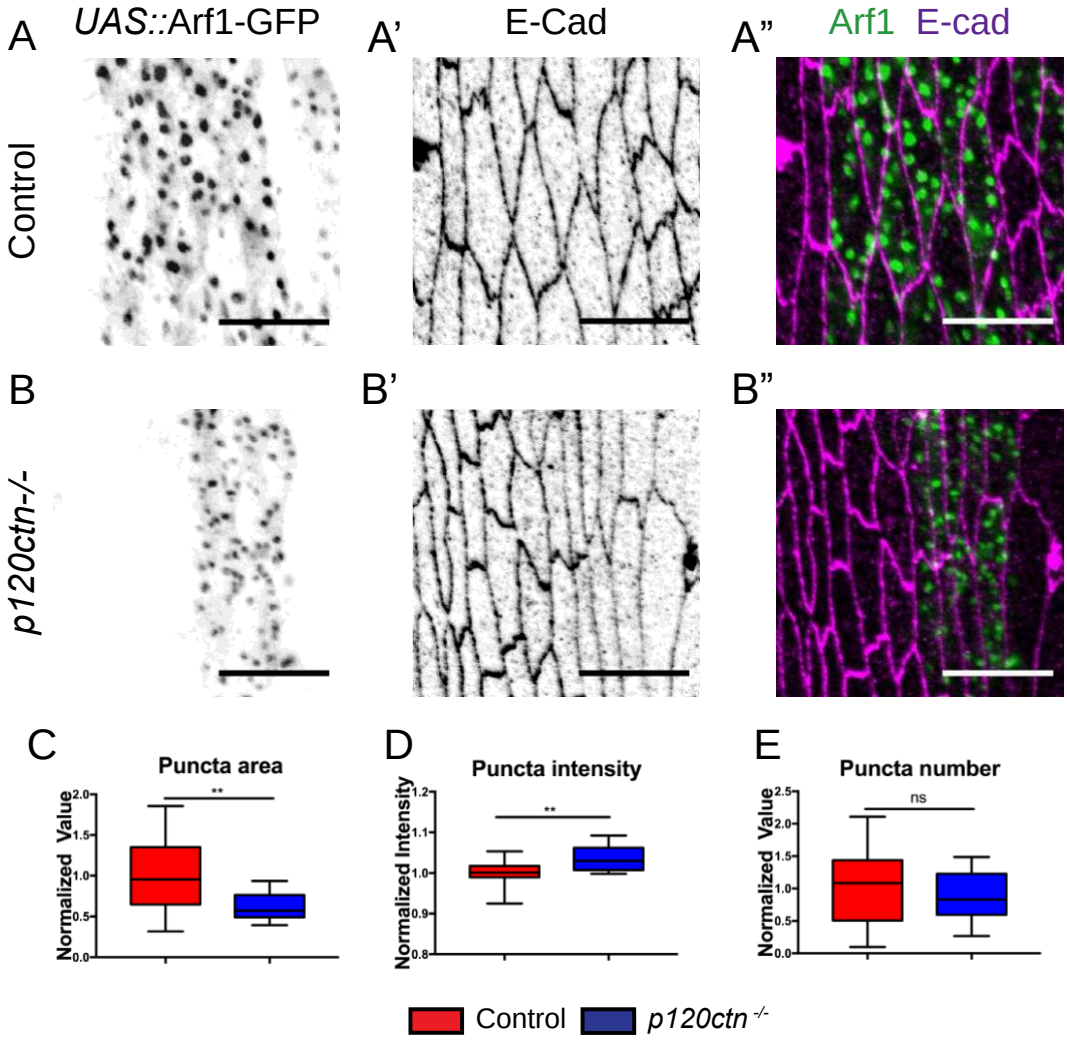

Figure 5.1. p120ctn ablation reduces the amount of Arf1 at the Golgi

A-B. Localisation of the *UAS::*Arf1-GFP puncta in the in the dorsolateral epidermis of stage 15 *Drosophila* in control (**A**) and *p120ctn*$^{-/-}$ mutant embryos (**B**), with cell borders visualized by E-cad immunostaining (central panel). Grey left and central images are the individual channels (Arf1-GFP and E-cad, respectively) the right panel is a merged image to show the signal of the two proteins respective to one another (Arf1 in green and E-cad in magenta). **C-E**. Quantification of the *UAS::*Arf1-GFP signal using the puncta script, all normalized and expressed relative to the control embryo values. (**C)** The area of the puncta as an average of all puncta. (**D**) The intensity of the puncta as an average of all measured in the images. (**E**) The number of puncta in the images as defined using a threshold set by the control. Statistical analysis was a two-tailed student t-test with Welches correction. *, $P < 0.05$; **, $P < 0.01$ ***, $P < 0.001$; ****, $P < 0.0001$. (n= 15-20 embryos per genotype) scale bar represents 10 µm.

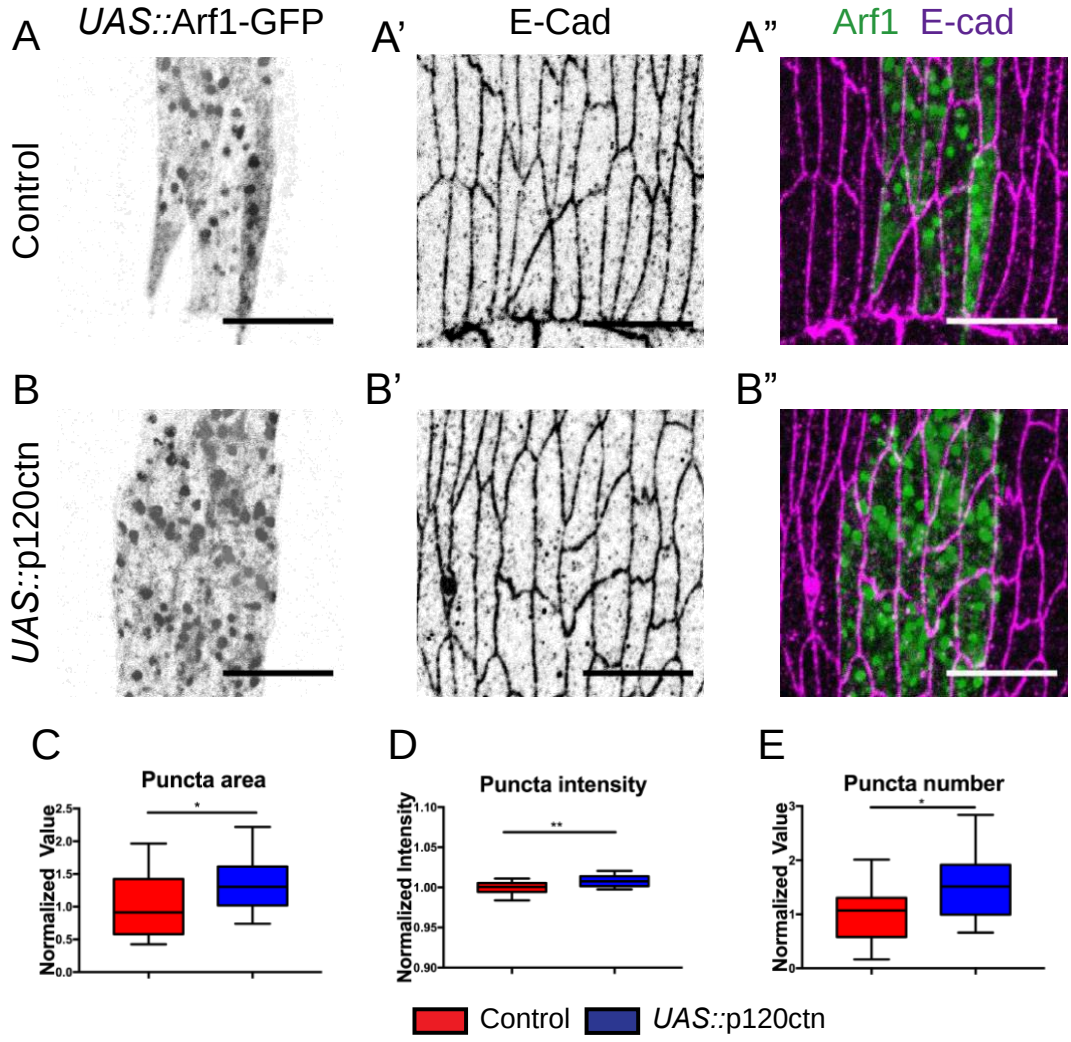

Figure 5.2. p120ctn overexpression increases the amount of Arf1 at the Golgi

A-B. Localisation of the *UAS::*Arf1-GFP puncta in the in the dorsolateral epidermis of stage 15 *Drosophila* in control (**A**) and p120ctn overexpressing embryos (**B**), with cell borders visualized by E-cad immunostaining (central panel). Grey left and central images are the individual channels (Arf1-GFP and E-cad, respectively) the right panel is a merged image to show the signal of the two proteins respective to one another (Arf1 in green and E-cad in magenta). **C-E**. Quantification of the *UAS::*Arf1-GFP signal using the puncta script, all normalized and expressed relative to the control embryo values. (**C)** The area of the puncta as an average of all puncta. (**D**) The intensity of the puncta as an average of all measured in the images. (**E**) The number of puncta in the images as defined using a threshold set by the control. Statistical analysis was a two-tailed student t-test with Welches correction. *, $P < 0.05$; **, $P < 0.01$ ***, $P < 0.001$; ****, $P < 0.0001$. (n= 15-20 embryos per genotype) scale bar represents 10 µm.

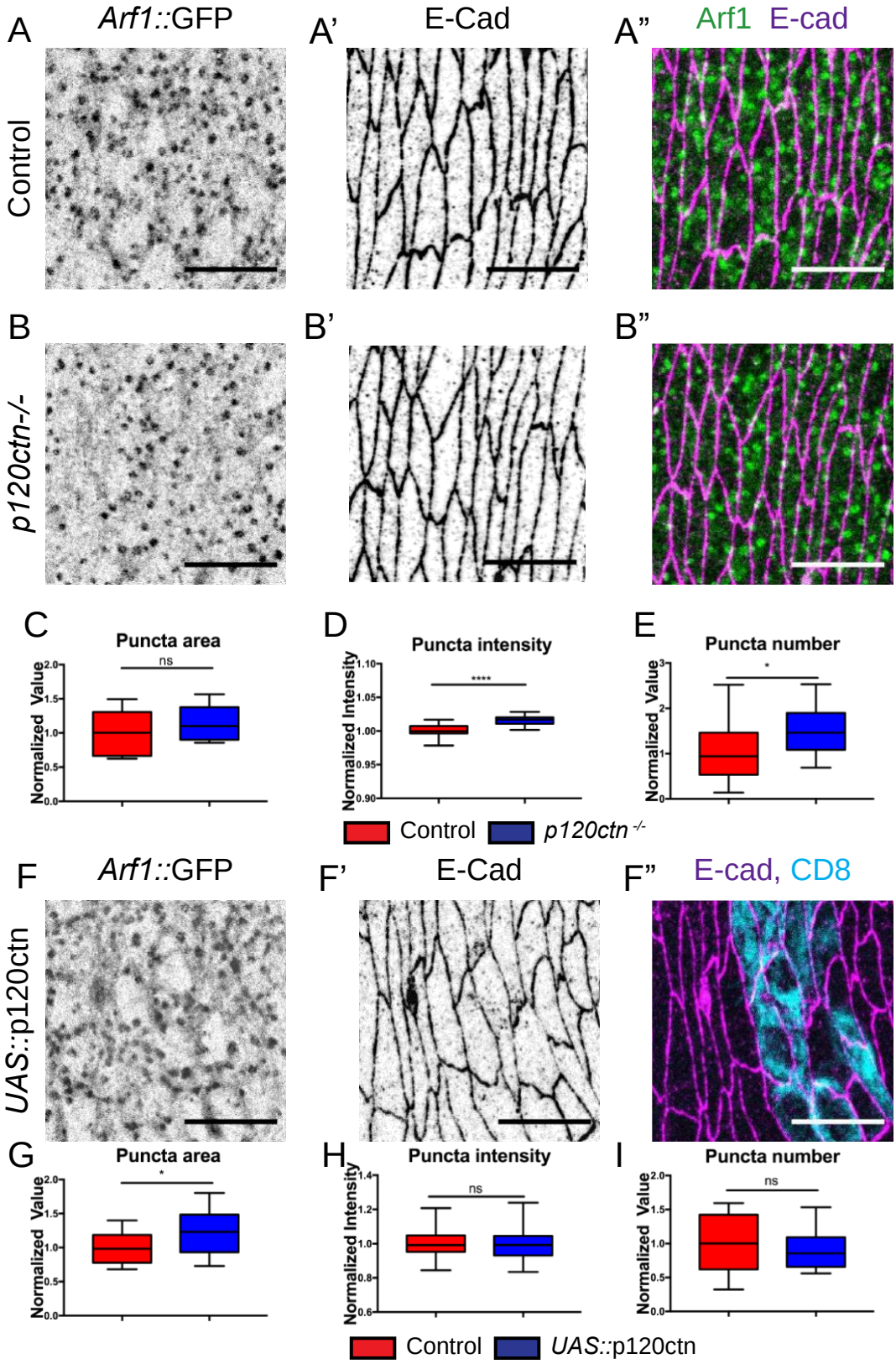
A
Arf1::GFP
A'
E-Cad
A"
Arf1 E-cad
Control
B
B'
B"
p120ctn-/-
C
Puncta area
ns
Normalized Value
D
Puncta intensity
****
Normalized Intensity
E
Puncta number
*
Normalized Value
Control
p120ctn -/-
F
Arf1::GFP
F'
E-Cad
F"
E-cad, CD8
UAS::p120ctn
G
Puncta area
*
Normalized Value
H
Puncta intensity
ns
Normalized Intensity
I
Puncta number
ns
Normalized Value
Control
UAS::p120ctn

Figure 5.3. CRISPR tagged endogenous Arf1-GFP does not replicate the results of the transgenic Arf-GFP with the alteration of p120ctn levels

A-B. Localisation of endogenously tagged Arf1-GFP puncta in the in the dorsolateral epidermis of stage 15 *Drosophila* in control (**A**) and *p120ctn*$^{-/-}$ mutant embryos (**B**), with cell borders visualized by E-cad immunostaining (central panel). Grey left and central images are the individual channels (Arf1-GFP and E-cad, respectively) the right panel is a merged image to show the signal of the two proteins respective to one another (Arf1 in green and E-cad in magenta). **C-E**. Quantification of the Arf1-GFP signal using the puncta script, all normalized and expressed relative to the control embryo values. (**C)** The area of the puncta as an average of all puncta. (**D**) The intensity of the puncta as an average of all measured in the images. (**E**) The number of puncta in the images as defined using a threshold set by the control. **F**. Localisation of the endogenous Arf1-GFP in *UAS::*p120ctn cells and adjacent internal control cells. Cells expressing the UAS::p120ctn construct are marked by the CD8 (F" Cyan in right panel) **G-I**. Quantification of the Arf1-GFP puncta in *UAS::*p120ctn overexpression. (**G)** The area of the puncta as an average of all puncta. (**H**) The intensity of the puncta as an average of all measured in the images. (**I**) The number of puncta in the images as defined using a threshold set by the control.

Statistical analysis was a two-tailed student t-test with Welches correction. *, $P < 0.05$; **, $P < 0.01$ ***, $P < 0.001$; ****, $P < 0.0001$. (n= 15-20 embryos per genotype) scale bar represents 10 µm.

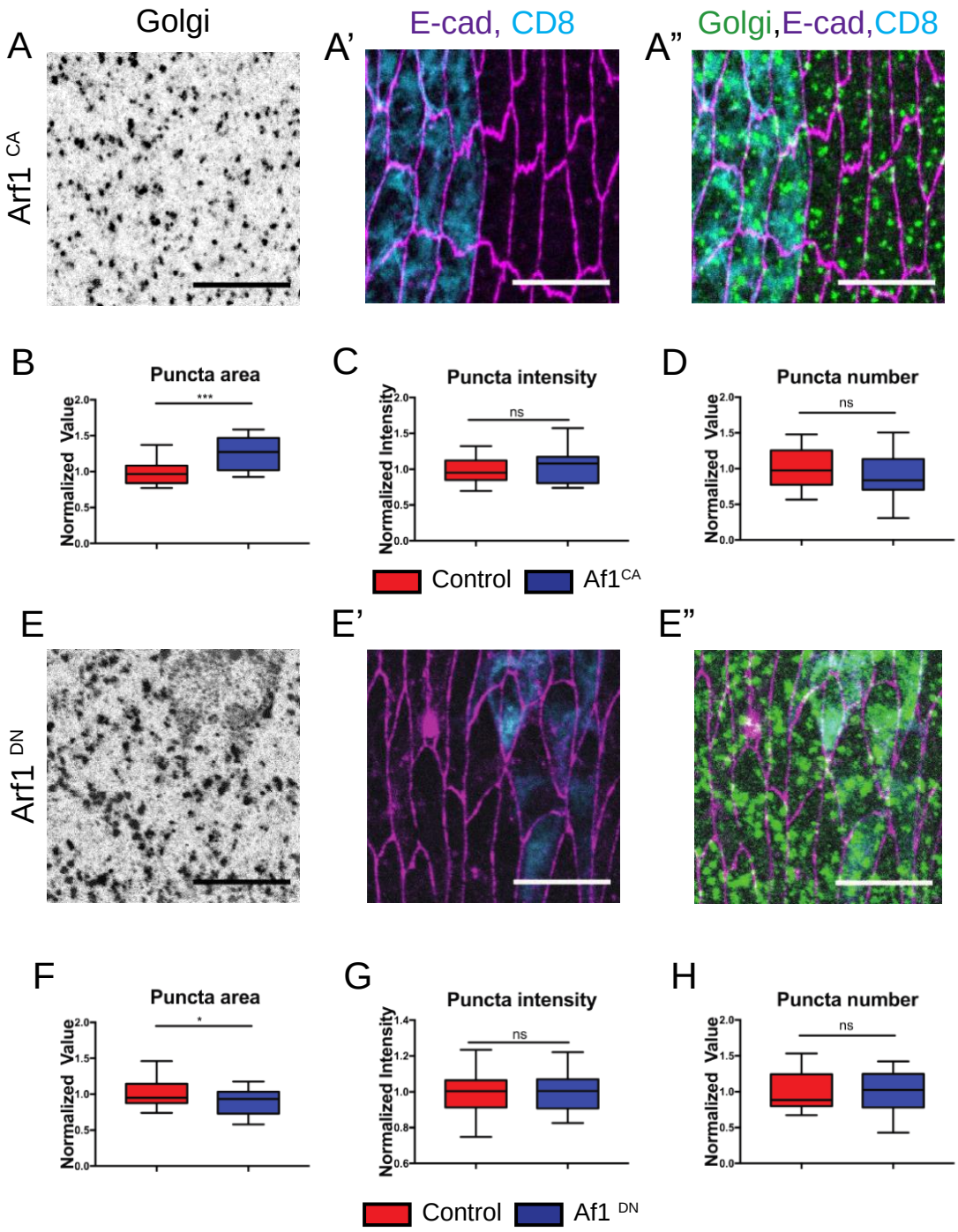
A
Golgi
A'
E-cad, CD8
A"
Golgi,E-cad,CD8
Arf1 CA
B
Puncta area
***
Normalized Value
C
Puncta intensity
ns
Normalized Intensity
D
Puncta number
ns
Normalized Value
Control
Af1 CA
E
E'
E"
Arf1 DN
F
Puncta area
*
Normalized Value
G
Puncta intensity
ns
Normalized Intensity
H
Puncta number
ns
Normalized Value
Control
Af1 DN

Figure 5.4. Arf1 regulatory constructs alter the Trans face of the Golgi

(A) Localisation of the Golgi puncta in the in the dorsolateral epidermis of stage 15 *Drosophila* with the expression of the Arf1 CA construct (cells marked by Cyan in central panel) and the internal control cells. Golgi staining is marked in green and cell borders visualized by E-cad-GFP (Magenta in central and right panel). **B-D.** Quantification of the Golgi signal using the puncta script, all normalized and expressed relative to the control embryo values. (**B)** The area of the puncta as an average of all puncta. (**C**) The intensity of the puncta as an average of all measured in the images. (**D**)
The number of puncta in the images as defined using a threshold set by the control. **(E)** Localisation of the Golgi puncta in the in the epidermis with the expression of the Arf1 DN construct (cells marked by Cyan in central panel) and the internal control cells. Golgi staining is marked in green and cell borders visualized by E-cad-GFP (Magenta in central and right panel). **F-H.** Quantification of the Golgi signal using the puncta script, all normalized and expressed relative to the control embryo values. (**F)** The area of the puncta as an average of all puncta. (**G**) The intensity of the puncta as an average of all measured in the images. (**H**) The number of puncta in the images as defined using a threshold set by the control. Statistical analysis was a two-tailed student t-test with Welches correction. *, $P < 0.05$; **, $P < 0.01$ ***, $P < 0.001$; ****, $P < 0.0001$. (n= 15-20 embryos per genotype) scale bar represents 10 µm.

Chapter 6: Characterization of the role of p120ctn in the endosomal trafficking pathway

6.1) Introduction

The endosomal system evolved to mediate the process of trafficking of proteins and organelles within cells (Bishop, 2003; Jovic et al., 2010; Naslavsky and Caplan, 2018). It targets and sorts cargo with multiple pathways involved in the decision of the destination and fate of cargo (Eaton and Martin-Belmonte, 2014; Roeth et al., 2009). This latter aspect has bearings upon the half-life of every protein within the cell and can determine the proteins lifespan by facilitating either the return of cargo to a particular destination or compartment or enabling the degradation of the protein to prevent the continued activity of an enzyme or structural component of the cell (Kerkhof et al., 2000; Sorkin and Duex, 2010). Further to the introduction to the endosomal system given in the introduction to this work (See Chapter 1, section 6) the current chapter will provide a focus on the intracellular trafficking pathways and the rationale behind the examination of them in the context of this work which was partially alluded to in the introductory section.

The endosomal system is functionally divided into sequential compartments which have been defined and indeed described by the Rab GTPases which are associated with these various compartments (Barr, 2013). The process of endosomal sorting is often described as a sequential event which starts with the early sorting endosome (Jovic et al., 2010). Most internalized vesicles which abscise from the plasma membrane are initially trafficked to this component before a trafficking decision is made (see Fig 1.2). After this a sorting decision occurs which selects, broadly, for one of two pathways: either recycling or degradation. However, this definition is somewhat unsatisfactory as it fails to account for the various other compartments involved in the process, specifically those involved in reprocessing such as the Golgi and the possible non-linear progressive shuttling of the protein between the various compartments. Further there are a plethora of molecular mediators which determine the decision path and destination of the cargo, which must be taken into account if one is to fully appreciate the nature and complexity of the endosomal sorting network (Eaton and Martin-Belmonte, 2014; Frankel and Audhya, 2018; Xie et al., 2016). Cargo can be sorted to the Golgi apparatus (see Chapter 5 section 5.1, for full description of the trans Golgi network): the reason for this is suggested to be the ability of the Golgi to modify or modulate the modifications of transmembrane proteins or even the extracellular domain of the proteins which are present on the cell surface and ordinarily unavailable to modifying enzymes. Evidence for this is scant and for the present it is mere conjecture (Lord and Roberts, 1998;

Progida and Bakke, 2016; Sivan et al., 2016). This supposition has been complicated by the technical difficulty of separating the two recycling pathways. From the Golgi the cargo can be recycled back to the plasma membrane by using the recycling pathway which is marked by the Rab11 GTPase (Takahashi et al., 2012). Failing this, the cargo can be transferred from the Golgi or the early endosome to the late endosomes which are marked by the Rab7 GTPase (Huotari and Helenius, 2011; Hyttinen et al., 2013; Poteryaev et al., 2010; Vanlandingham and Ceresa, 2009; Vonderheit and Helenius, 2005). The conventional view is that these are destined for degradation by fusing to the lysosomes, however some limited evidence indicates that they could perform some recycling function (Charette and Cosson, 2006).

As mentioned earlier, prior to this work the endocytic function of p120ctn was inferred by the measurement of the immunostaining for internal vesicles containing E-cad or using a pulse-chase assay to measure the rate and amount of internalization over a given time (Bulgakova and Brown, 2016; Lohia et al., 2012; Miyashita and Ozawa, 2007; Paterson et al., 2003). Previous work which formed the foundation for the work presented here indicated that in the absence of p120ctn an independent route of internalizing E-cad exists which appears to target the E-cad for degradation (Bulgakova and Brown, 2016). This was shown using a pulse-chase assay in the presence of chloroquine to block lysosomal fusion within the wing disc of p120ctn mutant larvae. This indicated an increase in the number of vesicles. However, the precise compartment which these vesicles represent was unknown. In light of this and my identification of a stark change in Clathrin localization in the p120ctn mutants, I wished to examine the various compartments within the endosomal system and determine which is the most affected.

To explore the effect that the loss of p120ctn has on the various pathways within the endosomal system, I undertook an examination of the various compartment of the endosomal system. I did this by using the genetic ablation of p120ctn, using the transheterozygotic knock-out, previously described (see Chapter 2: Materials and Methods) and measured the effect on either immunostained or YFP tagged variants of the Rab GTPases which mark the various stages and compartments of the endocytic pathway.

6.2) Rab5 is reduced in the absence of p120ctn

The first compartment I examined was the early endosome which is the first sorting station for all internalized cargo (Jovic et al., 2010). To measure this, I first attempted use an endogenously tagged YFP-Rab5, and upon examination this yielded no distinct pattern or signal under observation by a confocal microscope (data not shown). Therefore, I turned to the use of immunostaining to mark the compartment. In the control embryos the Rab5 signal localized in distinct puncta (Fig 6.1A). These were of various sizes and were dispersed throughout the cytoplasm at the level of the AJs, with some signal apparent at the plasma membrane colocalizing with the E-cad signal (Fig 6.1A"). This localization is consistent with the known cellular function and previous reports. In the *p120ctn* mutant embryos the Rab5 signal was visually reduced with fewer puncta apparent by eye (Fig 6.1B). To precisely quantify the effect of the loss of p120ctn I used the puncta script previously used to measure clathrin and Golgi puncta (see Chapters 3 and 4, Materials and methods). This quantification identified that in the absence of p120ctn the Rab5 puncta were significantly reduced in area ($p<0.0001$, Fig 6.1C), increased in intensity ($p=0.0083$, Fig 6.1D), and were significantly fewer in number at the level of the AJs ($p<0.0001$, Fig 6.1E). suggesting that a reduced volume of cargo is being processed in the early endosomal compartment.

6.3) Rab11-YFP is also reduced in absence of p120ctn

The next compartment I examined was the recycling endosome. There are two recycling pathways which are distinguished by their kinetic rates (Choudhury et al., 2004; Grant and Donaldson, 2009; van der Sluijs et al., 1992). Fast recycling is directly from the early endosome back to the plasma membrane, mediated by Rab4 and Rab11 (Li et al., 2008); the slow recycling pathway originates from the Golgi back to the plasma membrane mediated by Rab11 alone (Li et al., 2008; Takahashi et al., 2012). As Rab11 is involved in both pathways and is considered the classical marker for endosomal recycling, I focused my attention on Rab11. I was able to obtain endogenously tagged Rab11, therefore unlike the previous use of immunostaining for Rab5, this analysis was based upon quantification of endogenous protein directly. The signal of Rab11-YFP in the control embryos presented in a more diffuse pattern than Rab5 with more tubular or connected structures interspaced with some puncta (Fig 6.2A). Some Rab11-YFP appeared to be present at the membranes localizing with E-cad, which in this instance is immunostained to provide the outline of the cell membranes (Fig 6.2A'). In the *p120ctn* mutant embryos the pattern of Rab11-YFP signal was visibly reduced but some localization was still apparent at the plasma membrane (Fig 6.2 B). Further, some

of the Rab11-YFP signal was clustered into more intense larger puncta (note the lower left quarter of the micrograph on Fig 6.2B). Quantification of these puncta revealed that they were smaller in area (p=0.029,Fig 6.2C), were not significantly different in intensity as an average (p=0.69,Fig 6.2D), and were significantly fewer in number (p<0.0001 ,Fig 6.2 E) at the level of the AJs. Overall these findings would suggest that a reduced amount of Rab11 mediated recycling was occurring in the plane of AJs in the *p120ctn* mutant condition.

6.4) Rab7-YFP puncta and number are increased in the absence of p120ctn

To examine the consequences for the late endosomal compartment in the absence of p120ctn I used an endogenously tagged Rab7-YFP, which is the classical marker of the late endosomes .

In control embryos Rab7-YFP was localized in large distinct puncta throughout the cytoplasm in cells (Fig 6.3A). These puncta were substantially larger than the Rab5 or Rab11 puncta previously measured (see Fig 6.1 and 6.2). This is consistent with many previous reports in cell culture conditions and is due to the large volume of the contents of the compartment, involving the formation of multivesicular bodies prior to fusion with the lysosomes (Luzio et al., 2010). In *p120ctn* mutant embryos the Rab7-YFP puncta presented in the same localization pattern but appeared larger in size by eye than the control embryos (Fig 6.3B). In many instances the Rab7-YFP puncta appear to be in close proximity or localized to the plasma membrane (Fig 6.3A-B). Measurement of these puncta indicated that in the *p120ctn* mutant embryos the Rab7-YFP puncta were larger in area (p=0.0086,Fig 6.3 C), were not significantly different in intensity (p=0.9175,Fig 6.3 D), and were greater in number (p=0.0069,Fig 6.3 E). These observations would suggest that in the *p120ctn* mutants there is an increase in the trafficking to the late endosomes resulting in an increase in the requirement for Rab7 that was detected by the puncta increase observed.

6.5) Conclusion

Prior to these findings the role of p120ctn in the endosomal trafficking of cargo had been inferred by the use of E-cadherin internalization and pulse-chase assays. I present the first direct observation of the various components of the trafficking pathway using the genetic ablation of p120ctn to ascertain the consequent effect on the endosomal system of the loss of the p120ctn mediated internalization of E-cad. Prior to this it was unclear what the precise effects on the various pathways within the endosomal system were, nor if the E-cad which is subject to p120ctn-independent internalisation (PII) is degraded or recycled. From the data I

present it would be reasonable to deduce that degradation is elevated in the absence of p120ctn.

I found that in the absence of p120ctn there was a decrease in the amount of Rab5 and Rab11, and an increase in Rab7 at the level of the AJs, as measured by quantitative microscopy. Naturally, the puncta measurement used is subject to the limitations described in the previous chapter, and the results presented are not a direct biochemical assays of function. However, they constitute an *in situ* examination of how the cellular machinery has been perturbed by the loss of a component of the AJs. Further, I have used the Rabs as proxy measurement of these endosomal compartments not merely because they are the classical markers used for this, but because Rabs are GTPases they are indicative of the activity of the pathways and cellular process examined (Hutagalung and Novik, 2011; Müller and Goody, 2018; Pfeffer, 2013).

The reduction of Rab5 and Rab11 could be explained by the reduction of the amount of cargo being internalized and sorted for recycling. This would be consistent with previous work in which the loss of p120ctn was shown to stabilize E-cad at the plasma membrane (Bulgakova and Brown, 2016). However, there is difficultly in disentangling the reduction of Rab5 early endosomal compartment and the reduction in Rab11 recycling, as one is dependent on the other. It is therefore difficult to say that p120ctn is directly involved in recycling from these data alone, however based on results in other systems it is a distinct possibility that p120ctn does participate directly in the recycling of cargo. By contrast the increase of Rab7 is consistent with an increase in degradation of E-cad in the absence of p120ctn. The question which naturally arises from this is what mechanism mediates the internalization of E-cad for degradation, and what causes an apparent increase in the activity of this pathway in the p120ctn mutants. This and the question of the balance between p120ctn-dependent internalization of E-cad which predisposes for recycling and p120ctn-independent internalization which predisposes for degradation, will be an interesting question for future work.

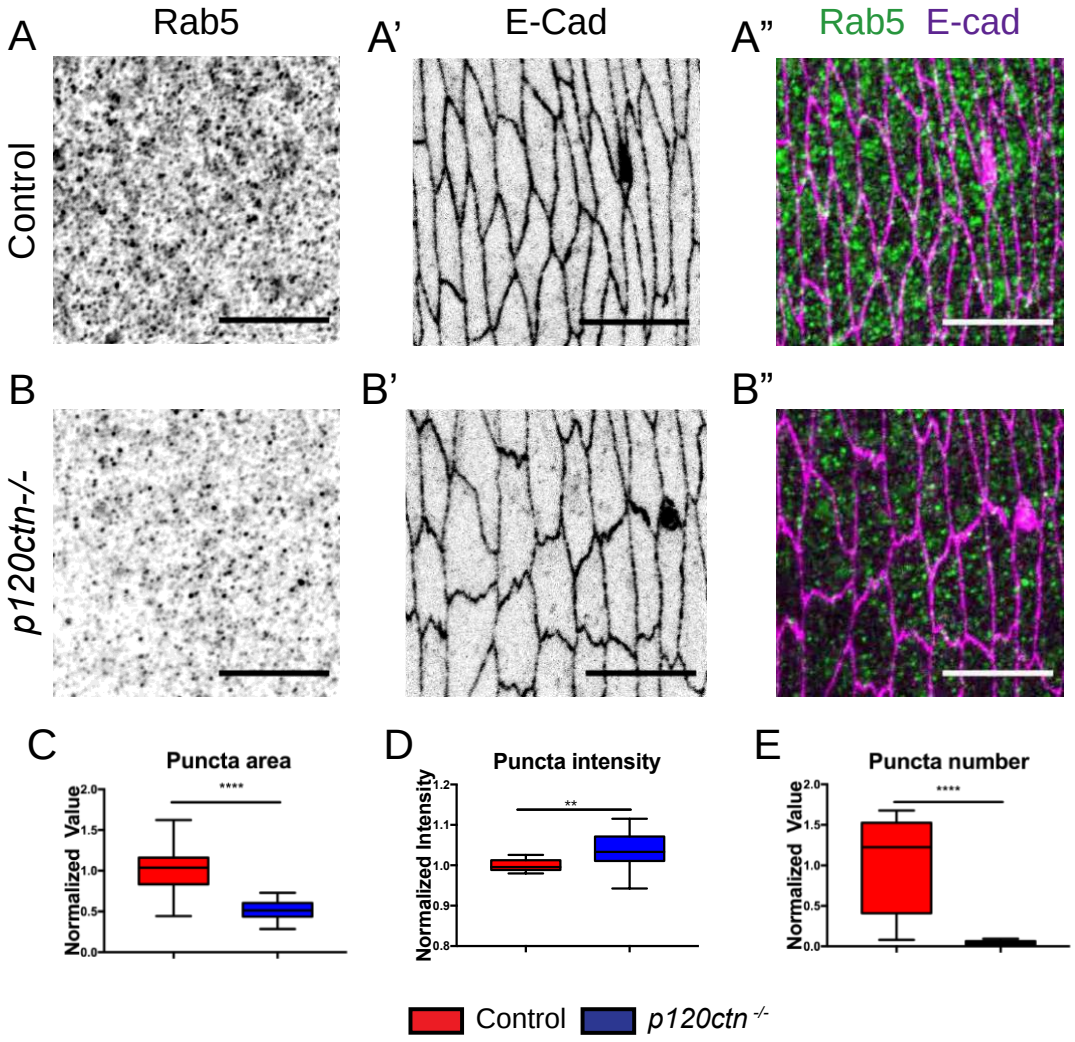

Figure 6.1. Rab5 is reduced in the plane of the AJs by the loss of p120ctn.

A-B. Localization of the Rab5 signal by immunostaining in the dorsolateral epidermis of stage 15 *Drosophila* in control (**A**) and *p120ctn*$^{-/-}$ mutant embryos (**B**), with cell borders visualized by E-cad-GFP. Grey left and central images are the individual channels (Rab5 and E-cad-GFP, respectively); the right panel is a merged image to show the signal of the two proteins respective to one another (Rab5 in green and E-cad in magenta). **C-E**. Quantification of the Rab5 signal using the puncta script, all normalized and expressed relative to the control embryo values. (**C)** The area of the puncta as an average of all puncta. (**D**) The intensity of the puncta as an average of all measured in the images. (**E**) The number of puncta in the images as defined using a threshold set by the control. Statistical analysis was a two-tailed student t-test with Welch's correction. *, $P < 0.05$; **, $P < 0.01$ ***, $P < 0.001$; ****, $P < 0.0001$. (n= 15-20 embryos per genotype) scale bar represents 10 µm.

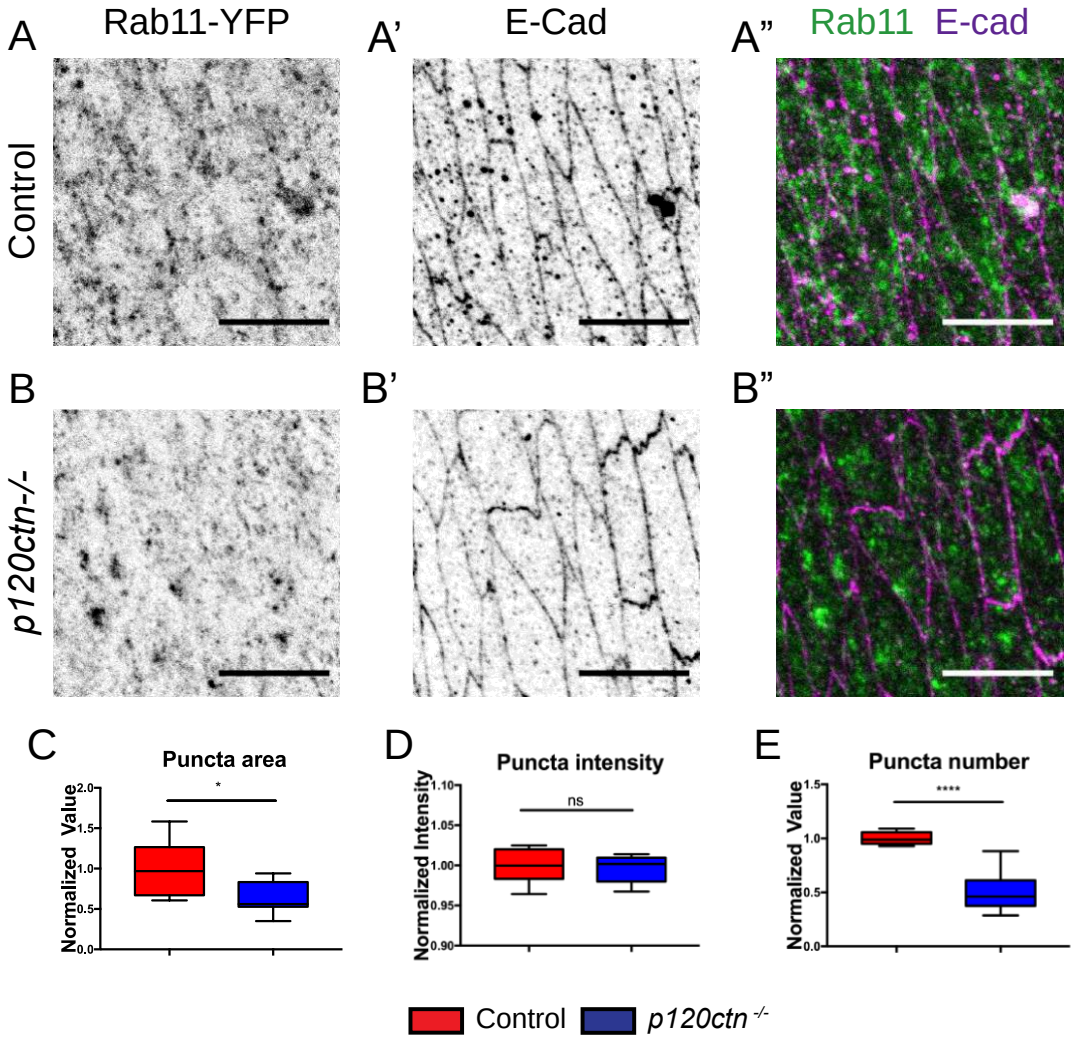

Figure 6.2. Rab11 is also reduced in the plane of the AJs by loss of p120ctn.

A-B. Localization of the endogenously tagged Rab11-YFP signal in the dorsolateral epidermis of stage 15 *Drosophila* in control (**A**) and *p120ctn*$^{-/-}$ mutant embryos (**B**), with cell borders visualized by E-cad immunostaining. Grey left and central images are the individual channels (Rab11-YFP and E-cad stained with Cy3, respectively); the right panel is a merged image to show the signal of the two proteins respective to one another (Rab11 in green and E-cad in magenta). **C-E**. Quantification of the Rab11 signal using the puncta script, all normalized and expressed relative to the control embryo values. (**C)** The area of the puncta as an average of all puncta. (**D**) The intensity of the puncta as an average of all measured in the images. (**E**) The number of puncta in the images as defined using a threshold set by the control. Statistical analysis was a two-tailed student t-test with Welch's correction. *, $P < 0.05$; **, $P < 0.01$ ***, $P < 0.001$; ****, $P < 0.0001$. (n= 15-20 embryos per genotype) scale bar represents 10 µm.

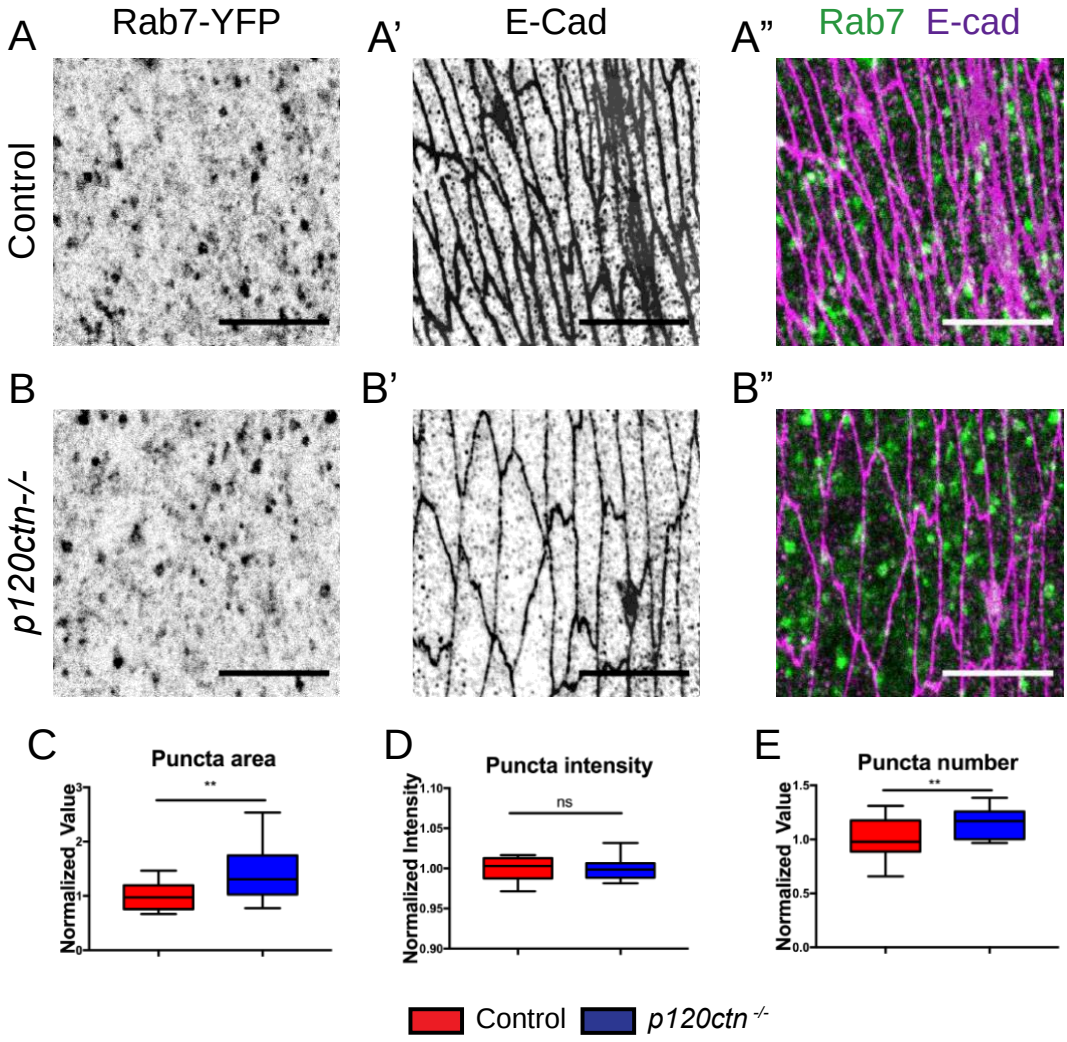

Figure 6.3. Rab7 is increased in the absence of p120ctn.

A-B. Localization of the endogenously tagged Rab7-YFP signal in the dorsolateral epidermis of stage 15 *Drosophila* in control (**A**) and *p120ctn*$^{-/-}$ mutant embryos (**B**), with cell borders visualized by E-cad immunostaining. Grey left and central images are the individual channels (Rab7-YFP and E-cad stained with Cy3, respectively); the right panel is a merged image to show the signal of the two proteins respective to one another (Rab7 in green and E-cad in magenta). **C-E**. Quantification of the Rab7 signal using the puncta script, all normalized and expressed relative to the control embryo values. (**C)** The area of the puncta as an average of all puncta. (**D**) The intensity of the puncta as an average of all measured in the images. (**E**) The number of puncta in the images as defined using a threshold set by the control. Statistical analysis was a two-tailed student t-test with Welch's correction. *, $P < 0.05$; **, $P < 0.01$ ***, $P < 0.001$; ****, $P < 0.0001$. (n= 15-20 embryos per genotype) scale bar represents 10 µm.

Chapter 7: Discussion and Final Conclusion

7.1) Overview

In this work I have presented a new insight into the mechanism of p120ctn dependent regulation of E-cad in the *Drosophila* system. This work has advanced the understanding of how p120ctn determines the amount of E-cad present at the cell surface and identified some of the mediators which operate downstream of p120ctn to facilitate this process. To my knowledge this is the first work which has undertaken a comprehensive analysis of the molecular pathways which operate downstream of p120ctn and the mechanism elucidated lend clarity on some previous work which has implicated but not studied the role of Rho and related GTPases.

In this work I present several key advances to the understanding of the role of p120ctn: First I have identified that p120ctn operates via a clathrin-mediated endocytic pathway, this is the first time the specific pathway that p120ctn uses has been identified and the stark effect on clathrin dynamics of modulating p120ctn has been demonstrated. Second I have shown that p120ctn activates the RhoA signalling pathway at the plasma membrane with the consequent effect that E-cad is retained and stabilized. Third, I identified a plasma membrane resident population of Arf1 which interacts with p120ctn, which is of interest in itself as Arf1 is considered to be primarily resident on the Golgi surface and traffics cargo in the anterograde pathway from the Golgi to the plasma membrane. My findings indicate that Arf1 has a functional role at the plasma membrane: to facilitate the internalization of E-cad and potentially other cargoes. This is the first demonstration of a functional role of this plasma membrane bound population. Fourth, I have undertaken a direct examination of the dynamics of p120ctn *in vivo* and shown that it localizes in a 1:1 stoichiometric manner with E-cad (taking advantage of the model system in which E-cad is asymmetrical distributed between two cell borders) and the dynamics of the p120ctn protein itself replicates precisely those of E-cad. Interestingly the recovery of p120ctn was reminiscent of the slow recovery phase observed in control E-cad. Fifth, I have undertaken a broader examination of the role of p120ctn in the vesicle trafficking pathways by using the Arf1-GFP resident population as a proxy for the activity of the TGN. The serendipitous identification of Arf1 as an interactor of p120ctn enabled us to study the TGN by proxy and infer the broader trafficking role that p120ctn has on the TGN. This analysis supports the view that p120ctn is a regulator of turnover and trafficking of E-cad in the cytoplasm. Finally, this work demonstrates for the first time a role for p120ctn in mechanotransduction. Using the laser ablation recoil of plasma

membranes, I studied mechanical tension within the cell membrane and found a p120ctn level dependent response. This aspect of p120ctn activity is entirely novel and is present for the first time in this work. I have identified that p120cn levels act as a determinant of tension and as a potential regulator of mechanotransduction of cell adhesion. As all of the findings presented in this work use proteins and cellular components which are widely expressed across evolutionarily diverse species it is likely that the mechanisms identified represent general features of cell biology.

In the following sections I discuss the several key findings of this work in turn and explore the implications of these findings within the field and the probable future direction of research into p120ctn.

7.2) p120ctn acts via a clathrin-mediated endocytic pathway

I have identified that p120ctn operates via a clathrin-mediated endocytic mechanism in multiple epithelial tissues. The significance of this finding is as the first to identify the pathway through which p120ctn regulates the turnover of E-cad at the plasma membrane. Previous work ascribed the mechanism of p120ctn to endocytosis but until this work none had explored the precise pathway. Multiple endocytic pathways exist in the mammalian system which internalize a range of cargo (Doherty and McMahon, 2009; Kaksonen and Roux, 2018; Mayor et al., 2014). This is a relatively unknown aspect in the *Drosophila* model, many studies have used the dominant negative or temperature inducted variant of the protein Dynamin (Baron, 2012; Damke et al., 2001; Kroll et al., 2015; Lee et al., 1999; Wülbeck et al., 2009) to prevent endocytosis but none have delved into the details of the individual endocytic pathways. Indeed, the existence of clathrin-independent endocytosis (CIE) pathways in *Drosophila* is still the subject of contention, with limited evidence in favour (Guha et al., 2003) and the primary objection arising from the absence of caveolin-encoding genes. Though one might argue that the CIE requires fewer components and would be therefore a probable pathway to emerge early in evolution, thus persisting in many organsims. In view of this, my finding that p120ctn interacts with clathrin may be unsurprising but the significance of this is broader than a mere identification of the specific internalization pathway. As I have also demonstrated that Arf1 recruits clathrin at the plasma membrane and p120ctn recruits Arf1, in view of the internalization for endocytic recycling evident in the presence of p120ctn, it is probable that the clathrin-mediated pathway targets the vesicles for trafficking to the Golgi and recycling: this aspect and evidence for this is discussed further below. The question which arises from this identification of a genetic or

network interaction between p120ctn and the clathrin-mediated internalization pathway is the nature of the molecular mechanism. The conventional view is that adaptor proteins (AP) recruit clathrin (Carvajal-Gonzalez et al., 2015; Ren et al., 2013), at the plasma membrane this has been the domain of AP2. However, as I have shown Arf1 at the plasma membrane with functional significance, in consideration of the known recruitment of AP1 by Arf1 at the Golgi (Ren et al., 2013), I could speculate that Arf1 is recruiting the same AP1 to the plasma membrane or is recruiting AP2, either possibility would be a novel finding. Indeed, the ongoing examination in the lab suggests the presence of AP1 at the plasma membrane (MRM, personal communication). Alternatively, p120ctn itself may recruit AP2, the counterargument to this proposition is the recruitment of Arf1, however this may not be the only means by which p120ctn initiates the process of internalization of cargo. Indeed, the nature of the cargo could determine the specific AP recruited. It is conceivable that, as p120ctn is in complex with all E-cad, and E-cad forms clusters of various sizes and dimensions, p120ctn can recruit different APs or other clathrin recruiters to initiate endocytosis relative to the cluster size. Further it may be possible that p120ctn is activating CIE, which is unstudied in this work. However, the argument against this is predicated on the finding that p120ctn mutants exhibit lower levels of E-cad at the membrane. If p120ctn were the only means by which E-cad could be internalized, then in the p120ctn mutant, E-cad would accumulate indefinitely on the plasma membrane. This highly indicates the existence of p120ctn independent pathway for E-cad internalization. Further I have shown that in the absence of p120ctn there is an increase in the endosomal degradation pathway (marked by Rab 7). This is a further indication of a separate p120ctn-independent and presumably CIE pathway for E-cad internalization, which predisposes the internalized E-cad for degradation. This identification of the gross pathway formed the basis for my subsequent dissection of the molecular meditators of p120ctn endocytic regulation of E-cad.

7.3) p120ctn activates the Rho signalling pathway at the plasma membrane

The study of the activity and function of the Rho signalling pathway in relation to cell adhesion and E-cad is a field heavy populated by publications. In the mammalian field it is widely viewed that p120ctn inhibits the action of Rho in the cytoplasm (Anastasiadis and Reynolds, 2001; Anastasiadis et al., 2000; Menke and Giehl, 2012). This has emerged from studies that uncoupled p120tn from E-cad and observed the consequent effect on Rho (Anastasiadis et al., 2000). Moreover, the specific binding and interaction with Rho has been mapped on the N-terminus of p120ctn along with several phosphorylation domains thought to

be important for the mediation of its interaction (Castaño et al., 2007; Mariner et al., 2001; Pieters et al., 2012). In the *Drosophila* system the possibility of any interaction with RhoA has been in question for some years (Fox and Peifer, 2007; Magie et al., 2002). I decided to evaluate this by using a broader measure of Rho signalling activity rather than focusing on RhoA specifically. By doing so I have shown that p120ctn activates Rho signalling at the plasma membrane and further that this has the function of altering the cortical actin to impede E-cad internalization and increase cortical tension. This is logical from the view of stabilization of the adherens junctional complexes to maintain and reinforce adhesion between cells. The interaction of the E-cad complex with cortical actin has been thought to be primarily mediated by α-catenin and vinculin (Dumbauld et al., 2013; Rangarajan and Izard, 2012; Yao et al., 2014). However, I have shown that this can be supplemented by p120ctn, indeed it is eminently possible that p120ctn has some direct action on α-catenin itself. But this particular aspect was not explored in the current work. It is conceivable that my results are compatible with those in the mammalian cells, if p120ctn is an activator of GTPase actin modulators at the plasma membrane, as is supposed as an evolutionarily ancient function for all catenins. It is entirely consistent with the notion that activity at the membrane would be complemented by an inhibition in the cytoplasm to prevent abnormal activity of Rho and undesirable contraction of the medial actin or other mechanism which could lead to aberrant cellular behaviour (Schackmann et al., 2011; van de Ven et al., 2015). This dual function of p120ctn would suggest that activation and inactivation of the actin modulation is conserved, further supposing the notion I present later that p120ctn is itself a mechanotransducer. By modulating actin dynamics and endocytosis of E-cad, p120ctn can both reinforce or reduce adhesion amount and strength. I have further identified a positive correlation of p120ctn levels at the membrane with the Rho signalling output. This allows the levels of p120ctn at the membrane to operate as an important determinant of Rho activity, an interaction which would also explain why Arf1 recruitment to the membranes is impaired in the case of p120cn overexpression, with the density of cortical actin potentially acting as a prohibitive barrier to the transportation of vesicles either to or from the plasma membrane. The nature of the balance between the promotion or inhibition of endocytosis by p120ctn in a Rho-dependant manner, and in consideration of the Arf1 data, would suggest that at a particular protein level p120ctn undergoes a switching action, or that the functional output of the Rho signalling pathway becomes sufficiently inhibitory for Arf1 to promote the internalization of vesicles. Alternatively, the system might depend on the ratio between the active and inactive p120ctn

fraction, However what accounts for, and moderates the levels of, p120ctn remains unknown and will be an interesting question for future work. Taking into consideration the membrane tension measures (discussed further below) it would be interesting to speculate about the border role that p120ctn has in actin dynamics and the effect on membrane rigidity and the impairment of endocytosis. Further it is an interesting question as to the nature of the interaction of p120ctn with Rho and other GTPases in the context of the different E-cad subpopulations and clusters in the plasma membrane. Presumably the immobile subcomplex are larger clusters which are tethered by strong attachments to the cortical actin, but for the moment this is inference and the role of p120ctn in these larger clusters is subject to conjecture.

7.4) The Arf1 population resident at the plasma membrane is used by p120ctn to internalize E-cad

My identification of Arf1 as an interactor of p120ctn has several novelties of its own. First the observation of Arf1 at the plasma member of cells is of interest as the conventional view was of Arf1 as a Golgi resident trafficking regulator of vesicles. Some previous publications had tangentially alluded to the presence of Arf1 at the plasma membrane (Kumari and Mayor, 2008), but none had examined if this population had a functional role. In my analysis I observed a large proportion of the Arf1 signal present at the trans face of the Golgi, however I consistently observed a population at the plasma membrane. This observation alone raises the question about how Arf1 comes to be localized to the plasma membrane. The first possibility is that it was an artefact of the overexpression, however this is countered by the localization I detected in the CRISPR tagged constructs I created during this work, which exhibits the same localization pattern as the transgenic construct (see Chapter 5). It could be conceivable that Arf1 is trafficked along with the vesicles between the Golgi and the plasma membrane, which would account for the existence of this secondary population. However, the majority of biochemical data available on Arf1 indicate that the N-terminal myristoylation is reversibly dependent on the activity of the protein when activated by GEFs (Franco et al., 1996; Harroun et al., 2005). It may be the non-punctate cytoplasmic signal represents an inactive hydrophilic pool of Arf1 and it requires specific GEF for localization, indeed some evidence for this is present at the Golgi surface (Rodrigues et al., 2016). For the moment it is impossible to say what precisely accounts for the existence of the secondary population of Arf1 at the plasma membrane, but it is most likely to be due to specific GEF

and the affinity of the different GEFs for the different Arf proteins (Jackson and Bouvet, 2014; Karandur et al., 2017).

The second element of novelty is my characterisation of a functional role of this population of Arf1 at the plasma membrane. I identified that Arf1 activity is required to promote the internalization of E-cad from the plasma membrane. As the effect is slight by comparison to the effect of the use of Rho dominant negative constructs, it is likely that Arf1 is not the only carrier used by p120ctn to facilitate the process of internalization. Moreover, the impairment of Rho destabilizes the entire cortical actin network, and by contrast the impairment of Arf1 function in later stages has a proportionally greater effect on the integrity of the Golgi itself. The functionality of the Arf1 population at the plasma membrane raises the further question about the nature of the trafficking between the plasma membrane and the Golgi in the context of the fraction of the E-cad population which is targeted for recycling as that which is degraded. In view of the data about Arf1 recruiting AP1, which is an Arf1 activity documented at the Golgi surface, and the loss of p120ctn abolishing the recycling component of E-cad, it is theoretically possible that the p120ctn interaction with Arf1 by some means determines the fate of the internalized E-cad cargo to be trafficked to the Golgi for recycling rather than degradation. This prospect is speculative for the present moment and will require further investigation to ascertian the veracity of the proposition, however it is an intriguing possibility that some measure of fate decision occurs at the plasma membrane.

7.5) The dynamics of p120tn replicate those of E-cad at the plasma membrane

In this work I have undertaken a direct examination of the stoichiometry of p120ctn in relation to E-cad at the plasma membrane and a study of the dynamics of p120ctn directly. This has allowed me to determine that p120ctn is in complex with both of the known subpopulations of E-cad, evident by the incomplete recovery of p120ctn at the plasma membrane, indicative of the existence of an immobile population of p120ctn at the plasma membrane. Further evidence of this is derived from the stoichiometry analysis, which is a special aspect of the tissue used in which E-cad is normally asymmetrically localized between the AP and DV cell borders. This asymmetry enabled me to assay the ratio comparability of E-cad and p120ctn. The use of the transgenic p120ctn construct induced a shift in the expressing cells of the E-cad asymmetry, however this was identical to the ratio of p120ctn between the AP:DV borders. Further the localization of p120ctn itself showed a high degree of membrane enrichment and co-localization with E-cad, within the limits of the resolution afforded by confocal microscopy. Prior to this work it had been tacitly assumed

that p120ctn was in complex with E-cad except in the cases in which dissociation was induced by other regulators which confer post-translation modification onto either p120ctn directly or onto the JMD to inhibit p120ctn binding and promote the internalization of E-cad (Fukumoto et al., 2008; Mariner et al., 2001; Piedra et al., 2003). Most of these studies used the mammalian cell system in culture, this has the disadvantages previously mentioned (Chapter 1 and 3) that the mammalian E-cad has evolved an additional endocytic motif on its JMD thus rendering it more sensitive to p120ctn loss, and the 2-Dimensional tissue cultures may not provide an accurate representation of the true forces and mechanism which responds to and regulates the turnover of cell adhesion *in vivo*. These critiques do not exclude the utility of the findings, they are merely stated to highlight the limitations of a single approach and to stipulate that they require validation in other model systems before they can be accepted as a general mechanism. As such no previous work has undertaken a stoichiometric assay of p120ctn to determine if association is a general feature in a system in which E-cad has not evolved additional sensitivity. My work addressed this point and showed that indeed E-cad-catenin complexes are the default configuration for the adherens junctions which is further supported in the *Drosophila* system by a recent publication from the Eaton lab (Iyer et al., 2019) .

The analysis of p120ctn dynamics presents its FRAP recovery as replicating those of E-cad in a wild-type genetic background. However, in these *UAS::*p120ctn-GFP expressing cells, this is not the case as the dynamics of E-cad itself are different due to it being stabilized at the plasma membrane by virtue of the overexpression of p120ctn induced by the use of the tagged construct (see Chapter 3). The reason for this discrepancy between E-cad and p120ctn dynamics, and the reason that p120ctn replicated the dynamics of WT E-cad in the p120ctn overexpression condition was rather perplexing. This is further complicated by the fact that p120ctn recovery, as fit by the model, conformed to a single exponential with a half-time which is similar to the slow recovery phase of E-cad recovery in the WT condition.

There are two separate but interconnected phenomena which require explanation in this case: first the discrepancy in the dynamics between E-cad and p120ctn in the overexpression cells, and second the reason for the elevation of E-cad at the membrane in these cells.

One can envision the following explanation for this discrepancy between E-cad and p120ctn recovery upon p120ctn overexpression. If p120ctn recovery is reaction limited and relies on uncoupling of this cytoplasmic protein from E-cad before or during vesicle formation, this uncoupling might still occur normally, despite inability to recruit Arf1 and

form vesicles will prevent the next step of E-cad endocytosis (Kang et al., 2010; Sprague and McNally, 2005). This would account for the primarily diffusional recovery in the single exponential curve, as measured by FRAP (See Chapter 4). Further, the saturation of p120ctn in these cells by virtue of the transgenic construct results in association with any available E-cad molecules, including those from newly synthesized E-cad, which would be indistinguishable from endocytic recycling in the FRAP experiment. The second phenomena which requires explanation is the elevation of E-cad at the plasma membrane in p120ctn overexpression. Assuming that p120ctn-independent internalization and the trafficking of newly synthesized protein are independent of direct regulation by p120ctn, it is theoretically possible that newly synthesized protein is still being trafficked to the membrane in the same amounts (assuming this is unaffected by membrane levels but is coupled to degradation). Due to the saturation mentioned above, p120ctn is binding all available E-cad therefore redirecting any that would be targeted for p120ctn-independent internalization (which predisposed for degradation) into the p120ctn-dependent recycling route. This system would operate in tandem with the signalling functions previously described to elevate Rho and provide the increased tension and physical barrier effect in the cortical actin. Determining the precise nature of these phenomena requires the examination of p120ctn dynamics at normal levels in an otherwise WT genetic background, which is a subject of ongoing research in the lab.

7.6) The TGN is also implicated in p120ctn dependent trafficking of E-cadherin

The identification of Arf1 as an interactor afforded the opportunity to explore the role of p120ctn in trafficking more broadly between the plasma membrane and the endosomal and Golgi system. As alluded previously the population of Arf1 on the Golgi surface allowed me to infer a proxy of the activity of the TGN. Having this in hand I was able to determine that the effect observed of altering p120ctn levels on the Arf1 population at the plasma membrane was replicated by the effect on the population of Arf1 which was resident at the Golgi surface. It was this which expanded the scope of the present work into the general function of p120ctn in trafficking of vesicles in the endosomal system in tandem with the direct analysis of the various compartments within the endosomal system directly (Chapter 6). Taking all of this data into account it is evident that p120ctn has a general function with the endosomal pathway, specifically the recycling pathway which operates via the Golgi. The loss of p120ctn induces a reduction in the volume of material being internalized to the Golgi, evident by the reduction of Arf1 at the Golgi in the p120ctn mutants and the reduction observed in

both Rab 5 and Rab 11 compartments. This is complemented by a concordant increase in the Rab 7 compartments, which is indicative of an elevation in the amount of degradation occurring in the absence of p120ctn. It is therefore evident that p120ctn is protective of E-cad by retaining it within the recycling circuit of cellular endosomal trafficking and sorting. The outstanding question from this is whether any direct recycling function of p120ctn is in evidence. If one examines the Rab 11 compartment and E-cad dynamics in the mutant condition it is apparent that recycling is impaired. However, it is not clear if this arises from a simple reduction in the volume which can be recycled by virtue of less being directed towards the Golgi or not being internalized at all. This raises two interesting propositions. The first it that recycling is coupled to internalization, a network interaction function which is logically sound, but which has not been previously demonstrated. Indeed, most studies prior to this work have examined the pathways in the endosomal system in isolation, it is more logical to my mind that one is dependent if not coupled to the other. Such a system would allow the cell to adjust and sense the proportion of one pathway and accordingly shift the other to adjust and modulate the system to maintain a degree of homeostatic balance. The second proposition is that fate decisions world appear to be determined at the plasma membrane. It is true that a p120ctn independent internalization pathway which directs E-cad towards degradation is in evidence, but how this is activated and why the E-cad which is internalized by this pathway (which is presumably also operating in the WT condition in the presence of and in tandem with the p120 dependent internalization pathway) remains an open question. It is possible that ubiquitination of the JMD in E-cad which has the p120ctn unbound by phosphorylation may predispose for this pathway. Evidence for this mechanism is apparent in mammalian cells but is lacking in *Drosophila* cells. Further such a mechanism would require the involvement of additional as yet unidentified mediators to ubiquitinate and phosphorylate the respective proteins.

As for p120ctn itself the identification and characterisation of its role beyond the regulation of endocytosis at the plasma membrane opens avenues for future work and provides the basis for several directions for investigation of the function of the protein and the role it plays throughout the cell to integrate multiple trafficking and signalling pathways. Finally, this work highlights and raises questions about cross-talk and interdependence of different pathways of intracellular trafficking and steps within each pathway.

7.7) Tension and membrane mechanical properties are influenced by p120ctn levels

The final discovery identified in this research represents an aspect of p120ctn which is presented for the first time in this work. The role of p120ctn in membrane tension could perhaps be inferred from the analysis previously presented of the effect of altering its levels on the Rho signalling pathway and MyosinII. However, this extends far beyond merely identification and characterization of a signalling pathway. The role of catenins in the regulation of the actin cytoskeleton has been documented as being the preserve of α-catenin, however I have shown that the levels of p120ctn not only have a linear correlative effect with the output of Rho signalling activity but also directly influence the tension present at the plasma membrane. At this juncture it is important to draw a distinction between the membrane and the cortical actin. Although I describe the effect of increasing or decreasing membrane tension it is not meant to suggest that p120ctn directly alters the properties of the lipid bilayer which composes the plasma membrane, but rather that the cortical actin is altered by the activity of p120ctn and this modification has a resultant effect on the dynamics of the membrane proper. It is entirely possible that an indirect alteration of the properties of the plasma membrane itself is induced by the alteration of the levels of E-cad at the membrane. This would result in an increased adhesion amount at the surface and possibly elevated rigidity of the lipid bilayer by virtue of the spatial restriction of the free movement of transmembrane proteins within the bilayer and the coupling of the E-cad with the molecules present on the adjacent surface of the neighbouring cell. Moreover, the viscoelastic properties of the membrane play a contributing factor in the measurement of the recoil and the tension present at the surface of the cell. These are the density of the cytoplasmic fluid within the plane of the AJ in his case which exhibits viscous properties (defined as the density and resistance of the liquid affecting the motion of the particles within a fluid medium) and second the elastic properties which are the capacity of the tissue to return to its original conformation or position once an eternal deforming force has been removed. From the mechanical view it is vital to take these elements into consideration when measuring the properties of the cell in relation to mechanotransduction and tension. From a biological view *in vivo*, it is difficult to measure these properties directly, but it is possible to infer using laser ablation. The use of the initial recoil to measure this property is reflective of this, the initial recoil is proportionally determined by the underlying tension in the system not the other viscoelastic properties. The latter metrics can be inferred and accounted for in calculation (Kelvin-Voigt model). Indeed, measuring and calculating the recoil during the entirety of the

experiment provided a measure of these elements by calculating the initial and total recoil of each condition. A recent publication has identified that p120ctn becomes more junctional as the pupal wing develops and the cells relax into a low tension state (Iyer et al., 2019). This work used an antibody to measure the proportion of p120ctn between the cytoplasm and the plasma membrane. Identifying an increase in junctional signal as cells become packed into a more regular hexagonal array, resulting in a lowering of the tension within the system. From this the authors describe p120ctn as being responsive to mechanical force. I show that p120ctn can directly influence the mechanical forces at the plasma membrane by altering the cortical actin. The two data can be reconciled by viewing p120ctn as a mechanosensitive mechanotransducer, that is to say it can both sense and influence force.

I have shown a direct role for p120ctn in modulating the tension of the cortical actin and the transduction of mechanical force. The questions which arise from this are many, but I anticipate that the nature of this interaction extends beyond the simple activation of Rho signalling into the direct mechanosensation and mechanotransduction directly: aspects which could represent a more general feature of the catenin family. Indeed, if p120ctn is both a mechanotransducer and regulator of E-cad endocytosis it would place it as a central regulatory hub for the entire adheres junction.

7.8) Conclusion

The protein p120ctn is a lesser known and studied member of the catenin protein family. This family bind to and regulate all aspects of cadherin dependent cell adhesion. Indeed, it is becoming more evident that during the course of evolution the catenin family, which initially were simply regulators of actin modulatory GTPases enzymes, were co-opted by the early cadherin molecules to co-ordinate the actin dependent intracellular cytoskeleton dynamics with the extracellular adhesion mediated by the cadherin proteins. The emergence of proteins which were specialized to attach cell to other adjacent cells, rather than to an extracellular protein matrix or secreted glycoprotein structure, required the integration of extracellular and intracellular adhesion. The other catenin family members, α- and β-, are responsible for the actin attachment and signalling functions respectively, indeed β-catenin has been extensively studied for its ability to interact with a multitude of proteins and signalling pathways. The repertoire of the catenin family is not however limited to these three members: several related sub-family proteins exist which contain the classical armadillo domains and cadherin interaction which defines the catenin family. It is becoming evident that the regulation of

actin and signalling is a core element of the catenin family, one might even go so far as to suggest that as a family they mediate all interactions between cell adhesion and the other functions and compartments of the cell. It is currently becoming more apparent that at least β-catenin and p120ctn itself can dissociate and interact with some transcription factors to mediate signalling response to growth factors or other transcription functions.

By contract to the other family members, p120ctn itself has garnered comparatively little attention. For the most part it has been the preserve of a select few groups mostly emerging from the lab in which it was identified. Though nothing is inherently wrong with this it does provide an interesting contrast with β-catenin which has been studied by dozens of groups from multiple fields in multiplicities contexts. Though it has been known that p120ctn is a regulator of E-cad at the plasma membrane and is highly correlated in cancerous conditions with the grade and metastasis of the primary tumours, knowledge about the precise molecular mediators which act downstream of p120tn have been lacking. The research undertaken in this doctorate has endeavoured to shed light upon this understudied aspect of p120ctn regulation of E-cad and to elucidate the molecular mechanisms of the identified interactors to enable a more comprehensive understanding of the function and activity of the protein. This work has identified novel interactors and mechanism for the activity of p120ctn which has lead us to propose that p120ctn act as a bi-directional regulator of E-cad in the same manner as a thermostat. It can adjust the levels of E-cad in both directions to increase or decrease adhesion at the surface as required. I discovered that p120ctn does this in tandem with altering the dynamics of the cytoskeleton in a tension and force dependent manner. It is this facet in particular which opens the most unexplored aspect for future work. I anticipate that the publications arising from this work and, at the time of writing, a more general increasing appreciation that appears to be emerging into the role of p120ctn more generally bodes well for the field. It is the view of this author that in the years to come data which reconciles mammalian and non-mammalian p120ctn data will emerge. Moreover, the effect of p120ctn in mechanotransduction, the understanding of which is in its infancy, will this author hope's lead to greater interest in p120ctn and more generally into the lesser appreciated E-cad interactors.

Acknowledgments

I would first like to acknowledge and express my gratitude to my supervisor, Dr Natalia Bulgakova. Not only for making available this project, but during its course for her consistent demand of academic and intellectual excellence in all matters. At times these seemed taxing, but they forced me to be more critical and to challenge all preconceptions of various subjects which were brought to bear. Because of this and for innumerable stimulating discourses and debates I am of the view that I have been forged into a better, and I hope wiser, scientist. For this she will ever have my respect and gratitude.

I wish next to acknowledge the other members of the lab who joined during my doctorate, they have all stimulated some interesting debate and provided a measure of personability and camaraderie which is much needed in the academic sphere.

Third, the friends and many acquaintances I have made during this time and on my travels to conferences. You all were curious specimens of the species and it was an honour and a privilege to see so many of all creeds and types.

Last and by no means least, I owe a debt which I cannot repay to my family. We have striven through dark time these last years and we are fewer in number but no less in spirt or love. With words I cannot say what is due, but know only that what I am this day began with what you were and are in all the days which came before.

References

Abedin, M., and King, N. (2008). The Premetazoan Ancestry of Cadherins. Science *319*, 946–948.

Abedin, M., and King, N. (2010). Diverse evolutionary paths to cell adhesion. Trends Cell Biol. *20*, 734–742.

Aberle, H., Schwartz, H., and Kemler, R. (1996). Cadherin-catenin complex: protein interactions and their implications for cadherin function. J. Cell. Biochem. *61*, 514–523.

Aiello, N.M., Bajor, D.L., Norgard, R.J., Sahmoud, A., Bhagwat, N., Pham, M.N., Cornish, T.C., Iacobuzio-Donahue, C.A., Vonderheide, R.H., and Stanger, B.Z. (2016). Metastatic progression is associated with dynamic changes in the local microenvironment. Nat. Commun. *7*.

Akkoca, A.N., Yanık, S., Özdemir, Z.T., Cihan, F.G., Sayar, S., Cincin, T.G., Çam, A., and Özer, C. (2014). TNM and Modified Dukes staging along with the demographic characteristics of patients with colorectal carcinoma. Int. J. Clin. Exp. Med. *7*, 2828–2835.

Anastasiadis, P.Z., and Reynolds, A.B. (2000). The p120 catenin family: complex roles in adhesion, signaling and cancer. J. Cell Sci. *113 (Pt 8)*, 1319–1334.

Anastasiadis, P.Z., and Reynolds, A.B. (2001). Regulation of Rho GTPases by p120-catenin. Curr. Opin. Cell Biol. *13*, 604–610.

Anastasiadis, P.Z., Moon, S.Y., Thoreson, M.A., Mariner, D.J., Crawford, H.C., Zheng, Y., and Reynolds, A.B. (2000a). Inhibition of RhoA by p120 catenin. Nat. Cell Biol. *2*, 637–644.

Anastasiadis, P.Z., Moon, S.Y., Thoreson, M.A., Mariner, D.J., Crawford, H.C., Zheng, Y., and Reynolds, A.B. (2000b). Inhibition of RhoA by p120 catenin. Nat. Cell Biol. *2*, 637–644.

Andl, C.D., Fargnoli, B.B., Okawa, T., Bowser, M., Takaoka, M., Nakagawa, H., Klein-Szanto, A., Hua, X., Herlyn, M., and Rustgi, A.K. (2006). Coordinated Functions of E-

Cadherin and Transforming Growth Factor β Receptor II In vitro and In vivo. Cancer Res. *66*, 9878–9885.

Arend, R.C., Londoño-Joshi, A.I., Straughn, J.M., and Buchsbaum, D.J. (2013). The Wnt/β-catenin pathway in ovarian cancer: a review. Gynecol. Oncol. *131*, 772–779.

Arzumanyan, A., Friedman, T., Kotei, E., Ng, I.O.L., Lian, Z., and Feitelson, M.A. (2012). Epigenetic repression of E-cadherin expression by hepatitis B virus x antigen in liver cancer. Oncogene *31*, 563–572.

Baron M (2012) Endocytic routes to Notch activation. Semin Cell Dev Biol 23: 437–442.

Bausek, N. (2013). JAK-STAT signaling in stem cells and their niches in Drosophila. JAK-STAT *2*.

Bishop, N.E. (2003). Dynamics of endosomal sorting. Int. Rev. Cytol. *232*, 1–57.

Bleichrodt, R.-J., Hulsman, M., Wösten, H.A.B., and Reinders, M.J.T. (2015). Switching from a Unicellular to Multicellular Organization in an Aspergillus niger Hypha. MBio *6*, e00111-15.

von Blume, J., Alleaume, A.-M., Cantero-Recasens, G., Curwin, A., Carreras-Sureda, A., Zimmermann, T., van Galen, J., Wakana, Y., Valverde, M.A., and Malhotra, V. (2011). ADF/cofilin regulates secretory cargo sorting at the TGN via the Ca2+ ATPase SPCA1. Dev. Cell *20*, 652–662.

Boguslavsky, S., Grosheva, I., Landau, E., Shtutman, M., Cohen, M., Arnold, K., Feinstein, E., Geiger, B., and Bershadsky, A. (2007). p120 catenin regulates lamellipodial dynamics and cell adhesion in cooperation with cortactin. Proc. Natl. Acad. Sci. U. S. A. *104*, 10882–10887.

Bonazzi, M., Veiga, E., Pizarro-Cerdá, J., and Cossart, P. (2008). Successive post-translational modifications of E-cadherin are required for InlA-mediated internalization of Listeria monocytogenes. Cell. Microbiol. *10*, 2208–2222.

Bonazzi, M., Lecuit, M., and Cossart, P. (2009). Listeria monocytogenes internalin and E-cadherin: from bench to bedside. Cold Spring Harb. Perspect. Biol. *1*, a003087.

Bonifacino, J.S., and Rojas, R. (2006). Retrograde transport from endosomes to the trans-Golgi network. Nat. Rev. Mol. Cell Biol. *7*, 568–579.

Boulant, S., Kural, C., Zeeh, J.-C., Ubelmann, F., and Kirchhausen, T. (2011). Actin dynamics counteract membrane tension during clathrin-mediated endocytosis. Nat. Cell Biol. *13*, 1124–1131.

Breuillard, D., Leunen, D., Chemaly, N., Auclair, L., Pinard, J.M., Kaminska, A., Desguerre, I., Ouss, L., and Nabbout, R. (2016). Autism spectrum disorder phenotype and intellectual disability in females with epilepsy and PCDH-19 mutations. Epilepsy Behav. EB *60*, 75–80.

Bryant, P.J. (1975). Pattern formation in the imaginal wing disc of Drosophila melanogaster: fate map, regeneration and duplication. J. Exp. Zool. *193*, 49–77.

Bryant, D.M., and Mostov, K.E. (2008). From cells to organs: building polarized tissue. Nat. Rev. Mol. Cell Biol. *9*, 887–901.

Bucher, D., Frey, F., Sochacki, K.A., Kummer, S., Bergeest, J.-P., Godinez, W.J., Kräusslich, H.-G., Rohr, K., Taraska, J.W., Schwarz, U.S., et al. (2018). Clathrin-adaptor ratio and membrane tension regulate the flat-to-curved transition of the clathrin coat during endocytosis. Nat. Commun. *9*, 1109.

Bulfoni, M., Turetta, M., Del Ben, F., Di Loreto, C., Beltrami, A.P., and Cesselli, D. (2016). Dissecting the Heterogeneity of Circulating Tumor Cells in Metastatic Breast Cancer: Going Far Beyond the Needle in the Haystack. Int. J. Mol. Sci. *17*.

Bulgakova, N.A., and Brown, N.H. (2016). Drosophila p120-catenin is crucial for endocytosis of the dynamic E-cadherin-Bazooka complex. J. Cell Sci. *129*, 477–482.

Bulgakova, N.A., Grigoriev, I., Yap, A.S., Akhmanova, A., and Brown, N.H. (2013). Dynamic microtubules produce an asymmetric E-cadherin–Bazooka complex to maintain segment boundaries. J. Cell Biol. *201*, 887–901.

Cailliez, F., and Lavery, R. (2006). Dynamics and Stability of E-Cadherin Dimers. Biophys. J. *91*, 3964–3971.

Campbell, K., and Casanova, J. (2015). A role for E-cadherin in ensuring cohesive migration of a heterogeneous population of non-epithelial cells. Nat. Commun. *6*, 7998.

Canel, M., Serrels, A., Frame, M.C., and Brunton, V.G. (2013). E-cadherin-integrin crosstalk in cancer invasion and metastasis. J. Cell Sci. *126*, 393–401.

Carnahan, R.H., Rokas, A., Gaucher, E.A., and Reynolds, A.B. (2010). The Molecular Evolution of the p120-Catenin Subfamily and Its Functional Associations. PLOS ONE *5*, e15747.

Carvajal-Gonzalez, J.M., Balmer, S., Mendoza, M., Dussert, A., Collu, G., Roman, A.-C., Weber, U., Ciruna, B., and Mlodzik, M. (2015). The clathrin adaptor AP-1 complex and Arf1 regulate planar cell polarity in vivo. Nat. Commun. *6*, 6751.

Casagolda, D., Valle-Pérez, B. del, Valls, G., Lugilde, E., Vinyoles, M., Casado-Vela, J., Solanas, G., Batlle, E., Reynolds, A.B., Casal, J.I., et al. (2010). A p120-catenin–CK1ε complex regulates Wnt signaling. J Cell Sci *123*, 2621–2631.

Castaño, J., Solanas, G., Casagolda, D., Raurell, I., Villagrasa, P., Bustelo, X.R., Herreros, A.G. de, and Duñach, M. (2007). Specific Phosphorylation of p120-Catenin Regulatory Domain Differently Modulates Its Binding to RhoA. Mol. Cell. Biol. *27*, 1745–1757.

Chao, Y.L., Shepard, C.R., and Wells, A. (2010). Breast carcinoma cells re-express E-cadherin during mesenchymal to epithelial reverting transition. Mol. Cancer *9*, 179.

Chappuis-Flament, S., Wong, E., Hicks, L.D., Kay, C.M., and Gumbiner, B.M. (2001). Multiple cadherin extracellular repeats mediate homophilic binding and adhesion. J. Cell Biol. *154*, 231–243.

Chen, W.V., and Maniatis, T. (2013). Clustered protocadherins. Development *140*, 3297–3302.

Chen, M.-W., Chan, C.-P., Lin, Y.-J., and Yen, H.-H. (2019). Anatomical location-based nodal staging system is superior to the 7th edition of the American Joint Committee on Cancer staging system among patients with surgically resected, histologically low-grade gastric cancer: A single institutional experience. PLOS ONE *14*, e0211836.

Chen, X., Kojima, S., Borisy, G.G., and Green, K.J. (2003). p120 catenin associates with kinesin and facilitates the transport of cadherin–catenin complexes to intercellular junctions. J. Cell Biol. *163*, 547–557.

Chen, Y.T., Stewart, D.B., and Nelson, W.J. (1999). Coupling assembly of the E-cadherin/beta-catenin complex to efficient endoplasmic reticulum exit and basal-lateral membrane targeting of E-cadherin in polarized MDCK cells. J. Cell Biol. *144*, 687–699.

Chi, Z., and Melendez, A.J. (2007). Role of Cell Adhesion Molecules and Immune-Cell Migration in the Initiation, Onset and Development of Atherosclerosis. Cell Adhes. Migr. *1*, 171–175.

Chia, P.Z.C., Gunn, P., and Gleeson, P.A. (2013). Cargo trafficking between endosomes and the trans-Golgi network. Histochem. Cell Biol. *140*, 307–315.

Chiasson, C.M., Wittich, K.B., Vincent, P.A., Faundez, V., and Kowalczyk, A.P. (2009). p120-catenin inhibits VE-cadherin internalization through a Rho-independent mechanism. Mol. Biol. Cell *20*, 1970–1980.

Choi, Y.S., and Gumbiner, B. (1989). Expression of cell adhesion molecule E-cadherin in Xenopus embryos begins at gastrulation and predominates in the ectoderm. J. Cell Biol. *108*, 2449–2458.

Christou, N., Perraud, A., Blondy, S., Jauberteau, M.-O., Battu, S., and Mathonnet, M. (2017). E-cadherin: A potential biomarker of colorectal cancer prognosis. Oncol. Lett. *13*, 4571–4576.

Chu, E.K., Kilic, O., Cho, H., Groisman, A., and Levchenko, A. (2018). Self-induced mechanical stress can trigger biofilm formation in uropathogenic Escherichia coli. Nat. Commun. *9*, 4087.

Chua, H.L., Bhat-Nakshatri, P., Clare, S.E., Morimiya, A., Badve, S., and Nakshatri, H. (2007). NF-kappaB represses E-cadherin expression and enhances epithelial to mesenchymal transition of mammary epithelial cells: potential involvement of ZEB-1 and ZEB-2. Oncogene *26*, 711–724.

Ciesiolka, M., Delvaeye, M., Van Imschoot, G., Verschuere, V., McCrea, P., van Roy, F., and Vleminckx, K. (2004). p120 catenin is required for morphogenetic movements involved in the formation of the eyes and the craniofacial skeleton in Xenopus. J. Cell Sci. *117*, 4325–4339.

Clevers, H., and Nusse, R. (2012). Wnt/β-Catenin Signaling and Disease. Cell *149*, 1192–1205.

Cobb, M. (2017). 60 years ago, Francis Crick changed the logic of biology. PLoS Biol. *15*.

Coelho, C., Brown, L.C., Maryam, M., Vij, R., Smith, D.F., Burnet, M.C., Kyle, J.E., Heyman, H.M., Ramirez, J., Prados-Rosales, R., et al. (2018). Listeria monocytogenes virulence factors, including Listeriolysin O, are secreted in biologically active Extracellular Vesicles. J. Biol. Chem. jbc.RA118.006472.

Collins, C., Denisin, A.K., Pruitt, B.L., and Nelson, W.J. (2017). Changes in E-cadherin rigidity sensing regulate cell adhesion. Proc. Natl. Acad. Sci. *114*, E5835–E5844.

Colpitts, C.C., Lupberger, J., and Baumert, T.F. (2016). Multifaceted role of E-cadherin in hepatitis C virus infection and pathogenesis. Proc. Natl. Acad. Sci. U. S. A. *113*, 7298–7300.

Cousin, H. (2017). Cadherins function during the collective cell migration of Xenopus Cranial Neural Crest cells: revisiting the role of E-cadherin. Mech. Dev. *148*, 79–88.

Damke, H., Binns, D.D., Ueda, H., Schmid, S.L., and Baba, T. (2001). Dynamin GTPase Domain Mutants Block Endocytic Vesicle Formation at Morphologically Distinct Stages. Mol. Biol. Cell *12*, 2578–2589.

Danen, E.H., de Vries, T.J., Morandini, R., Ghanem, G.G., Ruiter, D.J., and van Muijen, G.N. (1996). E-cadherin expression in human melanoma. Melanoma Res. *6*, 127–131.

Daniel, J.M. (2007). Dancing in and out of the nucleus: p120ctn and the transcription factor Kaiso. Biochim. Biophys. Acta BBA - Mol. Cell Res. *1773*, 59–68.

Daniel, J.M., and Reynolds, A.B. (1995). The tyrosine kinase substrate p120cas binds directly to E-cadherin but not to the adenomatous polyposis coli protein or alpha-catenin. Mol. Cell. Biol. *15*, 4819–4824.

Dannhauser, P.N., and Ungewickell, E.J. (2012). Reconstitution of clathrin-coated bud and vesicle formation with minimal components. Nat. Cell Biol. *14*, 634–639.

Daugherty, R.L., and Gottardi, C.J. (2007). Phospho-regulation of β-Catenin Adhesion and Signaling Functions. Physiol. Bethesda Md *22*, 303–309.

Davis, M.A., Ireton, R.C., and Reynolds, A.B. (2003). A core function for p120-catenin in cadherin turnover. J Cell Biol *163*, 525–534.

Day, K.J., Staehelin, L.A., and Glick, B.S. (2013). A Three-Stage Model of Golgi Structure and Function. Histochem. Cell Biol. *140*, 239–249.

D'Costa, Z.J., Jolly, C., Androphy, E.J., Mercer, A., Matthews, C.M., and Hibma, M.H. (2012). Transcriptional Repression of E-Cadherin by Human Papillomavirus Type 16 E6. PLoS ONE *7*.

Dejana, E., Orsenigo, F., and Lampugnani, M.G. (2008). The role of adherens junctions and VE-cadherin in the control of vascular permeability. J. Cell Sci. *121*, 2115–2122.

Delon, I., and Brown, N. (2008). Cell–Matrix Adhesion: The Wech Connection. Curr. Biol. *18*, R389–R391.

Delon, I., and Brown, N.H. (2009). The integrin adhesion complex changes its composition and function during morphogenesis of an epithelium. J. Cell Sci. *122*, 4363–4374.

Delva, E., and Kowalczyk, A.P. (2009). Regulation of Cadherin Trafficking. Traffic Cph. Den. *10*, 259–267.

Desai, R., Sarpal, R., Ishiyama, N., Pellikka, M., Ikura, M., and Tepass, U. (2013). Monomeric α-catenin links cadherin to the actin cytoskeleton. Nat. Cell Biol. *15*, 261–273.

Dickinson, D.J., Nelson, W.J., and Weis, W.I. (2011). A Polarized Epithelium Organized by β- and α-Catenin Predates Cadherin and Metazoan Origins. Science *331*, 1336–1339.

Dillon, D.A., D'Aquila, T., Reynolds, A.B., Fearon, E.R., and Rimm, D.L. (1998). The expression of p120ctn protein in breast cancer is independent of alpha- and beta-catenin and E-cadherin. Am. J. Pathol. *152*, 75–82.

Doherty, G.J., and McMahon, H.T. (2009). Mechanisms of Endocytosis. Annu. Rev. Biochem. *78*, 857–902.

Donaldson, J.G., and Honda, A. (2005). Localization and function of Arf family GTPases. Biochem. Soc. Trans. *33*, 639–642.

Donaldson, J.G., and Jackson, C.L. (2011). ARF family G proteins and their regulators: roles in membrane transport, development and disease. Nat. Rev. Mol. Cell Biol. *12*, 362–375.

Donaldson, J.G., Honda, A., and Weigert, R. (2005). Multiple activities for Arf1 at the Golgi complex. Biochim. Biophys. Acta *1744*, 364–373.

Dorudi, S., Sheffield, J.P., Poulsom, R., Northover, J.M., and Hart, I.R. (1993). E-cadherin expression in colorectal cancer. An immunocytochemical and in situ hybridization study. Am. J. Pathol. *142*, 981–986.

Drees, F., Reilein, A., and Nelson, W.J. (2005a). Cell Adhesion Assays: Fabrication of an E-cadherin Substratum and Isolation of Lateral and Basal Membrane Patches. Methods Mol. Biol. Clifton Nj *294*, 303–320.

Drees, F., Pokutta, S., Yamada, S., Nelson, W.J., and Weis, W.I. (2005b). α-Catenin Is a Molecular Switch that Binds E-Cadherin-β-Catenin and Regulates Actin-Filament Assembly. Cell *123*, 903–915.

D'Souza-Schorey, C., and Chavrier, P. (2006). ARF proteins: roles in membrane traffic and beyond. Nat. Rev. Mol. Cell Biol. *7*, 347–358.

Dumbauld, D.W., Lee, T.T., Singh, A., Scrimgeour, J., Gersbach, C.A., Zamir, E.A., Fu, J., Chen, C.S., Curtis, J.E., Craig, S.W., et al. (2013). How vinculin regulates force transmission. Proc. Natl. Acad. Sci. *110*, 9788–9793.

Duñach, M., Valle-Pérez, B.D., and Herreros, A.G. de (2017). p120-catenin in canonical Wnt signaling. Crit. Rev. Biochem. Mol. Biol. *0*, 1–13.

Dupre-Crochet, S., Figueroa, A., Hogan, C., Ferber, E.C., Bialucha, C.U., Adams, J., Richardson, E.C.N., and Fujita, Y. (2007). Casein kinase 1 is a novel negative regulator of E-cadherin-based cell-cell contacts. Mol. Cell. Biol. *27*, 3804–3816.

El-Amraoui, A., and Petit, C. (2010). Cadherins as Targets for Genetic Diseases. Cold Spring Harb. Perspect. Biol. *2*.

El-Amraoui, A., and Petit, C. (2013). Cadherin defects in inherited human diseases. Prog. Mol. Biol. Transl. Sci. *116*, 361–384.

Elisha, Y., Kalchenko, V., Kuznetsov, Y., and Geiger, B. (2018). Dual role of E-cadherin in the regulation of invasive collective migration of mammary carcinoma cells. Sci. Rep. *8*, 4986.

Ellis, P.E., Cano, S.D., Fear, M., Kelsell, D.P., Ghali, L., Crow, J.C., Perrett, C.W., and MacLean, A.B. (2008). Reduced E-cadherin expression correlates with disease progression in Paget's disease of the vulva but not Paget's disease of the breast. Mod. Pathol. *21*, 1192–1199.

Ernst, A.M., Syed, S.A., Zaki, O., Bottanelli, F., Zheng, H., Hacke, M., Xi, Z., Rivera-Molina, F., Graham, M., Rebane, A.A., et al. (2018). S-Palmitoylation Sorts Membrane Cargo for Anterograde Transport in the Golgi. Dev. Cell *47*, 479-493.e7.

Escobar, D.J., Desai, R., Ishiyama, N., Folmsbee, S.S., Novak, M.N., Flozak, A.S., Daugherty, R.L., Mo, R., Nanavati, D., Sarpal, R., et al. (2015). α-Catenin phosphorylation promotes intercellular adhesion through a dual-kinase mechanism. J. Cell Sci. *128*, 1150–1165.

Fang, D., Hawke, D., Zheng, Y., Xia, Y., Meisenhelder, J., Nika, H., Mills, G.B., Kobayashi, R., Hunter, T., and Lu, Z. (2007). Phosphorylation of β-Catenin by AKT Promotes β-Catenin Transcriptional Activity. J. Biol. Chem. *282*, 11221–11229.

Ferreira, A.P.A., and Boucrot, E. (2018). Mechanisms of Carrier Formation during Clathrin-Independent Endocytosis. Trends Cell Biol. *28*, 188–200.

Ferreira, A.C., Suriano, G., Mendes, N., Gomes, B., Wen, X., Carneiro, F., Seruca, R., and Machado, J.C. (2012). E-cadherin impairment increases cell survival through Notch-dependent upregulation of Bcl-2. Hum. Mol. Genet. *21*, 334–343.

Foty, R.A., and Steinberg, M.S. (2005). The differential adhesion hypothesis: a direct evaluation. Dev. Biol. *278*, 255–263.

Fox, D.T., and Peifer, M. (2007). Cell Adhesion: Separation of p120's Powers? Curr. Biol. *17*, R24–R27.

Fox, D.T., Homem, C.C.F., Myster, S.H., Wang, F., Bain, E.E., and Peifer, M. (2005). Rho1 regulates Drosophila adherens junctions independently of p120ctn. Development *132*, 4819–4831.

Franco M, Chardin P, Chabre M, Paris S (1996) Myristoylation-facilitated Binding of the G Protein ARF1 to Membrane Phospholipids Is Required for Its Activation by a Soluble Nucleotide Exchange Factor. J Biol Chem 271: 1573–1578.

Frankel, E.B., and Audhya, A. (2018). ESCRT-dependent cargo sorting at multivesicular endosomes. Semin. Cell Dev. Biol. *74*, 4–10.

Friston, K., Brown, H.R., Siemerkus, J., and Stephan, K.E. (2016). The dysconnection hypothesis (2016). Schizophr. Res. *176*, 83–94.

de la Fuente-Núñez, C., Reffuveille, F., Fernández, L., and Hancock, R.E. (2013). Bacterial biofilm development as a multicellular adaptation: antibiotic resistance and new therapeutic strategies. Curr. Opin. Microbiol. *16*, 580–589.

Fukumoto, Y., Shintani, Y., Reynolds, A.B., Johnson, K.R., and Wheelock, M.J. (2008). The regulatory or phosphorylation domain of p120 catenin controls E-cadherin dynamics at the plasma membrane. Exp. Cell Res. *314*, 52–67.

Füllekrug, J., and Nilsson, T. (1998). Protein sorting in the Golgi complex. Biochim. Biophys. Acta BBA - Mol. Cell Res. *1404*, 77–84.

Geng, F., Zhu, W., Anderson, R.A., Leber, B., and Andrews, D.W. (2012). Multiple post-translational modifications regulate E-cadherin transport during apoptosis. J. Cell Sci. *125*, 2615–2625.

Ghadimi, B.M., and Grade, M. (2010). Cancer gene profiling for response prediction. Methods Mol. Biol. Clifton NJ *576*, 327–339.

Gilbert, S.F. (2000). Early Drosophila Development. Dev. Biol. 6th Ed.

Gloerich, M., Bianchini, J.M., Siemers, K.A., Cohen, D.J., and Nelson, W.J. (2017). Cell division orientation is coupled to cell–cell adhesion by the E-cadherin/LGN complex. Nat. Commun. *8*, 13996.

Gold, J.S., Reynolds, A.B., and Rimm, D.L. (1998). Loss of p120ctn in human colorectal cancer predicts metastasis and poor survival. Cancer Lett. *132*, 193–201.

Goldenring, J.R. (2015). Recycling endosomes. Curr. Opin. Cell Biol. *35*, 117–122.

Goldstein, B., and Macara, I.G. (2007). The PAR Proteins: Fundamental Players in Animal Cell Polarization. Dev. Cell *13*, 609–622.

Gommel DU, Memon AR, Heiss A, Lottspeich F, Pfannstiel J, Lechner J, Reinhard C, Helms JB, Nickel W, Wieland FT (2001) Recruitment to Golgi membranes of ADP-ribosylation factor 1 is mediated by the cytoplasmic domain of p23. EMBO J 20: 6751–6760.

Gong, H., Guo, Y., Linstedt, A., and Schwartz, R. (2010). Discrete, continuous, and stochastic models of protein sorting in the Golgi apparatus. Phys. Rev. E Stat. Nonlin. Soft Matter Phys. *81*, 011914.

González Flecha, F.L. (2017). Kinetic stability of membrane proteins. Biophys. Rev. *9*, 563–572.

Gou, J., Lin, L., and Othmer, H.G. (2018). A Model for the Hippo Pathway in the Drosophila Wing Disc. Biophys. J. *115*, 737–747.

Grabowska, M.M., and Day, M.L. (2012). Soluble E-cadherin: more than a symptom of disease. Front. Biosci. Landmark Ed. *17*, 1948–1964.

Grammont, M. (2007). Adherens junction remodeling by the Notch pathway in Drosophila melanogaster oogenesis. J. Cell Biol. *177*, 139–150.

Grant, B.D., and Donaldson, J.G. (2009). Pathways and mechanisms of endocytic recycling. Nat. Rev. Mol. Cell Biol. *10*, 597–608.

Greene, N.D.E., and Copp, A.J. (2014). Neural Tube Defects. Annu. Rev. Neurosci. *37*, 221–242.

Grigoraş, M.L., Arghirescu, T.S., Folescu, R., Talpoş, I.C., Gîndac, C.M., Zamfir, C.L., Cornianu, M., Anghel, M.D., and Levai, C.M. (2017). Expression of E-cadherin in lung carcinoma, other than those with small cells (NSCLC). Romanian J. Morphol. Embryol. Rev. Roum. Morphol. Embryol. *58*, 1317–1325.

Gross, J.C., Schreiner, A., Engels, K., and Starzinski-Powitz, A. (2009). E-cadherin surface levels in epithelial growth factor-stimulated cells depend on adherens junction protein shrew-1. Mol. Biol. Cell *20*, 3598–3607.

Gu, C., Liu, M., Zhao, T., Wang, D., and Wang, Y. (2015). Protective role of p120-catenin in maintaining the integrity of adherens and tight junctions in ventilator-induced lung injury. Respir. Res. *16*, 58.

Gu, F., Crump, C.M., and Thomas, G. (2001). Trans-Golgi network sorting. Cell. Mol. Life Sci. CMLS *58*, 1067–1084.

Guha, A., Sriram, V., Krishnan, K.S., and Mayor, S. (2003). Shibire mutations reveal distinct dynamin-independent and -dependent endocytic pathways in primary cultures of Drosophila hemocytes. J. Cell Sci. *116*, 3373–3386.

Guillen, I., Mullor, J.L., Capdevila, J., Sanchez-Herrero, E., Morata, G., and Guerrero, I. (1995). The function of engrailed and the specification of Drosophila wing pattern. Development *121*, 3447–3456.

Gul, I.S., Hulpiau, P., Saeys, Y., and van Roy, F. (2017). Evolution and diversity of cadherins and catenins. Exp. Cell Res. *358*, 3–9.

Gumbiner, B.M. (2000). Regulation of Cadherin Adhesive Activity. J. Cell Biol. *148*, 399–404.

Gumbiner, B.M., and Kim, N.-G. (2014). The Hippo-YAP signaling pathway and contact inhibition of growth. J. Cell Sci. *127*, 709–717.

Guo, Y., Sirkis, D.W., and Schekman, R. (2014). Protein Sorting at the trans-Golgi Network. Annu. Rev. Cell Dev. Biol. *30*, 169–206.

Halbleib, J.M., and Nelson, W.J. (2006). Cadherins in development: cell adhesion, sorting, and tissue morphogenesis. Genes Dev. *20*, 3199–3214.

Hanahan, D., and Weinberg, R.A. (2000). The Hallmarks of Cancer. Cell *100*, 57–70.

Hanahan, D., and Weinberg, R.A. (2011). Hallmarks of Cancer: The Next Generation. Cell *144*, 646–674.

Harrison, O.J., Jin, X., Hong, S., Bahna, F., Ahlsen, G., Brasch, J., Wu, Y., Vendome, J., Felsovalyi, K., Hampton, C.M., et al. (2011). The Extracellular Architecture of Adherens Junctions Revealed by Crystal Structures of Type I Cadherins. Structure *19*, 244–256.

Harroun TA, Bradshaw JP, Balali-Mood K, Katsaras J (2005) A structural study of the myristoylated N-terminus of ARF1. Biochim Biophys Acta BBA - Biomembr 1668: 138–144.

Hartsock, A., and Nelson, W.J. (2012). Competitive Regulation of E-Cadherin JuxtaMembrane Domain Degradation by p120-Catenin Binding and Hakai-Mediated Ubiquitination. PLOS ONE *7*, e37476.

Haruki, S., Imoto, I., Kozaki, K., Matsui, T., Kawachi, H., Komatsu, S., Muramatsu, T., Shimada, Y., Kawano, T., and Inazawa, J. (2010). Frequent silencing of protocadherin 17 , a candidate tumour suppressor for esophageal squamous cell carcinoma. Carcinogenesis *31*, 1027–1036.

Hatzfeld, M. (2005). The p120 family of cell adhesion molecules. Eur. J. Cell Biol. *84*, 205–214.

Hayashi, S., and Takeichi, M. (2015). Emerging roles of protocadherins: from self-avoidance to enhancement of motility. J. Cell Sci. *128*, 1455–1464.

He, H., Shulkes, A., and Baldwin, G.S. (2008). PAK1 interacts with beta-catenin and is required for the regulation of the beta-catenin signalling pathway by gastrins. Biochim. Biophys. Acta *1783*, 1943–1954.

van Hengel, J., and van Roy, F. (2007). Diverse functions of p120ctn in tumors. Biochim. Biophys. Acta BBA - Mol. Cell Res. *1773*, 78–88.

Heuberger, J., and Birchmeier, W. (2010). Interplay of Cadherin-Mediated Cell Adhesion and Canonical Wnt Signaling. Cold Spring Harb. Perspect. Biol. *2*, a002915.

Hou, J.C., Shigematsu, S., Crawford, H.C., Anastasiadis, P.Z., and Pessin, J.E. (2006). Dual regulation of Rho and Rac by p120 catenin controls adipocyte plasma membrane trafficking. J. Biol. Chem. *281*, 23307–23312.

Hsu, V.W., and Prekeris, R. (2010). Transport at the Recycling Endosome. Curr. Opin. Cell Biol. *22*, 528–534.

Hsu, M.-Y., Meier, F.E., Nesbit, M., Hsu, J.-Y., Van Belle, P., Elder, D.E., and Herlyn, M. (2000). E-Cadherin Expression in Melanoma Cells Restores Keratinocyte-Mediated Growth Control and Down-Regulates Expression of Invasion-Related Adhesion Receptors. Am. J. Pathol. *156*, 1515–1525.

Hu, G. (2012). p120-Catenin: a novel regulator of innate immunity and inflammation. Crit. Rev. Immunol. *32*, 127–138.

Huang, S., and Wang, Y. (2017). Golgi structure formation, function, and post-translational modifications in mammalian cells. F1000Research *6*.

Hulpiau, P., Gul, I.S., and van Roy, F. (2013). New insights into the evolution of metazoan cadherins and catenins. Prog. Mol. Biol. Transl. Sci. *116*, 71–94.

Hunter, K.W., Crawford, N.P., and Alsarraj, J. (2008). Mechanisms of metastasis. Breast Cancer Res. BCR *10*, S2.

Hwang, S., Zimmerman, N.P., Agle, K.A., Turner, J.R., Kumar, S.N., and Dwinell, M.B. (2012). E-cadherin Is Critical for Collective Sheet Migration and Is Regulated by the Chemokine CXCL12 Protein During Restitution. J. Biol. Chem. *287*, 22227–22240.

Hynes, R.O., and Zhao, Q. (2000). The Evolution of Cell Adhesion. J. Cell Biol. *150*, F89–F96.

Ichii, T., and Takeichi, M. (2007). p120-catenin regulates microtubule dynamics and cell migration in a cadherin-independent manner. Genes Cells Devoted Mol. Cell. Mech. *12*, 827–839.

Ireton, R.C., Davis, M.A., van Hengel, J., Mariner, D.J., Barnes, K., Thoreson, M.A., Anastasiadis, P.Z., Matrisian, L., Bundy, L.M., Sealy, L., et al. (2002). A novel role for p120 catenin in E-cadherin function. J. Cell Biol. *159*, 465–476.

Irvine, K.D., and Harvey, K.F. (2015). Control of Organ Growth by Patterning and Hippo Signaling in Drosophila. Cold Spring Harb. Perspect. Biol. *7*.

Ishiyama, N., Lee, S.-H., Liu, S., Li, G.-Y., Smith, M.J., Reichardt, L.F., and Ikura, M. (2010). Dynamic and Static Interactions between p120 Catenin and E-Cadherin Regulate the Stability of Cell-Cell Adhesion. Cell *141*, 117–128.

Iyer, K.V., Piscitello-Gómez, R., Paijmans, J., Jülicher, F., and Eaton, S. (2019). Epithelial Viscoelasticity Is Regulated by Mechanosensitive E-cadherin Turnover. Curr. Biol. *29*, 578-591.e5.

Janowski, B.A., Huffman, K.E., Schwartz, J.C., Ram, R., Hardy, D., Shames, D.S., Minna, J.D., and Corey, D.R. (2005). Inhibiting gene expression at transcription start sites in chromosomal DNA with antigene RNAs. Nat. Chem. Biol. *1*, 216–222.

Jawhari, A.U., Noda, M., Pignatelli, M., and Farthing, M. (1999). Up-regulated cytoplasmic expression, with reduced membranous distribution, of the src substrate p120(ctn) in gastric carcinoma. J. Pathol. *189*, 180–185.

Jeanes, A., Gottardi, C., and Yap, A. (2008). Cadherins and cancer: how does cadherin dysfunction promote tumor progression? Oncogene *27*, 6920–6929.

Jian, X., Cavenagh, M., Gruschus, J.M., Randazzo, P.A., and Kahn, R.A. (2010). Modifications to the C-terminus of Arf1 alter cell functions and protein interactions. Traffic Cph. Den. *11*, 732–742.

Jinek, M., Chylinski, K., Fonfara, I., Hauer, M., Doudna, J.A., and Charpentier, E. (2012). A programmable dual-RNA-guided DNA endonuclease in adaptive bacterial immunity. Science *337*, 816–821.

Jovic, M., Sharma, M., Rahajeng, J., and Caplan, S. (2010). The early endosome: a busy sorting station for proteins at the crossroads. Histol. Histopathol. *25*, 99–112.

Kaksonen, M., and Roux, A. (2018). Mechanisms of clathrin-mediated endocytosis. Nat. Rev. Mol. Cell Biol. *19*, 313–326.

Kanazawa, N., Oda, T., Gunji, N., Nozue, M., Kawamoto, T., Todoroki, T., and Fukao, K. (2002). E-cadherin expression in the primary tumors and metastatic lymph nodes of poorly differentiated types of rectal cancer. Surg. Today *32*, 123–128.

Kang, M., Day, C.A., DiBenedetto, E., and Kenworthy, A.K. (2010). A Quantitative Approach to Analyze Binding Diffusion Kinetics by Confocal FRAP. Biophys. J. *99*, 2737–2747.

Karim, M.R., Haruta, T., Matsumoto, T., Oda, H., and Taniguchi, H. (2016). Imaging of Cell Shape Alteration and Cell Movement in Drosophila Gastrulation Using DE-cadherin Reporter Transgenic Flies. J. Vis. Exp. JoVE.

Kashiwagi, S., Yashiro, M., Takashima, T., Nomura, S., Noda, S., Kawajiri, H., Ishikawa, T., Wakasa, K., and Hirakawa, K. (2010). Significance of E-cadherin expression in triple-negative breast cancer. Br. J. Cancer *103*, 249–255.

Kelly, B.T., and Owen, D.J. (2011). Endocytic sorting of transmembrane protein cargo. Curr. Opin. Cell Biol. *23*, 404–412.

Kienzle, C., and Blume, J. von (2014). Secretory cargo sorting at the trans-Golgi network. Trends Cell Biol. *24*, 584–593.

Kim, H., Han, J.-R., Park, J., Oh, M., James, S.E., Chang, S., Lu, Q., Lee, K.Y., Ki, H., Song, W.-J., et al. (2008). Delta-catenin-induced dendritic morphogenesis. An essential role of p190RhoGEF interaction through Akt1-mediated phosphorylation. J. Biol. Chem. *283*, 977–987.

Kim, T.-J., Zheng, S., Sun, J., Muhamed, I., Wu, J., Lei, L., Kong, X., Leckband, D.E., and Wang, Y. (2015). Dynamic visualization of α-catenin reveals rapid, reversible conformation switching between tension states. Curr. Biol. CB *25*, 218–224.

Klymenko, Y., Johnson, J., Bos, B., Lombard, R., Campbell, L., Loughran, E., and Stack, M.S. (2017). Heterogeneous Cadherin Expression and Multicellular Aggregate Dynamics in Ovarian Cancer Dissemination. Neoplasia N. Y. N *19*, 549–563.

Koesters, R., Ridder, R., Kopp-Schneider, A., Betts, D., Adams, V., Niggli, F., Briner, J., and von Knebel Doeberitz, M. (1999). Mutational activation of the beta-catenin proto-oncogene is a common event in the development of Wilms' tumors. Cancer Res. *59*, 3880–3882.

Kohmura, N., Senzaki, K., Hamada, S., Kai, N., Yasuda, R., Watanabe, M., Ishii, H., Yasuda, M., Mishina, M., and Yagi, T. (1998). Diversity revealed by a novel family of cadherins expressed in neurons at a synaptic complex. Neuron *20*, 1137–1151.

Kondylis, V., and Rabouille, C. (2009). The Golgi apparatus: lessons from Drosophila. FEBS Lett. *583*, 3827–3838.

Kowalczyk, A.P., and Reynolds, A.B. (2004). Protecting your tail: regulation of cadherin degradation by p120-catenin. Curr. Opin. Cell Biol. *16*, 522–527.

Kragh, K.N., Hutchison, J.B., Melaugh, G., Rodesney, C., Roberts, A.E.L., Irie, Y., Jensen, P.Ø., Diggle, S.P., Allen, R.J., Gordon, V., et al. (2016). Role of Multicellular Aggregates in Biofilm Formation. MBio *7*.

Kraus, C., Liehr, T., Hülsken, J., Behrens, J., Birchmeier, W., Grzeschik, K.-H., and Ballhausen, W.G. (1994). Localization of the Human β-Catenin Gene (CTNNB1) to 3p21: A Region Implicated in Tumor Development. Genomics *23*, 272–274.

Krishnamurthy, N., and Kurzrock, R. (2018). Targeting the Wnt/beta-catenin pathway in cancer: Update on effectors and inhibitors. Cancer Treat. Rev. *62*, 50–60.

Kristensen, G.B., Abeler, V.M., Risberg, B., Trop, C., and Bryne, M. (1999). Tumor size, depth of invasion, and grading of the invasive tumor front are the main prognostic factors in early squamous cell cervical carcinoma. Gynecol. Oncol. *74*, 245–251.

Kroll, J.R., Wong, K.G., Siddiqui, F.M., and Tanouye, M.A. (2015). Disruption of Endocytosis with the Dynamin Mutant shibirets1 Suppresses Seizures in Drosophila. Genetics *201*, 1087–1102.

Kucera, A., Borg Distefano, M., Berg-Larsen, A., Skjeldal, F., Repnik, U., Bakke, O., and Progida, C. (2016a). Spatiotemporal Resolution of Rab9 and CI-MPR Dynamics in the Endocytic Pathway. Traffic Cph. Den. *17*, 211–229.

Kucera, A., Bakke, O., and Progida, C. (2016b). The multiple roles of Rab9 in the endolysosomal system. Commun. Integr. Biol. *9*, e1204498.

Kumari, S., and Mayor, S. (2008). ARF1 is directly involved in dynamin-independent endocytosis. Nat. Cell Biol. *10*, 30–41.

Kweon, H.-S., Beznoussenko, G.V., Micaroni, M., Polishchuk, R.S., Trucco, A., Martella, O., Di Giandomenico, D., Marra, P., Fusella, A., Di Pentima, A., et al. (2004). Golgi Enzymes Are Enriched in Perforated Zones of Golgi Cisternae but Are Depleted in COPI Vesicles. Mol. Biol. Cell *15*, 4710–4724.

Labernadie, A., Kato, T., Brugués, A., Serra-Picamal, X., Derzsi, S., Arwert, E., Weston, A., González-Tarragó, V., Elosegui-Artola, A., Albertazzi, L., et al. (2017). A mechanically active heterotypic E-cadherin/N-cadherin adhesion enables fibroblasts to drive cancer cell invasion. Nat. Cell Biol. *19*, 224–237.

Lackner, D.H., Carré, A., Guzzardo, P.M., Banning, C., Mangena, R., Henley, T., Oberndorfer, S., Gapp, B.V., Nijman, S.M.B., Brummelkamp, T.R., et al. (2015). A generic strategy for CRISPR-Cas9-mediated gene tagging. Nat. Commun. *6*, 10237.

Lamouille, S., Xu, J., and Derynck, R. (2014). Molecular mechanisms of epithelial–mesenchymal transition. Nat. Rev. Mol. Cell Biol. *15*, 178–196.

Larson, D.E., Liberman, Z., and Cagan, R.L. (2008). Cellular behavior in the developing Drosophila pupal retina. Mech. Dev. *125*, 223–232.

Laurson, J., Khan, S., Chung, R., Cross, K., and Raj, K. (2010). Epigenetic repression of E-cadherin by human papillomavirus 16 E7 protein. Carcinogenesis *31*, 918–926.

Le, T.L., Yap, A.S., and Stow, J.L. (1999). Recycling of E-Cadherin: A Potential Mechanism for Regulating Cadherin Dynamics. J. Cell Biol. *146*, 219–232.

Le Bras, G.F., Taubenslag, K.J., and Andl, C.D. (2012). The regulation of cell-cell adhesion during epithelial-mesenchymal transition, motility and tumor progression. Cell Adhes. Migr. *6*, 365–373.

Lecuit, M. (2005). Understanding how Listeria monocytogenes targets and crosses host barriers. Clin. Microbiol. Infect. *11*, 430–436.

Lecuit, M., Nelson, D.M., Smith, S.D., Khun, H., Huerre, M., Vacher-Lavenu, M.-C., Gordon, J.I., and Cossart, P. (2004). Targeting and crossing of the human maternofetal barrier by Listeria monocytogenes: Role of internalin interaction with trophoblast E-cadherin. Proc. Natl. Acad. Sci. *101*, 6152–6157.

Lee, T.I., and Young, R.A. (2013). Transcriptional Regulation and Its Misregulation in Disease. Cell *152*, 1237–1251.

Lee, A., Frank, D.W., Marks, M.S., and Lemmon, M.A. (1999). Dominant-negative inhibition of receptor-mediated endocytosis by a dynamin-1 mutant with a defective pleckstrin homology domain. Curr. Biol. CB *9*, 261–264.

Lee, Y.-C., Bååth, J.A., Bastle, R.M., Bhattacharjee, S., Cantoria, M.J., Dornan, M., Gamero-Estevez, E., Ford, L., Halova, L., Kernan, J., et al. (2017). Impact of detergents on membrane protein complex isolation. J. Proteome Res.

Lefevre, M., Rousseau, A., Rayon, T., Dalstein, V., Clavel, C., Beby-Defaux, A., Pretet, J.-L., Soussan, P., Polette, M., Lacau Saint Guily, J., et al. (2017). Epithelial to mesenchymal transition and HPV infection in squamous cell oropharyngeal carcinomas: the papillophar study. Br. J. Cancer *116*, 362–369.

Lemonidis, K., Gorleku, O.A., Sanchez-Perez, M.C., Grefen, C., and Chamberlain, L.H. (2014). The Golgi S-acylation machinery comprises zDHHC enzymes with major differences in substrate affinity and S-acylation activity. Mol. Biol. Cell *25*, 3870–3883.

Leong, C.-M., Doorbar, J., Nindl, I., Yoon, H.-S., and Hibma, M.H. (2010). Deregulation of E-cadherin by human papillomavirus is not confined to high-risk, cancer-causing types. Br. J. Dermatol. *163*, 1253–1263.

Levayer, R., Pelissier-Monier, A., and Lecuit, T. (2011). Spatial regulation of Dia and Myosin-II by RhoGEF2 controls initiation of E-cadherin endocytosis during epithelial morphogenesis. Nat. Cell Biol. *13*, 529–540.

Li, G., Pan, T., Guo, D., and Li, L.-C. (2014). Regulatory Variants and Disease: The E-Cadherin −160C/A SNP as an Example.

Li, Q., Sodroski, C., Lowey, B., Schweitzer, C.J., Cha, H., Zhang, F., and Liang, T.J. (2016). Hepatitis C virus depends on E-cadherin as an entry factor and regulates its expression in epithelial-to-mesenchymal transition. Proc. Natl. Acad. Sci. U. S. A. *113*, 7620–7625.

Li, Q., Hutchins, A.P., Chen, Y., Li, S., Shan, Y., Liao, B., Zheng, D., Shi, X., Li, Y., Chan, W.-Y., et al. (2017). A sequential EMT-MET mechanism drives the differentiation of human embryonic stem cells towards hepatocytes. Nat. Commun. *8*, 15166.

Li, X., Young, N.M., Tropp, S., Hu, D., Xu, Y., Hallgrímsson, B., and Marcucio, R.S. (2013). Quantification of shape and cell polarity reveals a novel mechanism underlying malformations resulting from related FGF mutations during facial morphogenesis. Hum. Mol. Genet. *22*, 5160–5172.

Lieu, Z.Z., Lock, J.G., Hammond, L.A., Gruta, N.L.L., Stow, J.L., and Gleeson, P.A. (2008). A trans-Golgi network golgin is required for the regulated secretion of TNF in activated macrophages in vivo. Proc. Natl. Acad. Sci. *105*, 3351–3356.

Lim, S.C., Jang, I.G., Kim, Y.C., and Park, K.O. (2000). The role of E-cadherin expression in non-small cell lung cancer. J. Korean Med. Sci. *15*, 501–506.

Lin, E., Cao, T., Nagrath, S., and King, M.R. (2018). Circulating Tumor Cells: Diagnostic and Therapeutic Applications. Annu. Rev. Biomed. Eng. *20*, 329–352.

Lin, Y.-L., Wang, Y.-P., Li, H.-Z., and Zhang, X. (2017). Aberrant Promoter Methylation of PCDH17 (Protocadherin 17) in Serum and its Clinical Significance in Renal Cell Carcinoma. Med. Sci. Monit. Int. Med. J. Exp. Clin. Res. *23*, 3318–3323.

Lipke, P.N. (2018). What We Do Not Know about Fungal Cell Adhesion Molecules. J. Fungi Basel Switz. *4*.

Liu, X., and Chu, K.-M. (2014). E-Cadherin and Gastric Cancer: Cause, Consequence, and Applications.

Liu, S., Sun, J., Wang, D., Pflugfelder, G.O., and Shen, J. (2016). Fold formation at the compartment boundary of Drosophila wing requires Yki signaling to suppress JNK dependent apoptosis. Sci. Rep. *6*.

Liu, Y.-N., Lee, W.-W., Wang, C.-Y., Chao, T.-H., Chen, Y., and Chen, J.H. (2005). Regulatory mechanisms controlling human E-cadherin gene expression. Oncogene *24*, 8277–8290.

Lock, J.G., Hammond, L.A., Houghton, F., Gleeson, P.A., and Stow, J.L. (2005). E-cadherin transport from the trans-Golgi network in tubulovesicular carriers is selectively regulated by golgin-97. Traffic Cph. Den. *6*, 1142–1156.

Lu, L., Bi, J., and Bao, L. (2018). Genetic profiling of cancer with circulating tumor DNA analysis. J. Genet. Genomics *45*, 79–85.

Luo, Y.T., Cheng, J., Feng, X., He, S.J., Wang, Y.W., and Huang, Q. (2018). The viable circulating tumor cells with cancer stem cells feature, where is the way out? J. Exp. Clin. Cancer Res. CR *37*.

Lyons, N.A., and Kolter, R. (2015). On The Evolution of Bacterial Multicellularity. Curr. Opin. Microbiol. *24*, 21–28.

MacDonald, B.T., Tamai, K., and He, X. (2009). Wnt/β-catenin signaling: components, mechanisms, and diseases. Dev. Cell *17*, 9–26.

Maeyama, Y., Mitsuyama, K., Noda, T., Nagata, S., Nagata, T., Yoshioka, S., Yoshida, H., Mukasa, M., Sumie, H., Kawano, H., et al. (2018). Prediction of colorectal tumor grade and invasion depth through narrow-band imaging scoring. World J. Gastroenterol. *24*, 4809–4820.

Magie, C.R., Pinto-Santini, D., and Parkhurst, S.M. (2002). Rho1 interacts with p120ctn and α-catenin, and regulates cadherin-based adherens junction components in Drosophila. Development *129*, 3771–3782.

Mah, K.M., and Weiner, J.A. (2017). Regulation of Wnt Signaling by Protocadherins. Semin. Cell Dev. Biol. *69*, 158–171.

Maib, H., Ferreira, F., Vassilopoulos, S., and Smythe, E. (2018). Cargo regulates clathrin-coated pit invagination via clathrin light chain phosphorylation. J Cell Biol *217*, 4253–4266.

Maiden, S.L., Petrova, Y.I., and Gumbiner, B.M. (2016). Microtubules Inhibit E-Cadherin Adhesive Activity by Maintaining Phosphorylated p120-Catenin in a Colon Carcinoma Cell Model. PLoS ONE *11*.

Mansoori, M., Madjd, Z., Janani, L., and Rasti, A. (2017). Circulating cancer stem cell markers in breast carcinomas: a systematic review protocol. Syst. Rev. *6*.

Mariner, D.J., Anastasiadis, P., Keilhack, H., Böhmer, F.D., Wang, J., and Reynolds, A.B. (2001). Identification of Src phosphorylation sites in the catenin p120ctn. J. Biol. Chem. *276*, 28006–28013.

Martorell, Ò., Merlos-Suárez, A., Campbell, K., Barriga, F.M., Christov, C.P., Miguel-Aliaga, I., Batlle, E., Casanova, J., and Casali, A. (2014). Conserved Mechanisms of Tumorigenesis in the Drosophila Adult Midgut. PLOS ONE *9*, e88413.

de Matos Simões, S., Blankenship, J.T., Weitz, O., Farrell, D.L., Tamada, M., Fernandez-Gonzalez, R., and Zallen, J.A. (2010). Rho-kinase directs Bazooka/Par-3 planar polarity during Drosophila axis elongation. Dev. Cell *19*, 377–388.

May, A.N., Crawford, B.D., and Nedelcu, A.M. (2018). In Vitro Model-Systems to Understand the Biology and Clinical Significance of Circulating Tumor Cell Clusters. Front. Oncol. *8*.

Mayor, S., Parton, R.G., and Donaldson, J.G. (2014). Clathrin-Independent Pathways of Endocytosis. Cold Spring Harb. Perspect. Biol. *6*.

McMahon, H.T., and Boucrot, E. (2011). Molecular mechanism and physiological functions of clathrin-mediated endocytosis. Nat. Rev. Mol. Cell Biol. *12*, 517–533.

Menke, A., and Giehl, K. (2012). Regulation of adherens junctions by Rho GTPases and p120-catenin. Arch. Biochem. Biophys. *524*, 48–55.

Miller, P.W., Clarke, D.N., Weis, W.I., Lowe, C.J., and Nelson, W.J. (2013). The Evolutionary Origin of Epithelial Cell-Cell Adhesion Mechanisms. Curr. Top. Membr. *72*, 267–311.

Millner, L.M., Linder, M.W., and Valdes, R. (2013). Circulating tumor cells: a review of present methods and the need to identify heterogeneous phenotypes. Ann. Clin. Lab. Sci. *43*, 295–304.

Miyashita, Y., and Ozawa, M. (2007). Increased Internalization of p120-uncoupled E-cadherin and a Requirement for a Dileucine Motif in the Cytoplasmic Domain for Endocytosis of the Protein. J. Biol. Chem. *282*, 11540–11548.

Mo, Y.Y., and Reynolds, A.B. (1996). Identification of murine p120 isoforms and heterogeneous expression of p120cas isoforms in human tumor cell lines. Cancer Res. *56*, 2633–2640.

Monks, J., Rosner, D., Geske, F.J., Lehman, L., Hanson, L., Neville, M.C., and Fadok, V.A. (2005). Epithelial cells as phagocytes: apoptotic epithelial cells are engulfed by mammary alveolar epithelial cells and repress inflammatory mediator release. Cell Death Differ. *12*, 107–114.

Morel, V., and Arias, A.M. (2004). Armadillo/β-catenin-dependent Wnt signalling is required for the polarisation of epidermal cells during dorsal closure in Drosophila. Development *131*, 3273–3283.

Montonen O, Aho M, Uitto J, Aho S (2001) Tissue Distribution and Cell Type-specific Expression of p120ctn Isoforms. J Histochem Cytochem 49: 1487–1495.

Murray, P.S., and Zaidel-Bar, R. (2014). Pre-metazoan origins and evolution of the cadherin adhesome. Biol. Open *3*, 1183–1195.

Myster, S.H., Cavallo, R., Anderson, C.T., Fox, D.T., and Peifer, M. (2003). Drosophila p120catenin plays a supporting role in cell adhesion but is not an essential adherens junction component. J Cell Biol *160*, 433–449.

Nagaoka, M., Koshimizu, U., Yuasa, S., Hattori, F., Chen, H., Tanaka, T., Okabe, M., Fukuda, K., and Akaike, T. (2006). E-Cadherin-Coated Plates Maintain Pluripotent ES Cells without Colony Formation. PLoS ONE *1*.

Nandadasa, S., Tao, Q., Menon, N.R., Heasman, J., and Wylie, C. (2009). N- and E-cadherins in Xenopus are specifically required in the neural and non-neural ectoderm, respectively, for F-actin assembly and morphogenetic movements. Dev. Camb. Engl. *136*, 1327–1338.

Nandadasa, S., Tao, Q., Shoemaker, A., Cha, S., and Wylie, C. (2012). Regulation of Classical Cadherin Membrane Expression and F-Actin Assembly by Alpha-Catenins, during Xenopus Embryogenesis. PLOS ONE *7*, e38756.

Nanes, B.A., and Kowalczyk, A.P. (2012). Adherens junction turnover: regulating adhesion through cadherin endocytosis, degradation, and recycling. Subcell. Biochem. *60*, 197–222.

Nanes, B.A., Chiasson-MacKenzie, C., Lowery, A.M., Ishiyama, N., Faundez, V., Ikura, M., Vincent, P.A., and Kowalczyk, A.P. (2012). p120-catenin binding masks an endocytic signal conserved in classical cadherins. J Cell Biol *199*, 365–380.

Nelson, W.J. (2008). Regulation of cell-cell adhesion by the cadherin-catenin complex. Biochem. Soc. Trans. *36*, 149–155.

Nelson, W.J., and Nusse, R. (2004). Convergence of Wnt, β-Catenin, and Cadherin Pathways. Science *303*, 1483–1487.

Nelson, W.J., Dickinson, D.J., and Weis, W.I. (2013). Roles of cadherins and catenins in cell-cell adhesion and epithelial cell polarity. Prog. Mol. Biol. Transl. Sci. *116*, 3–23.

Nichols, S.A., Roberts, B.W., Richter, D.J., Fairclough, S.R., and King, N. (2012). Origin of metazoan cadherin diversity and the antiquity of the classical cadherin/β-catenin complex. Proc. Natl. Acad. Sci. U. S. A. *109*, 13046–13051.

Niessen, C.M., and Gottardi, C.J. (2008). Molecular Components of the Adherens Junction. Biochim. Biophys. Acta *1778*, 562–571.

Nilsson, T., Au, C.E., and Bergeron, J.J.M. (2009). Sorting out glycosylation enzymes in the Golgi apparatus. FEBS Lett. *583*, 3764–3769.

Noren, N.K., Liu, B.P., Burridge, K., and Kreft, B. (2000). P120 Catenin Regulates the Actin Cytoskeleton via Rho Family Gtpases. J. Cell Biol. *150*, 567–580.

Oda, H., and Takeichi, M. (2011). Structural and functional diversity of cadherin at the adherens junction. J. Cell Biol. *193*, 1137–1146.

Oda, H., Tsukita, S., and Takeichi, M. (1998). Dynamic behavior of the cadherin-based cell-cell adhesion system during Drosophila gastrulation. Dev. Biol. *203*, 435–450.

Ohkubo, T., and Ozawa, M. (1999). p120(ctn) binds to the membrane-proximal region of the E-cadherin cytoplasmic domain and is involved in modulation of adhesion activity. J. Biol. Chem. *274*, 21409–21415.

Onder, T.T., Gupta, P.B., Mani, S.A., Yang, J., Lander, E.S., and Weinberg, R.A. (2008). Loss of E-cadherin promotes metastasis via multiple downstream transcriptional pathways. Cancer Res. *68*, 3645–3654.

Osato, N., Suzuki, Y., Ikeo, K., and Gojobori, T. (2007). Transcriptional Interferences in cis Natural Antisense Transcripts of Humans and Mice. Genetics *176*, 1299–1306.

Ozawa, M. (2002). Lateral Dimerization of the E-cadherin Extracellular Domain Is Necessary but Not Sufficient for Adhesive Activity. J. Biol. Chem. *277*, 19600–19608.

Pachmayr, E., Treese, C., and Stein, U. (2017). Underlying Mechanisms for Distant Metastasis - Molecular Biology. Visc. Med. *33*, 11–20.

Pacquelet, A., Lin, L., and Rorth, P. (2003). Binding site for p120/delta-catenin is not required for Drosophila E-cadherin function in vivo. J. Cell Biol. *160*, 313–319.

Paczkowski, J.E., Richardson, B.C., and Fromme, J.C. (2015). Cargo adaptors: structures illuminate mechanisms regulating vesicle biogenesis. Trends Cell Biol. *25*, 408–416.

Palaghia, M., Mihai, C., Lozneanu, L., Ciobanu, D., Trofin, A.M., Rotariu, A., Târcoveanu, F., and Cijevschi Prelipcean, C. (2016). E-cadherin expression in primary colorectal

cancer and metastatic lymph nodes. Romanian J. Morphol. Embryol. Rev. Roum. Morphol. Embryol. *57*, 205–209.

Park, S.Y., and Guo, X. (2014). Adaptor protein complexes and intracellular transport. Biosci. Rep. *34*.

Pawlizak, S., Fritsch, A.W., Grosser, S., Ahrens, D., Thalheim, T., Riedel, S., sling, T.R.K., Oswald, L., Zink, M., Manning, M.L., et al. (2015). Testing the differential adhesion hypothesis across the epithelial-mesenchymal transition. New J. Phys. *17*, 083049.

Pećina-Šlaus, N. (2003). Tumor suppressor gene E-cadherin and its role in normal and malignant cells. Cancer Cell Int. *3*, 17.

Pećina-Slaus, N., Zigmund, M., Kusec, V., Martić, T.N., Cacić, M., and Slaus, M. (2007). E-cadherin and beta-catenin expression patterns in malignant melanoma assessed by image analysis. J. Cutan. Pathol. *34*, 239–246.

Peglion, F., and Etienne-Manneville, S. (2013). p120catenin alteration in cancer and its role in tumour invasion. Phil Trans R Soc B *368*, 20130015.

Peifer, M., and Yap, A.S. (2003). Traffic control: p120-catenin acts as a gatekeeper to control the fate of classical cadherins in mammalian cells. J. Cell Biol. *163*, 437–440.

Peifer, M., Berg, S., and Reynolds, A.B. (1994). A repeating amino acid motif shared by proteins with diverse cellular roles. Cell *76*, 789–791.

Peinado, H., Portillo, F., and Cano, A. (2004). Transcriptional regulation of cadherins during development and carcinogenesis. Int. J. Dev. Biol. *48*, 365–375.

Perez, T.D., and Nelson, W.J. (2004). Cadherin Adhesion: Mechanisms and Molecular Interactions. Handb. Exp. Pharmacol. 3–21.

Perez-Moreno, M., Song, W., Pasolli, H.A., Williams, S.E., and Fuchs, E. (2008). Loss of p120 catenin and links to mitotic alterations, inflammation, and skin cancer. Proc. Natl. Acad. Sci. *105*, 15399–15404.

Petrova, Y.I., Schecterson, L., and Gumbiner, B.M. (2016). Roles for E-cadherin cell surface regulation in cancer. Mol. Biol. Cell *27*, 3233–3244.

Pettitt, J., Cox, E.A., Broadbent, I.D., Flett, A., and Hardin, J. (2003). The Caenorhabditis elegans p120 catenin homologue, JAC-1, modulates cadherin-catenin function during epidermal morphogenesis. J. Cell Biol. *162*, 15–22.

Peyriéras, N., Louvard, D., and Jacob, F. (1985). Characterization of antigens recognized by monoclonal and polyclonal antibodies directed against uvomorulin. Proc. Natl. Acad. Sci. U. S. A. *82*, 8067–8071.

Piedra, J., Miravet, S., Castaño, J., Pálmer, H.G., Heisterkamp, N., Herreros, A.G. de, and Duñach, M. (2003). p120 Catenin-Associated Fer and Fyn Tyrosine Kinases Regulate β-Catenin Tyr-142 Phosphorylation and β-Catenin-α-Catenin Interaction. Mol. Cell. Biol. *23*, 2287–2297.

Pieters, T., van Roy, F., and van Hengel, J. (2012). Functions of p120ctn isoforms in cell-cell adhesion and intracellular signaling. Front. Biosci. Landmark Ed. *17*, 1669–1694.

Pieters, T., Goossens, S., Haenebalcke, L., Andries, V., Stryjewska, A., De Rycke, R., Lemeire, K., Hochepied, T., Huylebroeck, D., Berx, G., et al. (2016). p120 Catenin-Mediated Stabilization of E-Cadherin Is Essential for Primitive Endoderm Specification. PLoS Genet. *12*, e1006243.

Poythress, R.H., Gallant, C., Vetterkind, S., and Morgan, K.G. (2013). Vasoconstrictor-induced endocytic recycling regulates focal adhesion protein localization and function in vascular smooth muscle. Am. J. Physiol. - Cell Physiol. *305*, C215–C227.

Praharaj, P.P., Bhutia, S.K., Nagrath, S., Bitting, R.L., and Deep, G. (2018). Circulating tumor cell-derived organoids: Current challenges and promises in medical research and precision medicine. Biochim. Biophys. Acta BBA - Rev. Cancer *1869*, 117–127.

Preuss, D., Mulholland, J., Franzusoff, A., Segev, N., and Botstein, D. (1992). Characterization of the Saccharomyces Golgi complex through the cell cycle by immunoelectron microscopy. Mol. Biol. Cell *3*, 789–803.

Putzke, A.P., Ventura, A.P., Bailey, A.M., Akture, C., Opoku-Ansah, J., Çeliktaş, M., Hwang, M.S., Darling, D.S., Coleman, I.M., Nelson, P.S., et al. (2011). Metastatic Progression of Prostate Cancer and E-Cadherin. Am. J. Pathol. *179*, 400–410.

Rabouille, C., Hui, N., Hunte, F., Kieckbusch, R., Berger, E.G., Warren, G., and Nilsson, T. (1995). Mapping the distribution of Golgi enzymes involved in the construction of complex oligosaccharides. J. Cell Sci. *108 (Pt 4)*, 1617–1627.

Rajput, C., Kini, V., Smith, M., Yazbeck, P., Chavez, A., Schmidt, T., Zhang, W., Knezevic, N., Komarova, Y., and Mehta, D. (2013). Neural Wiskott-Aldrich Syndrome Protein (N-WASP)-mediated p120-Catenin Interaction with Arp2-Actin Complex Stabilizes Endothelial Adherens Junctions. J. Biol. Chem. *288*, 4241–4250.

Ramis-Conde, I., Drasdo, D., Anderson, A.R.A., and Chaplain, M.A.J. (2008). Modeling the Influence of the E-Cadherin-β-Catenin Pathway in Cancer Cell Invasion: A Multiscale Approach. Biophys. J. *95*, 155–165.

Rangarajan, E.S., and Izard, T. (2012). The Cytoskeletal Protein α-Catenin Unfurls upon Binding to Vinculin. J. Biol. Chem. *287*, 18492–18499.

Rawlins, E.L., and Hogan, B.L.M. (2008). Ciliated epithelial cell lifespan in the mouse trachea and lung. Am. J. Physiol. Lung Cell. Mol. Physiol. *295*, L231-234.

Redies, C., Hertel, N., and Hübner, C.A. (2012). Cadherins and neuropsychiatric disorders. Brain Res. *1470*, 130–144.

Ren, X., Farias, G.G., Canagarajah, B.J., Bonifacino, J.S., and Hurley, J.H. (2013). Structural Basis for Recruitment and Activation of the AP-1 Clathrin Adaptor Complex by Arf1. Cell *152*, 755–767.

Renaud-Young, M., and Gallin, W.J. (2002). In the First Extracellular Domain of E-cadherin, Heterophilic Interactions, but Not the Conserved His-Ala-Val Motif, Are Required for Adhesion. J. Biol. Chem. *277*, 39609–39616.

Reynolds, A.B. (2007). p120-catenin: Past and present. Biochim. Biophys. Acta BBA - Mol. Cell Res. *1773*, 2–7.

Reynolds, A.B., and Roczniak-Ferguson, A. (2004). Emerging roles for p120-catenin in cell adhesion and cancer. Oncogene *23*, 7947–7956.

Reynolds, A.B., Roesel, D.J., Kanner, S.B., and Parsons, J.T. (1989). Transformation-specific tyrosine phosphorylation of a novel cellular protein in chicken cells expressing oncogenic variants of the avian cellular src gene. Mol. Cell. Biol. *9*, 629–638.

Reynolds, A.B., Daniel, J., McCrea, P.D., Wheelock, M.J., Wu, J., and Zhang, Z. (1994). Identification of a new catenin: the tyrosine kinase substrate p120cas associates with E-cadherin complexes. Mol. Cell. Biol. *14*, 8333–8342.

Reynolds, A.B., Daniel, J.M., Mo, Y.Y., Wu, J., and Zhang, Z. (1996). The novel catenin p120cas binds classical cadherins and induces an unusual morphological phenotype in NIH3T3 fibroblasts. Exp. Cell Res. *225*, 328–337.

Roberts, B., Haupt, A., Tucker, A., Grancharova, T., Arakaki, J., Fuqua, M.A., Nelson, A., Hookway, C., Ludmann, S.A., Mueller, I.A., et al. (2017). Systematic gene tagging using CRISPR/Cas9 in human stem cells to illuminate cell organization. Mol. Biol. Cell *28*, 2854–2874.

Roche, J. (2018). The Epithelial-to-Mesenchymal Transition in Cancer. Cancers *10*.

Rodrigues FF, Shao W, Harris TJC (2016) The Arf GAP Asap promotes Arf1 function at the Golgi for cleavage furrow biosynthesis in Drosophila. Mol Biol Cell 27: 3143–3155.

Rosquete, M.R., Davis, D.J., and Drakakaki, G. (2018). The Plant Trans-Golgi Network: Not Just a Matter of Distinction. Plant Physiol. *176*, 187–198.

Rosso, M., Majem, B., Devis, L., Lapyckyj, L., Besso, M.J., Llauradó, M., Abascal, M.F., Matos, M.L., Lanau, L., Castellví, J., et al. (2017). E-cadherin: A determinant molecule associated with ovarian cancer progression, dissemination and aggressiveness. PLOS ONE *12*, e0184439.

Roy, F.M. van, and McCrea, P.D. (2005). A role for Kaiso–p120ctn complexes in cancer? Nat. Rev. Cancer *5*, 956–964.

van Roy, F., and Berx, G. (2008). The cell-cell adhesion molecule E-cadherin. Cell. Mol. Life Sci. CMLS *65*, 3756–3788.

Ruiz-May, E., Kim, S.-J., Brandizzi, F., and Rose, J.K.C. (2012). The secreted plant N-glycoproteome and associated secretory pathways. Front. Plant Sci. *3*, 117.

Saito, T., Yoshida, K., Matsumoto, K., Saeki, K., Tanaka, Y., Ong, S.-M., Sasaki, N., Nishimura, R., and Nakagawa, T. (2014). Inflammatory cytokines induce a reduction in E-cadherin expression and morphological changes in MDCK cells. Res. Vet. Sci. *96*, 288–291.

Sandig, M., Voura, E.B., Kalnins, V.I., and Siu, C.H. (1997). Role of cadherins in the transendothelial migration of melanoma cells in culture. Cell Motil. Cytoskeleton *38*, 351–364.

Sato, K., Watanabe, T., Wang, S., Kakeno, M., Matsuzawa, K., Matsui, T., Yokoi, K., Murase, K., Sugiyama, I., Ozawa, M., et al. (2011). Numb controls E-cadherin endocytosis through p120 catenin with aPKC. Mol. Biol. Cell *22*, 3103–3119.

Schackmann, R.C.J., van Amersfoort, M., Haarhuis, J.H.I., Vlug, E.J., Halim, V.A., Roodhart, J.M.L., Vermaat, J.S., Voest, E.E., van der Groep, P., van Diest, P.J., et al. (2011). Cytosolic p120-catenin regulates growth of metastatic lobular carcinoma through Rock1-mediated anoikis resistance. J. Clin. Invest. *121*, 3176–3188.

Schäfer, G., Narasimha, M., Vogelsang, E., and Leptin, M. (2014). Cadherin switching during the formation and differentiation of the Drosophila mesoderm – implications for epithelial-to-mesenchymal transitions. J Cell Sci *127*, 1511–1522.

Schneider, M.R., and Kolligs, F.T. (2015). E-cadherin's role in development, tissue homeostasis and disease: Insights from mouse models: Tissue-specific inactivation of the adhesion protein E-cadherin in mice reveals its functions in health and disease. BioEssays News Rev. Mol. Cell. Dev. Biol. *37*, 294–304.

Schrader, E.K., Harstad, K.G., and Matouschek, A. (2009). Targeting proteins for degradation. Nat. Chem. Biol. *5*, 815–822.

Scott, B.L., Sochacki, K.A., Low-Nam, S.T., Bailey, E.M., Luu, Q., Hor, A., Dickey, A.M., Smith, S., Kerkvliet, J.G., Taraska, J.W., et al. (2018). Membrane bending occurs at all stages of clathrin-coat assembly and defines endocytic dynamics. Nat. Commun. *9*.

Sengupta, P., Satpute-Krishnan, P., Seo, A.Y., Burnette, D.T., Patterson, G.H., and Lippincott-Schwartz, J. (2015). ER trapping reveals Golgi enzymes continually revisit the ER through a recycling pathway that controls Golgi organization. Proc. Natl. Acad. Sci. *112*, E6752–E6761.

Shao, K., Chen, Z.Y., Gautam, S., Deng, N.H., Zhou, Y., and Wu, X.Z. (2016). Posttranslational modification of E-cadherin by core fucosylation regulates Src activation and induces epithelial-mesenchymal transition-like process in lung cancer cells. Glycobiology *26*, 142–154.

Shapiro, L., and Weis, W.I. (2009). Structure and biochemistry of cadherins and catenins. Cold Spring Harb. Perspect. Biol. *1*, a003053.

Sharif, G.M., and Wellstein, A. (2015). Cell density regulates cancer metastasis via the Hippo pathway. Future Oncol. *11*, 3253–3260.

Sharma, P., and McNeill, H. (2013). Fat and Dachsous cadherins. Prog. Mol. Biol. Transl. Sci. *116*, 215–235.

Shen, T., Zhang, K., Siegal, G.P., and Wei, S. (2016). Prognostic Value of E-Cadherin and β-Catenin in Triple-Negative Breast Cancer. Am. J. Clin. Pathol. *146*, 603–610.

Shibamoto, S., Hayakawa, M., Takeuchi, K., Hori, T., Miyazawa, K., Kitamura, N., Johnson, K.R., Wheelock, M.J., Matsuyoshi, N., and Takeichi, M. (1995). Association of p120, a tyrosine kinase substrate, with E-cadherin/catenin complexes. J. Cell Biol. *128*, 949–957.

Shimizu, T., Yabe, T., Muraoka, O., Yonemura, S., Aramaki, S., Hatta, K., Bae, Y.-K., Nojima, H., and Hibi, M. (2005). E-cadherin is required for gastrulation cell movements in zebrafish. Mech. Dev. *122*, 747–763.

Shrestha, H., Ryu, T., Seo, Y.-W., Park, S.-Y., He, Y., Dai, W., Park, E., Simkhada, S., Kim, H., Lee, K., et al. (2017). Hakai, an E3-ligase for E-cadherin, stabilizes δ-catenin through Src kinase. Cell. Signal. *31*, 135–145.

Sidibé, A., and Imhof, B.A. (2014). VE-cadherin phosphorylation decides: vascular permeability or diapedesis. Nat. Immunol. *15*, 215–217.

Skoudy, A., Gomez, S., Fabre, M., and Garcia de Herreros, A. (1996). p120-catenin expression in human colorectal cancer. Int. J. Cancer *68*, 14–20.

Smyth, D., Leung, G., Fernando, M., and McKay, D.M. (2012). Reduced Surface Expression of Epithelial E-Cadherin Evoked by Interferon-Gamma Is Fyn Kinase-Dependent. PLoS ONE *7*.

Snapp, E. (2005). Design and Use of Fluorescent Fusion Proteins in Cell Biology. Curr. Protoc. Cell Biol. Editor. Board Juan Bonifacino Al *CHAPTER*, Unit-21.4.

Solanas, G., Porta-de-la-Riva, M., Agustí, C., Casagolda, D., Sánchez-Aguilera, F., Larriba, M.J., Pons, F., Peiró, S., Escrivà, M., Muñoz, A., et al. (2008). E-cadherin controls beta-catenin and NF-kappaB transcriptional activity in mesenchymal gene expression. J. Cell Sci. *121*, 2224–2234.

Sousa, R., Liao, H.-S., Cuéllar, J., Jin, S., Valpuesta, J.M., Jin, A.J., and Lafer, E.M. (2016). Clathrin-coat disassembly illuminates the mechanisms of Hsp70 force generation. Nat. Struct. Mol. Biol. *23*, 821–829.

Spoel, S.H. (2018). Orchestrating the proteome with post-translational modifications. J. Exp. Bot. *69*, 4499–4503.

Sprague, B.L., and McNally, J.G. (2005). FRAP analysis of binding: proper and fitting. Trends Cell Biol. *15*, 84–91.

Staddon, J.M., Smales, C., Schulze, C., Esch, F.S., and Rubin, L.L. (1995). p120, a p120-related protein (p100), and the cadherin/catenin complex. J. Cell Biol. *130*, 369–381.

Stavreva, D.A., Varticovski, L., and Hager, G.L. (2012). Complex Dynamics of Transcription Regulation. Biochim. Biophys. Acta *1819*, 657–666.

Steeg, P.S. (2016). Targeting metastasis. Nat. Rev. Cancer *16*, 201–218.

Stefanatos, R.K., Bauer, C., and Vidal, M. (2013). p120 catenin is required for the stress response in Drosophila. PloS One *8*, e83942.

Steinberg, M.S. (1996). Adhesion in Development: An Historical Overview. Dev. Biol. *180*, 377–388.

Steinberg, M.S., and Gilbert, S.F. (2004). Townes and Holtfreter (1955): directed movements and selective adhesion of embryonic amphibian cells. J. Exp. Zoolog. A Comp. Exp. Biol. *301*, 701–706.

Strous, G.J. (1986). Golgi and secreted galactosyltransferase. CRC Crit. Rev. Biochem. *21*, 119–151.

Sui, L., Alt, S., Weigert, M., Dye, N., Eaton, S., Jug, F., Myers, E.W., Jülicher, F., Salbreux, G., and Dahmann, C. (2018). Differential lateral and basal tension drive folding of Drosophila wing discs through two distinct mechanisms. Nat. Commun. *9*, 4620.

Swarup, S., and Verheyen, E.M. (2012). Wnt/Wingless Signaling in Drosophila. Cold Spring Harb. Perspect. Biol. *4*.

Syrigos, K.N., Karayiannakis, A., Syrigou, E.I., Harrington, K., and Pignatelli, M. (1998). Abnormal expression of p120 correlates with poor survival in patients with bladder cancer. Eur. J. Cancer Oxf. Engl. 1990 *34*, 2037–2040.

Szathmáry, E., and Smith, J.M. (1995). The major evolutionary transitions. Nature *374*, 227.

Takeichi, M. (1977). Functional correlation between cell adhesive properties and some cell surface proteins. J. Cell Biol. *75*, 464–474.

Takeichi, M., Shirayoshi, Y., Hatta, K., and Nose, A. (1986). Cadherins: their morphogenetic role in animal development. Prog. Clin. Biol. Res. *217B*, 17–27.

Tan, Y.-P., Li, S., Jiang, X.-J., Loh, W., Foo, Y.K., Loh, C.-B., Xu, Q., Yuen, W.-H., Jones, M., Fu, J., et al. (2010). Regulation of protocadherin gene expression by multiple neuron-restrictive silencer elements scattered in the gene cluster. Nucleic Acids Res. *38*, 4985–4997.

Thiery, J.P. (2003). Cell adhesion in development: a complex signaling network. Curr. Opin. Genet. Dev. *13*, 365–371.

Thievessen, I., Seifert, H.-H., Swiatkowski, S., Florl, A.R., and Schulz, W.A. (2003). E-cadherin involved in inactivation of WNT/β-catenin signalling in urothelial carcinoma and normal urothelial cells. Br. J. Cancer *88*, 1932–1938.

Thoreson, M.A., Anastasiadis, P.Z., Daniel, J.M., Ireton, R.C., Wheelock, M.J., Johnson, K.R., Hummingbird, D.K., and Reynolds, A.B. (2000). Selective Uncoupling of P120ctn from E-Cadherin Disrupts Strong Adhesion. J. Cell Biol. *148*, 189–202.

Tian, X., Liu, Z., Niu, B., Zhang, J., Tan, T.K., Lee, S.R., Zhao, Y., Harris, D.C.H., and Zheng, G. (2011). E-Cadherin/β-Catenin Complex and the Epithelial Barrier. J. Biomed. Biotechnol. *2011*.

Tronchin, G., Bouchara, J.P., Annaix, V., Robert, R., and Senet, J.M. (1991). Fungal cell adhesion molecules in Candida albicans. Eur. J. Epidemiol. *7*, 23–33.

Troyanovsky, S. (2012). Adherens Junction Assembly. Subcell. Biochem. *60*, 89–108.

Troyanovsky, R.B., Laur, O., and Troyanovsky, S.M. (2007). Stable and Unstable Cadherin Dimers: Mechanisms of Formation and Roles in Cell Adhesion. Mol. Biol. Cell *18*, 4343–4352.

Tsai, N.-P., and Huber, K.M. (2017). Protocadherins and the social brain. Biol. Psychiatry *81*, 173–174.

Tsukasaki, Y., Miyazaki, N., Matsumoto, A., Nagae, S., Yonemura, S., Tanoue, T., Iwasaki, K., and Takeichi, M. (2014). Giant cadherins Fat and Dachsous self-bend to organize properly spaced intercellular junctions. Proc. Natl. Acad. Sci. *111*, 16011–16016.

Tunn, S., Nass, R., Ekkernkamp, A., Schulze, H., and Krieg, M. (1989). Evaluation of average life span of epithelial and stromal cells of human prostate by superoxide dismutase activity. The Prostate *15*, 263–271.

Uemura, T., Oda, H., Kraut, R., Hayashi, S., Kotaoka, Y., and Takeichi, M. (1996). Zygotic Drosophila E-cadherin expression is required for processes of dynamic epithelial cell rearrangement in the Drosophila embryo. Genes Dev. *10*, 659–671.

Van den Bossche, J., Malissen, B., Mantovani, A., De Baetselier, P., and Van Ginderachter, J.A. (2012). Regulation and function of the E-cadherin/catenin complex in cells of the monocyte-macrophage lineage and DCs. Blood *119*, 1623–1633.

Van den Bossche, J., Laoui, D., Naessens, T., Smits, H.H., Hokke, C.H., Stijlemans, B., Grooten, J., De Baetselier, P., and Van Ginderachter, J.A. (2015). E-cadherin

expression in macrophages dampens their inflammatory responsiveness in vitro, but does not modulate M2-regulated pathologies in vivo. Sci. Rep. *5*.

van de Ven, R.A.H., Tenhagen, M., Meuleman, W., van Riel, J.J.G., Schackmann, R.C.J., and Derksen, P.W.B. (2015). Nuclear p120-catenin regulates the anoikis resistance of mouse lobular breast cancer cells through Kaiso-dependent Wnt11 expression. Dis. Model. Mech. *8*, 373–384.

Vestweber, D. (2015). Cadherins in tissue architecture and disease. J. Mol. Med. Berl. Ger. *93*, 5–11.

Wang, F., Dumstrei, K., Haag, T., and Hartenstein, V. (2004). The role of DE-cadherin during cellularization, germ layer formation and early neurogenesis in the Drosophila embryo. Dev. Biol. *270*, 350–363.

Wang, W., Wang, L., Mizokami, A., Shi, J., Zou, C., Dai, J., Keller, E.T., Lu, Y., and Zhang, J. (2017a). Down-regulation of E-cadherin enhances prostate cancer chemoresistance via Notch signaling. Chin. J. Cancer *36*, 35.

Wang, Y., Zhang, H., Shi, M., Liou, Y.-C., Lu, L., and Yu, F. (2017b). Sec71 functions as a GEF for the small GTPase Arf1 to govern dendrite pruning of Drosophila sensory neurons. Development *144*, 1851–1862.

Wehrendt, D.P., Carmona, F., Wusener, A.E.G., González, Á., Martínez, J.M.L., and Arregui, C.O. (2016). P120-Catenin Regulates Early Trafficking Stages of the N-Cadherin Precursor Complex. PLOS ONE *11*, e0156758.

Weiner, J.A., and Jontes, J.D. (2013). Protocadherins, not prototypical: a complex tale of their interactions, expression, and functions. Front. Mol. Neurosci. *6*.

Wells, A., Yates, C., and Shepard, C.R. (2008). E-cadherin as an indicator of mesenchymal to epithelial reverting transitions during the metastatic seeding of disseminated carcinomas. Clin. Exp. Metastasis *25*, 621–628.

Wendt, M.K., Taylor, M.A., Schiemann, B.J., and Schiemann, W.P. (2011). Down-regulation of epithelial cadherin is required to initiate metastatic outgrowth of breast cancer. Mol. Biol. Cell *22*, 2423–2435.

Wickström, S.A., and Niessen, C.M. (2018). Cell adhesion and mechanics as drivers of tissue organization and differentiation: local cues for large scale organization. Curr. Opin. Cell Biol. *54*, 89–97.

Widmann, T.J., and Dahmann, C. (2009). Wingless signaling and the control of cell shape in Drosophila wing imaginal discs. Dev. Biol. *334*, 161–173.

Wiedenheft, B., Sternberg, S.H., and Doudna, J.A. (2012). RNA-guided genetic silencing systems in bacteria and archaea. Nature *482*, 331–338.

Wildenberg, G.A., Dohn, M.R., Carnahan, R.H., Davis, M.A., Lobdell, N.A., Settleman, J., and Reynolds, A.B. (2006). p120-Catenin and p190RhoGAP Regulate Cell-Cell Adhesion by Coordinating Antagonism between Rac and Rho. Cell *127*, 1027–1039.

Winklbauer, R. (2012). Cadherin function during Xenopus gastrulation. Subcell. Biochem. *60*, 301–320.

Wu, X., Quondamatteo, F., Lefever, T., Czuchra, A., Meyer, H., Chrostek, A., Paus, R., Langbein, L., and Brakebusch, C. (2006). Cdc42 controls progenitor cell differentiation and β-catenin turnover in skin. Genes Dev. *20*, 571–585.

Wu, Y., Jin, X., Harrison, O., Shapiro, L., Honig, B.H., and Ben-Shaul, A. (2010). Cooperativity between trans and cis interactions in cadherin-mediated junction formation. Proc. Natl. Acad. Sci. U. S. A. *107*, 17592–17597.

Wülbeck, C., Grieshaber, E., and Helfrich-Förster, C. (2009). Blocking endocytosis in Drosophila's circadian pacemaker neurons interferes with the endogenous clock in a PDF-dependent way. Chronobiol. Int. *26*, 1307–1322.

Xiao, C., Ogle, S.A., Schumacher, M.A., Schilling, N., Tokhunts, R.A., Orr-Asman, M.A., Miller, M.L., Robbins, D.J., Hollande, F., and Zavros, Y. (2010). Hedgehog signaling regulates E-cadherin expression for the maintenance of the actin cytoskeleton and tight junctions. Am. J. Physiol. - Gastrointest. Liver Physiol. *299*, G1252–G1265.

Xiao, K., Oas, R.G., Chiasson, C.M., and Kowalczyk, A.P. (2007). Role of p120-catenin in cadherin trafficking. Biochim. Biophys. Acta BBA - Mol. Cell Res. *1773*, 8–16.

Xiong, H., Hong, J., Du, W., Lin, Y., Ren, L., Wang, Y., Su, W., Wang, J., Cui, Y., Wang, Z., et al. (2012). Roles of STAT3 and ZEB1 Proteins in E-cadherin Down-regulation and Human Colorectal Cancer Epithelial-Mesenchymal Transition. J. Biol. Chem. *287*, 5819–5832.

Xu, L., and Qu, Z. (2012). Roles of Protein Ubiquitination and Degradation Kinetics in Biological Oscillations. PLoS ONE *7*.

Xu, R., Zhang, Y., Gu, L., Zheng, J., Cui, J., Dong, J., and Du, J. (2015). Arf6 regulates EGF-induced internalization of E-cadherin in breast cancer cells. Cancer Cell Int. *15*, 11.

Yadav, S., and Linstedt, A.D. (2011). Golgi positioning. Cold Spring Harb. Perspect. Biol. *3*.

Yadav, B.S., Chanana, P., and Jhamb, S. (2015). Biomarkers in triple negative breast cancer: A review. World J. Clin. Oncol. *6*, 252–263.

Yadav, S., Puri, S., and Linstedt, A.D. (2009). A Primary Role for Golgi Positioning in Directed Secretion, Cell Polarity, and Wound Healing. Mol. Biol. Cell *20*, 1728–1736.

Yanagisawa, M., Kaverina, I.N., Wang, A., Fujita, Y., Reynolds, A.B., and Anastasiadis, P.Z. (2004). A novel interaction between kinesin and p120 modulates p120 localization and function. J. Biol. Chem. *279*, 9512–9521.

Yang, M.-H., Imrali, A., and Heeschen, C. (2015). Circulating cancer stem cells: the importance to select. Chin. J. Cancer Res. *27*, 437–449.

Yano, H., Yamamoto-Hino, M., Abe, M., Kuwahara, R., Haraguchi, S., Kusaka, I., Awano, W., Kinoshita-Toyoda, A., Toyoda, H., and Goto, S. (2005). Distinct functional units of the Golgi complex in Drosophila cells. Proc. Natl. Acad. Sci. U. S. A. *102*, 13467–13472.

Yao, M., Qiu, W., Liu, R., Efremov, A.K., Cong, P., Seddiki, R., Payre, M., Lim, C.T., Ladoux, B., Mège, R.-M., et al. (2014). Force-dependent conformational switch of α-catenin controls vinculin binding. Nat. Commun. *5*, 4525.

Yap, A.S., Niessen, C.M., and Gumbiner, B.M. (1998). The juxtamembrane region of the cadherin cytoplasmic tail supports lateral clustering, adhesive strengthening, and interaction with p120ctn. J. Cell Biol. *141*, 779–789.

Yap, A.S., Gomez, G.A., and Parton, R.G. (2015). Adherens Junctions Revisualized: Organizing Cadherins as Nanoassemblies. Dev. Cell *35*, 12–20.

Yoshida, C., and Takeichi, M. (1982). Teratocarcinoma cell adhesion: identification of a cell-surface protein involved in calcium-dependent cell aggregation. Cell *28*, 217–224.

Zebda, N., Tian, Y., Tian, X., Gawlak, G., Higginbotham, K., Reynolds, A.B., Birukova, A.A., and Birukov, K.G. (2013). Interaction of p190RhoGAP with C-terminal domain of p120-catenin modulates endothelial cytoskeleton and permeability. J. Biol. Chem. *288*, 18290–18299.

Zecca, M., and Struhl, G. (2002). Control of growth and patterning of the Drosophila wing imaginal disc by EGFR-mediated signaling. Development *129*, 1369–1376.

Zhu, Y.-T., Han, B., Li, F., Chen, S.-Y., Tighe, S., Zhang, S., and Tseng, S.C.G. (2014). Knockdown of both p120 catenin and Kaiso promotes expansion of human corneal endothelial monolayers via RhoA-ROCK-noncanonical BMP-NFκB pathway. Invest. Ophthalmol. Vis. Sci. *55*, 1509–1518.